TAL TECH

DOCTORAL THESIS

Load Current Harmonic Sensitivity of AC/DC Power Converters of Energy Efficient Devices

Kamran Daniel

TALLINNA TEHNIKAÜLIKOOL
TALLINN UNIVERSITY OF TECHNOLOGY
TALLINN 2024

TALLINN UNIVERSITY OF TECHNOLOGY
DOCTORAL THESIS
35/2024

Load Current Harmonic Sensitivity of AC/DC Power Converters of Energy Efficient Devices

KAMRAN DANIEL

TAL TECH PRESS

TALLINN UNIVERSITY OF TECHNOLOGY
School of Engineering
Department of Electrical Power Engineering and Mechatronics
This dissertation was accepted for the defence of the degree 18/06/2024

Supervisor: Dr Lauri Kütt
School of Engineering
Department of Electrical Power and Mechatronics
Tallinn University of Technology
Tallinn, Estonia

Opponents: Prof Ilya Galkin
Institute of Industrial Electronics and Electrical Engineering
Riga Technical University
Riga, Latvia

Prof David Raisz
Department of Electric Power Engineering
Budapest University of Technology and Economics
Budapest, Hungary

Defence of the thesis: 15/08/2024, Tallinn

Declaration:
Hereby I declare that this doctoral thesis, my original investigation and achievement, submitted for the doctoral degree at Tallinn University of Technology has not been submitted for doctoral or equivalent academic degree.

Kamran Daniel

---
signature

European Union
European Regional
Development Fund

Investing
in your future

ISSN 2585-6898 (publication)
ISBN 978-9916-80-164-2 (publication)
ISSN 2586-6901 (PDF)
ISBN 978-9916-80-165-9 (PDF)
DOI https://doi.org/10.23658/taltech.35/2024
Printed by Koopia Niini & Rauam

Daniel, K. (2024). *Load Current Harmonic Sensitivity of AC/DC Power Converters of Energy Efficient Devices* [TalTech Press]. https://doi.org/10.23658/taltech.35/2024

TALLINNA TEHNIKAÜLIKOOL
DOKTORITÖÖ
35/2024

Energiatõhusate seadmete vahelduv-alalisvoolumuundurite koormusvoolu harmoonikute tundlikkus

KAMRAN DANIEL

TAL TECH
KIRJASTUS

Contents

List of publications

The list of author's publications, on the basis of which the thesis has been prepared:

I **K. Daniel**, L. Kütt, M. N. Iqbal, N. Shabbir and M. Jarkovoi, "Description of Practical Load Harmonic Current Emission due to Voltage Harmonic Variation," *2021 IEEE 62nd International Scientific Conference on Power and Electrical Engineering of Riga Technical University (RTUCON)*, Riga, Latvia, 2021, pp. 1–6, doi: 10.1109/RTUCON53541.2021.9711594.

II **K. Daniel**, L. Kütt, M. N. Iqbal, A.U. Rehman, M. Shafiq, H. Hamam, "Current Harmonic Aggregation Cases for Contemporary Loads," *Energies*, vol. 15, no. 2, 2022, doi: 10.3390/en15020437.

III **K. Daniel**, L. Kütt, M. N. Iqbal, N. Shabbir, M. Parker and M. Jarkovoi, "Waveform Variation Defined Model for Harmonic Current Emissions Including Cross-Order Supply Voltage Harmonics Influence," in *IEEE Access*, vol. 11, pp. 42276–42289, 2023, doi: 10.1109/ACCESS.2023.3270805.

IV **K. Daniel**, L. Kütt, M. N. Iqbal, N. Shabbir, M. Jarkovoi and M. Parker, "Voltage Main Harmonic Level Influence on Harmonic Current Emission Modeling," *2023 International Conference on Future Energy Solutions (FES)*, Vaasa, Finland, 2023, pp. 1–6, doi: 10.1109/FES57669.2023.10183302.

V **K. Daniel**, L. Kütt, M. N. Iqbal, N. Shabbir, M. Jarkovoi and M. Parker, "Load Current Harmonic Model Complexity Reduction through Empirical Pattern Analysis," *2023 IEEE 17th International Conference on Compatibility, Power Electronics and Power Engineering (CPE-POWERENG)*, Tallinn, Estonia, 2023, pp. 1–6, doi: 10.1109/CPE-POWERENG58103.2023.10227474.

VI **K. Daniel**, L. Kütt, M. N. Iqbal, N. Shabbir and M. Jarkovoi, "Estimation of Peak Voltage value and Its Occurrence Timing upon Non-Sinusoidal Supply Voltage," *2024 IEEE 18th International Conference on Compatibility, Power Electronics and Power Engineering (CPE-POWERENG)*, Gdynia, Poland, 2024, pp. 1–6.

Author's contribution to the publications

Contribution to the papers in this thesis are:

I K. Daniel was the main author and wrote the manuscript.

II K. Daniel was the main author, conducted experiment, performed analysis, and wrote the manuscript.

III K. Daniel was the main author, prepared the test bench, conducted experiment, performed simulations, and wrote the manuscript.

IV K. Daniel was the main author, performed measurement, simulation, and wrote the manuscript.

V K. Daniel was the main author, conducted the experiment, analysed results, and wrote the manuscript.

VI K. Daniel was the main author, conducted experiment, performed analysis, and wrote the manuscript.

Abbreviations

AC	Alternating current
CFL	Compact fluorescent lamp
DC	Direct current
DAQ	Data acquisition module
DFT	Discrete Fourier transform
DN	Distribution network
DSP	Digital signal processing
FCM	Frequency coupling matrix
EMC	Electromagnetic compatibility
EMI	Electromagnetic Interference
EV	Electric vehicle
EU	European Union
FFT	Fast Fourier transform
IEC	International electrotechnical commission
IEEE	Institute of electrical and electronics engineers
KCL	Kirchhoff's current law
LED	Light emitting diode
LV	Low voltage
NL	Nonlinear
PCC	Point of common coupling
PQ	Power quality
RMS	Root mean square
RMSE	Root mean square error
SMPS	Switch mode power supply
WVDM	Waveform variation defined model

Symbols

ω	Angular frequency
$\mathcal{F}$	Fourier transform
$\mathcal{F}^{-1}$	Inverse Fourier transform
φ	Phase angle
$\varphi_{h,c}$	Calculated value of phase angle
$\varphi_{h,m}$	Measured value of phase angle
φ_{init}	Initiation angle of capacitor charging /current conduction
φ_{term}	Termination-angle of capacitor charging/end-of-conduction angle
$\varphi_{x,c}$	Angle difference between zero crossing of harmonic and supply peak
φ_n	Harmonic phasor angle in Fourier series
$\Delta\varphi_{charge}$, Δt_{charge}	Charging duration of capacitor
$\Delta\varphi_{peak}$	Angle difference between supply peak and 90°
ω_1	Fundament component frequency
A_m	Coefficient for nonlinear magnitude portion
a_n	Amplitude of the sinusoidally oscillating (cosine)component of order *n,* in Fourier series
A_n	Harmonic phasor magnitude in Fourier series
a_o	Static component of Fourier series
A_p	Phase component for nonlinear magnitude portion
b_n	Amplitude of the sinusoidally oscillating (sine) component of order *n,* in Fourier series
C	Capacitance
C_B	Bulk capacitor
C_m	Coefficient for nonlinear phase portion
C_p	Phase component for nonlinear phase portion
f_1	Fundamental component frequency
f_h	Frequency of harmonic *h*
f_s	Sampling frequency
G_x	Hamonic magnitude sensitivity coefficient
h	Harmonic number
$k_{b\varphi}$	Phase coefficient of relative voltage level U_1
K_{Gconst}	Constant term of magnitude sensitivity coefficient
K_{Glin}	Linear term of magnitude sensitivity coefficient
k_{IM}	Coefficient of magnitude response
kM	Multiplier defining nonlinear coefficient's trend
$k_{RVL,q}$	Relative voltage level coefficient
$k_{SEN,xy}$	y-to-x order sensitivity coefficient
k_{WF}	Waveform coefficient
k_x	Harmonic phase sensitivity coefficient

k_{φ}	Coefficient of phase response
L	Inductor
N	Number of data points
Q	Quadratic unknown
R_{INR}	In-rush limiting resistor
r_{pp}	Peak to peak ripple
t	Time
T	Time period
t_{init}	Current initiation moment
t_{peak}	Peak instant of supply voltage
t_s	Sampling interval
t_{term}	Current termination moment
t_{Upeak}	Supply voltage peak moment
U_y	Voltage harmonic amplitude
x	Current harmonic order
Y	Admittance
y	Voltage harmonic order
Z	Impedance
α_{xy}	Base phase shift component of current harmonic x and voltage harmonic y
γ_{Upeak}	Argument function for peak voltage value
$\gamma_{\varphi peak}$	Argument function for peak voltage time
δ	Deviations
τ	Time constant
τ_{LOADRC}	Time constant for RC-load circuit
$i'_{y,h,k}$	Imaginary component of current harmonic of load k
$i'_{x,h,k}$	Real component of current harmonic of device k

1 Introduction

EU has set goals for carbon neutrality in 2025 (Fit for 55) [1], [2]. The revised European Energy Efficiency Directive (2023/1791/EU) from September 2023 sets goal to have 11.7% reduction in energy consumption by 2030, compared to 2023 levels. This will aim to reduce CO_2 emissions and targets all energy consumption on all major levels from industry and domestic functions**.** Along other means, significant attention is put on residential targets, such as of buildings' energy utilization and increase in efficiency of in-building functions. To support the Energy Efficiency and Fit for 55 targets the Eco design directive is in effect (2022/671/EU) [3]. All in all it sets the minimum requirements to basically every functioning electrical device, with specific limits to the standby power, average energy efficiency etc [4]. For example, a 50 W AC/DC power supply is required to have minimum 88% efficiency [5].

The energy efficiency targets for electric appliances power conversion are basically realized through power electronic converters. Basic operation of such a converter uses switching components and electronic control providing proportional reaction towards the load of power supply. Switching mode power supplies (SMPS) can be found on all commercial power levels and are universally available in forms of, for example, mobile device chargers, laptop power supplies, TV power supplies etc [6].

Commonly such devices are supplied energy through alternating current (AC) electric power grids. For the operation the power supply units the AC is first converted to direct current (DC) through rectifiers, followed by electronically commutated and efficiently controlled circuits. These high-efficient SMPS are presenting a non-linear load to the AC grid. Linear load, such as a resistor, always draws current proportionally to the supplying voltage waveform. The rectifier-based power supplies are usually having a non-sinusoidal current draw and thus are called non-linear loads[7], [8].

Due to widening requirements on energy efficiency the SMPS are paving way to all fields of activity [9]. Nonlinear loads are known to introduce significantly distorted load currents, leading to non-sinusoidal voltage drops and sinewave supply voltage degradation. In general expression the distortions are described by a series of harmonic frequency components of current and voltage, termed as current and voltage harmonics respectively. Harmonics are inevitable and in general unwanted phenomena associated with SMPS operation.

High levels of voltage harmonics can bring problems into the electrical system, leading to added inefficiencies, overheating, and potential damage to infrastructure. Understanding how these harmonic components are influenced by and interact with voltage distortions is key to ensuring the reliability and efficiency of power supplies [10].

Moreover, as electrical networks evolve with the integration of renewable energy non-linear sources and the push towards more manageable and islanded grid configurations, it is becoming increasingly important to have relevant models that can predict and mitigate potential upcoming unwanted electrical phenomena [11], [12]. While the models to investigate main frequency power flow are abundant, the harmonic distortions and even the details on the harmonic loads are being discussed in the early adoption terms.

This thesis aims to bridge one of the key issues in the modelling of the contemporary power electronic load devices. Within the thesis, a novel approach has been taken to provide more accurate estimation on the consumer devices' harmonic load current dependency on supply voltage waveform harmonics' parameters. A general term signed to this relation is harmonic load current sensitivity.

1.1 Power quality, waveform distortions, harmonics

Power quality as a term refers to the conditions and parameters of the voltage and current supply in a power system. The Institute of Electrical and Electronics Engineers (IEEE) defines it as the electromagnetic phenomena that describe the voltage and current at a specific time and location [13]. IEC uses power quality for characterisation of the electric current, voltage and frequency at a point in an electric power system, evaluated against a set of reference technical parameters [IEC 614-01-01]. Deviations from the expected range of parameters are seen as reduced power quality and degraded power quality could potentially lead to issues in the power system, affecting the normal operation of equipment used by end-users. The quality of the supply voltage is often considered critical as it has a broader impact on load endpoints and their functioning.

The International Electrotechnical Commission (IEC) outlines power quality in terms of electromagnetic compatibility (EMC). Power quality represents characteristics of the electric current, voltage and frequencies at a given point in an electric power system, evaluated against a set of reference technical parameters [14]. Electromagnetic disturbances can degrade the operation of electrical equipment or systems, potentially leading to malfunctions or improper functioning [15]–[17].

The IEC 61000-2-5 defines three environment categories that characterize the levels of expected supply voltage parametric deviations in power systems [18]. In broader view, supply voltage parameters are seen as electromagnetic compatibility aspects, whereby the 61000-series standards assist in defining the characteristics of the expected nominal value and deviation total range.

The distortion of current and voltage waveforms first became apparent in power systems during the early 20th century [19]. The term “power quality” began to appear in literature in the 1970s, coinciding with the emergence of circuits in electrical loads that contained nonlinear and switching devices like diodes, thyristors, and transistors. The presence of nonlinear loads and components within the power system is the primary cause of waveform degradation, which can manifest in several forms:

1. Harmonic Distortion: This is the most common form of waveform distortion and arises due to the presence of nonlinear loads, such as variable speed drives, compact fluorescent lights, and other electronic devices. These loads draw current in a non-sinusoidal manner, represented by current harmonics with integer multiples of the fundamental frequency (50 or 60 Hz). Harmonic currents can lead to the generation of harmonic voltages, which distort the supply waveform.
2. Inter-harmonics: These are voltages or currents that appear at frequencies that are non-integer multiples of the fundamental frequency. Inter-harmonics can be introduced by power electronics and some types of variable loads. They can cause problems in the operation of electronic devices and power monitoring equipment.
3. Voltage fluctuations and flicker: Rapid variations in the voltage level can cause lighting devices to flicker, which is particularly noticeable in incandescent bulbs. This type of distortion is often caused by loads that change rapidly, such as electric arc furnaces.
4. Notching: This distortion happens when electronic devices, like variable frequency drives, switch on and off rapidly. They create a series of voltage notches, or transient disturbances, in the waveform that can interfere with the operation of other equipment.

5. Transient disturbances: These are sudden, brief deviations from the ideal waveform, caused by events such as lightning strikes, power line faults, or switching large loads. Transients can be very damaging due to their high energy content.
6. Voltage unbalance: When the voltages in a three-phase system are unequal or not precisely 120 degrees out of phase, it results in an unbalance. This condition can cause additional heating in motors and reduce their efficiency and life span.

The present thesis has a focus on the waveform harmonic distortions. Waveform distortion in power systems refers to a deviation from the pure sinusoidal AC voltage and current waveforms that are ideal for efficient power delivery. In general, the harmonic voltage distortions are seen as most critical in regard to waveform evaluation. The voltage harmonic distortions can have a range of adverse effects on power systems, which include:

1. High-frequency harmonics can lead to overloading and eventual destruction of capacitors in power factor correction devices due to the relationship between capacitor current and harmonic voltage components; with higher-order harmonics causing more thermal stress than lower-order ones.
2. The inherent characteristics of capacitors, when combined with inductance from the power system, set a specific resonant frequency. Significant voltage distortion might occur if the frequency of any current harmonics aligns with this resonant point [20].
3. Transformers experience increased losses and decreased life span due to the heat generated by harmonic frequencies. These additional losses can also degrade transformer insulation, added to which the transformer core may become saturated and the asymmetric nature of harmonics can exacerbate this issue [21], [22].
4. In electric motors, harmonic voltages induce non-productive magnetic flux, which doesn't contribute to the motor's torque, leading to reduced efficiency and increased heat, noise, and vibration.
5. Harmonic currents raise transmission line losses, negatively affecting their capacity due to heightened skin and proximity effects. They also induce voltage drops across system impedances and amplify dielectric stress on the cables.
6. Measurement tools may register errors since they are typically calibrated for sinusoidal currents and voltages.
7. Protection devices within the power system may also fail to operate correctly due to harmonics. This can result in the malfunction of relays and the potential shifting of circuit breakers' tripping thresholds due to the additional heating of solenoids.
8. Household devices such as computers, televisions, and lighting fixtures can be adversely affected by voltage harmonics, impacting their performance and longevity.

1.2 Overview of requirements and normative for power quality respective to network-connected appliances

In electrical engineering and power system design, the requirements for distribution grid to provide service with high power quality is an essence. However, the parties responsible for ensuring the power quality levels are both the distribution grid and the customers' loads connected to the grid. The requirements for the loads are thus driven and have to account for the expected distribution grid characteristics. First and most important are the rules for safety, followed by rules of operation and life-cycle management. For example, EU has set frameworks of directives implying on stating the minimum and mandatory requirements to safety (LVD directive), on efficiency, on waste management (WEEE directive) etc.

Additionally, power supplies and connected devices have to be designed with the capability to handle fluctuations in supply voltage qualities without compromising the performance, which includes maintaining a steady output despite irregular input. Stating this in aspects of reliability for voltage harmonics, the power supply has to be resilient to the harmonics produced by other equipment and at the same time has to avoid any operation that could introduce significant harmonic distortion increase in the grid. This is further addressed in the Electromagnetic compatibility directive (2014/30/EU) [23], whereby it is more generally stated that devices must neither emit unacceptable levels of electromagnetic interference (EMI) nor be overly susceptible to EMI from external sources. Compliance with the directive is ensured, for example, through meeting criteria in the EMC standards like the IEC 61000 series. Criteria given in normative documents ensures that devices perform reliably without disturbing the function of other equipment.

For safety and consumer protection, certifications such as the European Union's CE marking denote that power supplies and network-connected appliances meet rigorous set of standards. A number of these standards also guide the design of power supplies, setting benchmarks for standby and operational power consumption to minimise energy waste and promote environmental conservation. The guidelines relating to the thresholds, mitigation, and measurements of harmonics have been outlined by IEC and IEEE within their respective standards. An overview and explication of various standards associated with harmonics has been presented below.

1. EN 50160: Details the characteristics of AC public networks at low, medium, and high voltage levels, encompassing voltage variations, harmonics, transients, flickers, dips, and swells in [17].
2. IEEE 519: Provide basis for managing harmonics in the electric power system, presenting specifics on the harmonic measurement procedure and recommended harmonic limits [24].
3. IEC 61000-2-2: Prescribes compatibility levels for conducted voltage disturbances within the range of up to 2 kHz, and furthermore from 2 kHz up to 150 kHz in public power supply networks [25].
4. IEC 61000-2-4: Specifies compatibility levels for conducted voltage disturbances in industrial sites within the range of up to 2 kHz [26].
5. IEC 61000-2-5: Outlines the description and classification of electromagnetic environments related to supply networks, covering phenomena associated with disturbances[27] including voltage harmonics.

6. IEC 61000-3-2: Establishes harmonic current emission limits for single units with current rating below 16 A [28].
7. IEC 61000-4-7: Specifies principles for the evaluation and measurement of harmonics in a power supply network [29].
8. IEC 61000-4-30: Defines the measurement methodology for power quality parameters and the interpretation of measurement results in the AC supply system [15].

Mitigating the impact of harmonic distortions is both a technical challenge and a regulatory concern, as standards and guidelines such as [25] and [26] have been established to limit the levels of harmonic voltage and current in power systems. Various strategies have been adopted to combat harmonic distortion, including the use of passive filters, active filters, and custom power devices [30]–[33].

To ensure proper and proportional mitigation, accurate modelling and estimation of harmonic distortions are key to managing power quality. While main frequency AC grids have linear circuit models employed, even the power flow analysis is calculation intensive. For harmonic distortions analysis further capable simulation tools and analytical techniques are required to describe the origins of voltage harmonics in the power grid. By providing where and how harmonics will manifest, engineers can proactively design systems to be more resilient to waveform distortions. Implementing such solutions are vital for sustaining the necessary power quality levels needed to support the growing complexity and connectivity of modern electrical grids and the plethora of devices that depend on them.

1.2.1 Challenges in harmonic sensitivity modelling

The dynamics of the modern power system are rapidly changing due to advancements in energy generation and consumption trends. The growing number of distributed generation units, like photovoltaic (PV) systems, and the increase in power electronic-based loads are evident. In addition to efficiency targets more and more small-power devices are introduced to the grid, this is to support also more capable living environments where more sensing and control is introduced. Trends in domestic energy storage unit implementations, electric vehicles charging set-ups and heat pump deployment will result in powerful SMPS being common load devices at each household. With PV generation requiring a SMPS (known as inverter) with output to the grid, energy storage will also use SMPS to supply the grid. However, SMPS as power sources are also non-linear sources, i.e. these will introduce also non-sinusoidal current infeed that would raise potential to the voltage waveform degradation.

Energy efficiency goals have already removed some high-power traditional linear loads such as incandescent lamps. First replacements by more energy-efficient compact fluorescent lamps (CFLs) already required SMPS to be part of every CFL lamp. Naturally, more efficient light-emitting diode (LED) lamps [34] use SMPS. Electric motor-based appliances are also being improved with the adoption of invert-based drives, which support various working modes, each with its own harmonic emission profile. These drives also are essentially operating as SMPS with non-linear characteristics.

Regarding the potential degradation of performance of grid components and devices (see 1.1) it is a critical consideration that a grid could operate with a good level of power quality. This refers the inclusion of supply voltage waveform to the criteria, where the distortions should not exceed limits required for safe and efficient operation. Controversy is evident when, for example, a highly efficient load is loading the grid in a way that the

losses in the grid are exceeding the “higher efficiency” margins of energy saved due to adding the SMPS. Also, it has to be kept in mind that while the individual devices may have acceptable harmonic distortion in their load current waveforms, the cumulative effect can impose limitations on the network’s power delivery capacity, particularly for transformers when the voltage waveform is compromised. Thus, an accurate assessments of harmonic emissions from present and future loads will be crucial for network operators to enhance capacity and plan for additional investments.

Modelling the operational behaviour of modern nonlinear devices, which exhibit stochastic characteristics, is challenging. While there are numerous studies on power flow modelling, nonlinear load modelling and harmonic estimations are relatively new. The traditional distribution grid models mainly focus on the energy consumption pattern evaluations and have limited time resolution, making it difficult to estimate current harmonic emissions accurately.

Harmonic currents provide an effect similar to the main harmonic frequency loads, considering linear line segments. However, the harmonic current source description and overall equivalent circuit presentation can be totally different. For example, it can be considered that the network transformer is acting as an emf source for mains frequency component, but for the harmonic component modelling the transformer could be presented as a short circuit or open circuit.

This thesis is looking at a harmonic load current modelling for a source approach. In particular, the load harmonic currents are seen to be emitted as a result of a device operation. Furthermore, aim is to include this source’s current model to be responsive to supply voltage waveform applied to a load device.

1.3 Hypothesis

The main hypothesis of the thesis are stated as

- Voltage and current harmonics coupling occurs primarily due to the time-domain variations of waveforms. This refers that any single frequency component coupling is insufficient for providing a systematic model basis. Impedance or admittance relations between voltage harmonics and current harmonics described in state-of-the-art models are lacking the physical expression of cross-order harmonic relations seen in measurements.
- Time-domain waveform variation of the current waveforms provides a defined relation towards voltage harmonic components across different order current harmonic components. These defined relations would be clearly seen through testing results of actual devices.
- Harmonic coupling models are to be defined based on the rectifier characteristic behavior instead of empirical impedance relations. The rectifier operation dynamic characteristics would indicate similar relations as seen from empirical testing outcome.

1.4 Research task definition

The aforementioned aspects pertain to the thorough examination of harmonic disturbances within power systems, focusing particularly on the loads’ current response to supply voltage distortions. Each item addressed below corresponds to a targeted stage in a comprehensive methodology to model and analyse harmonic effects.

A: Testing the loads for the empirical model definition of current harmonics

This stage involves practical experimentation with electrical loads to gather empirical data on how these loads contribute to current harmonics within a power system, particularly under non-ideal supply voltage conditions. The process typically requires subjecting loads to various voltage distortions and accurately recording the current waveforms under these conditions. The purpose is to establish a clear set of definitions and source for characterization of current harmonics that are observed in the presence of supply voltage distortions, creating a reference for further modelling and analysis.

B: Identification of the empirical model basic physical behaviour sources

This step involves analysing the collected data to determine patterns and underlying relationships between the distorted supply voltage and resultant harmonics. The aim is to understand the basic physical principles and mechanisms within the load circuitry that give rise to harmonics. This understanding can then inform the development of more refined model that seek not just to describe but also to explain harmonic propagations.

C: Defining the particular physical model for the harmonic current analytic analysis

Based on the observational data and the identification of physical behaviour of the components present in the energy-efficient devices, such as capacitors, a specific analytical model can be defined to account for the physical operation of rectifier circuit switching. This model represents the behaviour of the load currents in mathematical terms, identifying the root mechanism of current harmonics. Such a model would allow for predictive analysis – giving researchers the ability to anticipate harmonic generation under various conditions without the need for additional empirical testing.

D: Modelling the load currents characteristics and variance parameters with multiple voltage harmonics in the supply voltage

Finally, with a clear analytical model defined, the task is to refine the model to account for the interactions that occur when multiple voltage harmonics are present in the supply voltage. This involves adjusting the parameters within the model to capture the characteristics of load currents as they are influenced by a spectrum of harmonic frequencies.

Thus the thesis is providing both theoretical and practical approach the harmonic load currents' estimations.

1.5 Novelty expression

Main items of novelty in this thesis can be listed as follows:

A: Time-domain expression analysis on the current harmonics, voltage harmonic to current harmonic coupling

In analysing the time-domain expression of current harmonics and their coupling with voltage harmonics, we consider the instantaneous relationship between voltage and current waveforms. The novelty in this approach for identifying and characterising nonlinear interactions provides direct physical explanations for cross-order effects between different orders of harmonics.

B: Relation identification of load current harmonic components phase behaviour related to waveform time-shifting

Usual approach to harmonic current phase angle characteristics is to use phase angle as a parameter itself. However, the focus on this thesis is to consider the

phase angle as a marker of waveform timing, not the phase as a quantity itself. Novel time-scale description of the parameters related to the harmonic load current components will provide a direct physical address to the emergence of variations in the harmonic component phase angle ranges.

C: Load current waveform variation definition upon multiple supply voltage component presence

The nonlinear characteristics of power electronics interfaces, such as inverters or rectifiers, and their interaction with grid harmonics, lead to complex cumulation of waveform distortion parameters. The explanation of the definition of multiple harmonic supply voltage components sensitivity will be delivered, a new aspect delivered with actual case examples.

D: Detailed analytical expression of the load current harmonic behaviour for the expected voltage harmonic content ranges

The analytic expressions defining the physical harmonic parameter's ranges' and potential variation extent are defined for the full-wave rectifier circuit. Previously sources reporting harmonic sensitivity presence either assume numerical or then physical measurement bases, but are missing explanations on the physical circuit operation formulations. Novel explanations are delivered to tie the rectifier physical operation analytics and practical harmonics outcome.

1.6 Thesis outline

- Chapter 2 provides an introduction to harmonic sensitivity, requirements and instruments for harmonic content measurement, harmonic aggregation and analysis of harmonic estimation models, and effect of magnitude and phase of voltage harmonics on resultant current harmonics.
- Chapter 3 presents the methodology used to construct the harmonic estimation model and analysis of the model including the physical operation of the element in the switching circuits.
- Chapter 4 focuses on the time domain analytical expression for the harmonic models considering the physical operation of components present in the rectifying/switching circuit in loads.

2 Harmonic sensitivity

The accurate assessment and analysis of harmonic currents are vital for the effective operation and management of power systems. The topic of harmonic sensitivity derives from the complexity to provide an accurate estimation of harmonic load currents. In essence, the measurements indicate that harmonic currents of even simple power supply have significant variations depending on the voltage waveform supplied to the load. Therefore, the load current characteristics are sensitive to the supply voltage waveform parameters (publication II). In this thesis a LED lamp as an example of a simple load is used to deliver more detailed understanding of voltage waveform to current waveform interactions.

Market available LED lamps can be distinguished based on the shape of load current waveform, drawn by LED [34] shown in Figure 2.17; the presence filter or waveform control circuit, influences the characteristics of the load current waveform [35]–[38]. Within the context of this study, Type A LED lamps, as categorised in (section 2.5.2) [34] were randomly selected for evaluation to assess their odd-order harmonic content and behaviour under the voltage harmonic orders of 3, 5, and 7.

2.1 Waveform definitions

The field of electrical engineering depends heavily on the design and analysis of power supply systems and loads, both linear and nonlinear. Linear power sources, for example transformers/regulators, are known for their reliability, perfect waveshape and simplicity, making them ideal for applications where precision and low noise are critical. However, their limitations in terms of efficiency and size make them less suitable. In contrast, nonlinear power supplies, especially switched-mode power supplies are gaining popularity due to their efficiency and compact design. The use of high frequency switching devices significantly reduces size and weight, making nonlinear power supplies ideal for portable electronic devices and power efficient applications. However, the complexity of SMPS designs introduces challenges related to electromagnetic interference (EMI) and the potential for harmonic distortion in the output waveform. When designing power supply systems, understanding and accommodating various loads is crucial.

AC power supply works well with linear loads, such as resistors and incandescent bulbs. Sinewave mains power supply voltage waveform is defined as a function of sine that is written as

$$u_{AC,SIN}(t) = U_{AC,M1}\, sin(\omega_1 t) \tag{2.1}$$

Where $U_{AC,M1}$ is the magnitude (or peak value) of the supply and ω_1 is the frequency of fundamental component.

Ideal linear power supply provides perfect sine waveshape load current draw.

A linear load, acting upon supplied with such voltage will have a load current

$$i_{AC,SIN}(t) = I_{AC,M1}\, sin(\omega_1 t + \vartheta_{I1}) \tag{2.2}$$

For the AC load a scalar load impedance ($\boldsymbol{Z_{LOAD}}$) quantity is used for trivial calculations, so the load current magnitude is calculated as

$$I_{M1} = \frac{U_{M1}}{|\boldsymbol{Z_{LOAD}}|} \tag{2.3}$$

The current can be also written as a complex quantity, having its magnitude and phase shift angle tied in single variable

$$\boldsymbol{I}_{\boldsymbol{AC,SIN}} = \frac{I_{M1}}{\sqrt{2}} \angle \vartheta_{I1} \tag{2.4}$$

$$\vartheta_{I1} = tan^{-1} \frac{Im\{\boldsymbol{I}_{\boldsymbol{AC,SIN}}\}}{Re\{\boldsymbol{I}_{\boldsymbol{AC,SIN}}\}} \tag{2.5}$$

General rule for transformation from sinusoidal voltage and current to phasor domain is presented in the Table 2.1 below; where *U* is the general expression of RMS value of voltage waveform and *I* is the RMS value of current waveform of a circuit element. Voltage phase angle 'φ' and current phase angle 'ϑ' is angular distance towards reference i.e. zero degree position. Table 2.2 illustrates an example of phasor-presentation of current and voltage appearing on the inductor component in common RL series arrangement; where 'U_L' is the voltage across inductor and 'I_L' is series current.

Table 2.1 Sinusoidal-phasor transformation

Time domain		Phasor domain
$U \cdot \cos(\omega t + \varphi)$	↔	$U \angle \varphi$
$U \cdot \sin(\omega t + \varphi)$	↔	$U \angle (\varphi - 90^o)$
$I \cdot \cos(\omega t + \vartheta)$	↔	$I \angle \vartheta$
$I \cdot \sin(\omega t + \vartheta)$	↔	$I \angle (\vartheta - 90^o)$

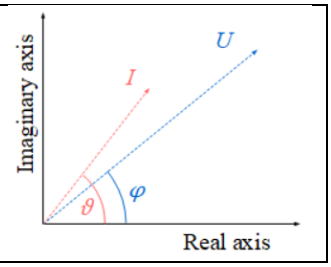

Table 2.2 Example of a phasor representations

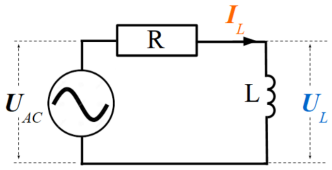

Mark IL, make inductance.

R = 1 kΩ, L = 0.1 H
Inductive reactance X_L = 31.4 Ω
U_{AC} = 230 V
$\boldsymbol{I}_L$ = current through inductor
$\boldsymbol{U}_L$ = voltage across inductor

Supply voltage of RL series circuit and phasor domain representation

$\boldsymbol{U}_{AC} = 230 \angle 0^o$ V

Voltage across the inductor terminals

$$\boldsymbol{U}_L = \frac{jX_L}{R + jX_L} \cdot \boldsymbol{U}_{AC}$$

$\boldsymbol{U}_L = 7.2 \angle 88.2^o$ V

Current through inductor is calculated as

$$\boldsymbol{I}_L = \frac{\boldsymbol{U}_{AC}}{R + jX_L}$$

$\boldsymbol{I}_L = 0.23 \angle -1.8^o$ A

Voltage and current time-domain waveform

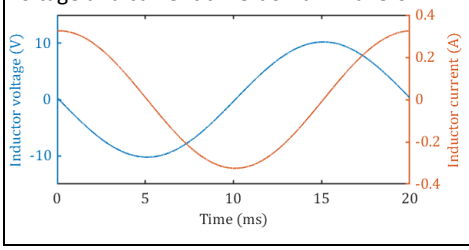

Phasor expression – plot

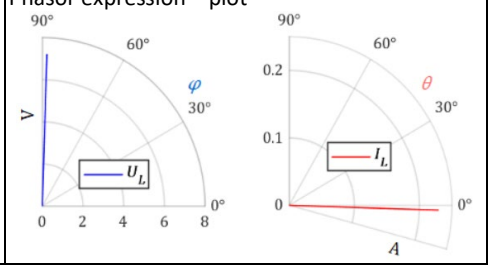

The actual voltage waveform in the grid is practically never a perfect sinusoid, but rather persistent if comparing, for example, two neighbouring cycles waveforms. This refers that these cyclic repeating waveforms could be observed as a main harmonic frequency sine component, with added higher order harmonic frequency sinewave components superposed on it. With inclusion of voltage harmonics, supply voltage waveform no longer maintains the original pure sine wave shape. Figure 2.1 illustrates voltage supply waveforms for fundamental frequency component and added harmonic frequency components.

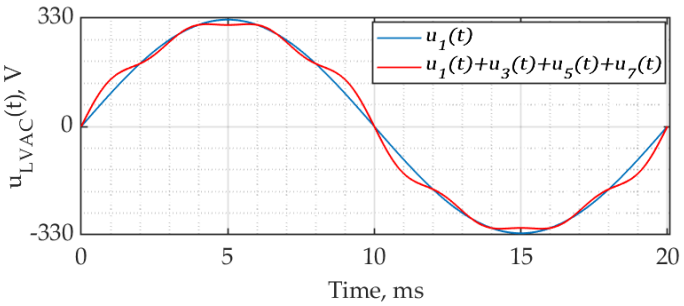

Figure 2.1 Supply waveform distortion example, with voltage harmonics imposed on the main harmonic waveform.

The distorted but cyclic voltage supply waveform can be represented using Fourier series expression as equation ((2.6), where multiple components make up the cumulative voltage waveform. Each Fourier series component can be considered independently, where term 'harmonic component' is used in conjunction with the 'harmonic order', where the 'order' refers to an integer multiple of the main cycle frequency. For example, the main harmonic component frequency of f_1 = 50 Hz corresponds to 1st order component representing main cycle occurrence frequency, f_5 = 250 Hz component is 5th order component etc. In the text, a "harmonic component" refers to either voltage or current component phasor, of a specific harmonic order. Denotation of the harmonic order is usually the subscript noted after the variable.

Therefore, the Fourier series presentation of grid voltage can be detailed as

$$\begin{aligned} u_{LVAC}(t) = {} & U_{M1}\, sin(\omega_1 t + \varphi_{U1}) \\ & + U_{M3}\, sin(3\omega_1 t + \varphi_{U3}) + U_{M5}\, sin(5\omega_1 t + \varphi_{U5}) \\ & + \dots\dots\, U_{Mh}\, sin(h\omega_1 t + \varphi_{Uh}) \end{aligned} \tag{2.6}$$

where U_{M1}, U_{M3}, U_{M5}, … U_{Mh} are the respective magnitudes and φ_{U1}, φ_{U3}, φ_{U5}, … φ_{Uh} are angular distances towards the reference position, and '$_h$' presents the total number of harmonic components considered, where ω_1 refer to angular frequency available as

$$\omega_1 = 2 \cdot \pi \cdot f_1$$

Each pair of voltage harmonic component level and phase angle make up a phasor expression, whereas the total voltage can be specified as an array of harmonic voltage components as

$$[\boldsymbol{U_{LVAC}}] = \begin{bmatrix} \boldsymbol{U_1} \\ \boldsymbol{U_3} \\ \dots \\ \boldsymbol{U_h} \end{bmatrix} = \begin{bmatrix} U_1 \angle \varphi_{U1} \\ U_3 \angle \varphi_{U3} \\ \dots \\ U_h \angle \varphi_{Uh} \end{bmatrix} \tag{2.7}$$

Equation (2.6) is modified Fourier series as it accounts only for odd harmonics; if the waveform in time domain is persistent regardless of cycle, the periodic waveform part will be described only by odd harmonics. In addition to supply voltage, load current can also be represented using similar Fourier series expression.

2.2 Fourier transform and harmonic components

The Figure 2.2 presents the load current waveform of a commercially available energy efficiency LED lamp. Due to the nonlinear nature of the lamp load, load current waveshape is not proportional to the sinusoidal supply voltage waveform, but has a clearly non-sinusoidal form. It has to be said that the current waveform, as presented in Figure 2.2 occurs both in cases when the supply voltage is of pure sinusoidal form but is rather similar also in cases, when the supply voltage has distortions such as presented in Figure 2.1.

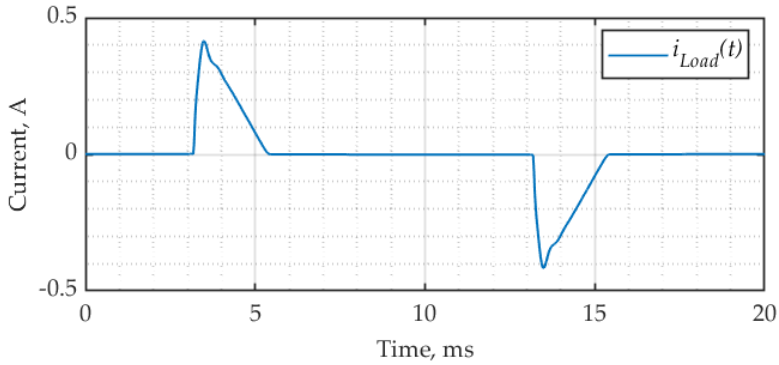

Figure 2.2 Typical load current of energy efficient LED lamp.

The load current can be expressed as a Fourier series as well, and such waveform composition representation through use of load current harmonic components is well respected by engineers. It emerges from aspect that a periodic function *f(t)* and its transform in frequency term *F(ω)* from the Fourier pair and one can be derived form the other.

$$f(t) \leftrightarrow F(\omega)$$

Frequency domain representation of the supply voltage and load current can be described using equations below

$$u_{LVAC}(t) \overset{F}{\rightarrow} U_{LVAC}(\omega) \tag{2.8}$$

$$i_L(t) \overset{F}{\rightarrow} I_L(\omega) \tag{2.9}$$

In general presentation, according to the *Fourier theorem*, any practical periodic function of frequency can be expressed as an infinite sum of sine or cosine functions that are integral multiples of main harmonic cycle frequency. Thus, assuming either voltage or current quantity time representation as a time-defined function f(t), general expression is

$$f(t) = a_0 + \sum_{n=1}^{\infty} (a_n \cos(n\omega_1 t) + b_n \sin(n\omega_1 t)) \tag{2.10}$$

where ω_1 is the *fundamental frequency* in radians per second. The sinusoid sin$(n\omega_0 t)$ or cos$(n\omega_1 t)$ is called the nth order harmonic of $f(t)$; it is an odd order harmonic if n is odd and an even order harmonic if n is even. Equation (2.10) is called the *trigonometric Fourier series* of $f(t)$. Fourier series coefficients – referred to as the Fourier coefficients – are available to reconstructing the waveform through inverse Fourier transform. The coefficient a_0 is the static component (for electric signals, the DC component) or the average value of $f(t)$ within main harmonic cycle. The coefficients a_n and b_n are the amplitudes of the sinusoidally oscillating components, but they also make up the phasor quantities of the harmonic components. Assuming linear trigonometric identities, one can specify the harmonic phasor magnitude A_n and phase φ_n through

$$A_n = \sqrt{a_n^2 + b_n^2} \quad , \quad \varphi_n = -\tan\left(\frac{b_n}{a_n}\right) \tag{2.11}$$

The engineers implement and measurement devices indicate these harmonic phasor quantities. The equation (2.10) can be rewritten as

$$f(t) = a_0 + \sum_{n=1}^{\infty} A_n \cos(n\omega t + \varphi_n) \tag{2.12}$$

Equation (2.12) can be re-written using the trigonometric identity $\cos(\alpha+\beta) = \cos\alpha\cdot\cos\beta - \sin\alpha\cdot\sin\beta$

$$f(t) = a_0 + \sum_{n=1}^{\infty} [A_n \cos(\varphi_n)\cos(n\omega t) - A_n \sin(\varphi_n)\sin(n\omega t)] \tag{2.13}$$

Equating (2.10) with (2.13) provides a representation using real and imaginary components as

$$a_n = A_n \cos(\varphi_n) \quad , \quad b_n = -A_n \sin(\varphi_n)$$

Thus the equivalent to the phasor presentation is the complex form of a harmonic component (2.11) of an order n

$$A_n \angle\varphi_n \leftrightarrow a_n - ib_n \tag{2.14}$$

To determine a_n for cosine terms and b_n for sine terms in the series, calculations using integrals of the original periodic function multiplied by the corresponding sine or cosine functions over one period of the function.

$$a_0 = \frac{1}{T}\int_0^T f(t)dt \tag{2.15}$$

$$a_n = \frac{2}{T}\int_0^T f(t)\cos(n\omega t)\,dt \tag{2.16}$$

$$b_n = \frac{2}{T}\int_0^T f(t)\sin(n\omega t)\,dt \tag{2.17}$$

Figure 2.3 illustrates the time and frequency domain representation of input voltage and load current of a common LED lamp; where the supply voltage is pure sine wave. Load current waveform is consisting of multiple current harmonic phasors, i.e. current

harmonic components with unique magnitude values and unique harmonic component phase angles. It has to be noted that the harmonic component phase angles are determined by assuming the 0-phase instant of the fundamental voltage component as reference point.

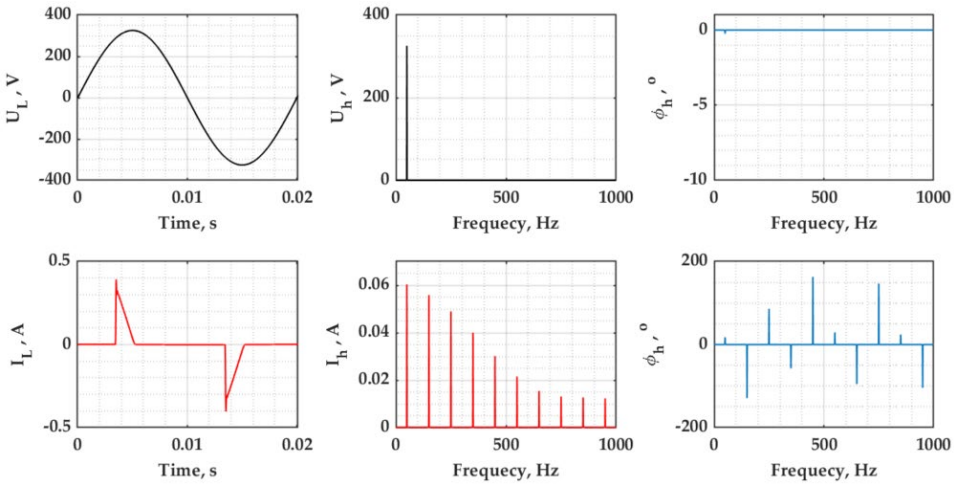

Figure 2.3 Voltage and current harmonic components definition for the voltage and current shapes.

Each cyclic repeating current waveform of any load can be described by a series of current harmonics similar to presentation in (*(2.6*). Non-linear loads' current harmonics have specific magnitude and phase angle values even when the supply voltage is pure sine-shaped.

As described in Chapter 1, the utility voltage available in customers' supply points (residential and industrial) could have different waveshape than pure sinusoid. However, load current harmonics parameter values are also sensitive to supply voltage harmonic parameters. Figure 2.4 shows an example of this, the effect of adding 5^{th} voltage harmonic to supply on one of the load current harmonics is observed from measurement results of a practical LED lamp device.

Harmonic sensitivity describes the influence of supply voltage harmonics on the current harmonics. The practical outcome of this sensitivity is visualized in Figure 2.4 and Figure 2.5; illustrating the effects of voltage harmonic phase angle. Voltage harmonic component magnitude is maintained constant at all these times.

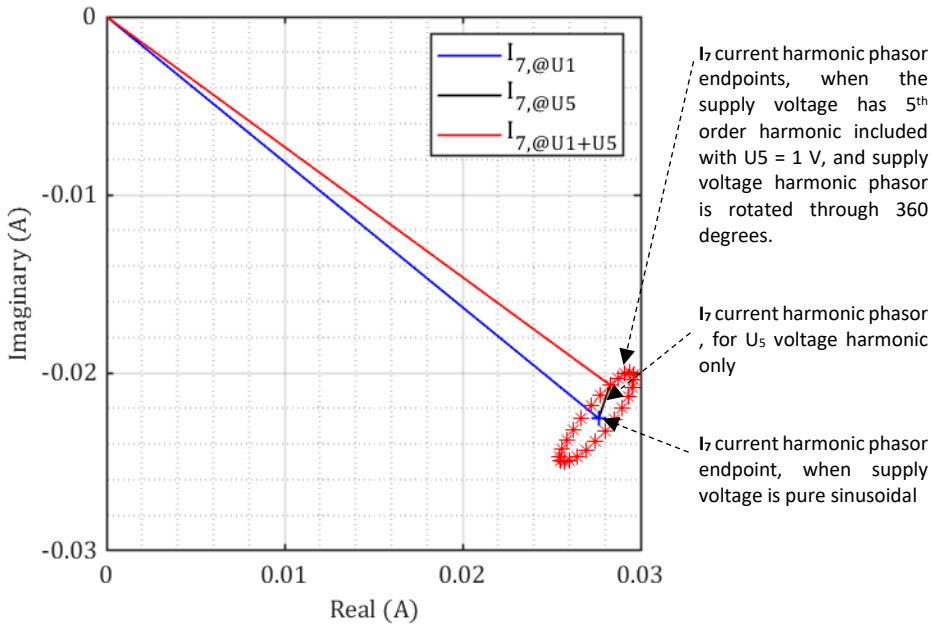

Figure 2.4 Variations in seventh harmonic current vectors for supply voltage containing $\boldsymbol{U_5}$ *(*U_5 *= 1 V) and phase* φ_{U5} *= 0, 15, 30…345°. (previously published in article I).*

2.3 Definition of harmonic sensitivity

In a low voltage distribution grid, the supply voltage waveform could be varying depending on the loads connected to the grid and their operation, for example according to daylight time, temperature, etc. [39]. As it is clear that the load current harmonics' parameters are dependent on the voltage supply waveform [40]–[42], in order to assess the total harmonic current in the LV grid, the voltage harmonics characteristics varying nature has to be accounted for.

General expression of variation of a load current phasor parameter is

$$\boldsymbol{I_{LOAD,T}} = \boldsymbol{I_{LOAD,REF}} + \Delta\boldsymbol{I_{LOAD,D}} \tag{2.18}$$

where $\boldsymbol{I_{LOAD,T}}$ is the total current phasor, $\boldsymbol{I_{LOAD,REF}}$ is the reference phasor and $\Delta\boldsymbol{I_{LOAD,D}}$ is the difference phasor. In terms of load current harmonic sensitivity, in this thesis the sensitivity is considered as dependence on the voltage harmonic characteristics referenced to the load harmonic current value in pure sinewave voltage supply conditions

$$\Delta\boldsymbol{I_{LOAD,h,SEN}} = \boldsymbol{I_{LOAD,h,ULVAC}} - \boldsymbol{I_{LOAD,h,USIN}} \tag{2.19}$$

where $\boldsymbol{I_{LOAD,h,ULVAC}}$ is the total load current harmonic phasor upon non-sinewave U_{LVAC} supply voltage, $\boldsymbol{I_{LOAD,h,USIN}}$ is the reference harmonic load current phasor when load is supplied with sinusoidal supply voltage, and $\Delta\boldsymbol{I_{LOAD,h,SEN}}$ is the difference phasor due to the sensitivity parameter.

Current harmonic sensitivity to the voltage harmonics in the first approach can be expressed as follows

$$\Delta\boldsymbol{I_{LOAD,h,SEN}} = k_{SEN,h} \cdot \boldsymbol{U_{LVAC,h}} \tag{2.20}$$

where k_{SEN} is the sensitivity coefficient describing the effect for the *h*-th harmonic.

The use of (2.19) is justified from evidence of test results. Figure 2.5 is showing the implication of variance in current waveforms due to added voltage harmonic [43], [44]. The total load harmonic currents are seen to be centred around a base point, which is identified as pure-sinewave supply voltage load current harmonic phasor. In addition, load harmonics also show cross-coupling and dependency to magnitude level of added voltage harmonics (see Figure 2.5); as Figure 2.5 presents the spread of harmonic component on the complex plane for various $\boldsymbol{U_{LVAC,h}}$ phase angle points and magnitude levels of the incident voltage harmonic.

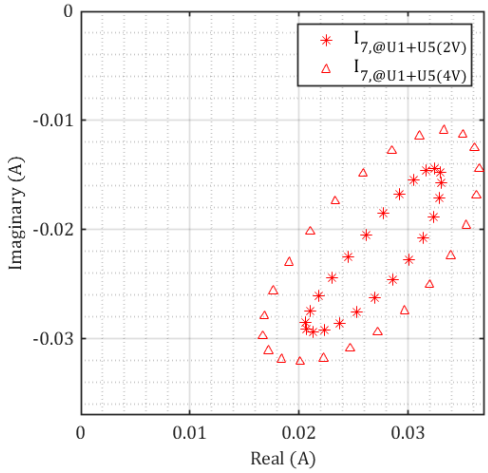

Figure 2.5 Seventh harmonic current phasors for supply voltage containing U_5 (2 V or 4 V) and phase φ_{U5} = 0,15,30…345°.

The sensitivity parameter is not a trivial constant, but is a rather sophisticated function with geometric origins. Furthermore, there is clear cross-order dependence of the voltage harmonic sensitivity – voltage harmonic of an order is providing influence to current harmonic of another order. This could be expressed as

$$\Delta \boldsymbol{I_{LOAD,x,SEN}} = k_{SEN,xy} \cdot \boldsymbol{U_{LVAC,y}} \tag{2.21}$$

where x is the current harmonic under observation, y is the influencing order of voltage harmonic and $k_{SEN,xy}$ is the y-to-x order sensitivity coefficient.

In this thesis, the target to investigate the harmonic sensitivity will be to develop into a model, that if input with voltage harmonic phasor values, would be able to output the current harmonics' phasor values. In the following chapter there will be a description on the approaches for modelling the harmonic current levels due to voltage harmonics' presence.

2.4 State of the art in harmonic sensitivity models

2.4.1 Frequency domain models

When modelling the waveform response of various power electronic converter loads in a distribution network (DN), analyses are commonly rooted in the frequency domain [45]–[47], predicated on an assumption of a sinusoidal voltage supply. One of the simplest presentations for harmonic fingerprint is assuming that each harmonic current emission is a constant current source $\boldsymbol{I_h} = I_{h,const} \angle \varphi_{h,const}$ [39][48].

$$\boldsymbol{I_{hTOT} = I_{hN} + I_{hZ}} \tag{2.22}$$

These sources of current harmonics operate independently from the input voltage. Thus this model does not take into account any sensitivity or influence parameters. Considering the voltage waveform in a distribution system is continuously altered due the variability and nature of the connected loads, current source models may face limitations in their effectiveness for comprehensive harmonic analysis. Harmonic load current coupling/sensitivity to voltage emerges clearly measurements reported commonly [18].

The Norton equivalent circuit model for this situation comprises two harmonic current elements – a constant current source $\boldsymbol{I_{x,Base}}$ and a linear impedance reaction $\boldsymbol{I_{x,Z}}$ [49], [50]. $\boldsymbol{I_{x,Base}}$ is recognised as a fixed value under an unaltered sinusoidal voltage. On a vector plot, the Norton model suggests that the actual current emission from a device should ideally remain close to an acceptable predetermined reference, which is the current emission under the ideal sinusoidal voltage condition (simulated as a constant current source) and follows a linear path for slight deviations. If impact of a voltage harmonic is detailed by a vector $\boldsymbol{U}_x = U_x \angle \varphi_{Ux}$, a response on the load's harmonic current would occur as

$$\boldsymbol{I_{hZ}} = \frac{U_h \angle \varphi_{Uh}}{Z_h \angle \varphi_{Zh}} \tag{2.23}$$

$$\boldsymbol{I_{hTOT} = I_{hN} + I_{hZ}} \tag{2.24}$$

Although this approach offers some advantages over the current source model it is unable to account for the cross-order dependency of harmonics. However, the Norton model, does not fully represent the extent of interactions noted in measured data. It does not adequately convey the influence between voltage and current harmonics of different orders – termed cross-order coupling (from Publication II). Additionally, it is not equipped to describe the variations in current harmonics due to different supply voltage magnitudes (main harmonic voltage level).

To address this shortcoming, the Frequency Coupling Matrix (FCM) model implements a cross-frequency admittance matrix [51]. In this improved approach, the harmonic currents are influenced not just by voltage harmonics of an identical frequency but also by those from other orders [52], [53]. The mathematical expression of the FCM model is presented in Equations (2.25) and (2.27). By integrating impedance (or conductance) metrics, the FCM refines the foundational Norton approach [54], recognising that the total $\boldsymbol{I_{x,FCM}}$ is the result of a cumulation of various sub-responses. That is, each *x*-th order harmonic current vector is the combined output of these distinct interactions. Using FCM, the *x*-th harmonic current vector could be written as

$$\boldsymbol{I_{x,FCM} = I_{x,Base} + [U][Y_{x,y}]} \tag{2.25}$$

where **[*U*]** is the total harmonic vector matrix of supply voltage, where each row is representing a supply voltage harmonic component vector, represented as

$$[\boldsymbol{U}] = \begin{bmatrix} \boldsymbol{U_1} \\ \boldsymbol{U_2} \\ \boldsymbol{U_3} \\ \vdots \\ \boldsymbol{U_h} \end{bmatrix} = \begin{bmatrix} U_1 \angle \varphi_{U1} \\ U_2 \angle \varphi_{U2} \\ U_3 \angle \varphi_{U3} \\ \vdots \\ U_h \angle \varphi_{Uh} \end{bmatrix} \tag{2.26}$$

and [$\boldsymbol{Y_{xy}}$] represents the frequency coupling admittance matrix. This matrix encapsulates the interactions between the *x*-th harmonic current component and each *y*-th voltage harmonic component presented in **[*U*]** [55].

$$\boldsymbol{I_{x,FCM}} = \begin{bmatrix} \boldsymbol{I_{1,Base}} \\ \boldsymbol{I_{2,Base}} \\ \boldsymbol{I_{3,Base}} \\ \vdots \\ \boldsymbol{I_{h,Base}} \end{bmatrix} + \begin{bmatrix} \boldsymbol{Y_{11}} & \boldsymbol{Y_{12}} & \boldsymbol{Y_{13}} & \cdots & \boldsymbol{Y_{1h}} \\ \boldsymbol{Y_{21}} & \boldsymbol{Y_{22}} & \boldsymbol{Y_{23}} & \cdots & \boldsymbol{Y_{2h}} \\ \boldsymbol{Y_{31}} & \boldsymbol{Y_{32}} & \boldsymbol{Y_{33}} & \cdots & \boldsymbol{Y_{3h}} \\ \vdots & \vdots & \vdots & \ddots & \vdots \\ \boldsymbol{Y_{h1}} & \boldsymbol{Y_{h2}} & \boldsymbol{Y_{h3}} & \cdots & \boldsymbol{Y_{hh}} \end{bmatrix} \cdot \begin{bmatrix} \boldsymbol{U_1} \\ \boldsymbol{U_2} \\ \boldsymbol{U_3} \\ \vdots \\ \boldsymbol{U_h} \end{bmatrix} \tag{2.27}$$

The FCM model is established on the principle that harmonics within a network are interdependent. Constructing an FCM model involves defining a matrix that represents the interaction intensity between different harmonic frequencies. Each element within this matrix corresponds to a coupling factor between two harmonic orders. These coupling factors are static in the characteristics of the power system components, and empirically determined. However, FCM model foundations lack in providing insight into the physical operation of rectifier circuits in devices. Measurements indicate that rectifier circuit load current is responding in magnitude level variation while voltage harmonic phasor phase angle only is modified.

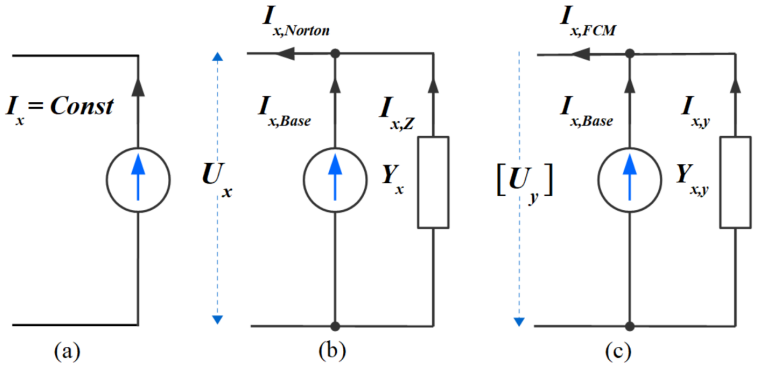

Figure 2.6 Harmonic load reaction models, (a) constant source (b) Norton equivalent (c) FCM [43][56] (previously published in article III).

The Frequency Coupling Matrix (FCM) method encounters challenges when applied to practical device modelling within actual network conditions, as these scenarios often lead to deviations. $\boldsymbol{I_x}$ outcome are circular vector plot result patterns where impedance-based products of harmonic voltage $\boldsymbol{U_y}$ phase influences are used [12]. However, $\boldsymbol{U_y}$ phase influence patterns on phasor plot are often elliptical in form (see Chapter 2). It has been detailed in [45], [57], [58], that further variables should be introduced via negative-sequence FCM or additional frequency component factor [59] to describe the elliptical result pattern; which inevitably increases the complexity and computational demand for the FCM method. While the FCM would be capable of providing a current harmonic magnitude response, there is any clear representation of physical phenomena that provides for harmonic cross-order coupling [60]–[62]. Remaining complexity and the deviation in $\boldsymbol{I_x}$ phase result will provide limitations of range for the FCM, as the cumulative assessment of total $\boldsymbol{I_y}$ different sub-reactions also means cumulation of deviations. Figure 2.13 illustrates equivalent circuit diagrams of above mention models.

2.4.2 Time domain models

The time-domain models provide comprehensive information about the load harmonic emission profile as they are based on the actual circuits of the loads. However, modelling every load connected to the grid using its circuit schematics is a challenging task. To overcome this challenge, a time-domain harmonic analysis approach is applied to nonlinear loads that are categorised based on their circuit topologies [63]. Since most electronic devices incorporate switch mode power supplies (SMPS), equivalent time-domain models of SMPS are made, and the current harmonic estimation is presented on simulated and measured waveforms. Similarly, a model is established for computer loads connected to a single transformer, and the results show harmonic cancellation and voltage waveform distortion at the transformer [64]. Mathematical models of low-power compact fluorescent lamps (CFL) were developed to study harmonic penetration in [65], where voltage and current waveforms were recorded and analysed using circuit simulation software.

2.4.3 Distinctive stochastic models

In the distinctive method of load modelling, the various types of loads connected to the power grid are classified by their electrical characteristics. These classifications are then used to develop probability distributions that predict the total harmonic distortion they contribute to the system. As an illustration, loads might be sorted into categories like linear or nonlinear, and further distinguished by their specific circuit configurations and power quality traits. This approach to modelling harmonics was initially suggested in 1987 [66]. That model arranged nonlinear loads into four distinct groups, categorised by their switching states and modes of operation. To analyse the collective effect of harmonics, the model applied the Monte Carlo method, leveraging probability density functions to manage variables like harmonic amplitudes and phase angles.

The study of how domestic appliances affect harmonics within low voltage networks employed actual appliance usage data and their operational patterns is discussed in [67]. This modelling compared its output against live network readings to ensure accuracy. An analogous method constructs usage profiles for home appliances based on resident behaviour, then analyses harmonic emissions using the appliances' equivalent circuit models [68].

Furthermore, research incorporating a probabilistic approach considered how waveform distortions are influenced by the widespread adoption of electric vehicles. This technique is valued for its capacity to incorporate uncertainties, especially regarding varied EV charging habits [69]. Propositions for grouped single and three-phase nonlinear loads according to their current total harmonic distortion levels, utilising energy consumption trends from different times to determine the participation of these load groups [70]. This process involved selecting customer database parameters with the assumption that data for any particular type of device would typically follow a normal distribution. Utilising this probability-based method, voltage distortions within the low voltage network are assessed.

2.5 Rectifier-based loads details

Rectifier circuits using diodes and thyristors for AC to DC conversion are well-known for introducing harmonics into power systems. Diode-based rectifiers are commonly used due to their simplicity and reliability. Thyristor-based rectifiers provide more control over the output voltage by adjusting the activation moment – called firing angle. This feature allows control over the timing of current conduction through the circuit. By controlling the point in the AC cycle at which the switches are triggered, it is possible to adjust the output voltage and current of the rectifier. Controlled rectifiers are especially valuable in applications requiring variable output for device-specific requirements, such as adjustable speed drives and power supplies that necessitate a variable output. Thus offering flexibility and precision in a wide array of power conversion applications in countless consumer, commercial, and industrial devices.

Within the context of this thesis the focus is on the uncontrolled rectifiers. Uncontrolled rectifiers use diodes that allow the current to flow in only one direction. As a result, the flow of current is determined by the inherent properties of the diodes, and there is no external control. The output voltage of uncontrolled rectifiers is fixed and depends on the input AC voltage and the specific rectifier circuit configuration.

2.5.1 Full-bridge rectifier

To optimise energy conversion using diode native conduction control, a full-wave rectifier is the ideal option. This type of rectifier can be constructed using bridge connection of 4 diodes. For reference, Figure 2.7 and Figure 2.8 demonstrate a typical bridge rectifier and its input and output voltages, with output having same DC current polarity regardless of AC cycle. Two diodes at time are responsible for each half-cycle current conduction.

Complexity arises from the parts of AC cycle with low instantaneous voltage. These cycle portions present a low DC output power also. In order to guarantee steady power availability on the DC side the solution is to add an element that provides energy to the load between these peaks cycle times. A bulk storage capacitor C_B in parallel with the load is a common choice for this purpose (see Figure 2.9).

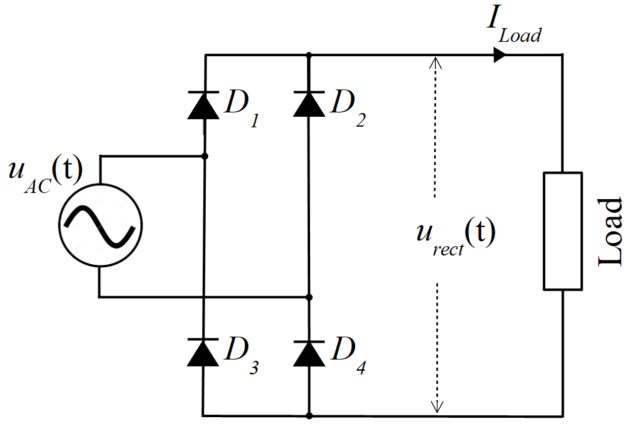

Figure 2.7 Ideal full bridge rectifier circuit.

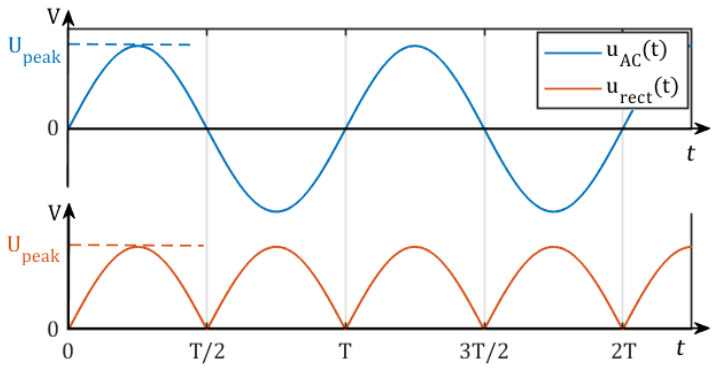

Figure 2.8 Input and output of full wave rectifier.

Figure 2.10 presents the general trends and capacitor voltage charging and discharging equations. When the rectifier output starts to decrease after attaining the peak voltage value (at $T/4$ or $3T/4$, T is the time period of the input wave, for 50 Hz AC supply, T = 20 ms); the capacitor's voltage $u_{CB}(t)$ exceeds the voltage supply momentary voltage value $u_{AC}(t)$, all the diodes conduction is cut off. It is under these conditions that the capacitor assumes its role of providing current to the load during the diode's non-conductive phase. The moment the capacitor begins delivering current to the load marks the start of a decline in the voltage $u_{CB}(t)$. Once the AC supply voltage momentary absolute value surpasses the capacitor's voltage, diodes D_2 and D_3 switch to a conductive state for the negative half-cycle, initiating a fresh charging cycle for the capacitor. The capacitor voltage will rise and follow the AC voltage, eventually again reach the peak output level U_{peak} of the supply voltage. The dynamics of this process are graphically depicted in Figure 2.11.

The conduction of diodes is between phase instances φ_{init} and φ_{term}, as initiation and termination instances of capacitor charging. Capacitor charging occurs during $\Delta\varphi_{charge}$

$$\Delta\varphi_{charge} = \varphi_{term} - \varphi_{init} \tag{2.28}$$

The voltage variation capacitor is ΔU_{ripple}, specified as

$$\Delta U_{ripple} = U_{CBmax} - U_{CBmin} \tag{2.29}$$

Capacitor voltage peaks after every $T/2$ for the full-bridge rectifier circuit. After conduction termination instant φ_{term}, voltage decay is determined by the time constant $\tau_{LOADRC} = R_{DCL} \cdot C_B$, where R_{DCL} is the resistance of the load connected to the capacitor (DC output). Equation (2.30 presents the equation to define the charging pattern of the C_B. For the condition when $\tau_{LOADRC} >> \{ T/2 - \Delta\varphi_{charge}($ or $\Delta t_{charge})\}$, the discharging of the capacitor could be considered as the straight line as the charge on capacitor reaches to U_{CBmin} from U_{CBmax}, shown in Figure 2.10 (blue line).

$$u_{CB}(t) = U_{CBinit} + (U_{CBmax} - U_{CBinit}) \left(1 - e^{-\frac{t - t_{term}}{\tau_{LOADRC}}}\right) \tag{2.30}$$

where t is time value greater than conduction termination t_{term} instant and less than next cycle rectifier conduction initiation instant t_{init} (see Figure 2.11).

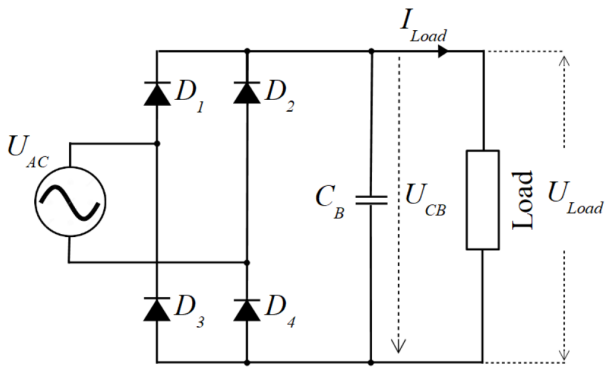

Figure 2.9 Full wave rectifier with capacitor.

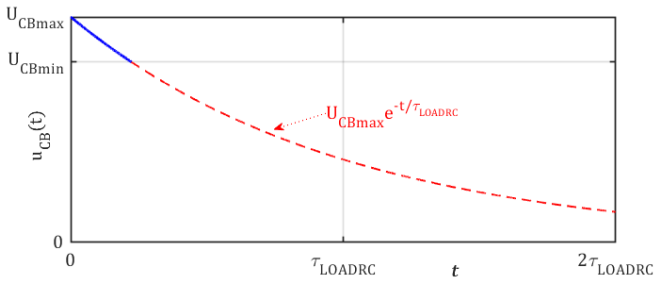

Figure 2.10 Capacitor discharging trend.

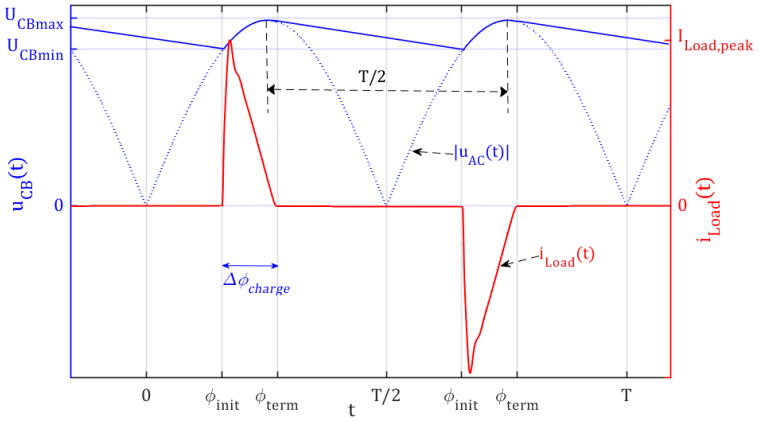

Figure 2.11 Characteristic waveforms for capacitor-equipped full-bridge rectifier.

2.5.2 Practical loads' behaviour

Energy-efficient LED lamps have become increasingly prevalent in both residential and commercial settings, and they are considered to be contributing to a significant share of today's electrical load. Traditional filament-based bulbs are highly inefficient, converting most of their energy input into heat – over 90% – rather than visible light [71]. On the other hand, Compact Fluorescent Lamps (CFLs) are designed to be much more energy-efficient, typically offering up to 15 times the lifespan and utilising about 70% less energy than their incandescent counterparts [72]. Efficiency and reliability are even

further increased in the LED emitter based lamps. However, energy-efficient lamps require specific lamp drivers to function and provide stabilized supply to light emitter component. Such drivers, by nature, possess nonlinear characteristics that leads to the loading of current harmonics in the electrical system. However, electronic drivers could also offer advantages, such as improved power input factors, reduced total harmonic distortion (THD) in the load current, and ability to eliminate the flickering effect and more. Due to price of the more advanced driver circuits, the most commonly deployed lamp type is equipped with rather primitive driver circuitry.

Recognising the issue of harmonic distortions in the grid, product standards such as the IEC 61000-3-2 [28] have been established to limit the harmonic currents emitted by electrical equipment, including low-power units in the domestic use. For the LED lamps, requirements can be listed as:

- The harmonic currents shall observe the power limits.
- The 3rd and 5th harmonic currents should not exceed 86% and 61% of the fundamental frequency current value, respectively.
- The current THD must not be greater than 70%, and the 3rd, 5th, and 7th harmonic currents must be equal or below 35%, 25% and 20%, respectively [73].

To formulate the base context for the analysis, practical LED lamps as loads were investigated through measurements of load current waveforms. Using assumptions of the circuit buildup, the LED lamps were sorted based on the apparent load current waveform characteristics. AC- and DC- side circuits inside the LED lamp (see Figure 2.12) could be identified and sorted into 4 categories.

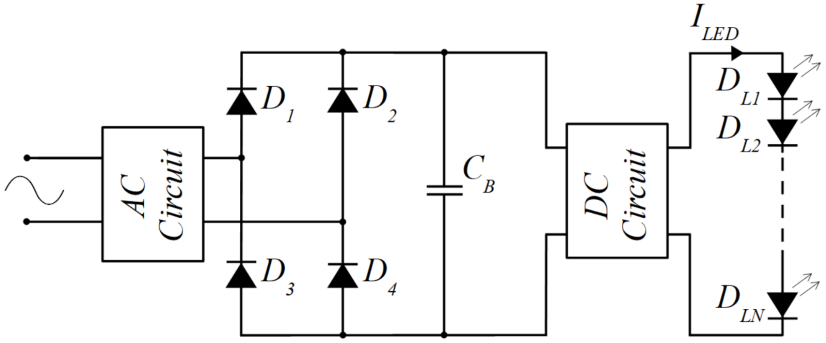

Figure 2.12 Typical circuit of LED lamp.

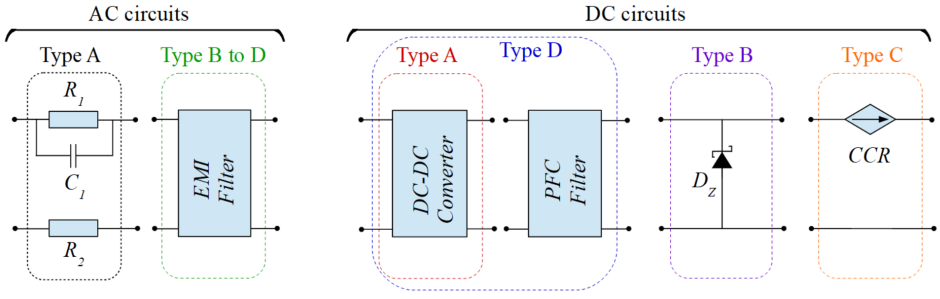

Figure 2.13 Types of commercially available LED lamps.

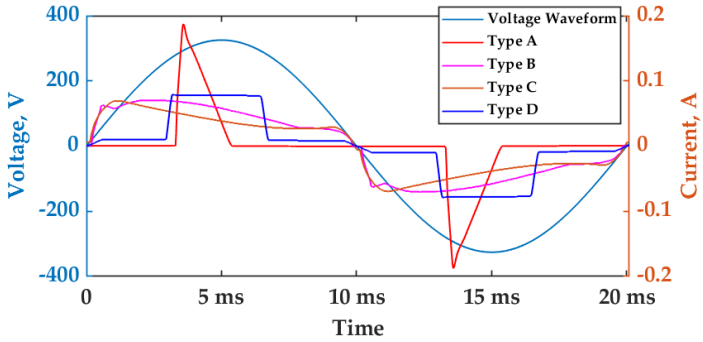

Figure 2.14 Load current waveform of different types of LED lamps.

The electrical characteristics of more than 150 commercially available LED lamps were empirically analysed in this study, focusing particularly on the current waveforms produced under a purely sinusoidal voltage application. The electrical circuit design distinctions among the various LED lamp types are visually represented in Figure 2.13.

The majority of tested LEDs, approximately 88%, exhibited a 'Type A' current waveform, graphically depicted in Figure 2.14. This waveform is reminiscent of a pulsed configuration, bearing resemblance to the current signature of CFLs [74]. A 'Type A' LED driver circuit typically comprises a full-bridge rectifying circuit, a DC-to-DC conversion module to stabilise the LED's input voltage, and EMI filtering components.

In contrast, 'Type B' LEDs initiate conduction in close proximity to the zero-cross points of the applied voltage, maintaining this conduction until the waveform's peak is attained. This results in a 50% extended conduction duration relative to 'Type A' LEDs. Within this configuration, a Zener diode is utilised to cap the forward voltage to the LED. It's notable that perturbations in input voltage could influence the DC potential experienced by the LEDs in such systems [74].

Regarding 'Type C' LEDs, the current manifests in a square waveform profile, attributed to the inclusion of a constant current regulator (CCR) within the circuit. The CCR is designed to uphold a steady current supply across a broad voltage spectrum, bolstering LED protection[75].

Lastly, 'Type D' LED lamps draw a current that approaches a sinusoidal shape, an outcome facilitated by the integration of an active power factor correction (PFC) converter [51]. To further suppress variations in current, resistive elements might be interspersed within the LED array [76].

2.6 Non-linear load current measurements

In the harmonic load currents' specifications in the product standards, such as IEC 61000-3-2 [28] the conditions on the load current have been specified in conditions with low-distorted supply voltage. The voltage waveform serving as a reference supply must be as ideal as possible; however, deviations are allowed compared to a near-perfect sinusoidal signal. In the following test scenarios, the main idea was not to test the loads (LED lamps') conformity to standard. Instead, the measurement was to provide voltage waveforms likely to occur in the LV AC power supply system. The conditions of the voltage harmonics, common to the LV public supply system, are given for example, in IEC 61000-2-2 [25].

2.6.1 Supply voltage waveform control

In order to simulate the different distorted supply voltage scenarios a test platform was set up to generate the supply voltage waveforms based on the specification table. The target of the voltage control was to enable precise adjustment of the voltage harmonics including level value and injection phase angle value.

For proper measurement of the current harmonic sensitivity, one has to consider that variations could be rather low in proportion; for a systematic sensitivity pattern determination, there have to be very stable voltage supply conditions. Thus voltage regulation has to ensure maintaining a constant output voltage level in spite of variations in the laboratory supply network input voltage or changes in load conditions. Software-generated waveform is one example of this, where the momentary values are calculated on a discrete basis and then forwards to digital-to-analogue (DA) converter.

A harmonic sensitivity identification system to support the persistent voltage supply conditions has been provided in Figure 2.16.

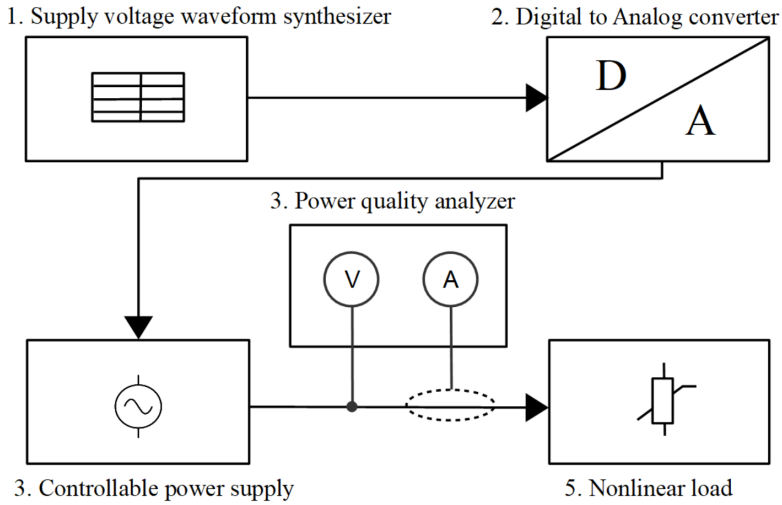

Figure 2.15 Measurement setup (previously published in article III).

For the comprehensive characterisation of the frequency approach, target of the measurement and waveform generation systems is to provide a platform to establish the harmonic sensitivity characterization. Harmonic current sensitivity will be observed using phasor approach – the voltage waveform will be established using magnitude and phase angle settings.

Scanning procedure is introduced to supply voltage that includes a specific voltage harmonic component with constant magnitude, while phase angle is variation range is complete 360 degrees in smaller steps. Harmonic current I_x was measured for each of the generated supply voltage conditions. Figure 2.16 presents the step-by-step flow for the generation of customised voltage waveform and result measurement of the test loads.

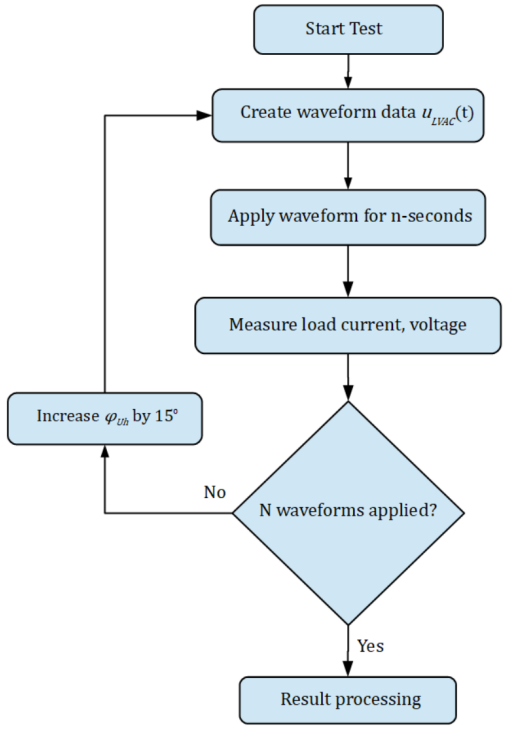

Figure 2.16 Generation of supply-voltage combinations with varying voltage phasor angle.

For particular sensitivity analysis patterns, comprehensive scan of load characteristics investigation scenarios as defined in Table 2.3 were used. The phase parameter was the main scanned quantity, where total of 24 settings each with 15° steps were used. Similarly, voltage steps were applied to harmonics and these remained in the range of 1 … 5 V corresponding to the expected levels in the grid (usually 1 V, 3 V, and 5 V levels were applied).

Table 2.3 presents an example for the 5th order harmonic along with fundamental voltage component kept at U_1 = 230 V. Initially, the load's harmonic currents were measured under a test supply voltage condition wherein only the fundamental voltage component U_1 was present. Subsequently, each input voltage scenario was sustained for a 10-second duration. A sequence of 24 distinct combinations was tested, each introducing a harmonic voltage into the supply, characterised by a consistent 5th harmonic voltage amplitude U_5 yet varying in phase angle by increments. Later on, this process was systematically replicated for various magnitudes of the influencer component U_5.

Table 2.3 Example of supply voltage combination with single harmonic added to supply voltage

Combinations	***U₁***	***U₃***		***U₅***		***U₇***	
	U_1, V	U_3, V	φ_{U3} °	U_5, V	φ_{U5} °	U_7, V	φ_{U7} °
1	230	0	0	0	0	0	0
24	230	0	0	3	0-15 …345	0	0

2.6.3 Measurement setup

A test bench has been created for load devices' measurements, with the capacity to support up to 16 loads simultaneously. The load outputs of a setup are connected to a controllable central distribution bus-bar through relays. A general purpose data acquisition system (DAQ) provides an analogue reference signal to the controllable power supply. To generate the desired voltage waveform, a controllable/programmable power supply Omicron-C356 is utilised. Power supply is controlled through the reference signal U_{refg} provided by the DAQ.

$$U_{refg} = \frac{U_{out}}{U_{range}} \times U_{coef} \tag{2.31}$$

Here U_{coef} is 7.072 and U_{range} is 300 V. A MATLAB script is used to generate the required reference voltage as well as digital signals for the relay management inside control box via data acquisition module. The magnitude and phase angles for each odd harmonic are utilised to synthesise the programmable power supply's reference signal. Equation below is used to calculate the $u_{test}(t)$ from the given amplitude and phase angle of the fundamental and odd harmonics up to the 19th harmonic.

$$u_{test}(t) = \sum_{y=1}^{n} \sqrt{2}\ U_h \sin(2\pi f_h t + \ \alpha_h) \tag{2.32}$$

U_h is the rms value of a particular harmonic. The α_h is the phase of particular harmonic. The harmonic frequency is shown by f_y and sampling interval by t_s. It is calculated from the sampling frequency f_s

$$t_s = \frac{1}{f_s} \tag{2.33}$$

The number of samples (N) for the specific duration (T_m) of the voltage output from the controllable power supply can be used to calculate sampling frequency, shown by following equation:

$$f_s = \frac{N}{T_m} \tag{2.34}$$

A pure sinusoidal voltage could be generated by the setup with a sampling frequency of 100 kHz. The A-Eberle PQ-BOX 200 has been used to measure the harmonic magnitude and phase angles, operating at a sampling frequency of 41 kHz for power quality measurements. The PQ-BOX 200 is capable of measuring power quality data with a 1-second resolution. The 1-second data is based on the average values calculated at 200-ms according to IEC 61000-4-30 standard. Figure 2.15 presents the block diagram of our measurement setup.

To ensure thermal stability in terms of harmonic profile of loads, measurements should be conducted after a 60-minute warm-up period. Continuous power was provided to the loads during testing breaks to maintain a consistent working temperature [77].

During the characteristic scan of the loads, small yet stable and repeatable variations in the phase and magnitude values of the harmonic current component were recorded. This was verified by performing a discrete Fourier transform (DFT) of the current waveform recorder on the measurement instrument.

2.7 Measurement outcome and initial observations

Selection of LEDs were tested to establish the harmonic sensitivity fine-scale dataset. The focus was on the circuit type A lamps (see section 2.5.2). In essence, the current waveforms of all the tested LEDs indicated similar type variation response characteristics to voltage harmonics added to the input voltage.

Time-domain observation of the scan outcome are presented Figure 2.17 as it compares the current waveform of an LED lamp when powered by a pure sinewave supply against when supply voltage has additional distinct harmonic voltage component at a specific magnitude and phased relative to the fundamental harmonic. It illustrates a scan result of the current waveforms outcome, when 5th voltage harmonic was introduced in supply with a fixed magnitude level, and the harmonic injection phase angle changed in 15-degree steps (denoted in Table 2.3). The synchronisation of measured current waveforms was with respect to the zero-phase instant of the voltage waveform's fundamental harmonic.

A distinguishing parameter of the load current waveform is the instant of rectifier conduction initiation time instant t_{init}. At this time instant or very near to it, load current provides highest slope and achieves its peaks value soon after this. Such rectifier's current instantaneous peaks provide a characteristic quantity for the rectifier's current magnitude.

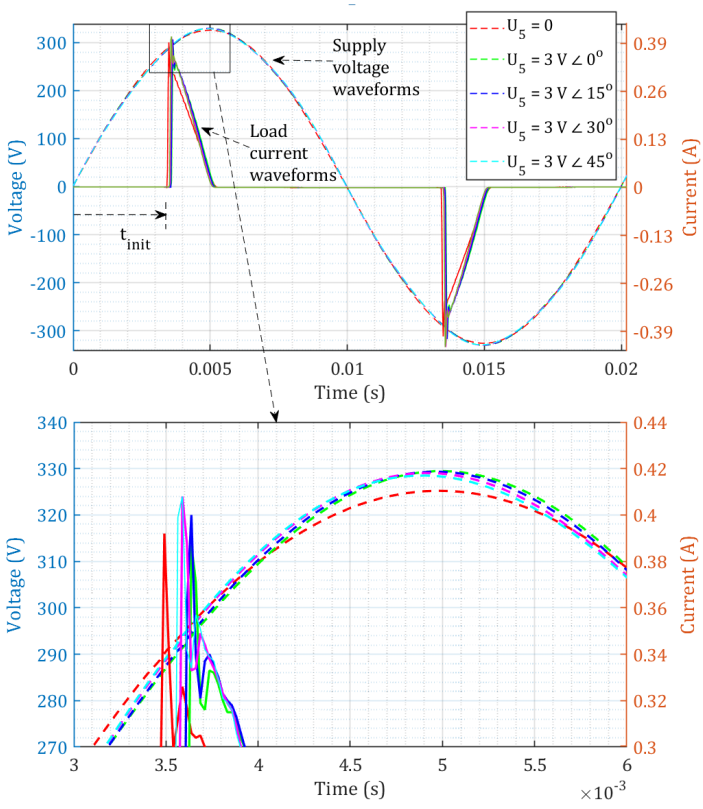

Figure 2.17 Current waveform initiation time and peak values affected by the 5th order voltage harmonic phase angle in supply. Supply waveforms (dashed lines), and I_L waveforms (continuous lines) (previously published in article III).

Harmonic current components considered, the outcome to each variation of the voltage harmonic component was directly and systematically observable in the harmonic current phasors' variations. Findings present a well-reported [54], [58], [78]–[80], though less-approached outcome.

- Voltage harmonics magnitude setting variation was providing variation to the load current harmonics both magnitude and phase.
    - Systematic cross-order dependence of the current and voltage components was observed.
- Voltage harmonics phase setting variation was providing variation to the load current harmonics both magnitude and phase.
    - Systematic cross-order dependence of the current and voltage components was observed.

Criticism arises towards the previously reported frequency domain models, as the cross-order coupling, and magnitude and phase manipulation cross-dependency is clearly evident. This is explained in the time-domain waveform measurement outcome displayed in Figure 2.17. This figure shows the former time-domain variation, displaying the impact of voltage variation on level and phase angle of the harmonic current phasor as the phase angle of the fifth voltage harmonic alters. This variation in time domain is clear to provide change in phase angle and level of multiple current harmonics. Thus the fifth voltage harmonic affects the harmonic currents across the spectrum. The conduction initiation moment given as the fundamental harmonic phase angle value (φ_{Init}), could be seen to determine the deviation of the load harmonic current pattern. Although time-domain initiation differences correlated with phase angle shifts are recognised in the literature [81][82]; however they have not been considered as one of the foundational assumptions of the analysis.

These observations of time domain outcome lead to establishing a hypothesis if the initiation phase angle φ_{Init} would be a determining factor for the load current harmonic phase angle variations throughout. The hypothesis proposed asserts correlation that the current harmonic phase angles will be directly affected by the rectifier's physical operation in the time-domain.

2.7.1 Phasor variation analysis

The main construct in the analysis of the harmonic sensitivity is to determine in which extent the voltage harmonic phasor provides a change the current harmonic phasor. Based on the measurement outcome, the effect of the voltage harmonic phasor on harmonic current indicates periodic relation. The graphical representation in Figure 2.18 illustrates a typical response when a 5th harmonic voltage component $\boldsymbol{U_5}$ is imposed onto a sinusoidal supply voltage, with its phase angle (φ_{U5}) completing a full rotation 360 degrees, while maintaining a constant magnitude ($U_5 = const$).

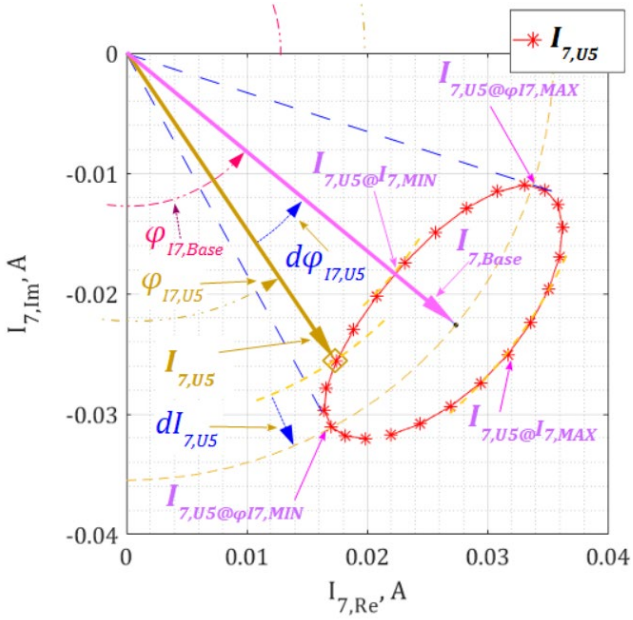

*Figure 2.18 Vector component plot for the harmonic load current component analysis. **I_7** vector endpoints' ellipse points plot, for U_5 = 3 V, φ_{U5} = 0, 15, 30 … 345°.*

The endpoints of ***I_7*** vectors make up the response with ellipse-like shape, but also $\varphi_{dI7,U5}$ is going through a rotation of exactly 360°. All other current harmonics show similar spread on complex plane, regardless of their frequency value.

Following the example of ***I_7*** in plot Figure 2.18, the harmonic current vector difference to base point ***$I_{x,Base}$*** is observed as

$$\begin{cases} dI_{x,Uy} = I_{x,Uy} - I_{x,Base} \\ d\varphi_{Ix,Uy} = \varphi_{Ix,Uy} - \varphi_{Ix,\mathrm{Base}} \end{cases} \tag{2.35}$$

where $dI_{x,Uy}$ is the measured harmonic current ***I_x*** magnitude difference due to included ***U_y***, compared to ***I_x*** magnitude $I_{x,Base}$ emerging in pure sinewave voltage supply conditions; $\varphi_{Ix,Uy}$ is the measured harmonic current ***I_x*** phase angle due to included ***U_y***, compared to ***I_x*** phase angle $\varphi_{Ix,Base}$ emerging in pure sinewave voltage supply conditions.

Although a linear impedance model [section 2.4] might explain the phase rotation of the current difference component for harmonics of the same order i.e., voltage and current harmonics having identical frequencies. However, this justification falls short as the phenomenon is exhibited by all current harmonics. For instance, introducing ***U_3*** rotated through φ_{U3} = {0 … 360°} again provides $\varphi_{dI7,U3}$ rotation through 360°, and cannot be considered an impedance-based relation. Therefore, there will be need to propose more sophisticated sensitivity coefficient for model, for calculating the harmonic current values.

The pattern of response plot appears to be symmetric towards the harmonic current base response to a pure sinusoidal voltage supply, denoted as ***$I_{x,Base}$***. The reaction vector in terms of both phase and magnitude is proportional to the magnitude of the influencer voltage harmonic, symbolised here as U_y. It raises the model description to the response as

$$\begin{cases} I_x = I_{x,\text{base}} + \Delta I_{x,y} \\ \varphi_{Ix} = \varphi_{Ix,\text{base}} + \Delta\varphi_{Ix,y} \end{cases} \quad (2.36)$$

where $\Delta I_{x,y}$ is the harmonic current $\boldsymbol{I_x}$ magnitude variation estimation due to included $\boldsymbol{U_y}$, compared to $\boldsymbol{I_x}$ magnitude $I_{x,Base}$ emerging in pure sinewave voltage supply conditions; $\Delta\varphi_{Ix,y}$ is the is the harmonic current $\boldsymbol{I_x}$ phase angle magnitude estimation due to included $\boldsymbol{U_y}$, compared to $\boldsymbol{I_x}$ phase angle $\varphi_{Ix,Base}$ emerging in pure sinewave voltage supply conditions.

This presentation aligns with basic Norton or frequency coupled matrix concepts [section 2.4.1]. However, on the basis of the physical operational characteristics of rectifiers, that it is justifiable to treat the magnitude and phase variation parameters as independent entities, rather than constraining them to a complex impedance relationship. Measurement results in Table 2.5 present the summary of the results, where

$$\begin{cases} d\varphi_{init,Uy} = \varphi_{init,Uy} - \varphi_{init,\text{base}} \\ d\varphi_{Ix,Uy} = \varphi_{Ix,Uy} - \varphi_{Ix,\text{base}} \end{cases} \quad (2.37)$$

where $\varphi_{init,Uy}$ is the initiation moment phase with $\boldsymbol{U_y}$ injected to the supply voltage; $\phi_{Ix,Uy}$ is the phase angle of the response current vector with $\boldsymbol{U_y}$ injected to the supply voltage, and "$_{Base}$" notates the values upon sinusoidal supply voltage conditions (i.e., only fundamental voltage component present).

2.7.2 Phase angle variation analysis

The time instance when the rectifier starts to conduct for charging capacitor is referred as initiation angle of the current conduction (φ_{init}); initiation angle is calculated using equation (2.38)

$$\varphi_{init} = f \cdot 360^o \cdot \mathrm{d}t_{init} \quad (2.38)$$

where $\mathrm{d}t_{init}$ – time-difference of the supply voltage main harmonic zero phase instant and current conduction initiation moment.

Shown in Table 2.4, initiation phase is referred to varying $\boldsymbol{U_5}$ added to the voltage supply. This table refers to the variation quantity of current harmonic phase only.

*Table 2.4 Initiation moment and phase angles of harmonics in load current, for different magnitude levels of harmonic voltage**

U_5, V	$\boldsymbol{\varphi_{U5}}$, °	$\boldsymbol{\varphi_{init,0}}$, ° **(50 Hz phase value)**	$\boldsymbol{\varphi_{I1}}$, °	$\boldsymbol{\varphi_{I3}}$, °	$\boldsymbol{\varphi_{I5}}$, °	$\boldsymbol{\varphi_{I7}}$, °
0	–	62.1	18.0	231.6	87.2	304.2
		$\Delta\varphi_{init}$, °	**$\Delta\varphi_{I1}$, °**	**$\Delta\varphi_{I3}$, °**	**$\Delta\varphi_{I5}$, °**	**$\Delta\varphi_{I7}$, °**
1	180	–0.9	0.6	2.0	3.6	5.5
	345	1.1	–0.8	–2.5	–4.2	–6.2
3	180	–2.9	2.0	6.5	11.5	17.7
	345	2.9	–2.4	–6.9	–11.8	–17.4
5	180	–4.7	3.6	11.3	20.4	32.0
	345	4.6	–3.6	–10.7	–18.3	–26.8

* Phase angle accuracy/resolution has been provided for more detailed comparison

Table 2.5 Difference in phase angles of harmonics in load current, for different magnitude levels of harmonic voltage, determined by (2.34)

U_5, V	φ_{U5}, °	φ_{init}, °	$\Delta\varphi_{ini}$, °	$\Delta\varphi'_{I1,U5}$, °	$\Delta\varphi'_{I3,U5}$, °	$\Delta\varphi'_{I5,U5}$, °	$\Delta\varphi'_{I7,U5}$, °
0	-	62.1					
1	180	61.2	0.9	-0.7	-0.7	-0.7	-0.8
	345	63.2	-1.1	0.8	0.8	0.8	0.9
3	180	59.2	2.9	-2.1	-2.2	-2.3	-2.5
	345	65.0	-2.9	2.3	2.3	2.4	2.5
5	180	57.4	4.7	-3.6	-3.8	-4.1	-4.6
	345	66.7	-4.6	3.5	3.6	3.7	3.8

* Phase angle accuracy/resolution has been provided for more detailed comparison

Normalising the phase angles towards the initiation influencing component $\boldsymbol{U_5}$, and observing the relation towards the current harmonic $\boldsymbol{I_x}$ of order x, it is revealed to have a ratio of closely common to

$$\Delta\varphi'_{I_{x,Uy}} = \Delta\varphi_{init,Uy} \cdot x \cdot k_{WF} \tag{2.39}$$

where k_{WF} – waveform coefficient, with almost same value for the discussed current harmonic orders (x = 3, 5, 7). As a result from a frequency domain transfer of t_{init} (φ_{init}) the initiation phase angle φ_{init} is in proportional ratio to the φ_{I1}. The aforementioned formula demonstrates that variations in the harmonic current phase angles due to the influence of $\boldsymbol{U_5}$, is directly relational and proportional to the initiation angle φ_{init}.

It is important to indicate that all harmonic current phase angle values exhibit vary, in response to changes in the phase angle of the voltage harmonic. This observation is a key aspect in explaining the harmonic cross-coupling phenomenon, considering that wherein phase angle shifts of a specific voltage harmonic $\boldsymbol{U_y}$ of a specific order will instigate a correlated phase angle response in a current harmonic of a different order.

Table 2.5 presents the maximum and minimum value of initiation moment of the current waveforms, corresponding to φ_{U5} value extreme points, calculated as

$$\Delta\varphi'_{I_{x,y}} = \frac{\Delta\varphi_{Ix,y}}{x} \tag{2.40}$$

where x is the current harmonic order, further confirming the equation (2.34). Moreover, any variation in the phase angle of the fundamental current harmonic component characterises the phase shifts of all other harmonic currents in the load, given through fundamental component phase shift multiplied by the observed harmonic current order number. It has to be observed that the magnitude of the incident voltage harmonic (U_5) provides a proportional impact on the initiation moment and the $\boldsymbol{I_x}$ phase angle φ_{Ix} variation range. The phase angles are seen to pose a high and low value responsive to φ_{U5} rotation of almost 180°.

2.7.3 Magnitude variation analysis

Similarly, the maximum value of the load currents ($I_{x,y,max}$) is also associated with the phase angle of influencing supply voltage harmonic (φ_{Uy}) on almost 180° rotation. Table 2.4 points out the behaviour of time-domain waveform $I_{L,peak}$, corresponding to φ_{U5}, providing maximum and minimum $\boldsymbol{I_x}$ magnitude I_x values with value range shown. It has to be noted, that the highest and lowest current magnitude occurrences are also found at nearly orthogonal (90°) values towards the φ_{U5} value for peak and minimum φ_{Ix} variation values.

Table 2.6 presents, as expected, the magnitudes of the harmonic currents demonstrate a direct proportionality to the amplitude of the superimposed voltage harmonic (in this case it is $\boldsymbol{U_5}$). The proportion origins are evident from time-domain waveform peak current levels, deployed to the current harmonics observed, presenting a physical background for the cross-order harmonic coupling appearance for the magnitude portion.

Table 2.6 Maximum and minimum of peak load current ($I_{L\ Peak}$) according to φ_{u5}

U_5, V	φ_{U5}, °	$I_{L\ Peak}$, A	$\Delta I_{L\ Peak}$, A	$\Delta I_{1,U5}$, mA	$\Delta I_{3,U5}$, mA	$\Delta I_{5,U5}$, mA	$\Delta I_{7,U5}$, mA
0	-	0.40					
1	270	0.38	0.02	0.05	0.30	0.67	1.13
	90	0.42	-0.02	-0.06	-0.28	-0.73	-1.19
3	270	0.34	0.06	0.21	0.83	1.74	3.0
	90	0.45	-0.06	-0.06	-0.76	-2.05	-3.5
5	255	0.30	0.10	0.29	1.50	3.8	6.3
	105	0.49	-0.10	-0.25	-1.21	-3.1	-5.1

3 Model development

3.1 Empirical model

Consequent to the analyses of variations in current harmonic magnitude and phase angle discussed in Chapter 2, it is evident that physical characterisation to the time-domain origins of the $\boldsymbol{I_x}$ components rationale to model the magnitude portions I_x and phase angle φ_{Ix} as independent entities. This is due to the non-impedance origins of the $\boldsymbol{I_x}$ variations in time-domain current presentation, as outlined in last chapter.

The following outlines a load current model that corresponds to the harmonic current variations previously detailed. For a particular harmonic order *x,* the load current harmonic vector $\boldsymbol{I_x}$ is composed of the components illustrated in Figure 3.1:

1. A constant current source part donated as $\boldsymbol{I_{x,Base}}$, having two components, magnitude component $I_{x,Base}$, and phase angle component $\varphi_{Ix,Base}$. $\boldsymbol{I_{x,Base}}$ is measured value from device test under pure sinusoidal supply voltage.
2. A linear part of harmonic current, symbolised as $\boldsymbol{\Delta I_{x,LIN}}$, consisting of current magnitude component $\Delta I_{x,LIN}$, and the current phase angle component $\Delta\varphi_{Ix,LIN}$. This segment is the accumulated result of all the linear responses attributed due to each voltage harmonic $\boldsymbol{U_y}$ in the supply, for every $\boldsymbol{I_x}$.
3. A nonlinear part presented as $\boldsymbol{\Delta I_{x,NL}}$, respective for magnitude nonlinear component $\Delta I_{x,\mathrm{NL}}$, and phase angle nonlinear component $\Delta\varphi_{Ix,\mathrm{NL}}$. The presence of this nonlinear part is inferred from non-symmetry depicted on an elliptical trajectory (see Figure 2.15). These parts are calculated as a cumulation of all nonlinear components due to each voltage harmonic $\boldsymbol{U_y}$ in the supply waveform, for every $\boldsymbol{I_x}$.

The interaction between the current harmonics phasor identified for separate evaluation of influence from voltage harmonic magnitude and voltage, has not been described previously for the commonly accepted frequency domain models (see section 2.4.1). Thus a new model concept is introduced here, where harmonic current will be presented as Waveform Variation Defined model presented as

$$\begin{cases} I_{x,WVDM} = I_{x,Base} + \Delta I_{x,LIN} + \Delta I_{x,NL} \\ \varphi_{Ix,WVDM} = \varphi_{Ix,Base} + \Delta\varphi_{Ix,LIN} + \Delta\varphi_{Ix,NL} \end{cases} \tag{3.1}$$

3.1.1 Linear part expression

The main proportion of the current harmonic level variation will be provided by the linear part, calculated as

$$\Delta I_{x,LIN} = \boldsymbol{U_y} \cdot \boldsymbol{G_x} \cdot \cos(\boldsymbol{\alpha_x} - \boldsymbol{\varphi_{Uy}}), \tag{3.2}$$

where U_y is the $\boldsymbol{U_y}$ magnitude matrix in form

$$\boldsymbol{U_y} = [U_3 \;\; U_5 \;\; \ldots \;\; U_N]$$

$\boldsymbol{G_x}$ is the current harmonic I_x magnitude sensitivity coefficient matrix in form.

$$\boldsymbol{G_x} = \begin{bmatrix} G_{x3} \\ G_{x5} \\ \ldots \\ G_{xN} \end{bmatrix}$$

where G_{x3} presents I_x sensitivity to the 3rd supply voltage harmonic magnitude U_3 respectively, (units A/V = S), and

$$\cos(\boldsymbol{\alpha_x} - \boldsymbol{\varphi_{Uy}}) = \begin{bmatrix} \cos(\alpha_{x3} - \varphi_{U3}) \\ \cos(\alpha_{x5} - \varphi_{U5}) \\ \cdots \\ \cos(\alpha_{xN} - \varphi_{UN}) \end{bmatrix},$$

The specific phase coefficient designated as α_{x3} is utilised for computing the phase angle of the harmonic current I_x related to phase angle φ_{U3} of the voltage harmonic component $\boldsymbol{U_3}$. Similarly, linear part of the current harmonic phase angle variation is modelled as:

$$\Delta\varphi_{Ix,LIN} = \boldsymbol{U_y} \cdot \boldsymbol{k_x} \cdot \sin(\boldsymbol{\alpha_x} - \boldsymbol{\varphi_{Uy}}), \tag{3.3}$$

$\boldsymbol{k_x}$ is the current harmonic $\boldsymbol{I_{x,LIN}}$ phase angle $\Delta\varphi_{Ix}$ sensitivity coefficient matrix in form

$$\boldsymbol{k_x} = \begin{bmatrix} k_{x3} \\ k_{x5} \\ \cdots \\ k_{xN} \end{bmatrix}$$

where k_{x3} presents $\Delta\varphi_{Ix}$ sensitivity to the 3rd supply voltage harmonic magnitude U_3 respectively, (units °/V), and

$$\sin(\boldsymbol{\alpha_x} - \boldsymbol{\varphi_{Uy}}) = \begin{bmatrix} \sin(\alpha_{x3} - \varphi_{U3}) \\ \sin(\alpha_{x5} - \varphi_{U5}) \\ \cdots \\ \sin(\alpha_{xN} - \varphi_{UN}) \end{bmatrix}.$$

Here the coefficients G_{xy}, k_{xy} and α_{xy} are determined through load measurements, presented in the next section.

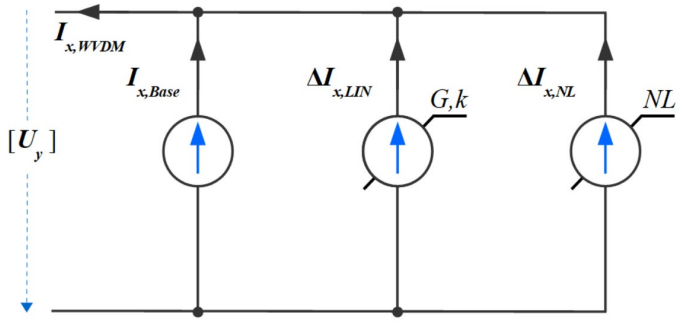

Figure 3.1 description for harmonic current component $\boldsymbol{I_x}$ of order x modelling (previously published in article III).

3.1.2 Nonlinear expressions

The nonlinear part of current will be calculated for supply voltage harmonic components as

$$\Delta I_{x,NL} = \boldsymbol{U_y} \cdot \left[\boldsymbol{A_{1m}} \sin\left(\boldsymbol{\varphi_{Uy}} + \boldsymbol{C_{1m}}\right) + \boldsymbol{A_{2m}} \sin\left(\boldsymbol{2\varphi_{Uy}} + \boldsymbol{C_{2m}}\right)\right] \quad (3.4)$$

where $\boldsymbol{A_{1m}}$, $\boldsymbol{A_{2m}}$, $\boldsymbol{C_{1m}}$, $\boldsymbol{C_{2m}}$ are first and second order polynomial expressions related to harmonic current order and harmonic voltage orders. Similarly nonlinear part for phase angle part will be calculated as

$$\Delta \varphi_{Ix,NL} = \boldsymbol{U_y} \cdot \left[\boldsymbol{A_{1p}} \sin\left(\boldsymbol{\varphi_{Uy}} + \boldsymbol{C_{1p}}\right) + \boldsymbol{A_{2p}} \sin\left(\boldsymbol{2\varphi_{Uy}} + \boldsymbol{C_{2p}}\right)\right] \quad (3.5)$$

where $\boldsymbol{A_{1p}}$, $\boldsymbol{A_{2p}}$, $\boldsymbol{C_{1p}}$, $\boldsymbol{C_{2p}}$ are second order polynomial expressions related to harmonic current order and harmonic voltage orders.

The polynomial expressions of the devices under test reveal a trend that can be observed through the measurement results. For instance, the Nonlinear part coefficient trend of third harmonic current I_3 can be seen in Figure 3.2 when the influencer harmonic order is $y = 5$. The coefficients are obtained for different levels of influencer, with the level variation for 5th voltage harmonic ranging from 1 V to 5 V. Each particular influencer level is rotated through 360°. Out of these expressions, A_{1m} and A_{1p} demonstrate a linear relationship to the value level of influencer harmonic magnitude. However, the other coefficients show their dependence on influencer levels using a polynomial of second order (as shown in Figure 3.2). The angle components are the remaining variables in equations 3.4 and 3.5 that play their role in adjusting the error value to reduce the overall root mean square error (RMSE) of the waveform variation defined model (WVDM) model. These also portray a similar second-order polynomial relation to harmonic voltage levels.

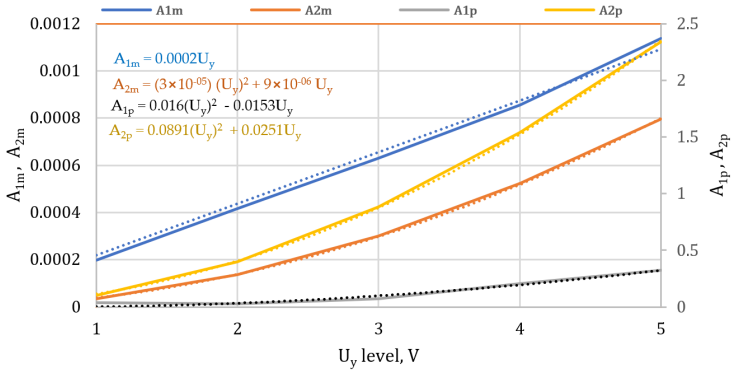

Figure 3.2 Trends of NL-polynomial coefficients vs influencer voltage level.

The general form of the equation(in figure 3.2) describing any nonlinear coefficient is

$$NL_{coef} = kM_{II}U_y^2 + kM_I U_y \quad (3.6)$$

Multipliers kM_I and kM_{II} are dependent on sensitivity coefficients, with the magnitude sensitivity coefficient G_{33} (current harmonic order $x = 3$ and voltage harmonic order $y = 3$) of the load device expressing the behaviours of these multiplying factors presented in Figure 3.3. The multiplying factors equations are linear and contain both linear and offset components. The relation presented in Figure 3.3 represents the accumulated response of the same current harmonic of several loads under identical input voltage conditions. All these trends are incorporated into the nonlinear portion of the empirical waveform variation-defined model (WVDM).

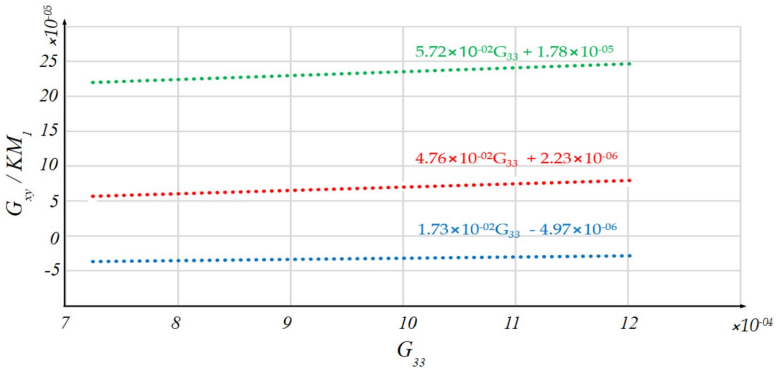

Figure 3.3 NL part coefficient description, G_{xy}/KM_I as a function of G_{33} .

In Figure 3.4, the roles of parts of the WVDM harmonic current model are provided. Corresponding to load current upon pure sinusoidal supply voltage, dot marking shows the response harmonic vector donated by $\boldsymbol{I_{7,Base}}$ (base response), the origin of this vector lies at reference coordinate. Measured harmonic current results are presented as red asterisks, when supply voltage including a single harmonic voltage $\boldsymbol{U_5}$ (with various phase angles $\Delta\varphi_{U5}$ but identical magnitude) is applied. A specific ellipse shape pattern emerges by adding the linear parts ΔI_7 and $\Delta\varphi_{I7}$, represented by triangles. There would be a noticeable difference between the linear-part-included harmonic current results and measurement results. So, adding the nonlinear part with linear modelling part improves compared to the actual measurement outcome. The final harmonic current response pattern, including the linear and nonlinear parts, is presented as circles' pattern.

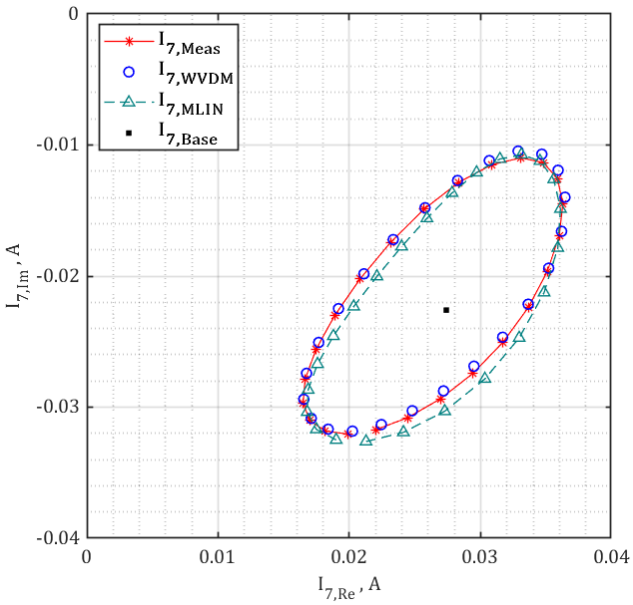

Figure 3.4 Presentation of roles of different harmonic current model components (previously published in article III).

3.1.3 Determination of coefficients

In order to implement WVDM the calculation of the coefficients, involved in harmonic load current calculation model, need to be outlined. In reference to Figure 2.18 of previous chapter, seventh current harmonic component $\boldsymbol{I_7}$ is used, which is the response by the effect of the $\boldsymbol{U_5}$ influencer voltage harmonic. Thus the influencing voltage harmonic order is $y = 5$ and the current harmonic order is $x = 7$. The quantities observed are referred to on the basis of Figure 2.18.

As ΔI_x is the difference between current vector magnitude to response magnitude of the sinusoidal supply voltage component response vector $I_{x,Base}$; in ideal situation, for ΔI_x to reach from $\Delta I_{x,MAX}$ to almost equal to zero, amount of voltage harmonic phase change φ_{Uy} almost 90 degrees. $\varphi_{Uy@\varphi Ix,MIN}$ is the influencing supply voltage phase angle when harmonic current phase deviation φ_{Ix} is at its highest value harmonic current magnitude I_x is of the same value as base magnitude. The base phase shift component α_{xy} can be specified by finding the influencing supply voltage phase angles φ_{Uy} corresponding to the minimum and maximum deviation of the magnitude I_x,

$$\alpha_{xy} = \frac{\varphi_{Uy@\varphi Ix,MAX} + \varphi_{Uy@\varphi Ix,MIN}}{2} \tag{3.7}$$

As the measurement steps are 15°, better accuracy is not available. Drawing upon the measurement data in Figure 2.15 and values present in Table 3.1, the α_{75} is determined to be close to value of 230°. By the orthogonal shift of $\varphi_{Uy} = 90°$ to find the maximum and minimum magnitude points, the base phase shift component $\boldsymbol{\alpha_{75}}$ could also be calculated as

$$\alpha_{xy} = \frac{\varphi_{Uy@Ix,MAX} + \varphi_{Uy@Ix,MIN}}{2} + 90° \tag{3.8}$$

Data in Table 3.1 provides that the $\boldsymbol{\alpha_{75}}$ will be around 240 degrees, calculated based on minimum and maximum magnitude. The proposed value of the coefficient of current magnitude sensitivity G_{xy} can be determined using maximum and minimum $\boldsymbol{I^*_x}$ magnitude difference value i.e., dI_x maximum and minimum values (referring to Figure 2.15)

$$G_{xy} = \frac{\left(\left| dI_{x,Uy@Ix,MAX} \right| - \left| dI_{x,Uy@Ix,MIN} \right| \right)}{2} \Big/ U_y \tag{3.9}$$

Analysing the results representations from Figure 2.18 and Figure 3.4, it becomes evident that base harmonic current vector $\boldsymbol{I_{x,Base}}$ does not lie in the centre of the ellipse (i.e. non-symmetric to centre), and the average of $|dI_{x,y@Ix,MAX}|$ and $|dI_{x,y@Ix,MIN}|$ is used to determine the G_{xy} using equation (3.9). The phase variation margins are well symmetrical to the ellipse centre, therefore measurement-derived $d\varphi_{Ix,Uy@\varphi Ix,MAX}$ or $d\varphi_{Ix,Uy@\varphi Ix,MIN}$ value could be used to calculate the initial proposed value of phase angle change coefficient 'k_{xy}', the as in (3.10)

$$k_{xy} = \frac{d\varphi_{Ix,Uy@\varphi Ix,MAX}}{U_y} \tag{3.10}$$

The influencer voltage harmonic U_y has a linear relation with magnitude of the harmonic current difference vectors. Consequently, for influencer voltage U_5 increase by 3 times (from 1 V to 3 V), results emerge for the $d\varphi_{Ix,Uy@\varphi Ix,MAX}$ and similarly $dI_{x,Uy@Ix,MAX}$ and $dI_{x,Uy@Ix,MIN}$ that provide the close values of linear scalar coefficients G_{xy} and k_{xy}.

Values of sensitivity-coefficients show remarkable consistency towards influencer magnitude, presented in Table 3.2. Using presented procedures in Equations ((3.7)(3.8)(3.10)) the linear coefficients for three loads discussed further are presented in Table 3.3.

Table 3.1 Results of α_{xy} values from measurements

		φ_{U5}	$\varphi_{U5\_MAX} - \varphi_{U5\_MIN}$	φ_{U5_CENTRE}	α_{75} for $dI_7 \approx 0$	α_{75}
dI_{7_MAX}	6.6 mA	225°	-150°	150°	240°	233°
dI_{7_MIN}	-4.9 mA	75°				
$d\varphi_{I7\_MAX}$	21.7°	315°	-165°	233°	233°	
$d\varphi_{I7\_MIN}$	-21.5°	150°				

Table 3.2 Comparison of voltage harmonic amplitude change to current harmonic phase deviation

Load	U_5	K_{35}, °/V	G_{35}, mA/V	K_{55}, °/V	G_{55}, mA/V	K_{75}, °/V	G_{75}, mA/V
1	1 V	3.17	0.22	5.3	0.63	7.5	1.08
	3 V	3.16	0.23	5.3	0.65	7.6	1.11
	5 V	3.16	0.27	5.3	0.70	7.5	1.14

Table 3.3 Model Parameters of Test Loads

	I_x order	3			5			7		
Load	U_y order	α_{3y}, °	G_{3y}, mA/V	k_{3y}, °/V	α_{5y}, °	G_{5y}, mA/V	k_{5y}, °/V	α_{7y}, °	G_{7y}, mA/V	k_{7y}, °/V
1	3	25	0.07	2.16	26	0.18	3.6	28	0.39	5.1
	5	218	0.24	3.2	220	0.67	5.3	223	1.13	7.5
	7	48	0.51	3.6	52	1.22	6.2	57	1.96	8.9
2	3	29	0.12	2.12	31	0.42	3.6	35	0.75	5.1
	5	223	0.51	2.95	226	1.27	5.0	233	1.91	7.3
	7	53	0.92	3.1	59	2.06	5.4	71	3.03	8.1
3	3	28	0.10	2.13	29	0.31	3.6	32	0.60	5.1
	5	221	0.39	2.99	224	1.01	5.1	229	1.58	7.3
	7	512	0.74	3.3	57	1.69	5.6	66	2.57	8.3

3.1.4 Single supply voltage harmonic component modelling

To conduct a more detailed assessment, linear component model results are stated for three similar type loads. The primary emphasis is on evaluating and comparing the measured vs model-calculated results. Coefficients from Table 3.3 have been implemented for the model calculation with linear part included (see equation (3.1)), as

$$\boldsymbol{I}_{x,MLIN} = \boldsymbol{I}_{x,Base} + \boldsymbol{\Delta I}_{x,LIN} \tag{3.11}$$

$$\varphi_{Ix,MLIN} = \varphi_{Ix,Base} + \boldsymbol{\Delta}\varphi_{Ix,LIN} \tag{3.12}$$

Deviation of calculation to measured magnitude value is presented as

$$\boldsymbol{\delta I}_{x,LIN} = \left|\boldsymbol{I}_{x,Meas}\right| - \left|\boldsymbol{I}_{x,Base} + \boldsymbol{\Delta I}_{x,LIN}\right|, \tag{3.13}$$

and similarly

$$\boldsymbol{\delta}\varphi_{Ix,LIN} = \left|\varphi_{Ix,Meas}\right| - \left|\varphi_{Ix,Base} + \boldsymbol{\Delta}\varphi_{Ix,LIN}\right|, \tag{3.14}$$

where $\delta I_{x,LIN}$ presents the magnitude difference of model (see (3.1)) result without nonlinear part included, compared to measurement outcome; $\delta\varphi_{Ix,LIN}$ presents the phase

difference of model (see (3.1)) result without nonlinear part included, compared to measurement outcome.

Complete model calculation outcome, including the nonlinear part is calculated according to (3.1). The deviation between the full model calculation and measurement outcome is determined as

$$\boldsymbol{\delta I_{x,WVDM}} = \left|\boldsymbol{I_{x,Meas}}\right| - \left|\boldsymbol{I_{x,WVDM}}\right|, \tag{3.15}$$

and similarly

$$\boldsymbol{\delta \varphi_{Ix,WVDM}} = \left|\boldsymbol{\varphi_{Ix,Meas}}\right| - \left|\boldsymbol{\varphi_{Ix,WVDM}}\right|. \tag{3.16}$$

For the whole $\boldsymbol{U_y}$ cycle (360°) rotation, the outcome deviation is evaluated using the root-mean-square error (RMSE), listed in Table 3.4 and Table 3.5 is calculated using the following equations,

$$RMSE_{Ix} = \sqrt{\frac{\sum_{i=0}^{N} \boldsymbol{\delta I_x}^2}{N}} \tag{3.17}$$

$$RMSE_{\varphi Ix} = \sqrt{\frac{\sum_{i=0}^{N} \boldsymbol{\delta \varphi_{Ix}}^2}{N}} \tag{3.18}$$

where *N* is total number of actual (measurement) points and predicted values (magnitude and phase).

Table 3.4 Comparison of measured and model calculated harmonic current values U_1 = 230 V; U_5 = 3 V $\boldsymbol{I_{7,Base,MEAS}}$ = (35.5 ∠ –40°) mA

I/P	***Measured values***				***Model with linear part result***				***Deviation for model with linear part***		***Full model result***		***Full model deviation from measurement***	
$\boldsymbol{\varphi_{U5}}$°	$\boldsymbol{I_{7,MEAS}}$, mA	$\boldsymbol{\varphi_{I7,MEAS}}$, °	$\boldsymbol{dI_{7,MEAS}}$, mA	$\boldsymbol{d\varphi_{I7,MEAS}}$, °	$\boldsymbol{\Delta I_{7,MLIN}}$, mA	$\boldsymbol{\Delta \varphi_{I7}}$, °	$\boldsymbol{I_{7,MLIN}}$, mA	$\boldsymbol{\varphi_{I7,MLIN}}$, °	$\boldsymbol{\delta I_{x,MLIN}}$, mA	$\boldsymbol{\delta \varphi_{Ix,MLIN}}$, °	$\boldsymbol{I_{7,WVDM}}$, mA	$\boldsymbol{\varphi_{I7,WVDM}}$, °	$\boldsymbol{\delta I_{x,WVDM}}$, mA	$\boldsymbol{\delta \varphi_{Ix,WVDM}}$, °
Max	40.4	-18	6.5	21.7	5.7	21.6	41.2	-18	1.8	1.7	40.3	-17	0.4	-0.2
Min	29.0	-61	-4.9	-21.5	-5.7	-21.6	29.8	-61	-1.0	-3.1	29.0	-61	0.0	-1.0
75	40.4	-34	-4.9	-5.8	-5.3	-8.1	40.8	-31	-0.4	-2.3	40.3	-33	0.1	-0.3
150	36.6	-18	-1.1	-21.5	0.7	-21.6	34.8	-18	1.8	-0.1	36.3	-17	0.3	-0.9
225	29.0	-37	6.5	-2.6	5.7	-3.0	29.8	-37	-0.9	-0.5	29.0	-36	0.0	-0.6
315	35.4	-61	0.1	21.7	0.8	21.5	34.7	-61	0.7	-0.2	35.3	-61	0.1	-0.3
RMS error for 24 U_5 phase angles injected									**0.9**	**2.1**			**0.2**	**0.5**

Individual results derived with model's linear part inclusion are relatively accurate (Table 3.4); however, if compared maximum linear part modelled magnitude ($\Delta I_{x,MLIN}$) of 5.7 mA, and the maximum linear part deviation ($\delta I_{x,MLIN}$) is 1.8 mA, which is roughly 30% of the full variation amplitude. Though suitable for single harmonic voltage component influence estimation, following section shows that for the cumulative multiple voltage harmonics influence model to have a reasonable outcome, the single harmonic voltage

influence would need to have as good correspondence as possible. Therefore, Table 3.4 presents low RMSE values of the modelled values when nonlinear part (see (3.1)) included in full model. This holds true for multiple loads tested (see Table 3.5), where the measured values and anticipated model calculated values shows very high match i.e. small RMSE.

Table 3.5 Difference of measurement and estimation for test loads; single supply harmonic U_5 = 3 V

Load		I_3						I_5						I_7					
		$I_{3,MEAS}$, mA	$I_{3,MLIN}$, mA	$I_{3,WVDM}$, mA	$\varphi_{I3,MEAS}$, °	$\varphi_{I3,MLIN}$, °	$\varphi_{I3,WVDM}$, °	$I_{5,MEAS}$, mA	$I_{5,MLIN}$, mA	$I_{5,WVDM}$, mA	φ_{I5_MEAS}, °	$\varphi_{I5,MLIN}$, °	$\varphi_{I5,WVDM}$, °	$I_{7,MEAS}$, mA	$I_{7,MLIN}$, mA	$I_{7,WVDM}$, mA	$\varphi_{I7,MEAS}$, °	$\varphi_{I7,MLIN}$, °	$\varphi_{I7,WVDM}$, °
1	Max	40.4	40.5	40.4	-118	-119	-118	36.3	36.8	36.4	103	103	104	31.0	31.7	31.0	-32	-32	-32
	Min	38.9	39.0	39.0	-137	-137	-137	32.3	32.8	32.4	72	72	72	24.2	24.9	24.4	-78	-78	-77
	RMSE		**0.3**	**0.1**		**0.9**	**0.1**		**0.5**	**0.1**		**1.3**	**0.2**		**0.6**	**0.1**		**2.0**	**0.4**
2	Max	59.4	59.7	59.6	-114	-114	-114	51.0	51.7	51.1	112	112	113	40.4	41.2	40.3	-18	-18	-17
	Min	56.4	56.7	56.5	-131	-131	-131	43.4	44.2	43.6	82	82	83	29.0	29.8	29.0	-61	-61	-61
	RMSE		**0.6**	**0.1**		**1.0**	**0.2**		**0.8**	**0.1**		**1.6**	**0.2**		**0.9**	**0.2**		**2.1**	**0.5**
3	Max	50.8	51.0	51.0	-117	-117	-117	44.3	44.9	44.4	106	106	107	35.9	36.7	35.8	-27	-27	-26
	Min	48.5	48.7	48.6	-135	-135	-135	38.3	38.9	38.4	76	76	76	26.5	27.2	26.5	-70	-70	-70
	RMSE		**0.5**	**0.1**		**1.0**	**0.1**		**0.7**	**0.1**		**1.5**	**0.2**		**0.8**	**0.2**		**2.1**	**0.4**

3.1.5 Cumulative response to voltage harmonics

The harmonic current calculation model (3.1) is composed by components referred through parts (3.2) & (3.3) which make up a scalar product of multiple effects from supply voltage harmonics of different order. This construction of model is able to account for aggregation of contributory influences from multiple supply voltage harmonic components on harmonic current I_x. To represent this, an analysis based on measurements assessing the aggregate influence is provided. The cumulative response is approached in a manner to keep one or multiple supply voltage harmonics as fixed vectors while the single other order harmonic voltage component U_y is varied through 360° with fixed-degree step, ensuring the magnitude keeping the magnitude U_y remains unchanged; illustrated in Table 3.6.

Table 3.6 Input-combination-2 when adding multiple harmonic voltages to fundamental voltage

supply voltage Combinations	U_1	U_3		U_5		U_7	
	U_1, V	U_3, V	φ_{U3} °	U_5, V	φ_{U5} °	U_7, V	φ_{U7} °
1	230	0	0	0	0	0	0
24	230	3	0-15…345	0	0	0	0
24	230	3	120	3	0-15…345	0	0
24	230	3	315	3	0-15…345	0	0

Beginning with fundamental voltage component response harmonic current $I_{7,base}$ reference point ("1" in Figure 3.5, for sinusoidal supply conditions), third harmonic U_3 is applied at first. The 360° rotation, with 15-degree step, of the U_3 provides an ellipse presented with black line and asterisks (as described in the previous chapter, see Figure 3.5. Two extreme points with minimum (point "2") and maximum phase value (point "3") of seventh harmonic current I_7 of are selected. Further, U_5 is introduced and rotated with 360° using former chosen points of U_3 as next point of interest on graph. The reported results provide additional ellipse patterns that have their centre-points in the previously identified points of interest. This enables a direct observation of the geometrical cumulation of influence vectors resulting from different harmonic orders of supply

voltages. Notably, the combined effects of U_3 and U_5 can be observed to induce 80° I_7 rotation. The plotted points of I_7 presented now serving as new origins of ellipses for U_5 influence ("2" and "3" on Figure 3.5) would facilitate an accurate integration of influence components for including more supply voltage harmonic.

The analysis of Figure 3.5 indicates that the harmonic current I_x components, computed using equation ((3.1)) for each supply voltage harmonic component U_y, have an individual influence that can be cumulatively summed up linearly

$$\Delta I_x = \sum_{n=1;y=2n+1}^{N} \Delta I_{x,y} \tag{3.19}$$

$$\Delta \varphi_{Ix} = \sum_{n=1;y=2n+1}^{N} \Delta \varphi_{Ix,y} \tag{3.20}$$

N is number of odd harmonic current components. Equations ((3.19) & (3.20)) are part of the matrix evaluation in ((3.2)–(3.5)). The cumulation approach is a useful technique for calculating supply voltage harmonics. However, it's only accurate for low magnitude levels. it may lead to significant deviation for higher levels of supply voltage harmonics. This can be traced to additional G_{xy} and K_{xy} dependence on the I_x ellipse cumulative base point positioning (see also chapter 3.2.2 Base point variations).

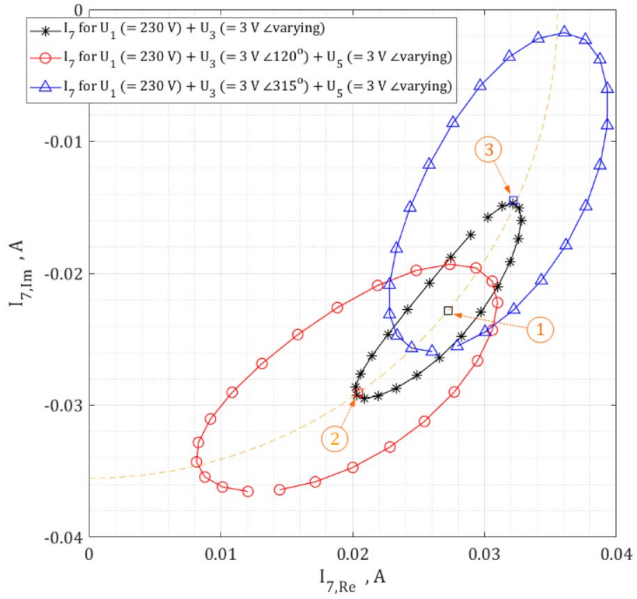

Figure 3.5 Explanation on harmonic current I_7 cumulative products results with U_1 = 230 V; U_3 and U_5 = 3 V. Red line: φ_{U3} = 105°, blue line: φ_{U3} = 300°, φ_{U5} phase values 0,15,30…345, plot of measured response. (previously published in article III).

3.1.6 Validation of proposed model

Even though acknowledged the limitations of cumulative harmonic current evaluation in the previous section, the linear cumulative I_x model has shown significant improvement in performance and accuracy compared to previous models. This will be demonstrated by using specific waveforms listed in Table 3.7.

Table 3.7 Harmonic voltage levels and phase angle present in residential grid, flat and pointed top waveforms

Waveform	U_1	U_3		U_5		U_7		U_9	
	U_1 , V	U_3 , V	φ_{U3} °	U_5 , V	φ_{U5} °	U_7 , V	φ_{U7} °	U_9 , V	φ_{U9} °
Grid-1	230	0.35	51	1.0	224	0.97	15	0	0
Grid-2	230	0.15	80	1.6	296	0.79	37	0	0
Flat top	230	5.5	0	3.8	180	2.0	0	0.57	180
Pointed top	230	6.6	0	4.7	180	1.4	180	0	0

The load current harmonics resulting from residential grid supply (as it contains harmonics with small magnitudes) tend to have a small magnitude, with the nonlinear part being insignificant compared to the linear part. In industrial grids, more extreme cases may occur with "pointed and flat-top" supply voltage waveforms, which exceed the accuracy range of the proposed model but can be used as a reference for different model presentations.

To estimate the load current harmonic fingerprint using the proposed harmonic model, two recorded residential grid voltage waveforms considered (Grid-1 and Grid-2, in Table 3.7). Additionally, "flat top" and "pointed top" waveforms in Table 3.7 for reference purposes, aimed at providing a more extensive industrial case presentation.

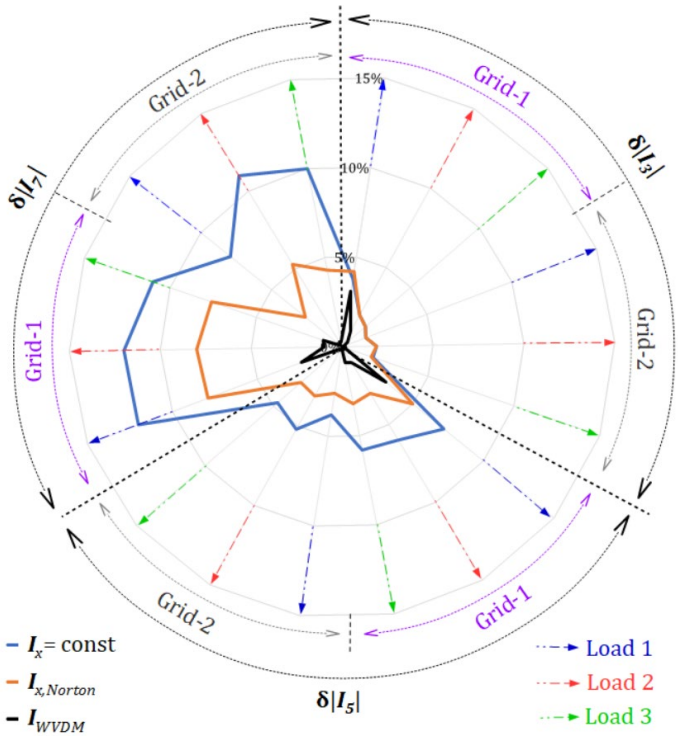

Figure 3.6 Deviation in magnitude between measurements and modelled (constant-current, Norton, proposed model) values, for two residential-area grid waveforms (published in article III).

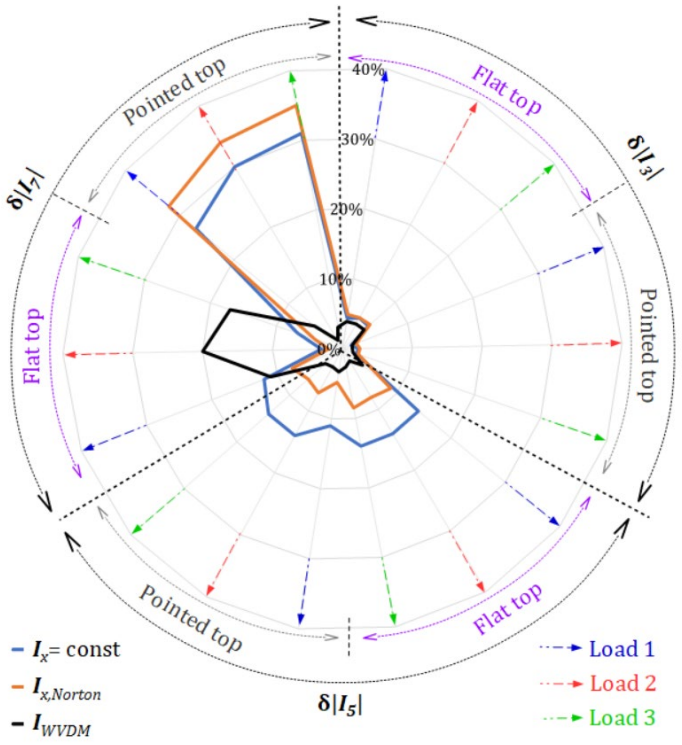

Figure 3.7 Deviation in magnitude between measurements and modelled (constant-current, Norton, proposed model) values, for Flat and pointed-top supply waveforms (previously published in article III).

The measurements for the loads mentioned in section 3.1.3 were carried out while supplying them with the supply waveforms mentioned in Table 3.3, using conditions (like thermal stability) and measurement setup detailed in section 2.1.3.

Table 3.8 provides a comparison between different techniques used to measure and estimate model accuracy by analysing the response of loads to specific waveforms using equations (3.2) through (3.5). The difference in the magnitude of harmonic currents, represented by $\delta|I_h|$, is shown for different harmonic models in Figure 3.6 and Figure 3.7. Comparison of results from constant harmonic current model (I_x = const) and Norton model ($I_{x,Norton}$) against the proposed model ($I_{x,WVDM}$), which shows a significant improvement in accuracy. Table 3.8 readings have been compared on Figure 3.6–Figure 3.7 for the magnitude result analysis. It has to be noted, that the phase angle values for all considered I_x observed, are showing less than 10^o difference compared to the measured values. Finally, Figure 3.8 provides a comparison between load current harmonic measurements and modelled responses of different harmonic modelling techniques for flat-top (FT) and pointed-top (PT) voltage waveforms.

The proposed model harmonic current estimation is rather usable even for the industrial cases presented. The phase margin tends to present more accurate estimation outcome, result of improved phase results due to cross-order harmonic coupling evaluation.

Table 3.8 Difference of estimations and measurement for tested residential and industrial voltage supply waveform

Load	Waveform type	Estimation technique	Difference					
			% $\delta\|I_3\|$	φ_{I3}	% $\delta\|I_5\|$	$\delta\varphi_{I5}$	% $\delta\|I_7\|$	$\delta\varphi_{I7}$
1	Grid-1	I_x = const	3.8	<1	7.2	1	12	3
		$I_{x,Norton}$	4.2	<1	5.0	2	7.9	4
		I_{WVDM}	3.1	1	3.1	2	2.4	3
	Grid-2	I_x = const	1.4	5	3.8	8	7.9	11
		$I_{x,Norton}$	1.4	5	2.6	<1	2.6	14
		I_{WVDM}	0.1	<1	0.1	1	0.1	2
	Flat top	I_x = const	4.3	20	14	40	12	65
		$I_{x,Norton}$	4.9	14	9.0	25	7.7	48
		I_{WVDM}	3.9	<1	3.7	3	12	9
	Pointed top	I_x = const	1.3	15	12	27	28	44
		$I_{x,Norton}$	2.1	8	4.8	8	33	53
		I_{WVDM}	1.5	1	3.3	2	5.1	5
2	Grid-1	I_x = const	2.0	1	6.0	3	12	7
		$I_{x,Norton}$	2.0	2	3.0	3	8.0	<1
		I_{WVDM}	1.0	<1	1	<1	1.0	<1
	Grid-2	I_x = const	1.9	5	5.2	7	11	9
		$I_{x,Norton}$	1.9	4	3.1	<1	5.3	12
		I_{WVDM}	0.2	<1	0.2	1	0.3	2
	Flat top	I_x = const	5.0	18	14	38	3.0	63
		$I_{x,Norton}$	5.0	12	8.0	22	2.0	47
		I_{WVDM}	4.0	2	2.0	1	20	3
	Pointed top	I_x = const	2.3	16	15	30	30	51
		$I_{x,Norton}$	2.5	8	7.1	10.	34	61
		I_{WVDM}	1.5	<1	2.9	2	1.4	6
3	Grid-1	I_x = const	1.7	1	5.8	3	12	7
		$I_{x,Norton}$	1.7	2	3.2	3	7.6	<1
		I_{WVDM}	0.4	<1	0.9	<1	1.1	<1
	Grid-2	I_x = const	1.8	5	4.7	8	10	9
		$I_{x,Norton}$	1.7	4	3.0	<1	4.3	13
		I_{WVDM}	0.1	<1	0.2	1	0.3	2
	Flat top	I_x = const	4.9	19	14	38	6.8	64
		$I_{x,Norton}$	5.2	12	8.5	23	4.2	47
		I_{WVDM}	4.1	2	2.6	2	17	6
	Pointed top	I_x = const	2.1	16	14	29	31	48
		$I_{x,Norton}$	2.4	8	6.5	9	35	58
		I_{WVDM}	1.6	<1	3.2	2	3.1	6

The proposed model for estimating harmonic current is applicable to presented industrial waveform cases; however, this is not valid for all industrial waveform presentations. Phase estimation tends to obtain precise estimation outcomes (see Figure 3.8), as obtained estimation results consider cross-order harmonic coupling.

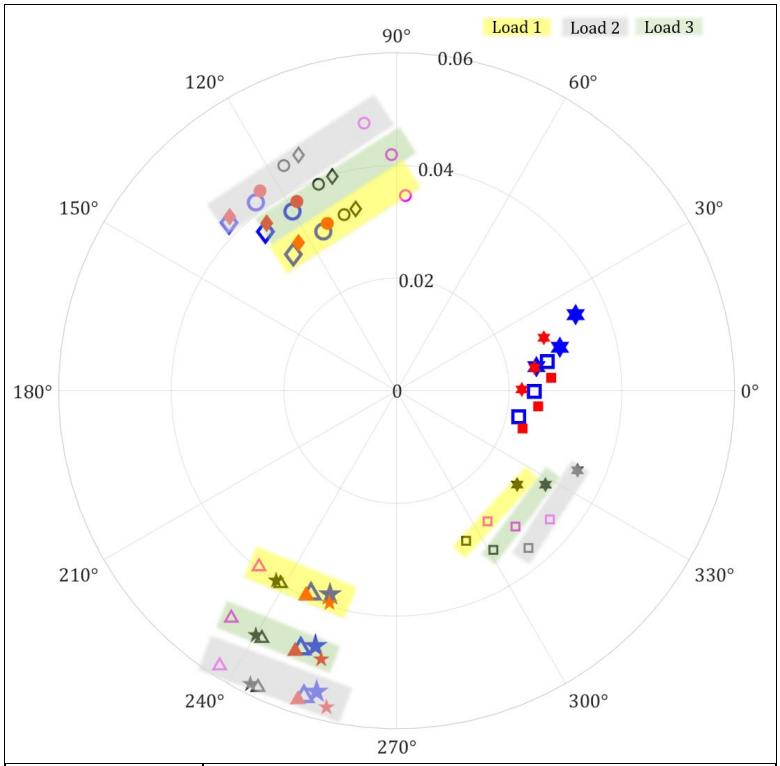

Waveform	Current harmonics		
Pure sine	△ $I_{3,Base}$	○ $I_{5,Base}$	□ $I_{7,Base}$
Flat top	△ $I_{3,Meas\_FT}$	○ $I_{5,Meas\_FT}$	□ $I_{7,Meas\_FT}$
	△ $I_{3,Norton\_FT}$	○ $I_{5,Norton\_FT}$	□ $I_{7,Norton\_FT}$
	▲ $I_{3,WVDM\_FT}$	● $I_{5,WVDM\_FT}$	■ $I_{7,WVDM\_FT}$
Pointed top	★ $I_{3,Meas\_PT}$	◇ $I_{5,Meas\_PT}$	✸ $I_{7,Meas\_PT}$
	★ $I_{3,Norton\_PT}$	◇ $I_{5,Norton\_PT}$	✸ $I_{7,Norton\_PT}$
	★ $I_{3,WVDM\_PT}$	◆ $I_{5,WVDM\_PT}$	✸ $I_{7,WVDM\_PT}$

Figure 3.8 Comparison of load current harmonic measurements and modelled response of different harmonic modelling techniques, for flat-top (FT) and pointed-top (PT) voltage waveforms (see Table 3.8) (previously published in article III).

3.2 Basepoint analysis for complexity reduction of proposed model

3.2.1 Main harmonic level Influence

The components of the current harmonic models are often considered as constants regardless of fundamental voltage component magnitude level U_1. This is not entirely accurate, as indicated by measurement, U_1 level significantly impacts the harmonic results. Significant experimental results are utilised in this section to propose a possible modelling approach that includes U_1 level. The measurement outcomes suggest that a linear relationship with respect to the relative U_1 level is suitable for representing the dependence of load current harmonics.

The waveform variation-dependent model (WVDM) targets the evaluation of phase and magnitude variations of the response and uses three components to describe the model [44]. The initial model is presented based on measurements at a rated voltage

230 V fundamental harmonic level. In subsequent measurements, however, it has been noted that any other supply level voltage value, particularly main harmonic U_1 level, results as an impact to basically all model components. This includes the base harmonic response $\boldsymbol{I_{x,base}}$ as well as model coefficients. This section elaborates on WVDM for load current harmonic estimation to include a U_1-dependent part, as the U_1 level influence has been inadequately described, if at all, in the literature.

Load current harmonics experience variations in response to supply voltage harmonics, and this current harmonics response is related to the time-domain waveform variation, see [44]. Specific behavioural patterns, such as, 3^o phase shift of 3rd order harmonic current, are attributed due to the variation in rectifier's conduction initiation moment. This subsequently leads to analogous phase shifts in higher order harmonics – 5^o in the fifth harmonic, 7^o in the seventh order current harmonic, and so on. Every voltage harmonic, injected to the power supply with the magnitude of U_y ('$_y$' is order of voltage harmonic) will provide a maximum current harmonic phase influence instance at specific phase value $\angle\varphi_{Uy}$, similarly minimum ($I_{x,min@Uy}$) and maximum ($I_{x,max@Uy}$) magnitude response phase values. These minimum and maximum points determine the WVDM coefficient values. The main load characteristic scan is performed using various input voltage supply combinations presented in Table 3.9.

Table 3.9 Supply voltage combination, with various level of fundamental, adding single voltage harmonic to supply waveform

Combi-nations	$\boldsymbol{U_1}$	$\boldsymbol{U_3}$		$\boldsymbol{U_5}$		$\boldsymbol{U_7}$	
	U_1, V	U_3, V	φ_{U3} °	U_5, V	φ_{U5} °	U_7, V	φ_{U7} °
5	207, 218, 230, 241, 253	0	0	0	0	0	0
120	207, 218, 230, 241, 253	3	0-15…345	0	0	0	0
120	207, 218, 230, 241, 253	0	0	3	0-15…345	0	0
120	207, 218, 230, 241, 253	0	0	0	0	3	0-15…345

3.2.2 Base point variations

Fundamental current harmonic responses (base point) $\boldsymbol{I_{5,base}}$ for various levels of U_1 (U_1 levels between 230 ± 10% V) are presented in Figure 3.9. It is observed that as U_1 magnitude increases, there is a corresponding gradual shift in the base point values for any given response harmonic. In addition, when an additional voltage harmonic ($\boldsymbol{U_x}$), is introduced in the supply voltage, the resultant current response vectors are shifted accordingly. The graphical representation includes '○' and '△' symbols to symbols to illustrate the $\boldsymbol{I_5}$ response vectors within the load current when the fifth-order supply voltage harmonic, $\boldsymbol{U_5}$, is introduced at two distinct U_1 magnitudes, specifically 207 V and 253 V. Table 3.10 presents the base point values, $\boldsymbol{I_{x,Base}}$, for the dominant low-order current harmonics across the aforementioned U_1 magnitude levels.

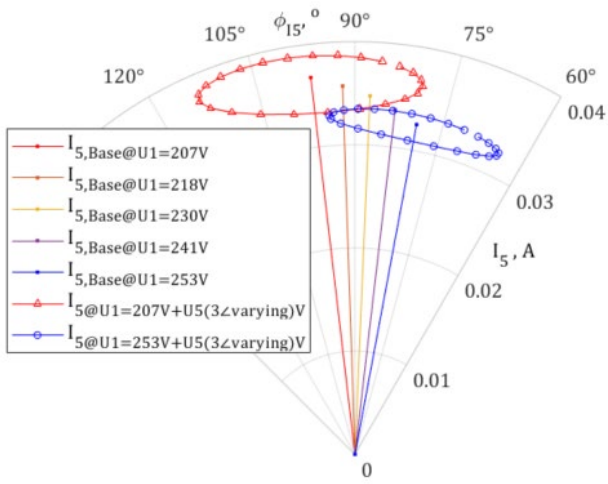

Figure 3.9 Harmonic response vectors for 5 levels of U_1 (previously published in article IV).

Table 3.10 Base point coordinates (3rd, 5th, 7th)

U_1 , V	$I_{3,Base}$, mA	$\varphi_{I3,Base}$, °	$I_{5,Base}$, mA	$\varphi_{I5,Base}$, °	$I_{7,Base}$, mA	$\varphi_{I7,Base}$, °
207	43.4	-123	36.8	97	28.5	-41
218	41.5	-125	35.7	92	28.4	-48
230	39.8	-128	34.8	88	28.3	-55
241	37.9	-130	33.6	83	27.9	-61
253	36.3	-133	32.5	79	27.5	-67

3.2.3 Phase and magnitude range variations

Figure 3.9 and Figure 3.10 illustrate the influence of voltage harmonics and amplitude value of the fundamental voltage component (U_1) in the supply upon the sensitivity of current harmonics. The seventh Harmonic component I_7 is presented here, as the base point magnitude I_7 is rather persistent; and phase angles of the base response are changing. Figure 3.10 demonstrates I_7 response when including third voltage harmonic U_3 inclusion with full 360-degree rotation ($\angle U_3$ 0 → 360° rotation) in supply voltage, for three scenarios of U_1 magnitude: a 10% increase to 253 V, the nominal 230 V, and a 10% decrease to 207 V. For each input scenario, there is a similar phase angle shift of the base points. The spread and compression of I_7 response vectors related to the U_1 levels are elaborated in Figure 3.10, supporting the cumulation hypothesis claimed by *WVDM* (referring to Figure 3.1 and equations (3.1)(3.5)).

The degree of dispersion in both phase and magnitude of load current harmonic components is quantifiable by the extent of their deviation from defined base vector point. The highest observed deviations are utilised as the metric for determining the deviation range to assess current variations as

$$dI_{x,y,MAX} = \frac{\left(\left| dI_{x,Uy@Ix,MAX} \right| + \left| dI_{x,Uy@Ix,MIN} \right| \right)}{2} \tag{3.21}$$

and for the phase angle variation

$$d\varphi_{Ix,y,MAX} = \frac{d\varphi_{Ix,Uy@\varphi Ix,MAX} - d\varphi_{Ix,Uy@\varphi Ix,MIN}}{2} \tag{3.22}$$

The highest observed deviations (calculated using equations 3.20 and 3.21) are presented in Table 3.11 for the input combination mentioned in Table 3.10.

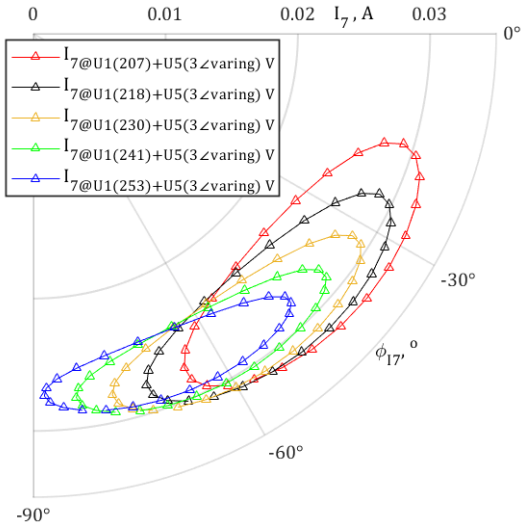

Figure 3.10 7^{th} harmonic response for supply containing U_1 (varying) + U_5 (3 V) (previously published in article IV).

Table 3.11 Maximum magnitude difference & maximum phase difference quantities, between base point & current harmonic vectors (3^{rd}, 5^{th}, 7^{th}) , (U_y = 3 V)

U_1 , V	Influencing U_h order, y	$dI_{3,max}$, mA	$d\varphi_{3,max,@dI3=0}$, °	$dI_{5,max}$, mA	$d\varphi_{5,max,@dI5=0}$, °	$dI_{7,max}$, mA	$d\varphi_{7,max,@dI7=0}$, °
207	3	0.3	07	1.0	12	1.9	17
	5	1.3	10	3.5	17	5.4	25
	7	2.6	11	6.1	19	9.1	28
218	3	0.2	07	0.8	12	1.6	16
	5	1.1	10	3.0	17	4.7	24
	7	2.2	11	5.3	19	8.2	28
230	3	0.2	07	0.6	11	1.3	15
	5	0.8	09	2.5	16	4.1	23
	7	1.9	11	4.6	19	7.3	27
241	3	0.2	06	0.5	10	1.1	15
	5	0.7	09	2.1	16	3.5	22
	7	1.6	11	4.1	18	6.5	26
253	3	0.2	06	0.4	10	0.9	14
	5	0.6	09	1.7	15	2.9	21
	7	1.4	11	3.5	18	5.8	26

In Waveform Variation-Dependent Model (WVDM), linear model coefficients represent the relationship between the magnitude of variation range and the parameters of the load current harmonic. The maximum deviation of current harmonics $dI_{x,y,MAX}$, due to supply voltage's influencing harmonic component U_y, yields the proportional coefficient G_{xy}, as defined by equation (3.20).

$$G_{xy} = \frac{dI_{x,MAX}}{U_y} \quad (3.23)$$

Similarly, the $d\varphi_{Ix,y,MAX}$ and supply voltage influencing voltage harmonic U_y proportional coefficient k_{xy} (see (3.21)) can be calculated as

$$k_{xy} = \frac{d\varphi_{Ix,y,MAX}}{U_y} \quad (3.24)$$

Current parameters' variation from Table 3.11, are used to determine sensitivity coefficients discussed in 3.22 and 3.23; these are presented in Table 3.12.

Table 3.12 G,k coefficient values for different harmonics combinations, measurement outcome. (U_y = 3 V), y = influencer harmonic order, and x = response harmonic order

U_1, V			G_{xy}, mA/V	k_{xy}, °/V	G_{xy}, mA/V	k_{xy}, °/V	G_{xy}, mA/V	k_{xy}, °/V
	y	*x*	**3**	**3**	**5**	**5**	**7**	**7**
207	3		0.09	2.4	0.29	4.0	0.56	5.6
218			0.08	2.3	0.23	3.8	0.47	5.3
230			0.07	2.2	0.18	3.6	0.39	5.1
241			0.07	2.1	0.14	3.4	0.32	4.8
253			0.07	2.0	0.10	3.3	0.26	4.6
207	5		0.37	3.4	0.96	5.7	1.52	8.2
218			0.30	3.3	0.80	5.5	1.31	7.9
230			0.24	3.2	0.66	5.3	1.13	7.6
241			0.19	3.1	0.55	5.2	0.96	7.3
253			0.15	3.0	0.45	5.0	0.81	7.0
207	7		0.71	3.7	1.63	6.4	2.50	9.4
218			0.59	3.7	1.40	6.3	2.22	9.2
230			0.50	3.6	1.20	6.1	1.96	8.9
241			0.42	3.6	1.03	6.1	1.70	8.7
253			0.35	3.6	0.88	6.0	1.49	8.6

3.2.4 Basepoint sensitivity model

The influence of the fundamental harmonic voltage U_1 on the resultant harmonic current is significant. The deviation of the base point itself could be modelled through impedance relation, although with negative value. As described in Table 3.12, the sensitivity coefficients G_{xy} and k_{xy} are dependent on U_1 level, introducing an additional dimension to the model. This allows for more precise calculations of expected harmonic current levels, taking into account the range of main-voltage values within the distribution network.

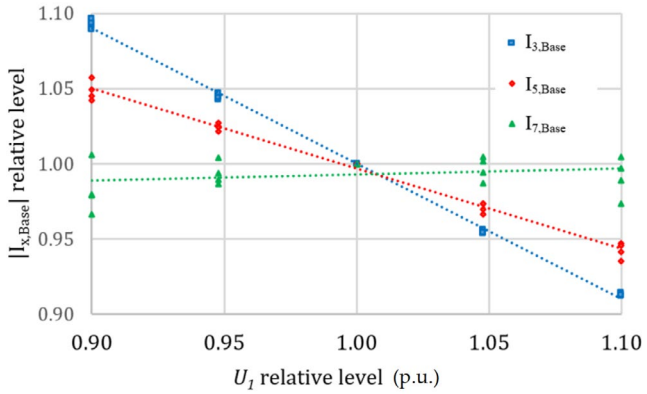

Figure 3.11 Relative relation between $|\boldsymbol{I_{x,Base}}|$ and fundamental harmonic voltage level (previously published in article IV).

Regarding model's predictive accuracy, the sensitivity on U_1 is well correlated to the main harmonic relation to the reference value, as indicated by the data in Figures 3.7, 3.8, and 3.9. Change in $I_{x,Base}$ are well illustrated by the trends shown in Figure 3.10. This dependency can be described using linear relation approach. The relation between U_1 levels and variables $\boldsymbol{I_{x,Base}}$, G_{xy}, and k_{xy} is quantitatively captured through a general empirical equations inferred from measurements. For example, appropriate relational expressions for the harmonic base points can be found as

$$m_{q,U1} = K_{RVL,q} \cdot \left(\frac{U_1}{230}\right) + (1 - K_{RVL,q}) \tag{3.25}$$

Term $k_{RVL,q}$ presents the empirical linear '*relative voltage level –RVL*' coefficient. The expression $(1 - k_{RVL,q})$ constitutes the offset component within the trend. '*q*' marks a coefficient identity, where multiplier is used (see Table 3.12). The corresponding scalar multiplier designated as $m_{q,U1}$ is expected to obtain value 1.0 when U_1 voltage relative value 1.0. To ascertain the magnitude of the harmonic base point $\boldsymbol{I_{x,Base,U1}}$ for a given actual U_1 voltage level, this scalar multiplier is employed.

$$\boldsymbol{I_{x,Base,U1}} = [m_{b3}\, m_{b5} \ldots m_{bN}] \cdot \boldsymbol{I_{x,Base}} \tag{3.26}$$

Phase value of Base point will be taken as reference for calculation of phase offset. This Phase value offset component is extracted utilising a linear trend relating with the relative level of U_1 voltage. The basepoint phase offset is an absolute phase shift quantity, added to the base point U_1 nominal level value

$$\boldsymbol{\varphi_{I,Base,U1}} = \boldsymbol{k_{b\varphi}} \cdot \left(\frac{U_1}{230} - 1\right) + \boldsymbol{\varphi_{I,Base}} \tag{3.27}$$

Where $k_{b\varphi}$ is the coefficient of base vector phase showing dependence of relative U_1 level.

The Figure 3.12 and Figure 3.13 demonstrate that the model coefficients G_{xy} and k_{xy} have a linear dependence on the relative value of U_1. The scalars m_{gU1} and m_{kU1} are multiplied with a value obtained at nominal U_1, and multipliers are included to $G_{x,U1}$ and $k_{x,U1}$ for correction based on the relative level of U_1. A general trend equation (3.24) can be suggested for all these coefficients. The $WVDM_{U1}$ model parameter values are then established using equations (3.25) and (3.26).

$$\boldsymbol{G_{x,U1}} = [m_{gX3}\ m_{gX5} \dots m_{gXN}] \begin{bmatrix} G_{x3} \\ G_{x5} \\ \dots \\ G_{xN} \end{bmatrix}$$

$$\boldsymbol{k_{x,U1}} = [m_{kX3}\ m_{kX5} \dots m_{kN}] \begin{bmatrix} k_{x3} \\ k_{x5} \\ \dots \\ k_{xN} \end{bmatrix}$$

The model equations are updated from (3.1) as

$$\begin{cases} I_{x,WVDM,U1} = I_{x,base,U1} + \Delta I_{x,LIN,U1} + \Delta I_{x,NL} \\ \varphi_{Ix,WVDM,U1} = \varphi_{Ix,Base,U1} + \Delta\varphi_{Ix,LIN,U1} + \Delta\varphi_{Ix,NL} \end{cases} \quad (3.28)$$

The WVDM model linear part, calculated using (3.27) will also be upgraded to U_1 sensitive variables.

$$\Delta I_{x,LIN,U1} = \boldsymbol{U_y} \cdot \boldsymbol{G_{x.U1}} \cdot \cos(\boldsymbol{\alpha_x} - \boldsymbol{\varphi_{Uy}}) \quad (3.29)$$

$$\Delta\varphi_{Ix,LIN,U1} = \boldsymbol{U_y} \cdot \boldsymbol{k_{x,U1}} \cdot \sin(\boldsymbol{\alpha_x} - \boldsymbol{\varphi_{Uy}}) \quad (3.30)$$

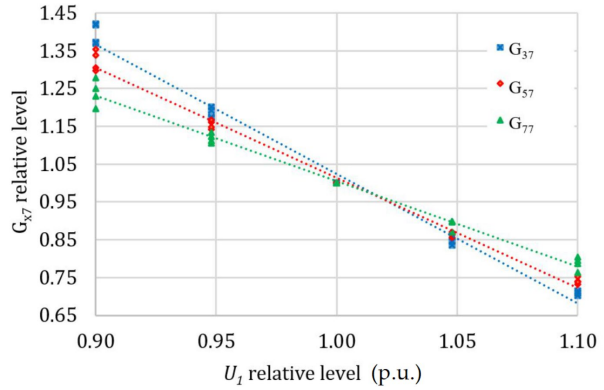

Figure 3.12 Relative relation between G_{xy} and fundamental harmonic voltage level (previously published in article IV).

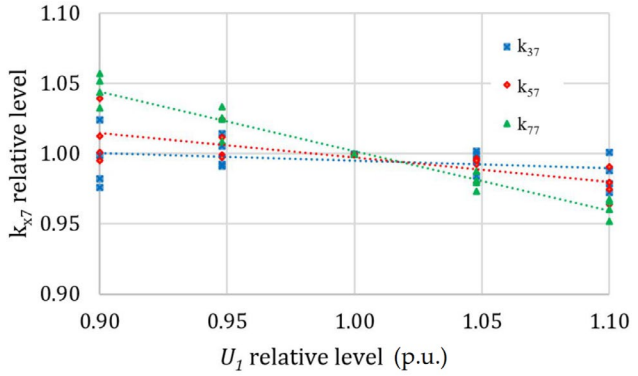

Figure 3.13 Relative relation between k_{xy} and fundamental harmonic voltage level (previously published in article IV).

3.2.5 Verification of WVDM with main harmonic influence

For verification of the abovementioned proposal on base point, Type-A LED lamps, as detailed in Chapter 2, have been employed. The harmonic current profiles for these loads were recorded across all input permutations indicated in Table 3.9. approach described in section 3.2.2 is deployed to evaluate accuracy of the proposed model. This involves the variation of the harmonic voltage component across 24 discrete phase angles and the gradual adjustment(increase) of the supply voltage magnitude U_1, ranging from 207 V (90% of the nominal 230 V) to 253 V (110% of the nominal 230 V). influencer voltage harmonics in supply voltage are rotated through a full 360^o, partitioned into 23 increments. For example, an added third harmonic U_3 makes rotation through phase angles $\varphi_{U3} = \{0 \dots 360^o\}$, while U_1 magnitude maintains a particular level.

Harmonic currents are then modelled using various estimation methodologies and compared against empirical measurements, with the root mean square error (RMSE) computed based on all 24-point deviations. Sensitivity coefficients relating to U_1 are established and presented in Table 3.12.

Comparison is presented using models as below:

1. $I_{h,const,230}$, assuming I_h persistence regardless of U_1 or any added U_y;
2. $I_{h,const,U1}$, assuming I_h relation to U_1 but persistence regardless of any added U_y;
3. *WVDM* (see equation (3.1))
4. $WVDM_{U1}$ (see equation (3.28))

Table 3.13 provides comparison of maximum deviation (δ_{MAX}) and the RMSE across various harmonic modelling methodologies applied to a singular load. The impact of voltage harmonic influencers has been addressed in literature [44]; however, the integration of U_1's influence into the estimation model enhances precision. The $WVDM_{U1}$ yields minimal RMSE values after estimation, regardless of order of current harmonic or influencer.

Table 3.13 Deviation comparison of modelled values for different harmonic modelling techniques. Influencing U_y level is 3 V (from publication IV)

x	y	U_1, V		$\lvert I_{x,Base}\rvert$, mA	$\delta\lvert I_x\rvert$, mA				$\varphi_{Ix,Base}$, °	$\delta\varphi_{Ix}$, °			
					$I_{h,\mathrm{const},230}$	$I_{h,\mathrm{const},U1}$	WVDM	$WVDM_{U1}$		$I_{h,\mathrm{const},230}$	$I_{h,\mathrm{const},U1}$	WVDM	$WVDM_{U1}$
		207		43.4	4.0	0.3	3.8	0.1	-123	12	7	6	<1
		218		41.5	1.9	0.2	1.7	0.2	-125	9	7	3	<1
3	3	230	δ_{MAX}	39.8	0.2	0.2	0.0	0.0	-128	7	7	<1	<1
		241		37.9	2.1	0.2	1.9	0.2	-130	9	6	3	<1
		253		36.3	3.7	0.2	3.6	0.1	-133	11	6	5	<1
		207			3.7	0.2	3.6	**0.1**		*7*	*5*	*5*	**<1**
		218			1.7	0.2	1.7	**0.2**		*5*	*5*	*2*	**<1**
3	*3*	230	***rmse***		0.2	0.2	0.0	**0.0**		*5*	*5*	<1	**<1**
		241			1.9	0.1	1.9	**0.2**		*5*	*4*	*2*	**<1**
		253			3.5	0.1	3.5	**0.1**		*6*	*4*	*5*	**<1**
		207		43.4	5.3	2.6	4.2	0.3	-123	16	11	5	2
		218		41.5	3.0	2.2	2.0	0.5	-125	13	11	2	2
3	7	230	δ_{MAX}	39.8	1.9	1.9	0.3	0.3	-128	11	11	1	1
		241		37.9	3.5	1.6	2.3	0.4	-130	13	11	4	1
		253		36.3	4.9	1.4	4.1	0.2	-133	15	11	6	<1
		207			3.8	1.5	3.5	**0.2**		*9*	*8*	*4*	**2**
		218			2.0	1.2	1.6	**0.4**		*8*	*8*	*1*	**2**
3	*7*	230	***rmse***		1.0	1.0	0.2	**0.2**		*8*	*8*	*1*	**1**
		241			2.1	0.8	2.0	**0.3**		*8*	*8*	*3*	**<1**
		253			3.7	0.7	3.6	**0.1**		*9*	*7*	*6*	**<1**
		207		36.8	4.2	3.5	2.7	0.5	97	26	17	11	1
		218		35.7	2.8	3.0	1.3	0.2	92	21	17	5	1
5	5	230	δ_{MAX}	34.8	2.5	2.5	0.2	0.2	88	16	16	<1	<1
		241		33.6	3.2	2.1	1.6	0.3	83	20	15	5	<1
		253		32.5	4.0	1.7	2.9	0.4	79	23	15	10	1
		207			2.8	2.0	2.1	**0.3**		*15*	*12*	*9*	**1**
		218			1.9	1.6	1.0	**0.1**		*12*	*12*	*4*	**1**
5	*5*	*230*	***rmse***		1.4	1.4	0.1	**0.1**		*11*	*11*	<1	**<1**
		241			1.7	1.1	1.2	**0.2**		*12*	*11*	*5*	**<1**
		253			2.5	0.9	2.3	**0.3**		*14*	*11*	*9*	**<1**
		207		28.5	5.3	5.4	1.3	1.2	-41	38	25	17	5
		218		28.4	4.6	2.7	0.7	0.7	-48	30	16	8	4
7	5	230	δ_{MAX}	28.3	4.1	4.1	0.2	0.2	-55	23	23	1	1
		241		27.9	3.8	3.5	0.9	0.4	-61	28	22	8	1
		253		27.5	3.7	2.9	1.6	0.8	-67	33	21	15	4
		207			3.2	3.2	0.9	**0.7**		*22*	*17*	*13*	**5**
		218			2.7	0.0	0.5	**0.5**		*18*	<1	*6*	**4**
7	*5*	*230*	***rmse***		2.3	2.3	0.1	**0.1**		*16*	*16*	<1	**<1**
		241			2.0	2.0	0.5	**0.2**		*17*	*15*	*7*	**<1**
		253			1.9	1.7	1.0	**0.7**		*20*	*15*	*13*	**4**

3.3 Sensitivity coefficient analysis for complexity reduction of proposed model

Empirical results show that the characterisation of load current's extreme points relating to phase and magnitude response to supply voltage distortion can be accurately represented using a linear relationship:

$$dI_{x,MAX} = k_{IM} \cdot U_y \tag{3.31}$$

$$d\varphi_{x,y,MAX} = k_{\varphi} \cdot U_y, \tag{3.32}$$

Where k_{IM} (units A/V) is the response coefficient of magnitude response and k_{φ} is coefficient of the phase response (units °/V, or rad/V). Proceeding subsections focus on defining the mathematical representation of sensitivity coefficients, G_{xy} and k_{xy}.

3.3.1 Magnitude coefficient trend model

The objective is to devise a relation whereby these coefficients can be determined from a limited dataset, eliminating the need for extensive measurements. The model under development will consider typical datasets containing supply voltage and load current parameters. Inputs supplied to model will include data on supply voltage harmonic components, which consist of the harmonic component's order *y*, the respective scalar voltage magnitude level U_y, and the phase angle φ_{Uy} of the voltage component.

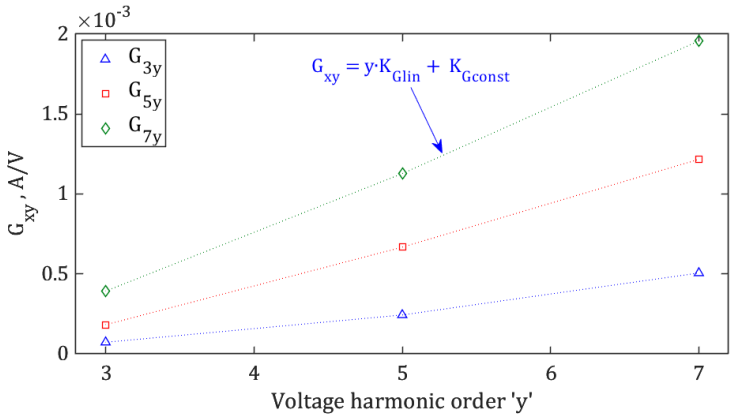

Figure 3.14 Magnitude variation coefficient patterns for WVDM against influencer voltage order y (previously published in article V).

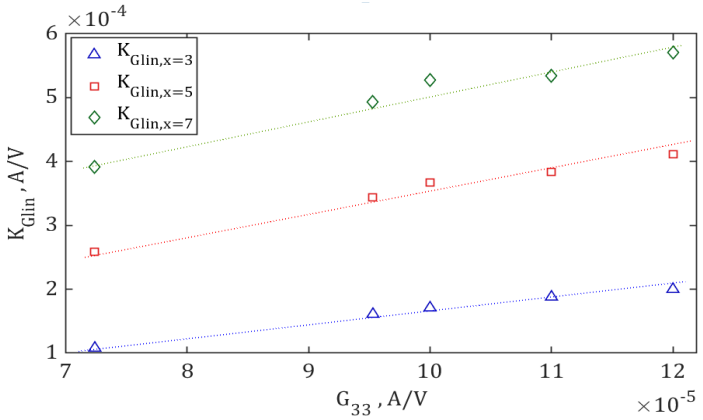

Figure 3.15 Linear variable K_{Glin} relation to G_{33} measured values (previously published in article V).

The relation between the influencer order, designated as '*y*', and the value of the sensitivity coefficient G_{xy} is represented in Figure 3.14. This figure suggests that a model comprising a linear term (K_{Glin}) alongside a constant term (K_{Gconst}) effectively captures the first-order relationship, written as

$$G_{xy} = K_{Glin} \cdot y + K_{Gconst} \tag{3.33}$$

Values of linear coefficient (K_{Glin}) and constant coefficient (K_{Gconst}) extracted from the five test loads are presented in Table 3.14. An analysis of these values against those obtained from empirical measurements displays a linear association of K_{Glin} with the G_{33} value, a relationship is illustrated in Figure 3.15. A good correlation to K_{Glin} can be specified as

$$K_{Glin} = 0.84 \cdot G_{33} \cdot (x - 1) \tag{3.34}$$

For example, in the case of I_7 , K_{Glin} = 5.07G_{33}; for the fifth and third order, slop values to find linear coefficient value are 3.55 and 1.66, respectively (see Figure 3.15).

The constant coefficient $K_{G\text{const}}$ is also linked with current harmonic order *x* and G_{33}. The following equation can be given for a constructing $K_{G\text{const}}$ coefficient of (3.33)

$$K_{Gconst} = 4 \cdot G_{33} + \left(\frac{-2(x-3)^2 + 20(x-3) + 1}{100000}\right) \tag{3.35}$$

G_{33} (a load-specific parameter), K_{Glin} and $K_{G\text{const}}$ values obtained in abovementioned analytical equations, can be used to determine other magnitude variation coefficients G_{xy} relating to any current and voltage harmonic order. This approach holds valid across all LED lamps in the test batch; however, it has to be mentioned that its applicability is confined to LED lamps of a similar type. In essence, such method of coefficient calculation offers a significant shortcut over direct measurement for the acquisition of the respective G_{xy} coefficients.

Table 3.14 Model linear coefficient and constant-coefficient parameters of test loads. Current harmonic order 'x' (from publication V)

	load 1		load 2		load 3		load 4		load 5	
x	K_{Glin}	K_{Gconst}	K_{Glin}	K_{Gconst}	K_{Glin}	K_{Gconst}	K_{Glin}	K_{Gconst}	K_{Glin}	K_{Gconst}
7	39.1	79.7	57.1	95.7	49.3	88.3	52.7	96.4	53.4	89.5
5	25.9	60.5	41.1	80.5	34.4	71.7	36.7	78.5	38.4	75.6
3	10.8	26.8	20	48.4	16.1	39.6	17.1	42.3	18.8	45.7

*all coefficient values are multiplied by 10^5 to enhance readability

Table 3.15 Model parameters of test loads, harmonic voltage order 'y'

Load	***y***	G_{3y}, **mA/V**		G_{5y}, **mA/V**		G_{7y}, **mA/V**		k_{3y}, **°/V**		k_{5y}, **°/V**		k_{7y}, **°/V**	
		meas	*calc*	*meas*	*calc*	*meas*	*calc*	*meas*	*calc*	*meas*	*calc*	*meas*	*calc*
1	3	0.07	0.07	0.18	0.11	0.39	0.32	2.16	2.12	3.60	3.54	5.08	4.95
	5	0.24	0.31	0.67	0.60	1.13	1.05	3.16	3.00	5.31	5.00	7.54	7.00
	7	0.51	0.55	1.22	1.08	1.96	1.78	3.63	3.67	6.17	6.12	8.91	8.57
2	3	0.12	0.12	0.42	0.40	0.75	0.85	2.12	2.12	3.56	3.54	5.10	4.95
	5	0.51	0.52	1.27	1.21	1.91	2.06	2.95	3.00	5.01	5.00	7.26	7.00
	7	0.92	0.92	2.0	2.0	3.03	3.27	3.11	3.67	5.39	6.12	8.08	8.57
3	3	0.1	0.09	0.31	0.25	0.6	0.57	2.13	2.12	3.57	3.54	5.07	4.95
	5	0.39	0.41	1.01	0.89	1.58	1.53	2.99	3.00	5.08	5.00	7.29	7.00
	7	0.74	0.73	1.69	1.53	2.57	2.49	3.25	3.67	5.59	6.12	8.26	8.57
4	3	0.1	0.09	0.32	0.28	0.62	0.62	2.15	2.12	3.60	3.54	5.11	4.95
	5	0.41	0.43	1.05	0.95	1.66	1.63	3.08	3.00	5.28	5.00	7.48	7.00
	7	0.78	0.77	1.79	1.62	2.73	2.64	3.39	3.67	5.79	6.12	8.51	8.57
5	3	0.11	0.10	0.39	0.34	0.7	0.73	2.12	2.12	3.57	3.54	5.10	4.95
	5	0.48	0.47	1.18	1.08	1.79	1.84	2.95	3.00	5.02	5.00	7.27	7.00
	7	0.86	0.84	1.93	1.82	2.83	2.95	3.12	3.67	5.39	6.12	8.07	8.57

3.3.2 Phase variation coefficient models

The phase variation coefficient k_{xy} is responsible for the WVDM modelled values spread on the complex plane. Empirical values for k_{xy}, as presented in Table 3.15, reveal a constant relationship between this phase variation coefficient, the current harmonic order *x*, and the voltage harmonic order *y*, represented by the following equation:

$$k\_ratio = \frac{k_{xy}}{x\sqrt{y}} \tag{3.36}$$

Moreover, while developing the solid relationship for k_{xy}, another coefficient is defined as

$$C_k = \frac{x}{\sqrt{2}} \tag{3.37}$$

C_k is consistent part of calculated k_{xy} ($k_{xy,calc}$). The relations used to determine the phase variation coefficient values, which can be further used to model harmonic current for any influencer order are presented in Table 3.16.

Table 3.16 Relation between phase variation coefficient, current and voltage harmonic order (from Publication V)

y	***x***	$k_{xy,calc}$
3	3	$\frac{x}{\sqrt{2}}$
	5	
	7	
5	3	$\frac{x(x-1)}{2}$
	5	
	7	
7	3	$\frac{x\sqrt{3}}{\sqrt{2}}$
	5	
	7	

3.3.3 Validation of sensitivity coefficient trend

For validation of the proposed model, firstly, accuracy must be determined. The accuracy of the modelled values of G_{xy} and k_{xy} could be established based on comparison with the measurement-originated sensitivity coefficients. The measurement specifics for sensitivity coefficient calculation have been presented in Chapter 2 (see Figure 2.15), where the sensitivity coefficient ($G_{xy,meas}$, $k_{xy,meas}$) values are obtained from direct results using equations (3.9) and (3.10). Proposed G_{xy} and K_{xy} calculation values are obtained using (3.32) and relations provided in Table 3.16. The statistical dispersion is stated as

$$\delta G_{xy,AVG} = average\left\{\left|G_{xy,meas}\right| - \left|G_{xy,calc}\right|\right\} \tag{3.38}$$

$$\delta k_{xy,AVG} = average\left\{\left|k_{xy,meas}\right| - \left|k_{xy,calc}\right|\right\} \tag{3.39}$$

The deviation average is determined by analysing the margin of difference across all five loads under test. Generally, the comparison does not reveal significant discrepancies between the estimated values for most harmonic orders. However, certain combinations of harmonic orders exhibit deviations up to 20%. In next validation step, calculated values of sensitivity coefficients ($G_{xy,calc}$, $K_{xy,calc}$) are used in total current deviation calculations.

The load current deviation evaluation, using load models with coefficients calculated according to the proposed scheme is critical point as this is related to the total harmonic current output estimation. Here for total load current estimation, accounting the voltage harmonic components effects, the waveform variation defined model [44] is used. The total current deviation is computed using

$$\begin{cases} dI_{x,WVDM} = \Delta I_{x,LIN} + \Delta I_{x,NL} \\ d\varphi_{Ix,WVDM} = \Delta\varphi_{Ix,LIN} + \Delta\varphi_{Ix,NL} \end{cases} \quad (3.40)$$

where $dI_{Ix,WVDM}$ and $d\varphi_{Ix,WVDM}$ is the deviation from the base load current component $I_{x,Base}$, and phase $\varphi_{Ix,Base}$; with the linear parts $\Delta I_{x,LIN}$ and $\Delta\varphi_{Ix,LIN}$ found as

$$\Delta I_{x,LIN} = \boldsymbol{U_y} \cdot \boldsymbol{G_x} \cdot \cos(\boldsymbol{\alpha_x} - \boldsymbol{\varphi_{Uy}}) \quad (3.41)$$

$$\Delta\varphi_{Ix,LIN} = \boldsymbol{U_y} \cdot \boldsymbol{k_x} \cdot \sin(\boldsymbol{\alpha_x} - \boldsymbol{\varphi_{Uy}}) \quad (3.42)$$

α_x is a load-specific phase offset quantity outlined by (3.7), φ_{Uy} signifies as the phase angle of the voltage harmonic component U_y of order y. Descriptions for the nonlinear part ($\Delta I_{x,NL}$ and $\Delta\varphi_{Ix,NL}$) is explained in section 3.1.2. For WVDM model coefficients, measurement-originated quantities, G_{xy} and k_{xy} are obtained using (3.9) and (3.10), while the WVDM results with proposed model to calculate coefficients G_{xy} and k_{xy} are provided for comparison. In order to present the highest variations, the deviation maximum values $dI_{x,MAX}$ are compared.

Table 3.15 presents the magnitudes of variation coefficients, which are determined following equation ((3.33) for all loads under test. Table 3.17 presents the percentage deviation of modelled G_{xy} from its measured counterpart (referenced in Table 3.15). Similarly, calculated phase variation coefficients (determined using variables established in Table 3.16) are presented in Table 3.15. Table 3.17 also shows the deviation in measured and modelled values of k_{xy} (See Table 3.15). The deviations between measurement and load current calculation results with WVDM-based values are presented in Table 3.18.

- $WVDM_{Gk,mea}$ uses G_{xy} and k_{xy} coefficients that are determined directly from measurements, and
- $WVDM_{Gk,calc}$ uses G_{xy} and k_{xy} variation coefficients calculated using (3.33) and relations provided in Table 3.16.

Table 3.17 Average deviation of modelled variation coefficients (from publication V)

		$\delta G_{xy,AVG}$			$\delta k_{xy,AVG}$		
y	***x***	**3**	**5**	**7**	**3**	**5**	**7**
3		6%	18%	9%	1%	1%	3%
5		8%	9%	5%	2%	2%	5%
7		3%	7%	6%	12%	9%	4%

Table 3.18 Comparison of modelled and measured values (from publication V)

y , (U_y=3V)	*Load*	*x*	*3*				*5*				*7*			
			dI_{max} , mA	$d\varphi_{max}$, °	$\delta(dI_{max})$, mA	$\delta(d\varphi_{max})$, °	dI_{max}, mA	$d\varphi_{max}$, °	$\delta(dI_{max})$, mA	$\delta(d\varphi_{max})$, °	dI_{max}, mA	$d\varphi_{max}$, °	$\delta(dI_{max})$, mA	$\delta(d\varphi_{max})$, °
3		*Measurement*	0.22	6.5			0.54	10.8			1.18	15.2		
	1	*WVDM*$_{Gk,mea}$	0.21	6.6	0.01	<1	0.53	11.0	0.01	<1	1.16	15.5	0.01	<1
		***WVDM*$_{Gk,calc}$**	0.21	6.7	0.01	<1	0.74	11.2	0.20	<1	1.39	15.9	0.22	<1
	2	*Measurement*	0.36	6.3			1.25	10.7			2.24	15.3		
		WVDM	0.36	6.5	0.00	<1	1.23	10.9	0.01	<1	2.24	15.5	0.00	<1
		***WVDM*$_{Gk,calc}$**	0.36	6.5	0.00	<1	1.27	10.9	0.02	<1	1.92	16.0	0.32	<1
	3	*Measurement*	0.29	6.4			0.94	10.7			1.79	15.2		
		WVDM$_{Gk,mea}$	0.28	6.5	0.00	<1	0.93	10.9	0.01	<1	1.79	15.4	0.00	<1
		***WVDM*$_{Gk,calc}$**	0.28	6.5	0.00	<1	1.11	11.0	0.17	<1	1.85	15.8	0.06	<1
	4	*Measurement*	0.30	6.4			0.95	10.8			1.86	15.3		
		WVDM$_{Gk,mea}$	0.30	6.5	0.00	<1	0.95	10.9	0.01	<1	1.85	15.4	0.00	<1
		***WVDM*$_{Gk,calc}$**	0.30	6.6	0.00	<1	1.05	11.1	0.10	<1	1.85	15.9	0.01	<1
	5	*Measurement*	0.33	6.3			1.16	10.7			2.09	15.3		
		WVDM$_{Gk,mea}$	0.33	6.5	0.00	<1	1.15	10.8	0.01	<1	2.09	15.4	0.01	<1
		***WVDM*$_{Gk,calc}$**	0.33	6.5	0.00	<1	1.29	10.9	0.13	<1	1.97	15.9	0.12	<1
7		*Measurement*	1.49	10.9			3.61	18.4			5.87	26.7		
	1	*WVDM*$_{Gk,mea}$	1.54	11.5	0.05	<1	3.71	19.4	0.10	0.9	5.93	28.5	0.07	1.8
		***WVDM*$_{Gk,calc}$**	1.44	11.4	0.05	<1	4.00	19.4	0.39	1.0	6.37	28.8	0.51	2.0
	2	*Measurement*	2.76	9.4			6.19	16.2			9.13	24.2		
		WVDM$_{Gk,mea}$	2.84	9.7	0.07	<1	6.34	16.3	0.16	<1	9.23	24.3	0.11	<1
		***WVDM*$_{Gk,calc}$**	2.83	8.1	0.06	1.3	6.45	14.2	0.26	2.0	8.61	22.8	0.52	1.4
	3	*Measurement*	2.21	9.8			5.08	16.8			7.70	24.8		
		WVDM$_{Gk,mea}$	2.27	10.2	0.06	<1	5.21	17.2	0.13	0.4	7.76	26.2	0.06	1.4
		***WVDM*$_{Gk,calc}$**	2.29	9.0	0.08	<1	5.62	15.7	0.54	1.1	7.97	26.1	0.27	1.3
	4	*Measurement*	2.34	10.2			5.36	17.4			8.18	25.5		
		WVDM$_{Gk,mea}$	2.41	10.5	0.07	<1	5.52	17.7	0.15	<1	8.26	25.9	0.07	<1
		***WVDM*$_{Gk,calc}$**	2.43	9.7	0.09	<1	5.94	16.7	0.58	0.7	8.49	25.7	0.31	<1
	5	*Measurement*	2.58	9.4			5.79	16.2			8.52	24.1		
		WVDM$_{Gk,mea}$	2.65	9.7	0.07	<1	5.93	16.3	0.15	<1	8.63	24.1	0.11	<1
		***WVDM*$_{Gk,calc}$**	2.69	8.0	0.11	1.3	6.21	14.1	0.42	2.0	8.33	22.6	0.19	1.5

4 Harmonic effect on rectifier circuits

4.1 Triangle expressions of time domain response

In advanced signal processing, triangular waveforms are employed both for system analysis and for signal synthesis due to their simplicity and basic harmonic structure. In their most fundamental form, triangular waves can be generated by the superposition of odd harmonics of a sine wave, with their amplitudes in the frequency domain inversely proportional to the square of the harmonic number, resulting in a clear, repetitive pattern that simplifies many types of analyses. Moreover, the linear rise and fall of triangular waveforms also make them suitable approximations for signals with sharp transitions, which can be advantageous in non-linear dynamic systems analysis.

Harmonic currents flow through the impedance of the power distribution system, which can cause voltage distortion, leading to higher peak voltage values. Supply voltage waveform can be represented as

$$u_{LVAC}(t) = U_{1M} \cdot sin(\omega_1 t + \varphi_1) + U_{2M} \cdot sin(\omega_2 t + \varphi_2) + \cdots + U_{NM} \cdot sin(\omega_N t + \varphi_N) \quad (4.1)$$

Ideally, series (*(2.10*) contains all harmonics but usually, odd order harmonics have much more dominant role in the waveshape. This is due to repeated shape of waveforms, and even order harmonics appear more dominant once there is variation in cycle waveforms. Thus in the following, attention is only paid on the odd order harmonics and even order harmonics are counted as having a magnitude of 0.

For the analytic expression formulation, it has to be emphasized that the harmonic components arise from the description of the time-domain waveform. Load current harmonic deviations emerge due to time-domain current waveform deviations. Therefore, analytic expression of the harmonic components will arise from time-domain current expression. The main expression for the LED lamp AC load will be defined through the operation of a rectifier.

Rectification operation time-domain waveforms are dependent on supply voltage waveform, evident from basic circuit analysis and measurements. The LED lamp structure employs a rectifier with a bulk capacitance C_B (reference to Figure 2.9), followed by a circuit to supply the light emitting component(s). In the literature, extensive investigation and circuit formulations are available for a typical rectifier, however for present thesis context only an ideal circuit is assumed. This is due to many simplifications on the path to describe the analytical structure of harmonic currents, described further in this chapter. Adding more detailed circuit model at this time, does not serve to provide better accuracy nor success; detailed circuit concept analysis will be part of future research.

The typical current waveshape of a common LED lamp is shown in Figure 4.1, which zooms in to the diode conduction starting and concluding time, during a positive half-cycle of the supply voltage. In voltage waveform, one of characteristic points is the peak voltage instant, time of peak (t_{peak}). When rectified voltage appearing on capacitor terminals reaches a value close to peak value U_{peak}, the current conduction stops. This is current conduction termination instant (t_{term}). Current conduction starts, when the supply voltage level intercepts the CB voltage level in the first quarter of supply voltage cycle. This is the conduction initiation instant (t_{init}). Along momentarily after the conduction initiation a peak current instant is occurring ($t_{i,peak}$), where the rectifier current has the peak level ($I_{Load,peak}$).

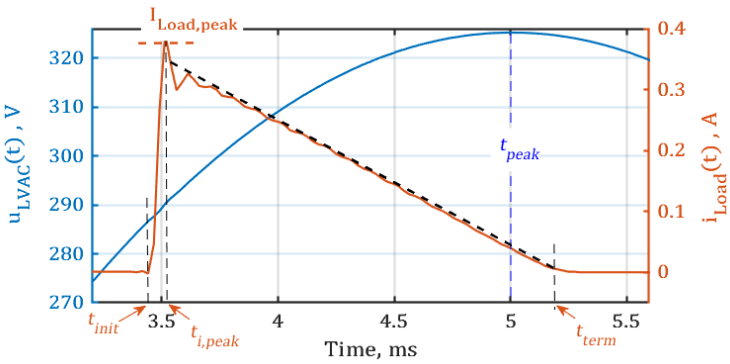

Figure 4.1 Close-up of conduction half-cycle of a rectifier current (published in article VI).

For the sake of simplicity in the analytical observation, several assumptions are made and the current waveform is reflected on a basis.

1) It is assumed that LED load current waveform is triangular shaped. The slope of the load current can be considered as linear function that depends on time (dotted black line, see Figure 4.1).
2) It is assumed that the t_{init} and $t_{i,peak}$ are very close, so that they are practically occurring in the same instant t_{init}.
3) Three vertexes of the triangle are observed, and the function the current (dotted black line) can be found using the slope of the two points ({t_{init}, $i_{L,peak}$} and {t_{peak}, 0}). The function the load current is calculated as using slope formula.

$$\frac{t - t_{init}}{t_{peak} - t_{init}} = \frac{i_{Load}(t) - I_{Load,peak}}{0 - I_{Laod,peak}} \tag{4.2}$$

$$i_{Load}(t) = \frac{-(t - t_{init})I_{Laod,peak}}{t_{peak} - t_{init}} + I_{Load,peak} \tag{4.3}$$

Where the $i_{L,peak}$ is the peak value of the load current.

4) t_{term} and t_{peak} are very close, so they are assumed to be same instant i.e. t_{peak}
5) U_{CBmax} will be assumed to be obtained when U_{LVAC} has peak value. Rectifier conduction will terminate after the peak instant.

The resulting triangle specification is provided in Figure 4.2.

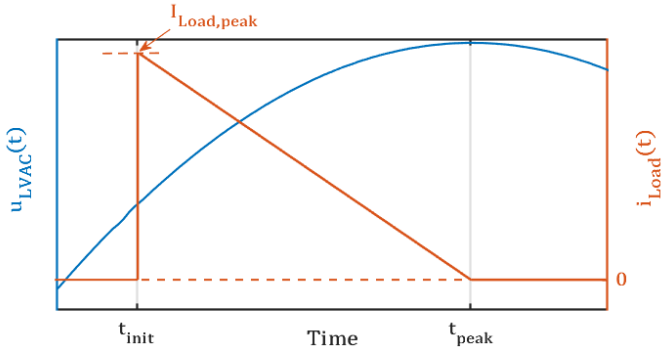

Figure 4.2 Triangular shape assumption of the load current.

Empirical results from (section 2.7) refer that the characteristics of harmonics are proportionally evident from t_{init} and I_{peak} values. The model waveform presented in Figure 4.2 is using thus same variables in the basis.

The waveshape of the current $i_{Load}(t)$ neither follows odd symmetry nor even symmetry, but it is *half-wave* symmetric. As the half-wave symmetry principle of the Fourier series

$$f\left(t-\frac{T}{2}\right) = -f(t) \tag{4.4}$$

And the Fourier coefficients for *half-wave* symmetry become

$$a_0 = 0 \tag{4.5}$$

$$a_n = \begin{cases} \frac{4}{T}\int_0^{T/2} f(t)\,cos(n\omega t)\,dt & for\ n\ odd \\ 0 & for\ n\ even \end{cases} \tag{4.6}$$

$$b_n = \begin{cases} \frac{4}{T}\int_0^{T/2} f(t)\,sin(n\omega t)\,dt & for\ n\ odd \\ 0 & for\ n\ even \end{cases} \tag{4.7}$$

So now using equations (4.6) & (4.7) the Fourier coefficients for the load current (a_{niL} & b_{niL})can be found as

$$a_{n_I} = \frac{4}{T}\int_0^{T/2} i_{Load}(t)\,cos(n\omega_1 t)\,dt \tag{4.8}$$

And value of the current exists only between t_{init} and t_{peak}, so the limits of the definite integral become

$$a_{n_I} = \frac{4}{T}\int_{t_{init}}^{t_{peak}} i_{Load}(t)\,cos(n\omega_1 t)\,dt \tag{4.9}$$

$$a_{n_{iL}} = \frac{4}{T}\left[\frac{i_{Load,peak}\{n\omega_1(t_{peak}-t_{init})\,sin(n\omega_1 t_{iinit}) - cos(n\omega_1 t_{init}) + cos(n\omega_1 t_{peak})\}}{n^2\omega_1^2\,(t_{init}-t_{peak})}\right] \tag{4.10}$$

Similarly

$$b_{n_I} = \frac{4}{T}\int_{t_{init}}^{t_{peak}} i_{Load}(t)\,sin(n\omega_1 t)\,dt \tag{4.11}$$

$$b_{n_{iL}} = \frac{4}{T}\left[\frac{i_{Load,peak}\{n\omega_1(t_{init}-t_{peak})\,cos(n\omega_1 t_{init}) - sin(n\omega_1 t_{init}) + sin(n\omega_1 t_{peak})\}}{n^2\omega_1^2\,(t_{init}-t_{peak})}\right] \tag{4.12}$$

The Fourier series of the current waveform can be found for using the equation (2.10) or (2.12), when the value of t_{init}, $t_{peak\ end}$, $I_{Load,peak}$ are known.

The derivations of the variables in (4.10) and (4.12) can be developed as follows:

1) t_{peak} where the peak $U_{LVAC,max} = U_{peak}$ instant occurs will be defined. This is most deterministic point of the supply waveform.

2) U_{peak} will be calculated knowing t_{peak} value. While this is basically available from (4.1), a more computationally efficient formula would be targeted.
3) U_{init} value will be determined, upon which the current conduction is initiated.
4) Knowing U_{init} value, a value for t_{init} will be determined.
5) Knowing t_{init} value, the value for $I_{Load,peak}$ will be determined.

In the scope of this thesis the first two expressions, t_{peak} and U_{peak} will be observed.

4.2 Analytical expression for peak voltage instants

In this section analytical approach has been defined that would provide a more detailed and general expression on the formulation of the rectifier circuit operation. Target of the expressions derivation is to provide analytical format to the peak voltage timing (related to rectifier diode conduction cut-off) and peak voltage level (related to the bulk capacitor voltage level at conduction cut-off). Discussion presented aims to provide base for the AC load current harmonic model development for rectifier circuit-based load devices taking into account supply voltage harmonics presence.

Majority of the energy efficient devices commercially available contains rectifier circuitry. Figure 4.3 shows the rectifier circuit commonly present in energy-efficient LED lamps. Rectification operation is dependent on supply voltage waveform shape; When rectified voltage appearing on capacitor terminal reaches its peak value, the current conduction stops [83]–[86]. The end-of-conduction time varies depending upon the peak value instant of the voltage waveform [87], [88]. The effect of different supply voltage harmonics, on the operation of rectifier circuits are analysed empirically in [42], [89], [90]. In the context of this thesis, an A-type waveshape common to LED lamp has been selected for analysis and is shown in Figure 4.4.

The time of peak (t_{peak}) value in voltage waveform is dependent on the amplitude and phase angle of the voltage harmonic present [91], [92]; this t_{peak} is end-of-conduction moment of the current of rectifier [93]. In case of pure sinusoidal supply, peak voltage is supposed to occur at 90 degrees phase instant. With voltage harmonic present in the supply, the resultant peak does will be offset from 90 degrees instant. This mean harmonics present in the load current also are affected dependent on the offset of instance of resultant peak voltage. Figure 4.4 shows some more extreme examples of supply voltage waveforms, flat and pointed top waveforms that could usually be available in the industrial LV network. In these cases, it is clear that the peak voltage available for the rectifier's capacitor charging operation will differ.

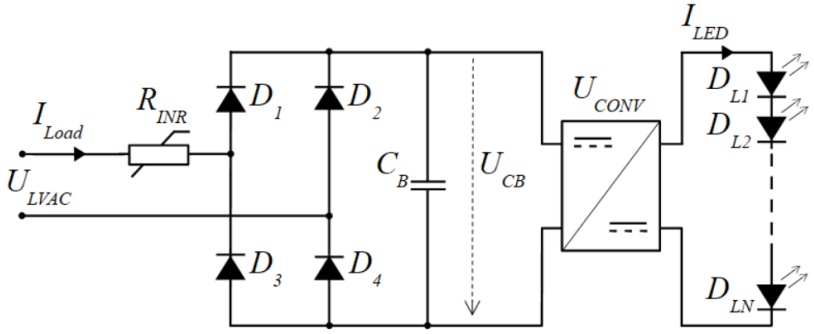

Figure 4.3 Rectifier circuit in LED lamp [94].

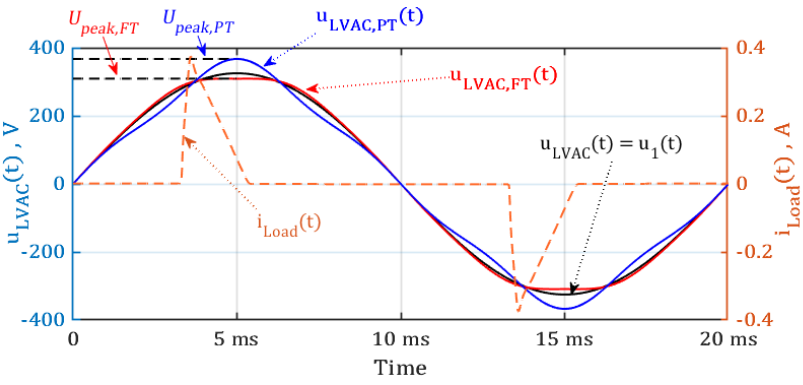

Figure 4.4 Supply voltage (pure-sine Flat-top(FT) & pointed-top(PT) waveforms and Current waveform of LED lamp (Previously published in article VI).

4.2.1 Voltage waveform numerical analysis

In discussing the influence of harmonics on peak voltage, it is essential to consider the role of the phase angle of harmonic voltage in altering the supply waveform. A significant factor in this alteration is the expected shift in peak value moments ($\triangle\varphi_{peak}$) associated with the phase shift of harmonic voltage, as illustrated in Figure 4.5. The resulting symmetrical shape, as depicted in Figure 4.6 and Figure 4.7, reflects the impact of a single voltage harmonic with varying amplitudes on the peak value moment shift.

In the following context, let us assume there is just two components present in the supply voltage waveform equation (4.1, the main harmonic with magnitude value U_1 and a harmonic component of order y with magnitude value U_y. In essence, the peak voltage value can be calculated at any time instant, using the common expression of sine components as

$$U_{Peak} = U_1 \cdot sin\left(\omega_1 \cdot t_{peak}\right) + U_y \cdot sin\left(y \cdot \omega_1 \cdot t_{peak} + \varphi_y\right) \tag{4.13}$$

or expressed phase-wise towards main harmonic 0 phase as

$$U_{Peak} = U_1 \cdot sin\left(\varphi_{Peak}\right) + U_y \cdot sin\left(y \cdot \varphi_{Peak} + \varphi_y\right) \tag{4.14}$$

It is noteworthy that the main harmonic initiation (zero phase) is assumed to occur at time $t = 0$. Here the φ_y is the harmonic voltage component U_y phase angle from the main harmonic zero phase value and U_y is the harmonic voltage component magnitude value.

Analytically, the peak instant (end of conduction time of capacitor) can be found where the voltage derivative approaches to zero; as expressed in the following equation.

$$max\{u_{LVAC}(t)\} \Rightarrow \frac{du_{LVAC}(t)}{dt} = 0 \tag{4.15}$$

The voltage on capacitor (U_{CB}) in rectifier circuit reaches to its peak when $u_{LVAC}(t)$ reaches its maximum.

$$U_{CB_{MAX}} = max\{u_{LVAC}(t)\}\,/_{T_{50Hz}} \tag{4.16}$$

Numerically the peak voltage value is straightforward to find. For any input U_y and φ_y the waveform could be assumed through finite time-step calculation and using (*4.13*) for any time step. An example of the outcome of numerical calculations is presented in Figure 4.9.

In order to find the analytical expressions of the characteristic parameters of the peak voltage absolute value and it's timing a more universal approach will be needed. Assuming the harmonic voltage component could have any phase angle and any magnitude the numerical descriptions may lack effectiveness for universal analysis. The complexity of the voltage peak moment timing is presented through expressions for peak phase value range in Figure 4.6 and Figure 4.7 for the peak value range. The eccentricity expression found in the numerical results refers to examples of Kepler equation, known to be unsolvable by geometric relations.

Details on the expressions of the peak voltage have more support from the analysis on dynamics of the supply voltage sinewave components. For the voltage peak time instant t_{peak}, the first order differentials of fundamental and influencer harmonic are equal in magnitude. Referring to equation (2.28)

$$\frac{d}{dt}u_1(t_{peak}) = -\frac{d}{dt}u_y(t_{peak}) \tag{4.17}$$

$$U_1 \cdot \omega_1 \cdot cos(\omega_1 t_{peak}) = -U_y \cdot \omega_1 \cdot y \cdot cos(y\omega_1 t_{peak} + \varphi_y) \tag{4.18}$$

Simplified into

$$U_1 \cdot cos(\omega_1 t_{peak}) = -U_y \cdot y \cdot cos(y\omega_1 t_{peak} + \varphi_y) \tag{4.19}$$

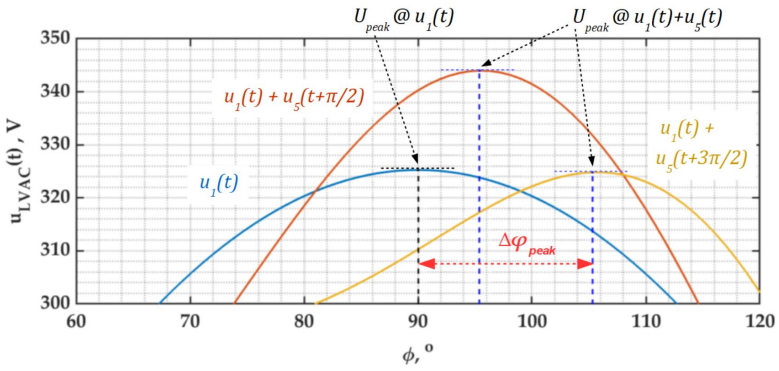

Figure 4.5 Peak instant response to harmonic phase angle (Previously published in article VI).

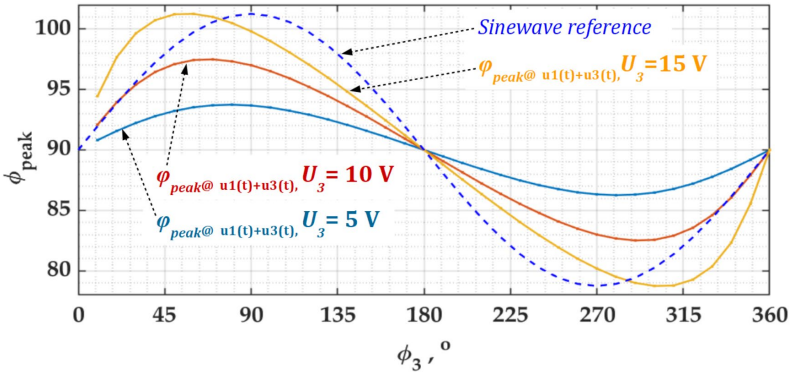

Figure 4.6 Variation in peak instant depending on harmonic phase angle (Previously published in article VI).

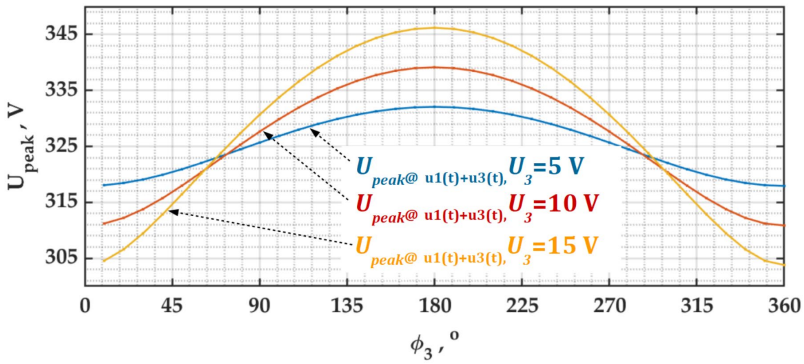

Figure 4.7 Variation in peak depending on harmonic phase angle (previously published in article VI).

From the numerical response results of φ_{peak} and U_{peak}, shown in Figure 4.6 and Figure 4.7 the corresponding eccentric periodic function can be seen to emerge. It can be seen that for any $\boldsymbol{U_y}$ phase φ_y rotation through 360° the function value will reoccur. For the description of the periodic function it will be assumed in the following

1) The function is basically a (co)sinusoidal form, where the argument is a function of U_y and φ_y.

$$U_{peak} = U_{1peak} + U_{peak,M} \cdot sin\left(\gamma_{Upeak}\right) \tag{4.20}$$

$$\varphi_{peak} = \varphi_{1peak} + \varphi_{peak,M} \cdot sin\left(\gamma_{\varphi peak}\right) \tag{4.21}$$

   Here $U_{peak,M}$ is the maximum difference between U_{1peak} and resultant peak voltage of waveform, and $\varphi_{peak,M}$ is the maximum difference between φ_{1peak} and peak-time of resultant waveform; γ_{Upeak} and $\gamma_{\varphi peak}$ are the function of added voltage harmonic level and phase angle.
2) The functions can be described for their characteristic points where U_{peak}=$U_{1,peak}$±$U_{peak,M}$, meaning the sin function argument in (4.20) is either 90° or 270°. This is termed as Case 1 points in the following subchapter.
3) The functions can be described for their characteristic points where t_{peak}=$t_{1,peak}$±$\Delta t_{peak,M}$, meaning the sin function argument in (4.21) is either 90° or 270°. This is termed as Case 2 points in the following subchapter.
4) The functions can be described for their characteristic points where U_{peak} = U_{1peak}, meaning the sin function argument in (4.20) is either 0° or 180°. This is termed as Case 3 points in the following subchapter.
5) The peak timing points where t_{peak}=$t_{1,peak}$ are essentially the same time instants as $t_{1,peak}$, meaning that the sin function argument in (4.21) is either 0° or 180°. This occurs at the same time instant as main harmonic 90° or 270° instants.

4.2.2 Dynamic expressions for peak voltage instant

The characteristic peak voltage observation cases will be listed below.

Case 1. Peak voltage highest and lowest magnitude expressions

Search for the peak voltage maximum possible value reveals that upon time instant when $u_1(t_{peak})$ and $u_y(t_{peak})$ components are both at maximum. Here sum of magnitude values will provide U_{peak}. This is when the sin components will both yield value of "1" i.e. the sin argument is π/2

$$U_{peak,max} = U_1 \cdot sin\left(\frac{\pi}{2}\right) + U_y \cdot sin\left(\frac{\pi}{2}\right) \quad (4.22)$$

given that harmonic phase angle is at *y* times higher than the main harmonic, the harmonic component angle which provides the π/2 at the time of U_1 magnitude peak will be

$$\varphi_{y,peak,max} = y \cdot \pi/2 \quad (4.23)$$

In case of odd harmonics, it should be noted that system with only 3rd harmonic added will provide peaking when $\varphi_{U3} = -90^o$ while for 5th harmonic added will respond with peak voltage maximum when $\varphi_{U5} = 90^o$. Similarly, the lowest magnitudes will be provided by harmonic phase angles with 180° modification.

Case 2. Maximum shift of the peak time instant from peak instant of only fundamental component (i.e. 90° or π/2) $\Delta\varphi_{peak,max}$.

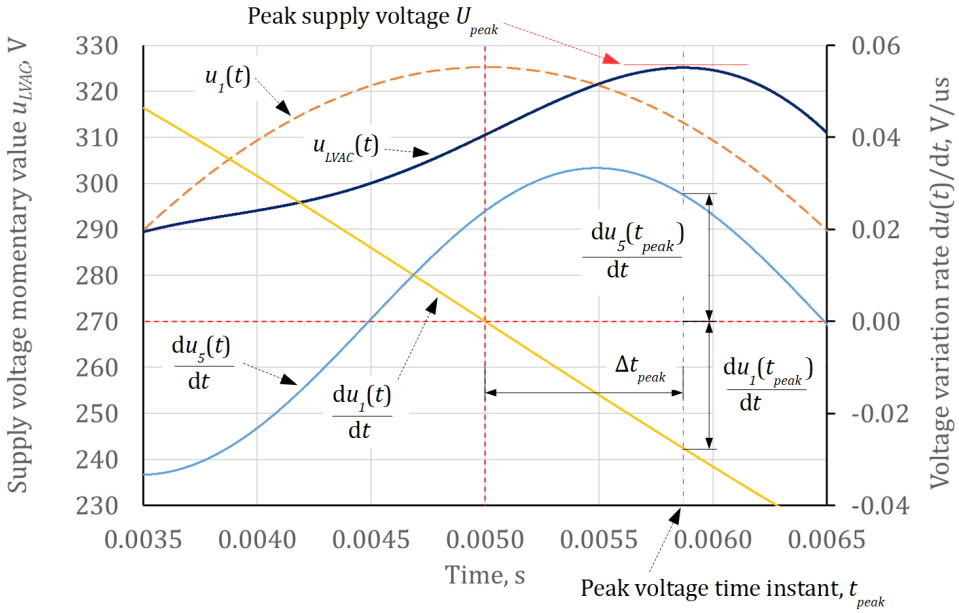

Figure 4.8 Variation in peak time instant depending on harmonic phase angle (previously published in article VI).

The peak time instant maximum shift $t_{peak,\Delta\varphi max}$ occurs when the first order derivative of the harmonic component variation is at its maximum; therefore

$$\left\{\frac{d}{dt}u_y\left(t_{peak,\Delta\varphi_{max}}\right)\right\}_{max} = U_y \cdot y \cdot \omega_1 \quad (4.24)$$

Assuming (4.22) this occurs at time instant when ($y \cdot \omega \cdot t_{peak} + \varphi_{Uy}$) provides total of 0. Therefore, the peak phase excursion occurs at instant for the harmonic when

$$\varphi_{Uy} = y \cdot \omega_1 \cdot t_{peak}$$

From (4.24)

$$cos\left(\omega_1 t_{peak,\Delta\varphi_{max}}\right) = \frac{U_y}{U_1} y \tag{4.25}$$

and replacing

$$A = \frac{U_1}{U_y} \tag{4.26}$$

the expression will be

$$t_{peak,\Delta\varphi_{MAX}} = \frac{cos^{-1}\frac{y}{A}}{\omega_1} \tag{4.27}$$

Case 3. Instant when peak voltage level of the combined waveform with $U_1 + U_y$ is ***equal*** to fundamental harmonic waveform peak; it is the point when there is peak voltage equal to magnitude level of U_1

$$U_1 = U_1\, sin(\omega_1 \cdot t) + U_x\, sin(y\omega_1 t + \varphi_y) \tag{4.28}$$

Here U_1 is the magnitude of fundamental component i.e. for 230 V_{rms} this will have level of 325 V. U_y is the amplitude of supply voltage harmonic component, φ_y is the phase angle of the voltage harmonic component.

Empirical value calculation of the crossing point of harmonic (U_y) near 90^o of fundamental harmonic on fundamental harmonic scale

$$t_{cross,y} = \frac{T_1}{y}\left(\frac{1}{4}(y+1) - \frac{\varphi_y}{2\pi}\right) \tag{4.29}$$

$$\varphi_{cross,y} = 2\pi\,\frac{t_{cross,y}}{T_1} \tag{4.30}$$

Where y is a harmonic number. T_1 = 0.02 s time-period of fundamental harmonic. Now, transforming the equations ((4.13) and ((4.17) to phase angle domain

$$U_1 = U_1\, sin\left(90^o - \varphi_{peak}\right) + U_y\, sin\,\varphi_{y,c} \tag{4.31}$$

$$U_1\, cos\left(90^o + \varphi_{peak}\right) = -y \cdot U_y \cdot cos\,\varphi_{y,c} \tag{4.32}$$

Here φ_{peak} is phase distance between peak of fundamental component (i.e. 90^o or π/2) and peak of $u_{LVAC}(t)$ expressed in degrees on fundamental harmonic scale and $\varphi_{y,c}$ is distance between peak of $u_{LVAC}(t)$ and the zero crossing instant of the voltage harmonic component.

From (4.31)

$$sin\,\varphi_{y,c} = \frac{U_1}{U_y} - \frac{U_1}{U_y} sin\left(90^o - \varphi_{peak}\right) \tag{4.33}$$

$$sin\,\varphi_{y,c} = A\,[1 - cos\,\varphi_{peak}] \tag{4.34}$$

From (4.32)

$$\frac{U_1}{U_y \cdot y} cos\left(90^o + \varphi_{peak}\right) = -\cos\varphi_{y,c} \tag{4.35}$$

As *cos* is an even function

$$\frac{A}{y} cos\left(90^o + \varphi_{peak}\right) = \cos\varphi_{y,c} \tag{4.36}$$

$$\frac{A}{y} cos\left(90^o + \varphi_{peak}\right) = 1 - [sin\,\varphi_{y,c}]^2 \tag{4.37}$$

$$sin\,\varphi_{y,c} = \sqrt{1 - \left[\frac{A}{y} cos\left(90^o + \varphi_{peak}\right)\right]^2} \tag{4.38}$$

Equating *(4.34*) and *(4.38*) provides

$$A^2\left[1 - cos\left(\varphi_{peak}\right)\right]^2 = 1 - \left[\frac{A}{y} cos\left(90^o + \varphi_{peak}\right)\right]^2 \tag{4.39}$$

and this can be developed into

$$\left[A^2 - \frac{A^2}{x^2}\right](cos\,\varphi_{peak})^2 - 2A^2\,cos\,\varphi_{peak} + +A^2 + \frac{A^2}{y^2} - 1 = 0 \tag{4.40}$$

Substituting $Q = \cos(\varphi_{peak})$

$$\left[1 - \frac{1}{y^2}\right] \cdot Q^2 - 2 \cdot Q + 1 + \frac{1}{y^2} - \frac{1}{A^2} = 0 \tag{4.41}$$

Coefficients of quadratic equations are

$$a = \left(1 - \tfrac{1}{y^2}\right), \text{ b = – 2 and c} = 1 + \tfrac{1}{y^2} - \tfrac{1}{A^2}$$

from value of $cos(\varphi_{peak})$ by quadratic solution, $\boldsymbol{\varphi_{peak}}$ can be determined.

Now in order to determine the value of $\boldsymbol{\varphi_{y,c}}$, similar expressions with (4.31) and (4.32) can be used. For development of relation for $\boldsymbol{\varphi_{y,c}}$, (4.31) will be expressed as

$$sin\left(90^o - \varphi_{peak}\right) = 1 + \frac{U_y}{U_1} sin\,\varphi_{y,c} \tag{4.42}$$

and

$$cos\,\varphi_{peak} = 1 + \frac{sin\,\varphi_{y,c}}{A} \tag{4.43}$$

Now (4.32) becomes

$$\cos\left(90^o + \varphi_{peak}\right) = -\frac{U_y}{U_1} \cdot y \cdot \cos\varphi_{y,c}$$

$$-sin\,\varphi_{peak} = -\frac{y \cdot cos\,\varphi_{y,c}}{A} \tag{4.44}$$

Squaring and adding (4.43) and (4.44)

$$\left(\frac{y \cdot cos\ \varphi_{y,c}}{A}\right)^2 + \left(1 + \frac{sin\ \varphi_{y,c}}{A}\right)^2 = 1 \tag{4.45}$$

$$(1 - y^2)\left(sin\ \varphi_{y,c}\right)^2 - 2A\ sin\ \varphi_{y,c} + y^2 = 0 \tag{4.46}$$

Coefficients of quadratic equations are

$$a = (1 - y^2),\ \text{b} = -2\text{A and } \text{c} = y^2\ .$$

from value of $sin(\varphi_{y,c})$ by quadratic solution, $\varphi_{y,c}$ can be determined.

4.2.3 Results and verification

From equation (4.41) and (4.46)

$$\varphi_{peak} = cos^{-1}\left\{\frac{-(-2) \pm \sqrt{(-2)^2 - 4\left(1 - \frac{1}{y^2}\right)\left(1 + \frac{1}{y^2} - \frac{1}{A^2}\right)}}{2\left(1 - \frac{1}{y^2}\right)}\right\} \tag{4.47}$$

$$\varphi_{y,c} = sin^{-1}\left\{\frac{-(-2A) \pm \sqrt{(-2A)^2 - 4(1 - y^2)y^2}}{2(1 - y^2)}\right\} \tag{4.48}$$

Mathematically, there are two possible solutions for every quadratic equation. And depending on the value of coefficients, one or both of the solutions can result a complex value. Equation (24) calculates the distance of zero crossing of the harmonic component and the modified peak of the resultant waveform; out of two quadratic solutions, the positive-real solution is taken as argument of inverse sine function (sin^{-1}), in equation (24). With U_{yRMS} = 10 V and U_{1RMS} = 230 V, 'A' becomes 23; the x = 5 for supply harmonic order 5. The quadratic solutions here are 0.442 and –2.36. As the argument of inverse sine can be {–1…1} one value of a solution remains

$$\varphi_{y,c} = \sin^{-1}(0.442) = \begin{cases} 26.3^o \\ -\ 26.3^\circ \end{cases}$$

It has to be noted that $\varphi_{y,c}$ is x-times smaller on the fundamental harmonic scale i.e. 5.3°. Furthermore, $\varphi_{y,c}$ refers to the exact instant where $u_1(t)$ and $u_{LVAC}(t)$ waveforms cross each other (see Figure 4.9). Similarly, the φ_{peak} can be calculated using the inverse cosine (cos^{-1}) function to the solution of quadratic equation mention in ((4.40). For the above-mentioned values of harmonic amplitudes and included voltage harmonic order, the calculated cos^{-1} argument value is 1.103 and 0.981. Similar to the inverse sine function, the argument of cos^{-1} also cannot exceed the range {–1…1}, so φ_{peak} is calculated as

$$\varphi_{peak} = \cos^{-1}(0.981) = 78.8^\circ$$

Hereby, the peak shift for the fundamental component timing will be

$$\Delta\varphi_{peak} = |90^o - 78.8^o| = 11.2^\circ.$$

These calculated values (φ_{peak} , $\Delta\varphi_{peak}$ *and* $\varphi_{y,c}$) match the measured values, as illustrated in Figure 4.9 below and Table 4.1. The value of $\Delta\varphi_{peak}$ can be converted to equivalent time precisely i.e. $t_{peak,\Delta U=0}$.

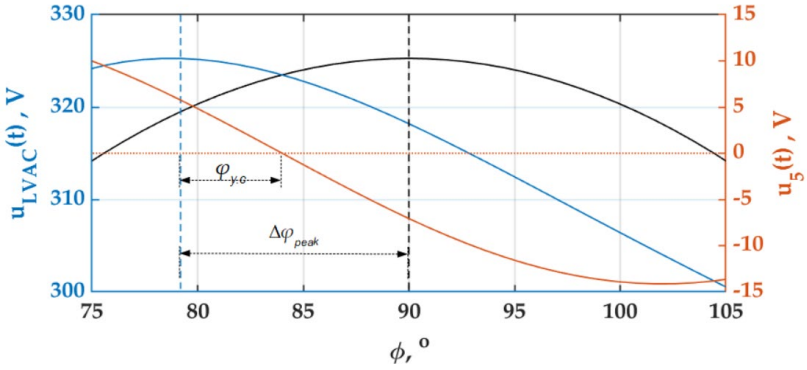

Figure 4.9 Distance calculation of zero crossing of influencer harmonic and fundamental-component's peak toward peak instant of $u_{LVAC}(t)$ (previously published in article VI).

Table 4.1 show the calculated values (referring to equation (4.27) of maximum shift of peak phase instant, $\Delta\varphi_{peak,max}$, peak time instant maximum shift $t_{peak,\Delta\varphi max}$, referred as **case 1**. It has to be noted that as the amplitude level of the higher harmonics (for example 7^{th}) increases, the resultant voltage waveform will have multiple peak or have two equal peaks. Therefore the calculation values can point out only one dominant value out of multiple peak values. Table II presents the comparison of measured and calculated values of peak instant phase values and harmonic component zero crossing instants; under the equations (4.46) & (4.47) mentioned under **case 2**. The value presented in Table 4.2 provides considerable accuracy to measurements. The proof of accuracy of the developed equation can be further acquired by comparing with measurements recorded (for a dedicated amplitude and phase of influencer harmonic) as mentioned in table III.

Table 4.1 Modelled/calculated value of maximum peak stretch on time axis for any level of influencer harmonic

Harmonic order	U_{yRMS} *level*	$\varphi_{peak,max}$		$t_{peak,\Delta\varphi max}$
y	**V**	**°**	**rad**	**ms**
3	5	86.3	1.51	4.79
	10	82.5	1.44	4.58
	15	78.7	1.37	4.37
	20	74.9	1.31	4.16
	25	71.0	1.24	3.94
5	5	83.8	1.46	4.65
	10	77.4	1.35	4.30
	15	71.0	1.24	3.94
	20	64.2	1.12	3.57
	25	57.1	0.99	3.17
7	5	81.2	1.42	4.51
	10	72.3	1.26	4.02
	15	62.8	1.1	3.49
	20	52.5	0.92	2.92
	25	40.5	0.706	2.25

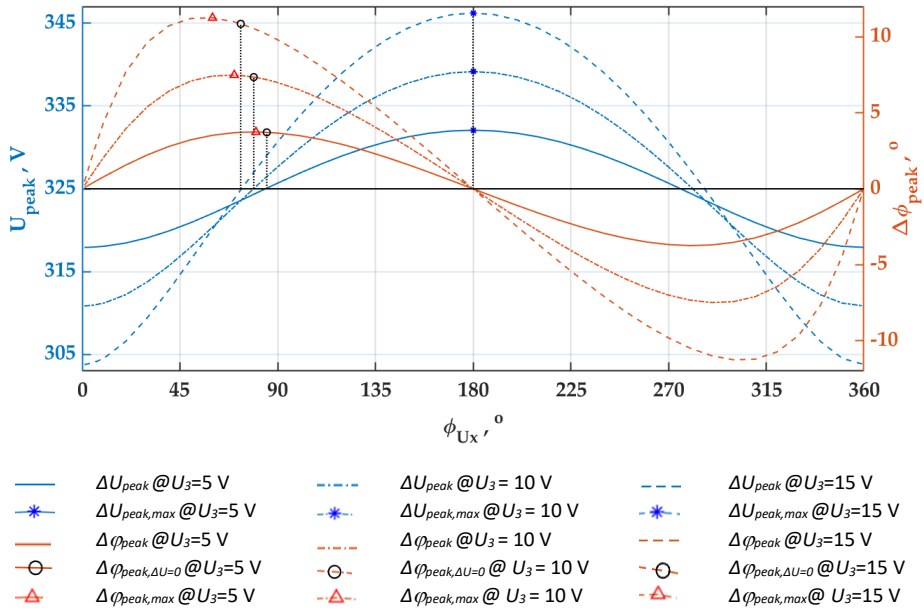

Figure 4.10 Results of U_{peak} and φ_{Upeak} instant of $u_{LVAC}(t)$ (previously published in article VI).

Table 4.2 Comparison of measured and calculated value of resultant peak stretch of $u_{LVAC}(t)$, magnitude identical to fundamental component

y	$U_{y,RMS}$, V	$\varphi_{peak,meas}$, °	$\varphi_{peak,calc}$ °	$\varphi_{y,c,meas}$, °	$\varphi_{y,c,calc}$, °	$\varphi_{cross,y,meas}$, °	$\varphi_{cross,y,calc}$, °
3	5	86.3	**86.3**	6.2	**5.6**	87.9	**88.1**
	10	82.6	**82.6**	11.1	**10.9**	86.3	**86.4**
	15	79.1	**79.2**	15.6	**15.9**	84.8	**84.7**
	20	75.9	**75.8**	20.4	**20.4**	83.2	**83.2**
	25	72.8	**72.7**	24.7	**24.5**	81.8	**81.8**
5	5	84.0	**84.0**	14.2	**14.8**	87.2	**87.0**
	10	78.8	**78.8**	26.2	**26.2**	84.8	**84.8**
	15	74.4	**74.4**	34.2	**34.4**	83.2	**83.1**
	20	70.7	**70.7**	40.5	**40.4**	81.9	**81.9**
	25	67.4	**67.4**	45.0	**45.0**	81.0	**81.0**
7	5	82.1	**82.1**	26.1	**25.7**	86.3	**86.3**
	10	76.6	**76.5**	40.6	**39.7**	84.2	**84.3**
	15	72.3	**72.1**	48.1	**47.7**	83.1	**83.2**

Table 4.3 Measured values at characteristic points of resultant peak phase stretch of $U_{LVAC}(t)$

case	***y***	**3**		**5**	
	U_{yRMS}, V	$\Delta\varphi_{peak}$, °	φ_y , °	$\Delta\varphi_{peak}$, °	φ_y , °
$\Delta\varphi_{peak}$ = max	5	3.8	80	6.2	120
	10	7.5	68	12.6	155
	15	11.3	55	18.8	185
ΔU_{peak} = 0	5	3.7	85	6.0	105
	10	7.4	79	11.3	120
	15	10.9	73	15.7	135
ΔU_{peak} = (max/min)	5	0	0; 180	0	0; 180
	10				
	15				

5 Conclusions and future work

5.1 Conclusions

This doctoral dissertation introduces an empirical and analytical methodology for estimating load current harmonic phasors characteristics within low-voltage networks. The proposed approach offers a direct and computationally less-intense estimation of the impact of nonlinear loads on distribution networks, compared to other state-of-the-art methods. Detailed attention is paid to energy-efficient loads, especially lighting loads as these are one of the most numerous and common ones in households. Contemporary energy efficient loads are basically all utilizing some switch-mode power supply as primary electric converter. The rectifier of the AC front-end with bulk capacitor is one of the common cores for every zero-carbon policy supporting load.

Thesis originates from the practical measurement results, whereas the sophistication of the relations between voltage and current harmonics has been clearly seen in the course of various measurement outcome. This has been reported previously in the literature, however without a specific physical relationship related to the phenomenon. It can be seen that either calculation methods selection or then engineering practical approach is often defining the scientific viewpoint of the approach taken. Common approach is purely frequency domain analysis. However, the naturally seeming relation between for example 250 Hz and 350 Hz components has to be explained outside the frequency domain.

The thesis develops a current harmonic estimation model foundation based on the nature of devices and power quality measurements across different voltage distortions. The harmonic profile of the load linked with the physical operation of the circuit component, like capacitor in converter circuit helps to understand the cross-order harmonic components relations. The models defined directly aid in estimating current harmonic emissions under real LV voltage distortions and addresses the cross-order coupling of the voltage harmonics on load current harmonics. In this case, the link of the cross-order coupling is not related to phasor relation common for the grid calculation methods. The link is in shown in time-domain timing shift of the load current waveform, a physically solid standpoint.

Deeper studies of base component effect and modelling of the sensitivity parameters of the estimation model demonstrate the effective and flexibility of the developed model, highlighting its potential to use reduced number of variables and less calculation and measurement burden. In recognizing the independence of the phase and magnitude variation characteristics, it has been provided that realistic measurement outcome in form of elliptic response to voltage harmonic phasors, can be effectively and in simpler relation calculated. The competing FCM waveform requires, for example, including tensor analysis for the characterization of the elliptic phasor endpoint response. The empirical model linear part in this thesis is providing already fair response, using straightforward geometric construct.

The WVDM proposed in the thesis assumes input data from the empirical measurements. Effective discretion between linear and nonlinear reaction parts allows to reach different outcome precision. The WVDM targets to include cross-harmonic influences for the final calculation of the realistic LV supply voltage waveform. WVDM is still empiric in its grounds and uses rather many measurement-based coefficients. It is shown that limits will emerge as WVDM is used for different levels of main harmonic *U1*.

The added coefficient burden is not in favour of empiric model and shows that for characterization of a particular load, number of identification measurements to determine the particular coefficient values will be very high.

Analytical definition of the harmonic current components is developed in the latest chapter of the thesis. It is clear from the start that inclusion of voltage harmonics adds to the initial complexity of Fourier transform. Functions identified to describe the analytic relations are non-linear and their outcome is formed from geometrical interrelations. Sophistication of the mathematical formulation requires fast reduction of complexity. Even as idealistic waveforms are presented for analysis, the expressions derived and proposed make up difficult-to-integrate concepts. Numerical results for the actual harmonics are referring to eccentric periodic functions usage. This type functions are known to the difficult to solve, Kepler function is available as an example of a classical analytically unsolved reference. Therefore, the reach is limited to only characteristic points estimation of analytical expressions. Expression development itself requires more detailed mathematical reasoning and is part of future work.

The proposed model harmonic current estimation is oriented towards residential grids, but is usable even for the industrial cases. However, proposed model is not valid for all industrial waveform presentations. Overall, the model serves as a crucial tool for estimating harmonic emissions, enhancing low voltage network operation detailing, and supporting network operators in planning upgrades or expansions, particularly in anticipation of increased penetration of nonlinear devices in the grid.

5.2 Future work

Distribution networks, particularly at low voltage (LV) levels, are encountering increasingly complicated challenges. Initiatives like constructing near-zero energy buildings, boosting renewable energy generation, adopting modern and efficient loads, and integrating domestic electric energy storage. However, these initiatives introduce powerful nonlinear power supply units, converters, and inverters into the distribution network, necessitating the network's ability to support them while maintaining specific operating characteristics, notably ensuring sufficient hosting capacity.

Thesis is looking at the load current harmonics modelling topics in a most trivial circuit cases. While common, this model is not aiming at loads using more AC-friendly devices. Approach to define also other loads' characterization options would be addressed in the next work, to include capabilities of estimation of power-factor-correction equipped harmonic response. This will be developed after the main relations for the type A LED lamp are identified and finalized. The circuit model improvement to incorporate the real rectifier waveform and its characteristics to harmonics modelling will be added.

The current model outlined in this thesis does not incorporate grid infeed units' (for example, photovoltaic (PV), battery storage) data. Additionally, while the implementation of battery storage may become essential in the future, it is not currently part of the model. Nonetheless, the model can presently assess the impact load current harmonics. Furthermore, there is potential to expand the model to include commercial (industrial) loads and upcoming penetration of high-power domestic energy management devices of 3-phase loading.

An additional possibility for development involves extending the model to incorporate a network model, building upon the results of the current harmonic estimation model. Utilising current and voltage values, this extension could provide network impedance values at different frequencies, thereby elucidating the influence of harmonics on grid

operation parameters. Moreover, ongoing efforts are directed towards refining a more detailed model that accounts for the influence of voltage waveform on load current harmonics emission.

Hosting capacity for more potent units is likely to reach its limits in at least some networks or network segments, potentially constraining the integration of new technologies until network improvements are made. Thus, the more capable load models serve as a crucial tool for assessing the impact of various policies and technologies on power supply system performance. For solutions such as energy conservation, distributed generation, smart buildings, electric vehicles etc it could be estimated that some limits of operation would be due to high distortion of the supply voltage. Thus the actuality of the topic of harmonic dependence will remain and be more prominent for the network engineers responding to upcoming challenges in distribution network.

List of figures

List of tables

References

[1] European Commission, “Directive (EU) 2023/959 of the European Parliament and of the Council of 10 May 2023 amending Directive 2003/87/EC establishing a system for greenhouse gas emission allowance trading within the Union and Decision (EU) 2015/1814 concerning the establishmen,” 2023.

[2] European Union, “PE-CONS 7/23 ECOFIN.2.B DMY/IC/cc,” vol. 2023, no. April, 2023.

[3] European Commission, *European Union (EcoDesign Requriements for certain Energy-related Products) (Amendment) Regulations 2022*, no. 8.5.2017. 2022, pp. 2003–2005.

[4] European Commission, “Non paper on complementary economic modelling undertaken by DG ENER analysing the impacts of overall energy efficiency target of 13% to 19% in the context of discussions in the European Parliament on the revision of the Energy Efficiency Directive,” 2022. [Online]. Available: https://energy.ec.europa.eu/data-and-analysis/energy-modelling/eu-reference-scenario-2020_en

[5] European Commission, “DIRECTIVE (EU) 2023/1791 OF THE EUROPEAN PARLIAMENT AND OF THE COUNCIL of 13 September 2023 on energy efficiency and amending Regulation (EU) 2023/955 (recast),” vol. 2016, no. 68, pp. 48–119, 2023.

[6] European Commission, “European Commission-Press release Simpler EU energy labels for lighting products applicable from 1 September,” no. March, 2021.

[7] European Commission, “Directive 2009/125/EC of the European Parliament and of the Council repealing Commission Regulations (EC) No 244/2009, (EC) No 245/2009 and (EU) No 1194/2012,” 2012.

[8] European Union, “Laying down ecodesign requirements for light sources and separate control gears pursuant to Directive 2009/125/EC of the European Parliament and of the Council,” 2013.

[9] M. N. Iqbal, L. Kütt, B. Asad, T. Vaimann, A. Rassõlkin, and G. L. Demidova, “Time dependency of current harmonics for switch-mode power supplies,” *Appl. Sci.*, vol. 10, no. 21, pp. 1–12, 2020, doi: 10.3390/app10217806.

[10] M. Jarkovoi, M. Naveed Iqbal, and L. Kutt, “Analysis of harmonic current stability and summation of LED lamps,” *2019 Electr. Power Qual. Supply Reliab. Conf. 2019 Symp. Electr. Eng. Mechatronics, PQ SEEM 2019*, pp. 1–8, 2019, doi: 10.1109/PQ.2019.8818237.

[11] B. Badrzadeh and M. Gupta, “Practical experiences and mitigation methods of harmonics in wind power plants,” *IEEE Trans. Ind. Appl.*, vol. 49, no. 5, pp. 2279–2289, 2013, doi: 10.1109/TIA.2013.2260314.

[12] Y. Xiao and X. Yang, “Harmonic summation and assessment based on probability distribution,” *IEEE Trans. Power Deliv.*, vol. 27, no. 2, pp. 1030–1032, 2012, doi: 10.1109/TPWRD.2012.2187124.

[13] IEEE-Std-519-2014 and IEEE Std 519-2014, “IEEE Recommended Practice and Requirements for Harmonic Control in Electric Power Systems,” *IEEE Stand. Assoc.*, 2014, doi: 10.1109/IEEESTD.2014.6826459.

[14] IEEE and IEEE Std 1159-2009, *IEEE Recommended Practice for Monitoring Electric Power Quality*, vol. 2019, no. 26 June. 2019. doi: 10.1109/IEEESTD.2009.5154067.

[15] IEC 61000-4-30: 2003, “Electromagnetic compatibility (EMC) Part 4-30: Testing and measurement techniques Power quality measurement methods,” *Int. Electrotech. Comm.*, 2003.

[16] IEC 61000-4-7:2009, “Electromagnetic compatibility (EMC) - Part 4-7: Testing and measurement techniques - General guide on harmonics and interharmonics measurements and instrumentation, for power supply systems and equipment connected thereto,” *Int. Electrotech. Comm.*, 2009.

[17] EVS-EN-50160: 2023, “Voltage characteristics of electricity supplied by public distribution networks.,” *CENELEC*, 2023.

[18] A. R. Kalair, N. Abas, A. R. Kalair, Z. Saleem, and N. Khan, “Review of harmonic analysis, modeling and mitigation techniques,” *Renew. Sustain. Energy Rev.*, vol. 78, no. February, pp. 1152–1187, 2017, doi: 10.1016/j.rser.2017.04.121.

[19] T. Theodoridis and J. Kraemer, *Electric Power Distribution Engineering*. 2015.

[20] A. Baggini, *Handbook of Power Quality*. 2008. doi: 10.1002/9780470754245.

[21] S. Chattopadhyay;, M. Mitra;, and S. Sengupta, *Electric Power Quality*.

[22] A. Elmoudi, M. Lehtonen, and H. Nordman, “Effect of harmonics on transformers loss of life,” *Conf. Rec. IEEE Int. Symp. Electr. Insul.*, vol. 2007, pp. 408–411, 2007, doi: 10.1109/elinsl.2006.1665344.

[23] European Union, “Directive 2014/30/EU Electromagnetic compatibility,” 2014.

[24] IEEE-Std-519-2014, “IEEE Recommended Practice and Requirements for Harmonic Control in Electric Power Systems,” *IEEE Stand. Assoc.*, 2014.

[25] IEC-61000-2-2:2002 and IEC 61000-2-2:2002, “Electromagnetic compatibility (EMC) - Environment - Compatibility levels for low-frequency conducted disturbances and signalling in public low-voltage power supply systems,” *Int. Electrotech. Comm.*, 2002.

[26] IEC 61000-2-4, “Environment- Compatibility levels in industrial plants for low-frequency conducted disturbances,” *Int. Electrotech. Comm.*, 2002.

[27] IEC 61000-2-5, “Environment – Description and classification of electromagnetic environments,” *Int. Electrotech. Comm.*, 2017.

[28] IEC 61000-3-2:2018, “Electromagnetic compatibility (EMC) - Part 3-2: Limits - Limits for harmonic current emissions (equipment input current ≤16 A per phase),” *Int. Electrotech. Comm.*, 2018.

[29] IEC-61000-4-7:2002, “Electromagnetic compatibility (EMC) - Part 4-7: Testing and measurement techniques - General guide on harmonics and interharmonics measurements and instrumentation, for power supply systems and equipment connected thereto,” *Int. Electrotech. Comm.*, 2002.

[30] D. Schwanz, M. Bollen, and A. Larsson, “A review of solutions for harmonic mitigation,” *Proc. Int. Conf. Harmon. Qual. Power, ICHQP*, vol. 2016-Decem, pp. 30–35, 2016, doi: 10.1109/ICHQP.2016.7783422.

[31] D. De Barcellos Martins, M. Oleskovicz, and B. R. Pereira Junior, “Application of Photovoltaic Generation for Harmonic Distortion Mitigation in a Microgrid,” *Proc. Int. Conf. Harmon. Qual. Power, ICHQP*, vol. 2022-May, 2022, doi: 10.1109/ICHQP53011.2022.9808606.

[32] N. Rugthaicharoencheep and S. Chaladying, “Technical and financial evaluation for investment of harmonic mitigation in power network,” in *2017 IEEE Manchester PowerTech, Powertech 2017*, 2017, pp. 1–5. doi: 10.1109/PTC.2017.7981079.

[33] D. Schwanz, M. Bollen, A. Larsson, and Ł. H. Kocewiak, “Harmonic mitigation in wind power plants: Active filter solutions,” *Proc. Int. Conf. Harmon. Qual. Power, ICHQP*, vol. 2016-Decem, pp. 220–225, 2016, doi: 10.1109/ICHQP.2016.7783321.

[34] M. N. Iqbal, L. Kutt, N. Shabbir, and B. Asad, “Comparison of Current Harmonic Emission by Different Lighting Technologies,” *2020 IEEE 61st Annu. Int. Sci. Conf. Power Electr. Eng. Riga Tech. Univ. RTUCON 2020 - Proc.*, pp. 1–5, 2020, doi: 10.1109/RTUCON51174.2020.9316615.

[35] J. Cunill-Solà and M. Salichs, “Study and Characterization of Waveforms From,” vol. 22, no. 4, pp. 2305–2311, 2007.

[36] D. Chakravorty, J. Meyer, P. Schegner, S. Yanchenko, and M. Schocke, “Impact of Modern Electronic Equipment on the Assessment of Network Harmonic Impedance,” *IEEE Trans. Smart Grid*, vol. 8, no. 1, pp. 382–390, 2017, doi: 10.1109/TSG.2016.2587120.

[37] A. J. Collin *et al.*, “Analysis of approaches for modeling the low frequency emission of LED lamps,” *Energies*, vol. 13, no. 7, pp. 1–33, 2020, doi: 10.3390/en13071571.

[38] J. Molina and L. Sainz, “Compact fluorescent lamp modeling for large-scale harmonic penetration studies,” *IEEE Trans. Power Deliv.*, vol. 30, no. 3, pp. 1523–1531, 2015, doi: 10.1109/TPWRD.2014.2363143.

[39] L. Kütt, E. Saarijarvi, M. Lehtonen, H. Mõlder, and J. Niitsoo, “Estimating the harmonic distortions in a distribution network supplying EV charging load using practical source data - Case example,” *IEEE Power Energy Soc. Gen. Meet.*, vol. 2014-Octob, no. October, pp. 4–8, 2014, doi: 10.1109/PESGM.2014.6939267.

[40] A. M. Blanco, S. Yanchenko, J. Meyer, and P. Schegner, “The impact of supply voltage distortion on the harmonic current emission of non-linear loads,” *DYNA*, vol. 82, no. 192, pp. 150–159, 2015, doi: 10.15446/dyna.v82n192.48591.

[41] M. N. Iqbal *et al.*, “Estimation of harmonic emission of electric vehicles and their impact on low voltage residential network,” *Sustain.*, vol. 13, no. 15, pp. 1–17, Aug. 2021, doi: 10.3390/su13158551.

[42] M. Rylander, W. M. Grady, and M. Narendorf, “Experimental apparatus, testing results, and interpretation of the impact of voltage distortion on the current distortion of typical single-phase loads,” *IEEE Trans. Power Deliv.*, vol. 24, no. 2, pp. 844–851, 2009, doi: 10.1109/TPWRD.2008.2002874.

[43] K. Daniel, L. Kütt, M. N. Iqbal, N. Shabbir, and M. Jarkovoi, “Description of Practical Load Harmonic Current Emission due to Voltage Harmonic Variation,” *2021 IEEE 62nd Int. Sci. Conf. Power Electr. Eng. Riga Tech. Univ. RTUCON 2021 - Proc.*, pp. 1–6, 2021, doi: 10.1109/RTUCON53541.2021.9711594.

[44] K. Daniel, L. Kütt, M. N. Iqbal, N. Shabbir, M. Parker, and M. Jarkovoi, “Waveform Variation Defined Model for Harmonic Current Emissions Including Cross-Order Supply Voltage Harmonics Influence,” *IEEE Access*, vol. 11, no. March, pp. 42276–42289, 2023, doi: 10.1109/ACCESS.2023.3270805.

[45] P. W. Lehn and K. L. Lian, “Frequency coupling matrix of a voltage-source converter derived from piecewise linear differential equations,” *IEEE Trans. Power Deliv.*, vol. 22, no. 3, pp. 1603–1612, 2007, doi: 10.1109/TPWRD.2006.886779.

[46] M. N. N. Iqbal, K. Lauri, L. Kütt, B. Asad, and N. Shabbir, “Impact of Cable Impedance on the Harmonic Emission of LED Lamps,” *21st Int. Sci. Conf. Electr. Power Eng.*, no. December, pp. 1–6, 2020, doi: 10.1109/EPE51172.2020.9269271.

[47] A. Gil-De-Castro, R. Medina-Gracia, S. K. Ronnberg, A. M. Blanco, and J. Meyer, “Differences in the performance between CFL and LED lamps under different voltage distortions,” *Proc. Int. Conf. Harmon. Qual. Power, ICHQP*, vol. 2018-May, pp. 1–6, 2018, doi: 10.1109/ICHQP.2018.8378918.

[48] A. J. Collin *et al.*, “Survey of harmonic emission of electrical vehicle chargers in the European market,” *2016 Int. Symp. Power Electron. Electr. Drives, Autom. Motion, SPEEDAM 2016*, pp. 1208–1213, 2016, doi: 10.1109/SPEEDAM.2016.7526005.

[49] D. Taghvaie, Amir; Zare, Firuz; Sharma, Rahul; Kumar, “Impacts of Grid Impedance on Power Quality of Converters in Distribution Networks,” in *IECON 2022-48th Annual Conference of The IEEE industrial Electronics Society*, 2022. doi: 10.1109/IECON49645.2022.9968362.

[50] H. Rathnayake, K. G. Khajeh, F. Zare, and R. Sharma, “Harmonic analysis of grid-tied active front end inverters for the frequency range of 0-9 khz in distribution networks: Addressing future regulations,” *Proc. IEEE Int. Conf. Ind. Technol.*, vol. 2019-Febru, pp. 446–451, 2019, doi: 10.1109/ICIT.2019.8755015.

[51] X. Xiao *et al.*, “Analysis and Modelling of Power-Dependent Harmonic Characteristics of Modern PE Devices in LV Networks,” *IEEE Trans. Power Deliv.*, vol. 32, no. 2, pp. 1014–1023, 2017, doi: 10.1109/TPWRD.2016.2574566.

[52] A. S. Koch, J. M. A. Myrzik, T. Wiesner, and L. Jendernalik, “Evaluation and validation of Norton approaches for nonlinear harmonic models,” in *2013 IEEE Grenoble Conference PowerTech, POWERTECH 2013*, 2013. doi: 10.1109/PTC.2013.6652270.

[53] C. F. M. Almeida and N. Kagan, “Harmonic coupled norton equivalent model for modeling harmonic-producing loads,” in *ICHQP 2010 - 14th International Conference on Harmonics and Quality of Power*, 2010. doi: 10.1109/ICHQP.2010.5625491.

[54] J. Yadav, K. Vasudevan, J. Meyer, and D. Kumar, “Frequency Coupling Matrix Model of a Three-Phase Variable Frequency Drive,” *IEEE Trans. Ind. Appl.*, vol. 58, no. 3, pp. 3652–3663, 2022, doi: 10.1109/TIA.2022.3156104.

[55] J. Yadav, K. Vasudevan, J. Meyer, and Di. Kumar, “Modelling Three Phase Variable Frequency Drive Using a Frequency Coupling Matrix,” *Proc. 2020 IEEE 1st Int. Conf. Smart Technol. Power, Energy Control. STPEC 2020*, 2020, doi: 10.1109/STPEC49749.2020.9297761.

[56] M. Ramzan, A. Othman, and N. R. Watson, “Accurate Harmonic Analysis of Distribution Systems,” *2022 7th IEEE Work. Electron. Grid, eGRID 2022*, 2022, doi: 10.1109/eGRID57376.2022.9990007.

[57] R. Savoor and K. Meier-Hellstern, “Estimating the Frequency Coupling Matrix From Network Measurements,” *IEEE Trans. Control Netw. Syst.*, vol. 7, no. 2, pp. 353–388, 2020, doi: 10.1201/9781315208787-16.

[58] R. Langella *et al.*, “On the use of fourier descriptors for the assessment of frequency coupling matrices of power electronic devices,” *Proc. Int. Conf. Harmon. Qual. Power, ICHQP*, vol. 2018-May, pp. 1–6, 2018, doi: 10.1109/ICHQP.2018.8378908.

[59] K. J. Son, G. S. An, K. D. Nam, and T. G. Chang, “An Advanced Frequency Estimation Algorithm Based on Analytic Compensation of Effects of Dominant Harmonic in Power Systems,” *IEEE Access*, vol. 9, pp. 146568–146577, 2021, doi: 10.1109/ACCESS.2021.3122469.

[60] J. Yadav, K. Vasudevan, J. Meyer, and D. Kumar, “Frequency Coupling Matrix Model of a Three Phase Variable Frequency Drive,” *IEEE Trans. Ind. Appl.*, vol. 9994, no. c, pp. 1–1, 2022, doi: 10.1109/tia.2022.3156104.

[61] Y. Sun, G. Zhang, W. Xu, and J. G. Mayordomo, “A Harmonically Coupled Admittance Matrix Model for AC/DC Converters,” *IEEE Trans. Power Syst.*, vol. 22, no. 4, pp. 1574–1582, 2007, doi: 10.1109/TPWRS.2007.907514.

[62] L. F. Beites, J. G. Mayordomo, and X. Yang, “The Harmonically Coupled Admittance Matrix of the Single-Phase Diode Rectifier,” *IEEE Access*, vol. 9, pp. 128023–128031, 2021, doi: 10.1109/ACCESS.2021.3110597.

[63] A. M. Blanco, S. Yanchenko, J. Meyer, and P. Schegner, “Impact of supply voltage distortion on the current harmonic emission of non-linear loads,” *DYNA*, vol. 82, no. 192, pp. 150–159, Aug. 2015, doi: 10.15446/dyna.v82n192.48591.

[64] E. E. Ahmed, W. Xu, and G. Zhang, “Analyzing systems with distributed harmonic sources including the attenuation and diversity effects,” *IEEE Trans. Power Deliv.*, vol. 20, no. 4, pp. 2602–2612, 2005, doi: 10.1109/TPWRD.2005.855441.

[65] J. Cunill-Sola and M. Salichs, “Study and Characterization of Waveforms From Low-Watt (<25 W) Compact Fluorescent Lamps With Electronic Ballasts,” *IEEE Trans. Power Deliv.*, vol. 22, no. 4, pp. 2305–2311, Oct. 2007, doi: 10.1109/TPWRD.2007.899551.

[66] Y. Baghzouz and O. T. Tan, “Probabilistic modeling of power system harmonics,” *IEEE Trans. Ind. Appl.*, vol. IA-23, no. 1, pp. 173–180, 1987, doi: 10.1109/TIA.1987.4504883.

[67] G. Ye, M. Nijhuis, V. Cuk, and J. F. G. Cobben, “Stochastic residential harmonic source modeling for grid impact studies,” *Energies*, vol. 10, no. 3, pp. 1–21, 2017, doi: 10.3390/en10030372.

[68] D. Salles, C. Jiang, W. Xu, W. Freitas, and H. E. Mazin, “Assessing the collective harmonic impact of modern residential loads-part I: Methodology,” *IEEE Trans. Power Deliv.*, vol. 27, no. 4, pp. 1937–1946, 2012, doi: 10.1109/TPWRD.2012.2207132.

[69] P. Caramia, D. Prroto, A. Russo, and P. Varilone, “Probabilistic Harmonic Analysis for Waveform Distortion Assessment of Low Voltage Distribution Systems with Plug-in Hybrid Electric Vehicles,” *1st Int. Conf. Energy Transit. Mediterr. Area (SyNERGY MED)*, 2019.

[70] M. T. Au and J. V. Milanović, “Establishing harmonic distortion level of distribution network based on stochastic aggregate harmonic load models,” *IEEE Trans. Power Deliv.*, vol. 22, no. 2, pp. 1086–1092, 2007, doi: 10.1109/TPWRD.2007.893193.

[71] E. J. Brunner, P. S. Ford, M. A. McNulty, and M. A. Thayer, “Compact fluorescent lighting and residential natural gas consumption: Testing for interactive effects,” *Energy Policy*, vol. 38, no. 3, pp. 1288–1296, 2010, doi: 10.1016/j.enpol.2009.11.003.

[72] N. Khan and N. Abas, “Comparative study of energy saving light sources,” *Renew. Sustain. Energy Rev.*, vol. 15, no. 1, pp. 296–309, 2011, doi: 10.1016/j.rser.2010.07.072.

[73] S. Uddin, H. Shareef, and A. Mohamed, “Power quality performance of energy-efficient low-wattage LED lamps,” *Meas. J. Int. Meas. Confed.*, vol. 46, no. 10, pp. 3783–3795, 2013, doi: 10.1016/j.measurement.2013.07.022.

[74] X. Xu, A. Collin, S. Z. Djokic, R. Langella, A. Testa, and J. Drapela, “Experimental evaluation and classification of LED lamps for typical residential applications,” in *IEEE PES Innovative Smart Grid Technologies Conference Europe (ISGT-Europe)*, 2017. doi: 10.1109/ISGTEurope.2017.8260292.

[75] S. C. Industries, U. States, F. D. A. Class, S. Buyer, E. Opportunity, and A. A. Employer, “Direct-AC, linear LED driver topology: CCR straight circuit (120 V AC, 230 V AC). Technical report, ON Semiconductor,” 2015.

[76] S. Uddin, H. Shareef, A. Mohamed, M. A. Hannan, and K. Mohamed, “LEDs as energy efficient lighting systems: A detail review,” *Proc. - 2011 IEEE Student Conf. Res. Dev. SCOReD 2011*, pp. 468–472, 2011, doi: 10.1109/SCOReD.2011.6148785.

[77] M. Naveed Iqbal, M. Jarkovoi, L. Kutt, and N. Shabbir, “Impact of LED thermal stability to household lighting harmonic load current modeling,” *2019 Electr. Power Qual. Supply Reliab. Conf. 2019 Symp. Electr. Eng. Mechatronics, PQ SEEM 2019*, 2019, doi: 10.1109/PQ.2019.8818226.

[78] D. Gallo, R. Langella, M. Luiso, A. Testa, and N. R. Watson, “A new test procedure to measure power electronic devices’ frequency coupling admittance,” *IEEE Trans. Instrum. Meas.*, vol. 67, no. 10, pp. 2401–2409, 2018, doi: 10.1109/TIM.2018.2819318.

[79] J. B. Kwon, X. Wang, F. Blaabjerg, C. L. Bak, A. R. Wood, and N. R. Watson, “Harmonic instability analysis of a single-phase grid-connected converter using a harmonic state-space modeling method,” *IEEE Trans. Ind. Appl.*, vol. 52, no. 5, pp. 4188–4200, 2016, doi: 10.1109/TIA.2016.2581154.

[80] D. Kumar and F. Zare, “Harmonic Analysis of Grid Connected Power Electronic Systems in Low Voltage Distribution Networks,” *IEEE J. Emerg. Sel. Top. Power Electron.*, vol. 4, no. 1, pp. 70–79, 2016, doi: 10.1109/JESTPE.2015.2454537.

[81] A. Alduraibi, J. Yaghoobi, and F. Zare, “Impacts of Grid Voltage Harmonics Amplitude and Phase Angle Values on Power Converters in Distribution Networks,” *IEEE Access*, vol. 9, pp. 92017–92029, 2021, doi: 10.1109/ACCESS.2021.3093026.

[82] J. Drapela *et al.*, “A New Analytical Model of Single-Phase Diode Bridge Rectifiers in the Presence of Interharmonics in Supply Voltage,” 2023, doi: 10.1109/OAJPE.2023.3244330.

[83] J. Liu, J. K. Motwani, D. Zhang, and D. Dong, “Unidirectional Hybrid Multilevel Rectifier Family for MV/HV Applications: Analysis and Comparative Evaluation,” *IEEE Trans. Power Electron.*, vol. 39, no. 3, pp. 1–13, 2023, doi: 10.1109/tpel.2023.3337772.

[84] S. Gupta, N. Vamanan, and V. John, “A Diode Bridge Rectifier with Improved Power Quality Using the Capacitive Network,” *IEEE Trans. Ind. Appl.*, vol. 54, no. 2, pp. 1563–1572, 2018, doi: 10.1109/TIA.2017.2785354.

[85] X. Yue and S. Du, “A Synchronized Switch Harvesting Rectifier With Reusable Storage Capacitors for Piezoelectric Energy Harvesting,” *IEEE J. Solid-State Circuits*, vol. 58, no. 9, pp. 2597–2606, 2023, doi: 10.1109/JSSC.2023.3260145.

[86] R. Devices, X. Xie, J. Zhang, Y. Sun, S. Member, and J. Fan, “A Measurement-Based Dynamic Harmonic Model for Single-Phase Diode Bridge,” *IEEE Trans. Instrum. Meas.*, vol. 73, pp. 1–13, 2024, doi: 10.1109/TIM.2024.3370782.

[87] J. K. Han, J. W. Kim, and G. W. Moon, “A High-Efficiency Asymmetrical Half-Bridge Converter with Integrated Boost Converter in Secondary Rectifier,” *IEEE Trans. Power Electron.*, vol. 32, no. 11, pp. 8237–8242, 2017, doi: 10.1109/TPEL.2017.2675283.

[88] S. Sharifi, M. Monfared, and M. Babaei, “Ferdowsi Rectifiers - Single-Phase Buck-Boost Bridgeless PFC Rectifiers with Low Semiconductor Count,” *IEEE Trans. Ind. Electron.*, vol. 67, no. 11, pp. 9206–9214, 2020, doi: 10.1109/TIE.2019.2955430.

[89] M. Melquíades Silva, M. Losada Y Gonzalez, and S. Rocha Silva, “A new analytical model for evaluating loads supplied by sinusoidal and non-sinusoidal voltage sources,” *2010 IEEE/PES Transm. Distrib. Conf. Expo. Lat. Am. T D-LA 2010*, pp. 824–831, 2011, doi: 10.1109/TDC-LA.2010.5762980.

[90] S. Elphick, P. Ciufo, and S. Perera, “Laboratory investigation of the input current characteristics of modern domestic appliances for varying supply voltage conditions,” *ICHQP 2010 - 14th Int. Conf. Harmon. Qual. Power*, pp. 1–7, 2010, doi: 10.1109/ICHQP.2010.5625397.

[91] R. S. Thallam, M. T. Doyle, S. D. Krein, M. J. Samotyj, A. Mansoor, and W. M. Grady, “Effect of Supply Voltage Harmonics on the Input Current of Single-Phase Diode Bridge Rectifier Loads,” *IEEE Trans. Power Deliv.*, vol. 10, no. 3, pp. 1416–1422, 1995, doi: 10.1109/61.400924.

[92] J. J. Mesas, L. Sainz, and J. Molina, “Parameter estimation procedure for models of single-phase uncontrolled rectifiers,” *IEEE Trans. Power Deliv.*, vol. 26, no. 3, pp. 1911–1919, 2011, doi: 10.1109/TPWRD.2011.2120629.

[93] Z. Chen, Y. Han, Y. Wu, Z. Lu, and X. Liu, “A Low Voltage Stress PFC Rectifier Based on Nonoverlapping Strategy Using Resonant Switched-Capacitor Converter,” *IEEE Trans. Ind. Electron.*, vol. 69, no. 12, pp. 12728–12738, 2022, doi: 10.1109/TIE.2021.3135643.

[94] K. Daniel, L. Kütt, M. N. Iqbal, N. Shabbir, M. Jarkovoi, and M. Parker, “Load Current Harmonic Model Complexity Reduction through Empirical Pattern Analysis,” *Int. Conf. Compat. Power Electron. Power Eng. (CPE-POWERENG 2023) JUNE 14 – 16, Tallinn, Est.*, pp. 1–6, 2023, doi: 10.1109/CPE-POWERENG58103.2023.10227474.

Acknowledgements

The work reported in this thesis was supported by the Estonian Research Council grant PSG142, “Synthesis of output current waveforms of power electronic converters for increasing the hosting capacity of renewable energy sources in the distribution networks”, and PRG-2055, “Efficient, reliable, and secure partial power electronic systems.”

The completion of this work would not have been possible without the expertise of my supervisor, Professor Lauri Kütt. I would also like to thank my mother, family and friends, especially my beloved wife, Rahat Chaudhry. Without their unconditional support and prayers, it would not have been possible.

Abstract

Load Current Harmonic Sensitivity of AC/DC Power Converters of Energy Efficient Devices

The wide deployment of energy-efficient modern power electronic converters has led to a progressive increase in loads with non-sinusoidal current draw within low voltage networks. While low voltage AC supply networks have some dispersion from sinewave voltage supply waveform added harmonic currents, injected by switch-mode converters, can potentially distort the supply voltage waveform up to failure and loss of reliability levels. This thesis explores the correspondence between voltage harmonics in supply grid and their impact on the characteristics of load current harmonic components in order to provide more accurate harmonic current modelling.

Focusing on non-linear load behaviour an experimental evaluation is conducted to assess the sensitivity of current harmonics to supply voltage harmonics. A novel empirical Waveform Variation Defined Model (WVDM) is proposed, emphasizing time-domain waveform variations over traditional impedance-based approaches. The WVDM provides improved correspondence with the actual physical operation of loads, particularly highlighting cross-order coupling between supply voltage and current harmonics variations. This model incorporates non-impedance relations and separates phase and magnitude response components, demonstrating accurate estimations of cumulative influence for different supply voltage harmonics, especially low order odd harmonics prevalent in residential grids.

Furthermore, this thesis investigates the systematic occurrence and variation of sensitivity characteristics of load current harmonics. With physical time-domain origins in the background, reduction and co-relations of sensitivity coefficients is shown. Empirical model limits are presented as relations to the main component level of the supply voltage emerge, highlighting the significant role of the fundamental voltage (U_1) in the characteristic coefficients' ranges.

Finally, research contributes to the development of analytical expressions related to the physical operation of components in rectifier circuits. These expressions offer a deeper understanding of harmonic load current dependency on supply voltage harmonics, facilitating the construction of more precise models for load current. Keeping the time-domain foundations in focus the basis for the Fourier transform expressions are defined. Simplified waveform characteristic time-instances and level-instances are listed and defined for analytical expressions.

A comprehensive exploration of the effects of voltage harmonics on current harmonics in low voltage networks observed in this thesis, presenting valuable insights and analytical tools essential for understanding and mitigating the effects of harmonic distortions on power distribution systems.

Lühikokkuvõte

Energiatõhusate seadmete vahelduv-alalisvoolumuundurite koormusvoolu harmoonikute tundlikkus

Laialdane energiatõhusate pooljuhtmuundurite kasutuselevõtt on madalpingevõrkudes toonud kaasa mittesiinuselise lainekujuga koormusvoolu tarbivate elektriliste koormuste hulga kasvu. Kuigi vahelduvvoolu jaotusvõrkudes on pingelainekuju siinuskujust vähene kõrvalekalle, siis pooljuhtmuundurite vooluharmoonikute täiendav koormus elektrivõrkudes võib tuua kaasa vahelduvpingekuju lubamatu moonutumise, mis võib viia rikete ja töökindluse kaotuseni. Käesolev doktoritöö uurib pingeharmoonikute ja vooluharmoonikute vahelisi seoseid, millele toetudes saab täpsemini modelleerida vooluharmoonikute tasemeid elektrivõrkudes.

Eksperimentaalne töö keskendub mittelineaarsete koormusseadmete vooluharmoonikute tasemete muutuste hindamisele seoses toitepinge harmoonikute tasemetega. Pakutakse välja uudne lainekuju muutusel põhinev mudel (WVDM), mis rõhutab ajavalla lainekuju muutuste rakendamist võrreldes tavapäraste näivtakistussuhetele tuginevate mudelitega. Teiste mudelitega võrreldes WVDM pakub analüüsiks koormuste füüsikalisele talitlusele parema vastavuse, eriti rõhutades vooluharmoonikute ja pingeharmoonikute erinevate järkude vahelist ristsidestust. Mudel rakendab mitte-näivtakistusseoseid ja käsitleb faasi- ja amplituudikomponentide eraldatud käsitluse. Tulemuseks on parem täpsus erinevate toitepinge harmoonikute kumulatiivse mõju hindamisel vooluharmoonikute parameetritele, eriti olmepiirkondade jaotusvõrkudes olevate olulisimate paaritute pingeharmoonikute kontekstis.

Täiendavalt käsitletakse siin uurimistöös pinge- ja vooluharmoonikute seoste ja varieeruvuse ilmingute süsteemsust. Tuginedes füüsikalistele ajavalla suurustele saab näidata tundlikkussuuruste hulga vähendamise võimalusi ja täiendavaid koosmõjusid. Empiiriliste mudelite piirid avalduvad muuhulgas pinge põhiharmooniku tasemega seoses, tõstes esile muuhulgas pinge põhiharmooniku olulise rolli seoseid kirjeldavate tegurite muutumisulatusele.

Lõpuosas annab uurimistöö panuse analüütiliste seoste väljatöötamiseks tuginedes alaldite komponentide füüsilisele talitlusele. Antud matemaatilised kirjeldused pakuvad põhjalikuma selgituse koormusvoolu harmoonikute seostest pingeharmoonikutega, pakkudes koormusvoolude mudelite täpsuse parandamist. Fourier' teisenduse aluseks olevad võrrandid defineeritakse püsides ajavallast teada olevatel alustel. Analüütiliste võrrandite konstrueerimiseks pakutakse välja lihtsustatud lainekuju ja seda defineerivad ajahetked ja hetkväärtused.

Uurimistöös esitatud põhjalik käsitlus toitepinge harmoonikute mõjust vooluharmoonikute parameetritele pakub täpsustatud selgitusi ja analüütilised vahendid, mis on vajalikud harmoonilismoonutuste tasemete kujunemise mõistmiseks ja ka moonutuste vältimiseks jaotusvõrkudes.

Appendix

Publication I

K. Daniel, L. Kütt, M. N. Iqbal, N. Shabbir and M. Jarkovoi, “Description of Practical Load Harmonic Current Emission due to Voltage Harmonic Variation,” *2021 IEEE 62nd International Scientific Conference on Power and Electrical Engineering of Riga Technical University (RTUCON)*, Riga, Latvia, 2021, pp. 1–6, doi: 10.1109/RTUCON53541.2021.9711594.

2021 IEEE 62nd International Scientific Conference on Power and Electrical Engineering of Riga Technical University (RTUCON) | 978-1-6654-3804-9/21/$31.00 ©2021 IEEE | DOI: 10.1109/RTUCON53541.2021.9711594

Description of Practical Load Harmonic Current Emission due to Voltage Harmonic Variation

Kamran Daniel, Lauri Kütt, Muhammad Naveed Iqbal, Noman Shabbir, Marek Jarkovoi
Department of Electrical Power Engineering and Mechatronics
Tallinn University of Technology
19086 Tallinn, Estonia
kdanie@taltech.ee

***Abstract*— An increase in harmonic currents in the low voltage networks is progressively observed, which is mainly caused due to increase in energy-efficient modern power electronic equipment. The current harmonics, injected by this power electronic equipment, tend to change the voltage waveform of the distribution network. The current harmonic emission of these loads is also susceptible to the input voltage waveform. Any amplitude and phase angle variation of the voltage harmonics, either combine or exclusively, has a visible impact on amplitude and phase angles of load's current harmonic emission. This paper presents the influence of amplitude and phase varying voltage harmonic, on amplitude and phase angle of current harmonics.**

Keywords—power quality, harmonic emission, harmonic sensitivity, phase angles

I. INTRODUCTION

The increasing number of nonlinear loads in the distribution grid is becoming a significant issue for utility companies since most of these loads have high harmonic emissions [1]. Harmonics currents that are injected upstream by these loads affect the devices connected at the point of common coupling (PCC) and alter the voltage waveform by interacting with the voltage harmonics injected by the network. Nonlinear loads contain switching devices that are based on power electronic circuits, such as switch-mode power supplies for power conversion. The aggregated harmonic emission of these devices depends on the phase and magnitude variations that can be caused by the supply voltage harmonics [2]. Previously, the research includes analyzing the voltage and current harmonics mainly based upon RMS value, and little importance given to matters of phase angle information. Similarly, high frequency harmonics can be treated as constant vectors if the phase angle of voltage harmonics is known [3][4].

In case of a linear harmonic response model, the voltage harmonic described as a vector $\boldsymbol{U_h} = U_{hM} \angle \theta_{Uh}$ will provide a response of the load's harmonic current with relation of

$$\boldsymbol{I_{hZ}} = \frac{U_{hM} \angle \theta_{Uh}}{Z_h \angle \theta_{Zh}} \quad (1)$$

Where Z_h is the complex impedance describing the harmonic response of the device to the h-th harmonic voltage. In this case the vector representation of harmonic load current for different harmonic voltage phase angle will be seen as a circle, having a constant phase shift towards the voltage harmonic phase shift θ_{Zh}. Fig. 1 presents the harmonic load reaction models.

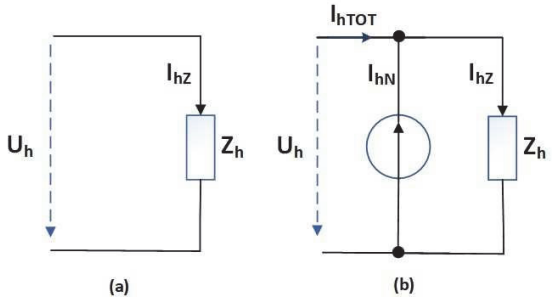

Fig. 1. Harmonic load reaction models, (a) linear load (b) Norton equivalent

However, it has been a well-known suggestion that the current response of a nonlinear-load is better represented by Norton model rather than purely linear model. In Norton model, there will be two current components, a constant current source having current $\boldsymbol{I_{hN}}$ and a linear impedance reaction $\boldsymbol{I_{hZ}}$. In this case, the response to the voltage harmonic will be composed of a circular pattern from the linear response branch and an offset due to the constant portion of the current source.

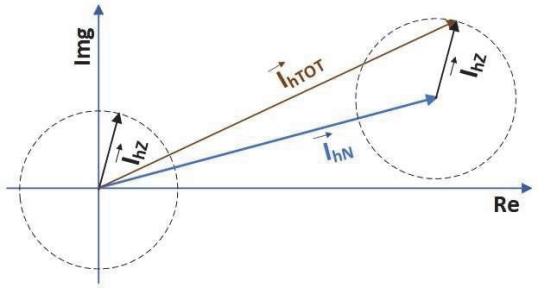

Fig. 2. Addition of harmonic components for linear and Norton models.

One distinction from the measurement results towards the current RMS values is that for the linear model the harmonic current is always proportional to harmonic voltage component level. The Norton model, however, presents that the current RMS is varying, dependent not only on the harmonic voltage component level but also on harmonic voltage component

The work reported was supported by the Estonian Research Council grant PSG142, "Synthesis of output current waveforms of power electronic converters for increasing the hosting capacity of renewable energy sources in the distribution networks"

978-1-6654-3804-9/21/$31.00 ©2021 European Union

phase angle value, shown in Fig. 2. This is due to the summing of the Norton model current source current component vector $\boldsymbol{I_{hN}}$ and the linear impedance current vector $\boldsymbol{I_{hZ}}$.

$$\boldsymbol{I_{hTOT} = I_{hN} + I_{hZ}} \quad (2)$$

$$\boldsymbol{I_{hTOT}} = I_{hNM} \angle \varphi_{hN}(t) + I_{hZM} \angle \varphi_{hZ}(t) \quad (3)$$

Fig. 3 illustrates the aggregation of harmonic vectors. For a complete 360-degree rotation of the harmonic voltage component, the current vector would make a variation of $\pm\Delta\varphi_{hTOT}$ while this is made up of 2 components: Norton current source harmonic current component with phase angle $\varphi_{hN\text{-}0}$, and the linear component with phase angle φ_{hZ}. While phase angle $\varphi_{hN\text{-}0}$ is assumed at persistent value, the φ_{hZ} would provide a 360^0 response angle in accordance to voltage harmonic component phase angle.

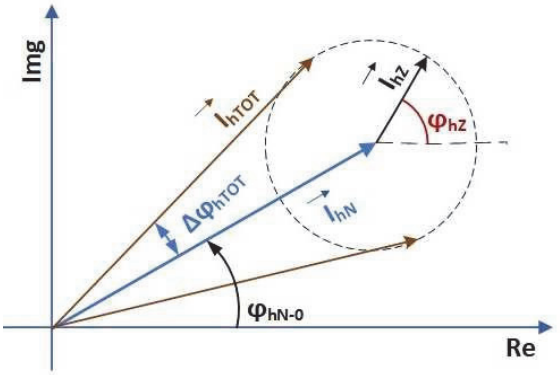

Fig. 3. Summation of two different harmonic currents with phase shift, referring to Norton model approach.

It can be expected that a purely resistive load harmonic current will correspond to the voltage harmonic level proportionally and to its phase angle at specific offset angle. On the other hand, nonlinear loads draw non-sinusoidal currents and the current waveform will contain high frequency harmonics even for sinusoidal input voltage.

The grid supply voltage waveform is not a pure sinewave as it is distorted because of effects due to various nonlinear network components and loads. In this paper, an approach is taken to characterize the practical loads and their response due to harmonic voltage components in the grid. In order to view the load current harmonic emission response for pure sinewave voltage waveform or any particular distorted voltage, an experimental setup is used that is able to generate desired voltage waveforms and harmonics.

This paper presents the measurement results on the effect of voltage harmonic components on the harmonic current profile of the loads. Current harmonics from resistive load and LED lamp are calculated and observed at different voltage harmonic input variations.

This paper is organized as follow. Section II describes the measurement procedure used for testing and the equipment used in creating the experimental setup. Section III contains the investigation of the measurement from loads and analysis of results. The summary is presented in chapter IV.

II. Experimental Setup

The experimental setup used in this study consists of a power quality (PQ) analyzer, a data acquisition (DAQ) module, load combination array, programmable power supply, and a personal computer. Fig. 4 shows the block diagram of the experimental setup. PQ analyzer realizes one-second measurement aggregated and recorded according to class-A standards [5]. MATLAB controls the generation of input voltage for measurement setup; as it programs the DAQ module to provide the signal to the programmable power supply. Supply waveform is generated with the sampling frequency of 100 kS/s; meaning 2000 points for every 50 Hz cycle. The same MATLAB script drives the load scenarios by supplying digital binary switching signal to relays which are embedded on 16-load combination array.

Two loads including LED lamps, and pure resistive loads, are tested in this study to observe harmonic response on input voltage harmonics variations. LED lamps are rather stable loads for their harmonic fingerprint [6], and here a 14 W LED lamp is measured at different input voltage waveforms with harmonic components included. At first, the harmonic currents of the LED are recorded for input voltage containing only the fundamental component. In the second step, measurement is recorded for the input voltage having fundamental and third harmonic with constant magnitudes. The phase of the fundamental component is taken as the zero, and third harmonic phase angles are changed periodically with step of either 15 or 30 degrees. All input voltage combinations are present for 10 s. PQ analyzer records with a resolution of 1 s measurements aggregated on 200 ms internal measurement data points. Phase angles of harmonic currents are recorded with respect to input fundamental voltage. The equipment is warmed up for an hour to attain thermal stability, which results in a near-constant harmonic profile [7] [8]. Continuous power is provided to LED lamps to maintain a working temperature during warmup period. PQ analyzer can also perform one second of complete voltage and current waveform recording with a sampling frequency of 40.1 kHz.

The discrete Fourier transform (DFT) is used to extract the magnitude and phase angles of both current and voltage waveform recording data. The DFT of the signal can provide the exact amplitude and phase angle of all the harmonic components present in the voltage or current waveform. The PQ analyzer used in this study is commercially certified to make an accurate and precise measurement of magnitude and phase angle values [9].

III. Measurements and Results

To study the harmonic coupling between the input voltage and load current of the device; at first, the resistive load is taken for testing. A resistive load is selected that could draw the RMS current equivalent to the RMS current drawn by the LED lamp. Unlike the nonlinear load, resistive loads do not inject current harmonics as the voltage and current are totally in phase.

Each harmonic in the input voltage generate the exclusive current harmonic component [10]. Current harmonic vectors of the resistive load are presented in Fig. 5.

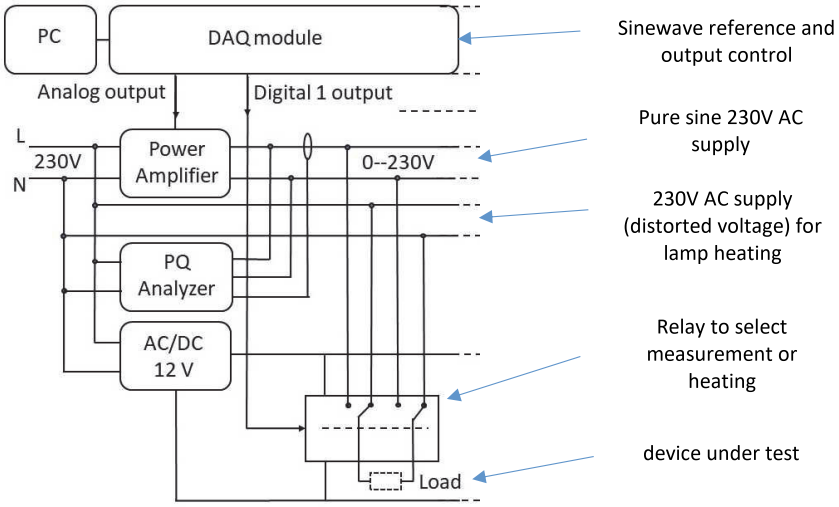

Fig. 4. Measurement setup [2]

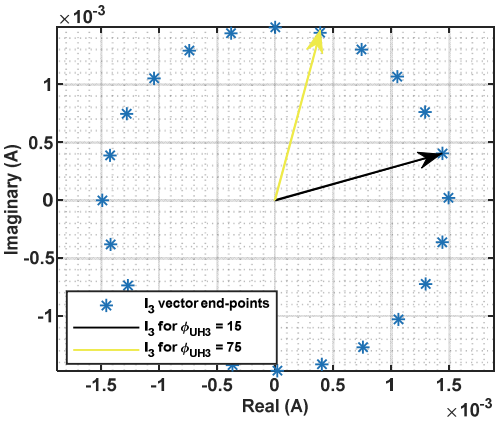

Fig. 5. I_3 vectors in resistive load for input U_{H3} =3V and changing φ_{UH3} only

The third harmonic current vector ($\boldsymbol{I_3}$) is generated in the response of third harmonic volatge ($\boldsymbol{U_{H3}}$); its phase angle changes accordingly with the phase of the third harmonic voltage.

$$\boldsymbol{I_3} = \frac{U_3 \angle \varphi_{U3}}{Z_3 \angle \varphi_{Z3}} \tag{4}$$

Current harmonics corresponding to a particular voltage harmonic will have no phase difference as the load type is resistive. With every change in the φ_{UH3}, there is a unique vector I_3 (black and yellow vectors). The third harmonic voltage phase angles (φ_{UH3}) are changed with a 15-degree step, and response vectors I_3 are generated in accordance to harmonic model with linear load; asterisks shown in Fig. 5 are endpoints of harmonic vectors as they rotate in circle with phase change of input voltage harmonic.

Fig. 6 presents the total load current in resistive load for varying voltage harmonic amplitude and phase values. It can be seen that there is practically identical total load current value present for all tests. The lack of RMS current change refers to the resistive harmonic response model. Therefore, for active/resistive loads, the Norton model is not necessary. Also, voltage harmonic injection of a particular harmonic order does not produce harmonic current of some other harmonic order.

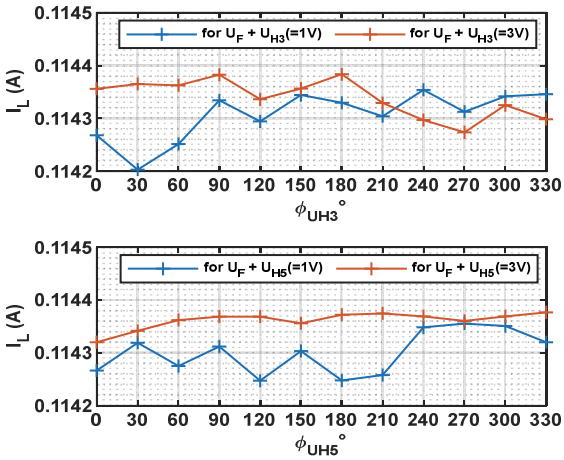

Fig. 6. Total RMS current in Resistive load, in presence of harmonic voltages

The second type of load used for testing is a LED lamp. LED lamps have built-in rectifier circuits for energy conversion, so they draw nonlinear current. The load current contains harmonics even if the input voltage is pure sinusoidal with no higher order harmonics. The lamp is tested at the input voltage containing a third harmonic voltage (U_{H3}) component added to the fundamental (U_F) voltage component. The levels and phase angle of U_{H3} are changed. The load current is sensitive to φ_{UH3}, and with the increase in the amplitude of U_{H3}, there is more variation in the load current, shown in Fig. 7.

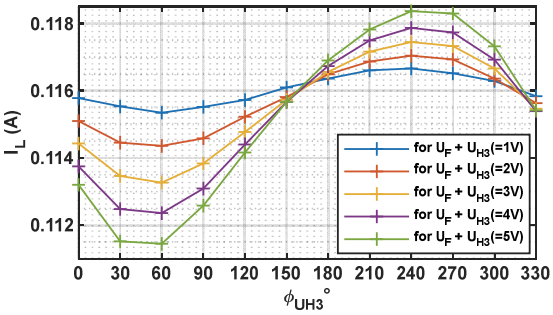

Fig. 7. Load current for fundamental (U_F) component + U_{H3}, keeping the U_F constant and varying amplitude U_{H3} and phase φ_{UH3}

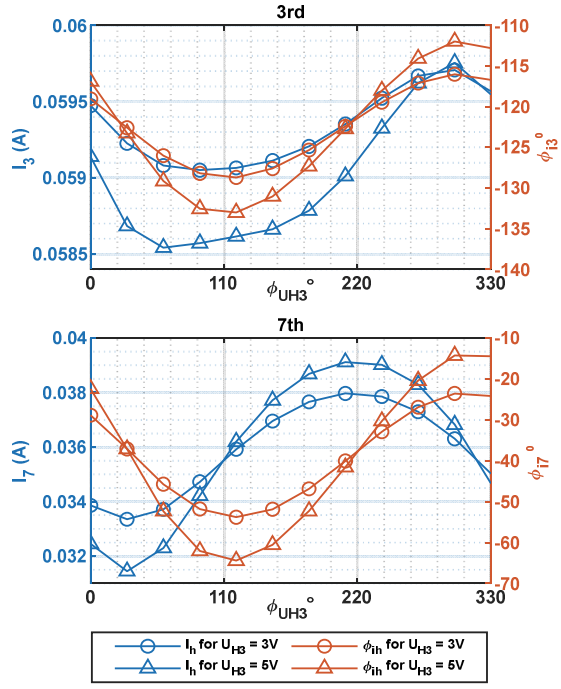

Fig. 8. Impact on harmonic currents for adding U_{H3}(amplitude and phase-varying) in input voltage

Fig. 8 shows the sensitivity of harmonic current to the harmonics in the input voltage. Suppose k_{th} voltage harmonic (U_{Hi}) is added to the input voltage. The change in the amplitude and phase of the U_{Hi} affects the i_{th} current harmonic, and it also affects the other current harmonics. With the change in phase angle (φ_{UH3}) of U_{H3}, the amplitude of I_3 shows more variation. Referring to Fig. 3, this response basically refers to expected correspondence of Norton model approach.

However, from the measurement results it is revealed that when the phase angle of 3rd harmonic voltage (φ_{HU3}) is varied, and both amplitude and phase of rest of the current harmonics ia also varying. Furthermore, variation in U_{H3} amplitude will also cause variation (again, in terms of amplitude and phase) in all other current harmonics. The seventh current harmonic (I_7) is also shown in the second (right side) diagram on Fig. 8.

When U_{H3}, along with fundamental, is present in the input voltage, the third harmonic current (I_3) is likely to be affected, as observed in the resistive load case. But in case of LED lamps, any input voltage harmonic affects all the current harmonics in load current.

$$\boldsymbol{I_{hk}} = \sum_{k=1}^{\infty} \boldsymbol{I_{h_{uk}}} \tag{5}$$

$\boldsymbol{I_{huk}}$ is the contribution of k_{th} harmonic voltage in the total value of any harmonic current $\boldsymbol{I_{hk}}$,

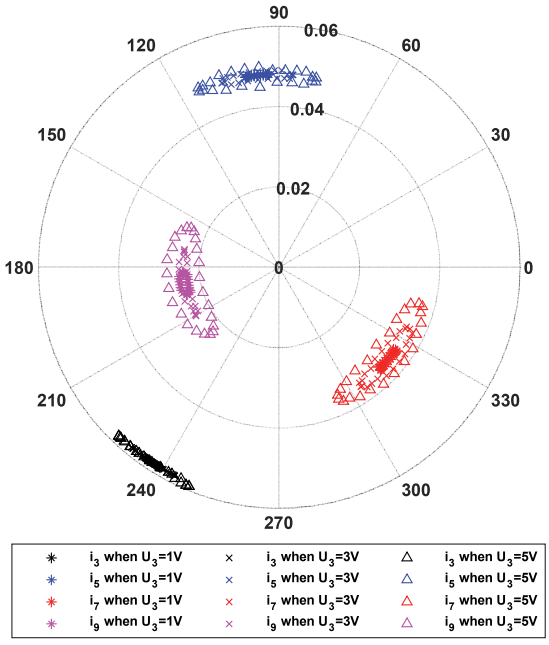

Fig. 9. Variations in harmonic currents for input voltage containing different levels of U_{H3} and phase φ_{UH3} = 0,15,30…345°.

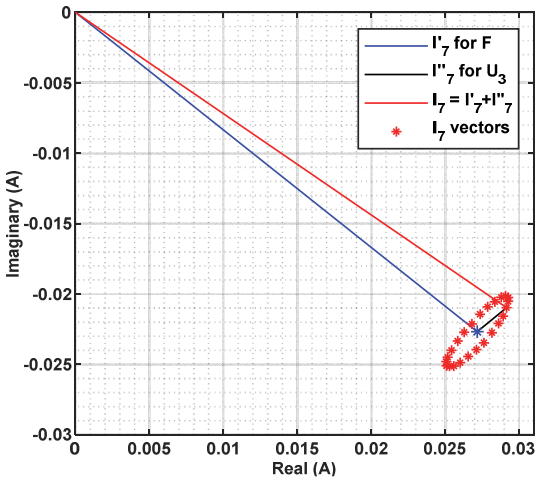

Fig. 10. Vvariations in seventh harmonic current for input voltage containing U_{H3} and phase φ_{UH3} = 0,15,30…345º.

Fig 9 and Fig. 10 illustrate the influence of voltage harmonics on the current harmonics. Any change in phase angle of U_{H3} in the input voltage, a change in amplitude and phase of seventh harmonic current I_7 can be observed as presented in Fig 10. All other current harmonics are affected also. By vector addition, the net total I_7 present in the load current is obtained. Red asterisks show the I_7 vectors corresponding to the change in φ_{UH3} when the amplitude U_{H3} is 1 V. The resultant vectors I_7 lies on the loci of the ellipse, whose center is almost at the tip of I'_7 (blue) vector.

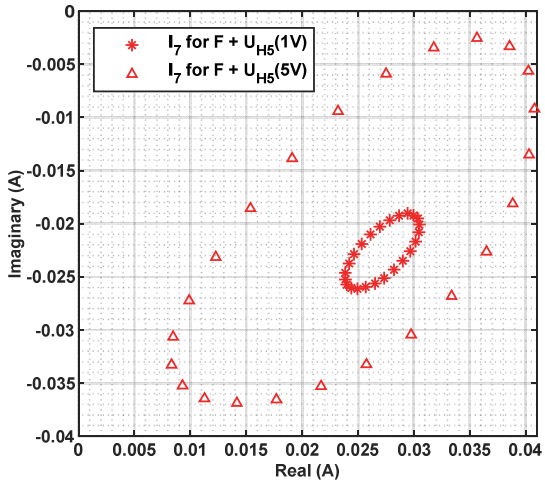

Fig. 11. Seventh harmonic current for input voltage containing U_{H5} (1V or 5V) and phase φ_{UH5} = 0,15,30…345º.

When the input harmonic voltage amplitude is changed, the amplitude and phase of current harmonics are altered. If the fifth voltage harmonic (U_{H5}) is present in the input voltage, it also affects all the harmonic currents including I_3, I_7, etc. The impact of U_{H5} on current harmonics is presented in Fig. 12. The resultant I_7 vectors for two amplitude levels (1 V and 5 V) of U_{H5} is shown in the Fig. 11. When the U_{H5} amplitude rises from 1 V to 5 V (phase angle step is identical), the amplitude of the I_7 current vectors, due to U_{H5}, is increased, resultant vector I_7 is presented with red delta. Asterisks are I_7 vectors when U_{H5} amplitude is 1 V, and red-deltas are I_7 vectors when U_{H5} amplitude is 5 V. Resulting current vectors seems to follow the loci of the ellipse.

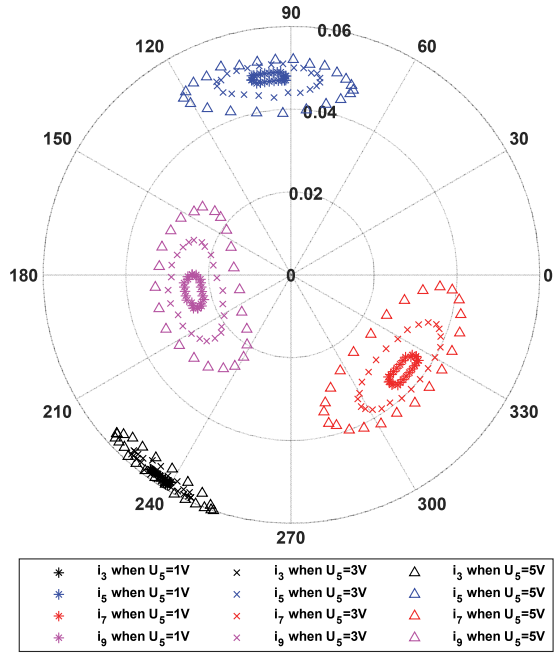

Fig. 12. Current harmonics for input voltage containing different levels of U_{H5} and phase φ_{UH5} = 0,15,30…345º.

As the measurement outcome presents, the reaction patterns are rather difficult to fully correlate to the Norton model. Given the reaction patterns, pure Norton model would explain the circular harmonic current reaction components.

It can be pointed out that the current source model can be used to describe the center of the reaction vector is at the same location regardless of the harmonic voltage presence. However, the impedance component model cannot fully describe that the reaction vector occurrence is of elliptical shape. In addition, the Norton model cannot explain that there is a reaction to other order current harmonics, not related to the frequency of the influencing voltage harmonic. For example, the physical coupling of the reaction of U_{H3} at 150 Hz frequency is rather difficult to associate to the variation of I_{H7} at 350 Hz frequency etc. The approach to use interharmonic coupling impedance matrices [11] does not provide a solution to the reactions at frequencies at non-integer multiple but also not to elliptical reaction pattern.

DISCUSSION

The voltage harmonics in the grid waveform are largely the upstream result of load current harmonics. Therefore, in order to model the grid voltage, the reaction between the voltage and current harmonics needs to the known. The impact of amplitude and phase-varying voltage harmonic on amplitude and phase angle of current harmonics are analyzed in this paper relying on measurement results. It can be seen that there is a considerable effect on amplitude and phase on current harmonic emission of load; when amplitude or phase angle of injected voltage is changed. If the harmonic currents are assumed to follow the parallelogram principle of vector addition they form an almost elliptical shape if only the phase angle of voltage harmonic is varied.

It has to be noted that the supply voltage waveform provided by the utility contains a prominent level of harmonics, which are injected by all the connected components. The analysis here only presents the effect of 3rd, 5th harmonic voltage on 3rd, 5th, 7th and 9th harmonic current drawn by both linear and nonlinear loads.

The significance of the outcome presented here is that the coupling of the different reaction current vectors to the harmonic voltage component is significant and it is occurring across different harmonics of different orders. This calls for establishment of more accurate model that could describe the reaction patterns on the physical level. Proposals of this model will be provided in the further upcoming papers. In this way, the models to estimate the distribution network voltage harmonic levels due to presence of more nonlinear loads and sources can be described with more accuracy. The more accurate models are needed to reliably estimate the hosting capacity of renewable sources and contemporary customer load units in the distribution networks.

REFERENCE

[1] M. N. Iqbal, L. Kütt, B. Asad, T. Vaimann, A. Rassõlkin, and G. L. Demidova, "Time Dependency of Current Harmonics for Switch-Mode Power Supplies," *Appl. Sci.*, vol. 10, no. 21, p. 7806, Nov. 2020, doi: 10.3390/app10217806.

[2] M. Jarkovoi, M. Naveed Iqbal, and L. Kutt, "Analysis of harmonic current stability and summation of LED lamps," *2019 Electr. Power Qual. Supply Reliab. Conf. 2019 Symp. Electr. Eng. Mechatronics, PQ SEEM 2019*, pp. 1–8, 2019, doi: 10.1109/PQ.2019.8818237.

[3] B. Badrzadeh and M. Gupta, "Practical experiences and mitigation methods of harmonics in wind power plants," *IEEE Trans. Ind. Appl.*, vol. 49, no. 5, pp. 2279–2289, 2013, doi: 10.1109/TIA.2013.2260314.

[4] Y. Xiao and X. Yang, "Harmonic summation and assessment based on probability distribution," *IEEE Trans. Power Deliv.*, vol. 27, no. 2, pp. 1030–1032, 2012, doi: 10.1109/TPWRD.2012.2187124.

[5] "IEC 61000-4-30: Electromagnetic compatibility (EMC) - Part 4-30: Testing and measurement techniques - Power quality measurement methods," Geneva.

[6] M. N. Iqbal, L. Kutt, N. Shabbir, and B. Asad, "Comparison of Current Harmonic Emission by Different Lighting Technologies," in *2020 IEEE 61th International Scientific Conference on Power and Electrical Engineering of Riga Technical University (RTUCON)*, Nov. 2020, pp. 1–6, doi: 10.1109/RTUCON51174.2020.9316615.

[7] M. Naveed Iqbal, M. Jarkovoi, L. Kutt, and N. Shabbir, "Impact of LED thermal stability to household lighting harmonic load current modeling," *2019 Electr. Power Qual. Supply Reliab. Conf. 2019 Symp. Electr. Eng. Mechatronics, PQ SEEM 2019*, 2019, doi: 10.1109/PQ.2019.8818226.

[8] M. N. Iqbal, L. Kütt, B. Asad, N. Shabbir, and I. Rasheed, "Time-dependent variations in current harmonic emission by LED lamps in the low-voltage network," *Electr. Eng.*, Jan. 2021, doi: 10.1007/s00202-020-01175-4.

[9] M. N. Iqbal, "Measurement Based Approach for Residential Customer Stochastic Current Harmonic Modelling," [Online]. Available: https://digikogu.taltech.ee/en/Item/cc2248c5-5530-44fb-8150-51de0e7832ad?_ga=2.233526238.1973071602.1633682412-1057891764.1633682412.

[10] Y. Xiao and X. Yang, "A grid harmonic summation method based on the probability assessment of harmonic phase angles," *ICHQP 2010 - 14th Int. Conf. Harmon. Qual. Power*, pp. 1–6, 2010, doi: 10.1109/ICHQP.2010.5625480.

[11] F. Yahyaie, S. Member, P. W. Lehn, and S. Member, "Using Frequency Coupling Matrix Techniques for the Analysis of Harmonic Interactions," vol. 31, no. 1, pp. 112–121, 2016.

Publication II

K. Daniel, L. Kütt, M. N. Iqbal, A.U. Rehman, M. Shafiq, H. Hamam, “Current Harmonic Aggregation Cases for Contemporary Loads,” *Energies*, vol. 15, no. 2, 2022, doi: 10.3390/en15020437.

energies

MDPI

Article

Current Harmonic Aggregation Cases for Contemporary Loads

Kamran Daniel [1,2], Lauri Kütt [1], Muhammad Naveed Iqbal [1,3,*], Noman Shabbir [1], Ateeq Ur Rehman [3], Muhammad Shafiq [4,*] and Habib Hamam [5,6,7]

1 Department of Power Engineering and Mechatronics, Tallinn University of Technology, Ehitajate tee 5, 19086 Tallinn, Estonia; kdanie@taltech.ee (K.D.); lauri.kutt@taltech.ee (L.K.); noshab@taltech.ee (N.S.)
2 Department of Electrical, Electronics and Telecommunication Engineering, FSD Campus, University of Engineering and Technology, Lahore 54890, Pakistan
3 Department of Electrical Engineering, Government College University, Lahore 54000, Pakistan; ateeq.rehman@gcu.edu.pk
4 Department of Information and Communication Engineering, Yeungnam University, Gyeongsan 38541, Korea
5 Faculty of Engineering, Université de Moncton, Moncton, NB E1A3E9, Canada; habib.hamam@umoncton.ca
6 Spectrum of Knowledge Production & Skills Development, Sfax 3027, Tunisia
7 Department of Electrical and Electronic Eng. Science, School of Electrical Engineering, University of Johannesburg, Johannesburg 2006, South Africa
* Correspondence: miqbal@taltech.ee (M.N.I.); shafiq@ynu.ac.kr (M.S.)

Abstract: Power electronic circuits in modern power supplies have improved the conversion efficiency on the one hand but have also increased harmonic emissions. Harmonic currents from the operation of these units affect the voltage waveforms of the network and could compromise the reliability of the network. Load and source non-linearity can, therefore, limit the renewable source's hosting capacity in the grid, as a large number of inverter units may increase the harmonic distortions. As a result, voltage and current distortions could reach unbearable levels in devices connected to the network. Harmonic estimation modelling often relies on measurement data, and differences may appear in mathematical simulations as the harmonic aggregation or cancellation may generate different results due to the inaccuracies and limitations of the measurement device. In this paper, the effect of harmonic currents cancellation on the aggregation of different load currents is evaluated to show its impact in the network by presenting a comparison between the measurement and mathematical aggregation of harmonics. Furthermore, the harmonic cancellation phenomenon is also qualified for multiple loads connected to the power supply.

Keywords: current harmonics; voltage distortions; power quality; hosting capacity; LED lighting; photovoltaics; electric vehicles

Citation: Daniel, K.; Kütt, L.; Iqbal, M.N.; Shabbir, N.; Rehman, A.U.; Shafiq, M.; Hamam, H. Current Harmonic Aggregation Cases for Contemporary Loads. *Energies* **2022**, *15*, 437. https://doi.org/10.3390/en15020437

Academic Editor: Alon Kuperman

Received: 5 December 2021
Accepted: 5 January 2022
Published: 8 January 2022

1. Introduction

Hosting capacity (HC) evaluation for the inclusion of renewable energy production and storage units, including photovoltaic inverters, battery chargers, etc., is one of the tasks that must be carried out in distribution network planning. In [1], the historical outline of HC assessment is explained and the HC of low voltage networks is illustrated by increasing the number of electric vehicle (EV) chargers or photovoltaic (PV) panels [2]. The performance index calculation requires a network model, partial input data, and Monte Carlo simulation to indicate the uncertainties. Different approaches for HC, which are deterministic, stochastic, and time-series are outlined in [3]. These approaches use unique uncertainties, computation time, precision, input data, and models. A detailed investigation and mitigation of challenges associated with power quality when renewable distribution systems are integrated into a grid are presented in [4] For example [5], ideas are presented to forecast the HC of the distribution network as they make up important tools to plan the distribution network and predict the impact on power quality due to the integration of the PV system.

HC can be more accurately assessed if the harmonic profile of contemporary loads is analyzed along with the harmonic profile of future loads and sources such as EV and PV inverters [6]. For environmentally sustainable electricity production and use, the number of solar plants and EVs is increasing annually; this impacts the distribution network in terms of power quality. Measurements can provide a closer insight into the solar inverter effect on THDv of the supply voltage [7].

As most contemporary loads implement power electronic converters at the load side, their non-linear characteristics are a reason for feeding harmonic currents into networks. This has an influence on the voltage distortion parameters of an AC power system. In order to have a power system with credible power quality indices [8,9], it is essential to determine the contribution of harmonic content injected devices connected to the electrical grid [10]. Voltage distortion not only influences a single consumer, but affects all other consumers sharing the same network [11,12]. To deliver the least distorted voltage to consumers, the network operator must take actions to leverage voltage distortions.

Current harmonics can be represented as phasors with RMS and phase angle values; in such a manner, harmonic components are rotating vectors with real and imaginary parts in the complex plane. In a distribution network where multiple non-linear loads are connected, it is likely that the different harmonic load currents not only have different RMS component values but also harmonic phase angle values. As a result, various combinations of similar loads could lead to variations in the aggregated harmonic current. In order to find the total harmonic currents loading the substation, the individual load harmonics have to be summed geometrically. The total harmonic current from the multiple devices can be significantly lower than the arithmetic sum of individual current magnitudes due to diversity in the harmonic phase angles [13].

Harmonic voltages with different magnitudes and phase angles can cause changes in load current harmonics both in RMS and phase [14]. In addition, both the voltage and current distortions vary with different loading levels and are time-varying PQ characteristics. Hence, it is highly complex to accurately determine current harmonics magnitude and phase angle values for every time instant [15]. Summation coefficients are provided by IEC standard 61000-3-6 to perform the summation of harmonic magnitudes [16]. The IEC standard has suggested rules based on summation coefficients, if using harmonic current magnitudes. Furthermore, there are several other influences to current harmonic RMS levels and phase angle values. The impact on harmonic current variation due to the impedance of cables attached to LED lamps was studied in [17].

One of the most straightforward approaches to determine the expected load harmonic current fingerprint is the measurement of the loads. This must also include aspects of sensitivity [18]. For example, the thermal stability of loads refers to the temperature stability when performing measurements; for example, LED lamps and power supplies require roughly forty minutes [19]. The average variation interrelation of higher-order harmonic currents increases with an increase in the number of loads connected simultaneously [20]. Similarly, in [21] the aggregation result was compared to measurement data with multiple loads connected simultaneously, showing that higher-order harmonics vary more significantly than lower-order harmonics. In addition, higher-order harmonic current vectors are spread out more compared to lower-order harmonics. THD_I was observed with an average reduction of up to 10% due to the harmonic currents' cancellation effect.

This paper focuses on the practical aspects of the aggregation of the harmonic emission at the point of common coupling; this is usable, for example, in the case of simplified measurements of RMS harmonic currents in the estimation of load and source HC. The scale and accuracy of harmonic component summation are measured and compared with the values obtained from a single load measurement. Combinations of loads are tested for the total harmonic load currents' estimation. The analysis is based on measurements performed for different numbers of combinations of loads operating simultaneously. The harmonic estimation of multiple loads operating at the same time presents an approximate occurrence of cancellation that may happen when multiple devices are operating. Not

accounting for the cancellation would lead to pessimistic harmonic estimation, in turn leading to lower hosting capacity estimation.

2. Harmonic Variation and Summation

Harmonic current can be represented as complex phasor quantities; measured values are RMS and phase angle. Therefore, in order to perform aggregation, the amplitude and phase form can be converted to real and imaginary components in the complex plane using the following formulas. Harmonic aggregation is performed using Equation (1).

$$i(t) = \sum_{h=1}^{\infty} I_{m,h} \cos(2\pi h f_1 t + \varphi_{I,h}) \tag{1}$$

f_1 is the frequency of fundamental component, h is the harmonic number, and $\varphi_{I,h}$ is the phase shift to corresponding h number. The real and imaginary values of the any harmonic phasor are:

$$i_{x,h} = \mathrm{Re}(I_h) = I_{m,h} \cos(\varphi_{i,h})$$
$$i_{y,h} = \mathrm{Im}(I_h) = I_{m,h} \sin(\varphi_{i,h})$$

and a modulus of them will be:

$$I_{m,h} = |I_h| = \sqrt{i_{x,h}^2 + i_{y,h}^2} \tag{2}$$

As root-mean-square values can be used to present phasor magnitudes, the RMS value of any harmonic and total RMS current can be calculated using the equation below.

$$I_h = \sqrt{\frac{i_{x,h}^2 + i_{y,h}^2}{2}} = \frac{I_{m,h}}{\sqrt{2}} \tag{3}$$

$$I = \sqrt{\sum_{h=1}^{\infty} \frac{I_{m,h}^2}{2}} \tag{4}$$

Harmonic currents are produced when a load draws a current with a non-sinusoidal waveform. According to the Kirchoff Current Law (KCL), the total sum of current at the point of common connection is zero when multiple loads are simultaneously connected. Every load device behaves as a source of harmonics and provides its share, so the total current at PCC is the aggregation of individual harmonics from all load devices according to superposition. In order to find total vector current, the real and imaginary components of individual loads should be added.

$$\begin{cases} i_{x\sum,h} = \sum_{k=1}^{K} i_{x,h,k} \\ i_{y\sum,h} = \sum_{k=1}^{K} i_{y,h,k} \end{cases} \tag{5}$$

$i_{x,h,k}$—real component of current harmonic of particular device k;
$i_{y,h,k}$—imaginary component of current harmonic of load k;
K—total loads at the point of common connection.
The resultant magnitude and RMS of a particular harmonic are:

$$I_{m\sum,h} = \sqrt{i_{x\sum,h}^2 + i_{y\sum,h}^2} \tag{6}$$

$$I_{\sum,h} = \frac{I_{m,h}}{\sqrt{2}} \tag{7}$$

Phase angle calculation is performed according to the quadrant of the phasor. The resultant phase-angle range is –180 to +180 degrees (–π to +π).

$$\theta_{I\sum,h}\begin{cases} \tan^{-1}\left(\frac{i_{y\sum,h}}{i_{x\sum,h}}\right), if\ i_{x\sum,h} > 0 \\ \tan^{-1}\left(\frac{i_{y\sum,h}}{i_{x\sum,h}}\right) + \pi, if\ i_{x\sum,h} < 0\ and\ i_{y\sum,h} \geq 0 \\ \tan^{-1}\left(\frac{i_{y\sum,h}}{i_{x\sum,h}}\right) - \pi, if\ i_{x\sum,h} < 0\ and\ i_{y\sum,h} < 0 \\ \frac{\pi}{2}, if\ i_{x\sum,h} = 0\ and\ i_{y\sum,h} > 0 \\ -\frac{\pi}{2}, if\ i_{x\sum,h} = 0\ and\ i_{y\sum,h} < 0 \end{cases} \quad (8)$$

To find the summation accuracy of harmonics, harmonic phasors of individual loads are aggregated to find the resulting harmonic current magnitudes and phase of investigated load combinations. The calculated values of phasors are then compared to measured phasor data of the respective combination of load, and the difference between the calculated and actual values is found. Figure 1 illustrates the difference between measured and aggregated harmonic vectors.

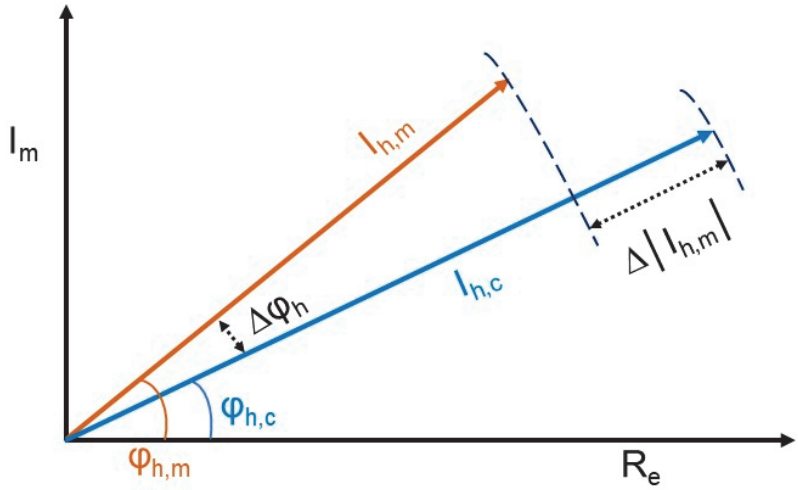

Figure 1. Determining the magnitude and phase angle difference of measured (brown) and calculated (blue) values.

3. Measurement Setup

Sixteen LED lamps are arbitrarily chosen as loads; lamps have a power rating range from 8 W to 17 W and a luminous flux between 800 and 1521 Lm. To reach thermal stability, the LED lamps and power amplifier/power supply were powered up for more than one hour prior to measurement [19]. Table 1 also shows the total harmonic distortion percentage of all the LED lamps used in the experiment. Three of the lamps have a THD_I in the range of 28 to 53%; the others have a THD_I above 100%.

Table 1. Parameters of lamps used for testing.

Lamp No.	Lamp Rated Power (W)	Lamp Rated Luminance (Lm)	Measured THDI (%)
1	14	1521	145
2	10	1055	164
3	9	810	135
4	12	1055	149
5	12	900	134
6	10	800	148
7	12	1055	152
8	9	1055	162
9	8	806	46
10	11	1060	28
11	9	806	139
12	10.5	1060	136
13	9.8	806	52.7
14	10	1055	135
15	11	1055	154
16	17	1521	134

The experimental setup consists of a power quality (PQ) analyzer, a data acquisition (DAQ) module, a load combination array, a programmable power supply, and a personal computer. The PQ analyzer realizes a one-second measurement that is aggregated and recorded according to class-A standards [22]. MATLAB controls the generation of input voltage for measurement setup as it programs the DAQ module to provide the signal to programmable power supply. Supply waveform is generated with the sampling frequency of 100 kS/s, meaning 2000 points for every 50 Hz cycle. The same MATLAB script drives the load scenarios by supplying a digital binary switching signal to dual-pole double-throw (DPDT) relays which are embedded on 16-load combination array [22,23].

Initially, harmonic current measurements are performed for each load/lamp individually. Afterwards, a combination of loads—for example, load numbers 1 and 2—are subjected to measurement. Different load combinations are used in each step. Each individual lamp or lamp combination is run for 10 s. The PQ analyzer records with a minimum interval of 1 s. The phase angles of harmonic currents are recorded with respect to the input fundamental voltage. Measurements are only conducted after the thermal stability of the load, with a warm-up period of 60 minutes. Continuous power is provided to LED lamps to maintain a working temperature.

Lamps are supplied either by a source to warm them up to a stable operating temperature or during the measurement from the pure sinewave source. Double throw relays provide power from the secondary source when lamps are unengaged. The outline of the measurement setup is presented in Figure 2.

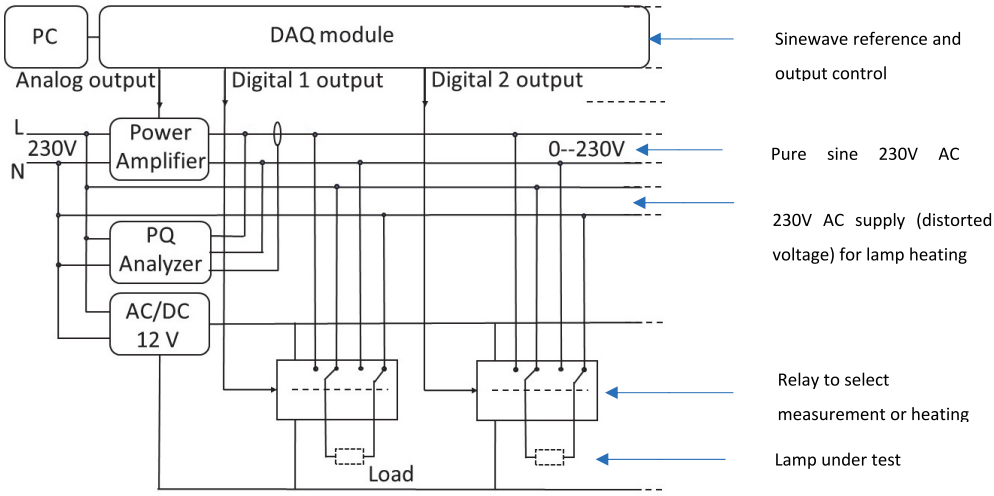

Figure 2. Measurement setup.

4. Measurement Results

4.1. Individual Load Measurements

The measured load currents of all sixteen lamps are shown in Figure 3, and measured RMS currents are in the 40 mA to 140 mA range. The figure also indicates the harmonic profile details of lamps used in this study. Only odd harmonic currents under the 1 kHz range are considered for analysis and the calculation is in the present context. The limit used is due to the measurement system capabilities and related uncertainty. However, it was verified that harmonics above 1 kHz have a negligible impact on the load current. LEDs' internal circuit topology can play an essential role in defining the harmonic current fingerprint of lamps, as some lamps can contain active or passive filters and power factor correction circuit for reducing the harmonic content in a current. More details on the lamp circuit topologies are presented in [21,23]. The number of circuit types selected here is assumed to present the statistical mix of lamps on the market. Every lamp follows approximately the same pattern: the RMS of the current harmonic components decreases as the order of the harmonic decreases. Table 2 represents the RMS and phase angle information of the test lamps, as the phase angle information must be observed during the estimation of the total harmonics of multiple devices.

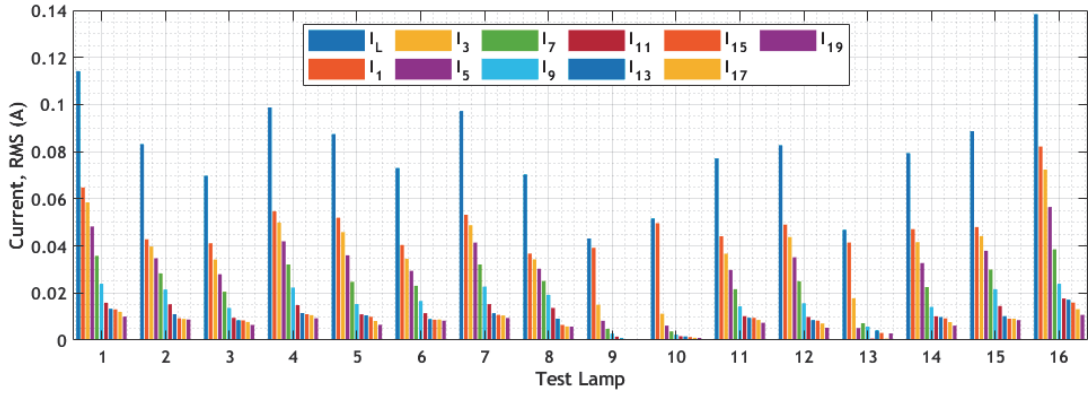

Figure 3. Current harmonics in lamps.

Table 2. Measured harmonics' current characteristics for individual lamps.

Lamp No.	I_3	θ_{I3}	I_5	θ_{I5}	I_7	θ_{I7}	I_{13}	θ_{I13}	I_{19}	θ_{I19}
1	0.059	−123	0.048	97	0.036	−40	0.013	−34	0.01	−38
2	0.04	−128	0.035	87	0.028	−55	0.011	−92	0.009	−100
3	0.034	−120	0.028	101	0.021	−33	0.008	−19	0.007	−18
4	0.05	−126	0.042	91	0.032	−49	0.012	−60	0.009	−69
5	0.046	−116	0.036	108	0.025	−22	0.011	13	0.007	32
6	0.035	−127	0.029	89	0.023	−52	0.009	−69	0.008	−81
7	0.049	−128	0.041	89	0.032	−53	0.011	−71	0.009	−82
8	0.034	−136	0.03	73	0.025	−76	0.009	−141	0.006	−154
9	0.015	−6	0.008	−10	0.005	−15	0.001	−39	0.0003	−84
10	0.011	−19	0.006	−17	0.004	−12	0.002	−44	0.001	−107
11	0.037	−117	0.03	107	0.022	−25	0.01	−1	0.007	10
12	0.044	−126	0.035	92	0.025	−46	0.009	−35	0.005	−40
13	0.018	−166	0.005	15	0.007	25	0.004	51	0.003	78
14	0.042	−117	0.033	108	0.023	−22	0.01	12	0.006	28
15	0.044	−135	0.038	75	0.03	−72	0.01	−114	0.009	−137
16	0.072	−114	0.057	113	0.039	−15	0.017	26	0.011	51

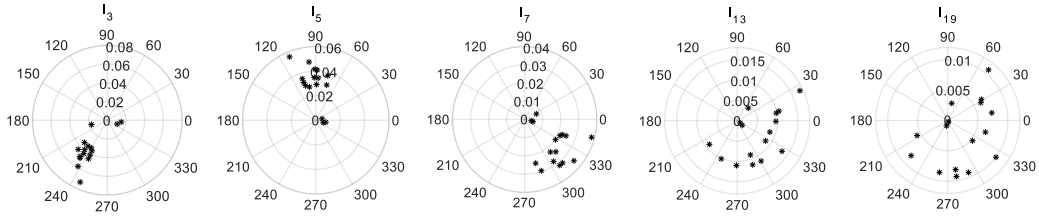

4.2. Aggregation Measurement Results

All possible combinations of the sixteen lamps are issued by switching two lamps at a time. The total number of possible lamp combinations is 120. Due to the limitation of the power in the voltage power supply, only two lamps are switched on at a time. For any combination, measurements of the individual lamps are taken and resultant harmonics are calculated by adding the individual current harmonics.

The RMS measurement data of all combinations of the lamps are illustrated in Figure 4. The trend shows the similar behavior of harmonics; that is, lower-order harmonics have more significant percentage than higher-order harmonics in total harmonic content. Very few lamp combinations show a small amount of harmonic content because these loads may contain harmonic filters; for those combinations, even lower-order harmonic content is negligible.

Figure 5 shows the third harmonic data of all the combinations used for comparison. The first graph represents the third harmonics' phasors recorded by the measurement device for all combinations. The second part of the figure shows all estimated harmonics, calculated by the geometric addition of the individual third harmonic current component values of lamps present in any particular combination using Formula (5) with K = 2.

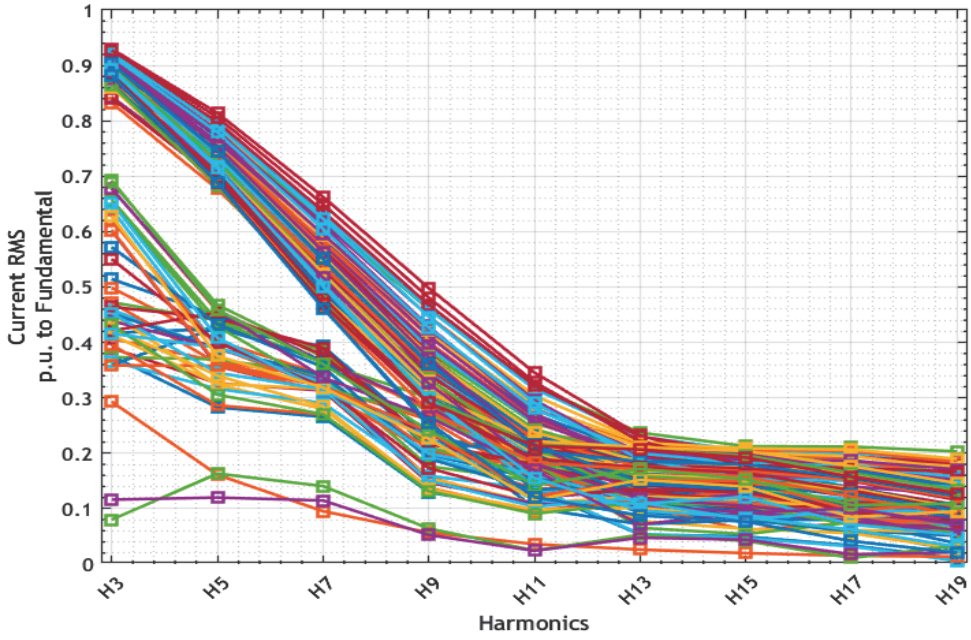

Figure 4. Measured harmonic currents' RMS levels (with respect to RMS of fundamental harmonic current components) of 120 lamp combinations.

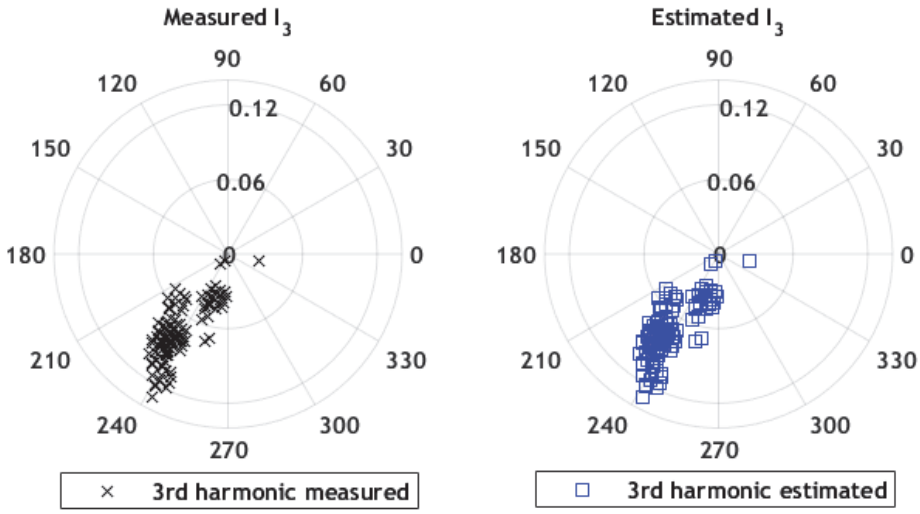

Figure 5. Third harmonic current vectors of all lamp combinations.

The actual measurement data of every load combination are compared with the respective aggregated sum of individual harmonic currents of lamps that are present in the combination. Each point is the difference in the estimated and measurement results from an exclusive combination. The magnitude difference is represented as a percentage. The difference in the phase angles of measured and estimated harmonics is expressed in degrees.

The geometric sum and measured values of the harmonics in different load combinations are demonstrated in Figure 6. Phase angles illustrate the spread of harmonic phasors. Harmonics with a broader spread of phase angle are likely to face more cancellation (see further); as shown in the second part of Figure 6, phase angles range practically from –180 to 180 degrees for the nineteenth harmonic. When multiple devices are connected at a common point, higher-order harmonics are more likely to face a harmonic cancellation effect.

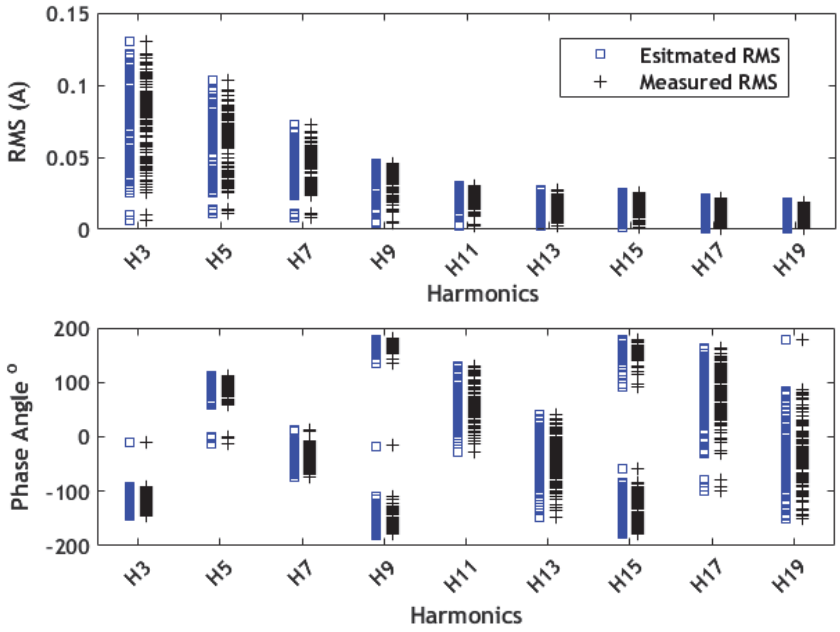

Figure 6. Harmonic RMS and phase values of all lamp combinations.

The top and bottom edges of the boxplot in Figure 7 show the 95th and 5th percentile values, while the middle red line indicates the mean value. The whiskers are extended towards extreme values. Figure 7 shows that a near-perfect harmonic summation is seen with a sinusoidal supply provided to loads. The mean difference in the estimated and measured values of all harmonics is very close to zero, which is evidence of the accurate estimation and measurement of load harmonics. The mean difference in the lower-order harmonics is close to zero from the third to the ninth harmonic. The previous study established that the higher-order harmonics have a wider spread on a complex plane, so the mean RMS difference in the higher-order comparison data is more significant than that of lower-order. In the second part of Figure 7, the phase difference in measured and estimated harmonic current increase with harmonic order is shown. The overall difference in phase angle remains below 0.5 degrees.

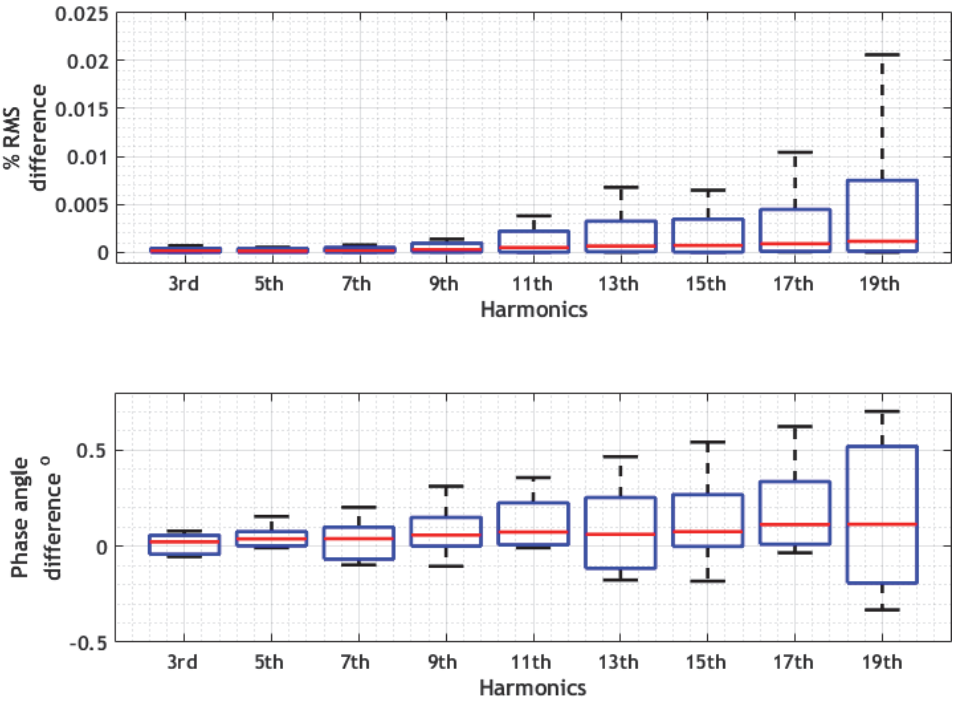

Figure 7. Percentage of RMS difference and phase angle difference in the calculated and measured results of LED loads.

The verification above is important for the following context:

(1) To verify that the harmonics presented with low magnitudes are handled with enough accuracy, and to reflect that if a higher number of such load current components with low magnitudes are accumulated, their totals are expected to have a relatively low order of error, both in magnitude and phase angle values.

(2) While the equipment used for performing measurements of the actual LED lamp combinations is not capable of reliably supplying more than two or three lamps at a time, the analytical cumulative harmonic current analysis using (5) will provide results that are also applicable for higher numbers of LED lamps assumed to be used at the same time.

These assumptions will be used in the following analysis for the combinations where higher numbers of LEDs are used at the same time (2–16).

5. Aggregation Analysis and Harmonic Cancellation Estimation

It has been suggested that renewable-source converters would have an impact on the distribution network power quality and create distortions similar to non-linear loads. Massive LED-lamp inclusion to the loads would provide a healthy increase in the harmonic currents' levels in the grids. More electric vehicles directly bring the high-power non-linear loads to the distribution networks. Utility engineers would need to be prepared to analyze the situation and determine the sufficient potential hosting capacity availability prior to the addition of new non-linear units to the grid.

Engineers usually do not have the tools to present harmonics' phase angles, and usually present the harmonic RMS. This is used to compare the actual situation to that of [24]. If there is a need to estimate the added units' impact on the distribution grid, observing the RMS harmonic currents only will create uncertainty in the estimation of the

total load harmonic current. The simplest way to estimate the total RMS harmonic current is to add these currents arithmetically [25].

The harmonic cancellation refers to the cumulation of the harmonic currents in such a manner that the resulting RMS harmonic current is lower than the arithmetic sum [26–28]. The cases with arithmetic sum (in case only RMS measurements are available) and geometric sum (RMS and phase angle data are available) is presented here. The effect of harmonic cancellation can be estimated using a cancellation factor.

$$K_{can} = 1 - \frac{I_{RMS,h,total}}{\sum_{n=1}^{N} I_{RMS,h,n}} \tag{9}$$

where N is the number of total individual loads.

Figure 8 represents the histogram of the harmonic cancellation coefficient when multiple LEDs are connected simultaneously. It can be seen that the cancellation coefficient is around 0.5 for the majority of load scenarios in higher-order harmonics. As for some load combinations, cancellation coefficients even reach unity. With a greater number of connected loads, the cancellation coefficient increases. $K_{can} = 1$ means that harmonic current will be cancelled out to 0 magnitude. It is examined in [23,29,30] that with the increase in the number of lamps, an individual current harmonic components reduction does not happen in a similar pattern for lower and higher-order harmonics. This is due to the fact that low-order harmonic phasors are closely aligned in comparison to high-order phasors on the complex plane. The resulting harmonic levels are decreased due to the cancellation effect, and high-order harmonics have more average reduction as compared to lower-harmonic orders.

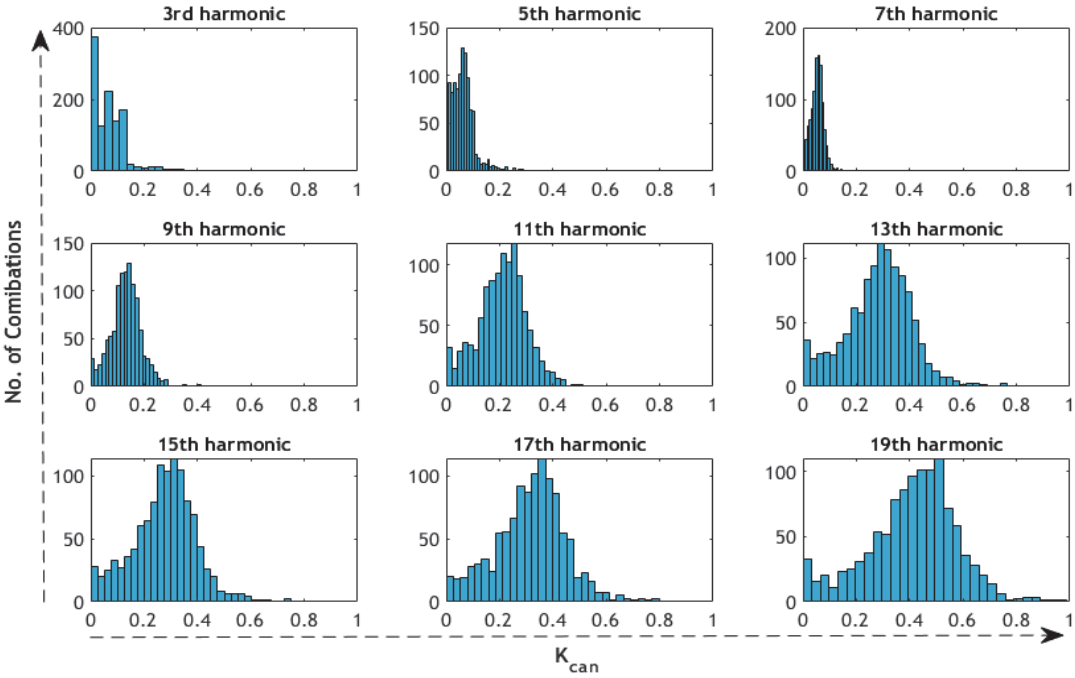

Figure 8. Harmonic cancellation effect of LED loads (no. of load scenarios/combinations on y-axis and cancellation coefficient on the x-axis) (number of combinations reported).

Figure 9 illustrates the cancellation coefficient for harmonics on the y-axis and the share of occurrence on the x-axis. More than a thousand different load scenarios are created

by changing the number of loads connected at the same time. The occurrence of K_{can} is higher and less scattered when the number of attached devices is increased.

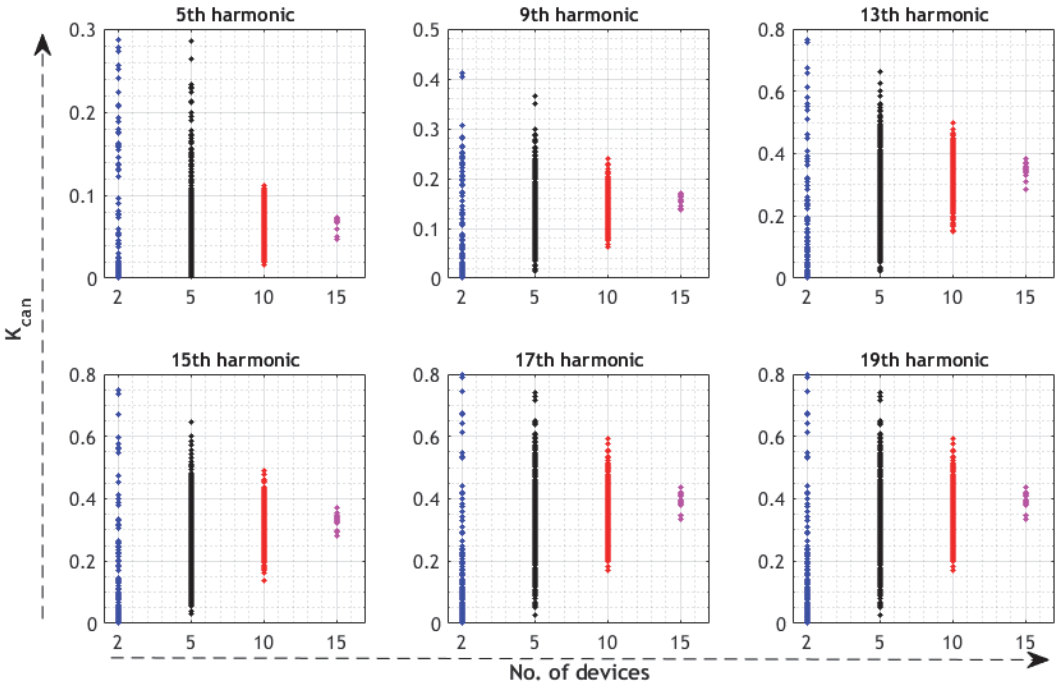

Figure 9. Harmonic cancellation coefficient of LED load devices operating at the same time.

The data presented in Table 3 were taken from [26]. This table summarizes the measured data EV onboard battery chargers for sinusoidal supply voltage and zero source impedance. Load scenarios are created by taking a particular combination of the EVs, and the harmonic cancellation factor is also calculated. The occurrence of K_{can} of EVs is similar to the K_{can} occurrence of LEDs for lower-order harmonics, as observed for the case of the fifth harmonic in Figures 9 and 10. However, the distributions of the cancellation coefficients are spread further as compared to the LED lamps. This is because the EV charging loads have a different harmonic current profile than LEDs.

Table 3. Measured harmonics for individual EVs.

EV No.	Prated (kW)	THD_I (%)	I_1	θ_{I1}	I_3	θ_{I3}	I_5	θ_{I5}	I_7	θ_{I7}
1	7.7	5.1	27.9	−1	0.7	165	0.2	12	0.1	33
2	7.4	4.4	31.0	−1	0.9	177	0.4	171	0.5	164
3	3.3	7.9	13.9	3	1.0	−154	0.2	−167	0.2	−172
4	3.3	2.9	15.1	7	0.2	−74	0.1	−129	0.1	−85
5	3.3	11.9	15.9	7	1.8	−110	0.1	47	0.1	−70
6	3.3	5.4	15.5	1	0.5	−177	0.3	−174	0.2	−179
7	7.2	2.9	15.4	5	0.2	−68	0.2	−128	0.1	−82

Table 3. *Cont.*

EV No.	Prated (kW)	THD_I (%)	I_1	θ_{I1}	I_3	θ_{I3}	I_5	θ_{I5}	I_7	θ_{I7}
8	3.3	3.1	9.6	3	0.3	−3	0.0	−25	0.0	−36
9	2.75	7.4	13.1	5	0.9	−141	0.0	6	0.0	−66
10	3.3	3.2	15.3	4	0.4	−126	0.1	−160	0.1	−168
11	16.8	5.9	28.7	14	1.6	−166	0.0	−94	0.1	−47
12	3.3	7.2	14.7	2	0.9	−166	0.5	−178	0.3	147
13	3.3	1.7	9.5	3	0.1	−155	0.1	−90	0.1	−139
14	3.3	5.7	9.0	0	0.3	137	0.2	27	0.1	−118
15	6.1	2.8	14.2	3	0.3	−173	0.1	167	0.1	−144
16	7.4/22	9.4	30.7	12	0.1	168	1.8	161	0.6	86

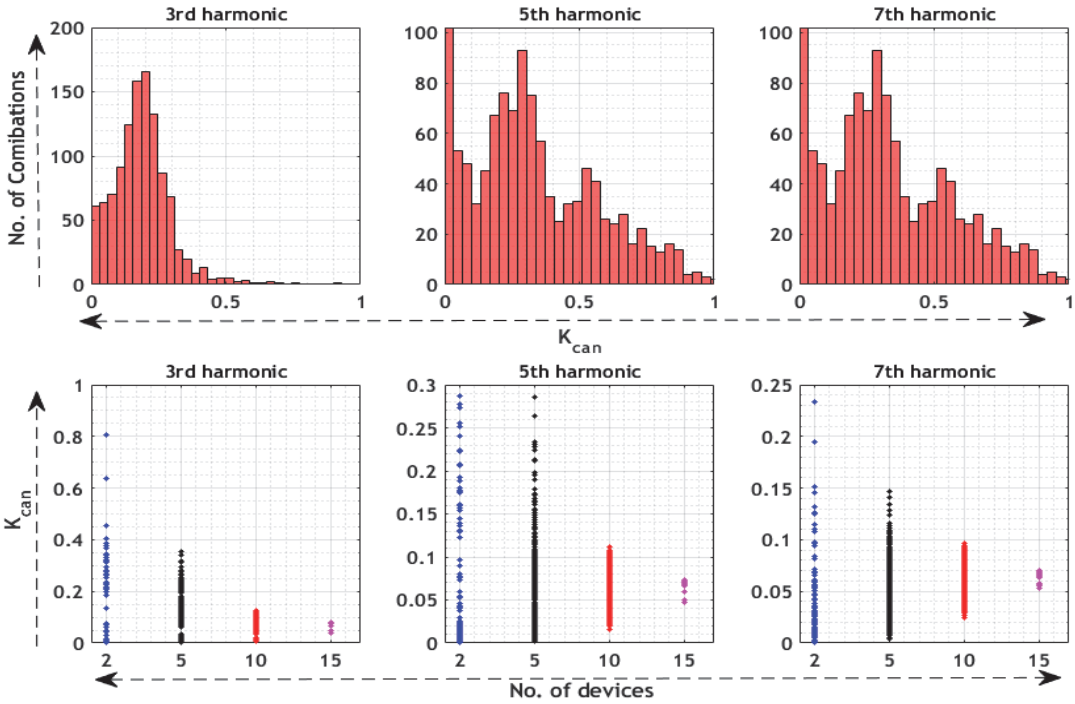

Figure 10. Harmonic cancellation effect of EV loads.

6. Conclusions

The harmonic currents are vital for any future load or renewable power infeed source assessment, as these are almost completely of non-linear nature. The presence of harmonic currents is in itself not a direct problem, as long as their levels in the grid are not too high. The supply will be compromised once the supply voltage harmonics of the grid increases, and will be above accepted standard levels due to the influence of the current harmonics. This means that exceeding the hosting capacity limits the capabilities of the grid. This paper addresses the basics of analysis for the addition of a significant number of non-linear endpoints to the grid, which are usable for the context of hosting capacity estimation.

The assessment of accuracy in harmonic summation and a brief investigation of the cancellation effect has been discussed in this study based on the analytic approach for the low-power load devices. Only odd harmonics are considered, starting from the 3rd to the 19th orders. Harmonic magnitudes and phase angles are seen to have a different spread of phasors on the complex plane. The harmonic cancellation effect is directly

related to the number of loads connected to the point of common connection and is more visible for higher-order harmonics. In the results for lower-order harmonics, fundamental component harmonic cancellation does not emerge significantly and is below . . . 0.2 (3rd, 5th, . . . orders).

A measurement setup with a pure sine wave supply voltage is used to inject harmonic phasors to analyze the load combinations so that the aggregation and cancellation can be observed clearly. Compared to summation calculations, the resultant harmonic phasors were found to have a very miniscule difference from the phasor values measured when load combinations were connected simultaneously. It was found that while higher-order harmonics show different dispersion in magnitude and angle values than lower-order components, there are rather insignificant differences between calculated and measured values.

It is presented that the cancellation effect is more significant when the number of connected devices is increased. The cancellation coefficient of EV charging current harmonics is also compared with that of LED loads. It was observed that the cancellation coefficients of both load types show a similar distribution.

It can be seen that for the higher current harmonics, RMS-based analysis for perspective loads inclusion is not advised. The reason for this is that there is a high chance of harmonic cancellation when a large number of devices are connected to the grid. RMS-based estimation is pessimistic. It could provide an indication of higher than-actual-results that could impose some unjustified limits—for example, on the renewable energy source hosting capacity of the distribution networks. For a better assessment, analysis using more sophisticated measurement capabilities, including harmonic phase angle reporting, is advised.

It has to be noted that the supply voltage waveform provided by the utility typically contains a notable level of harmonics, which are injected by all the components connected to a utility grid. The analysis here is only presented for the sinewave voltage supply. For the real grid voltage waveform, the LED and EV harmonic currents could differ from the values provided in this paper. This will be investigated in more detail in upcoming research.

Author Contributions: Conceptualization, K.D. and L.K.; methodology, M.N.I.; software, K.D. and N.S.; validation, A.U.R., M.S. and H.H.; formal analysis, K.D. and M.S.; writing—original draft preparation, K.D.; writing—review and editing, L.K., M.N.I. and M.S. All authors have read and agreed to the published version of the manuscript.

Funding: This work was supported by the Estonian Council grant (PSG142).

Institutional Review Board Statement: Not applicable.

Informed Consent Statement: Not applicable.

Data Availability Statement: Data is contained within the article.

Acknowledgments: The authors thank the Natural Sciences and Engineering Research Council of Canada (NSERC) and New Brunswick Innovation Foundation (NBIF) for the financial support of the global project. These granting agencies did not contribute to the design of the study or the collection, analysis, and interpretation of data.

Conflicts of Interest: The authors declare no conflict of interest.

References

1. Bollen, M.H.J.; Rönnberg, S.K. Hosting capacity of the power grid for renewable electricity production and new large consumption equipment. *Energies* **2017**, *10*, 1325. [CrossRef]
2. Iqbal, M.N.; Kütt, L.; Lehtonen, M.; Millar, R.J.; Püvi, V.; Rassõlkin, A.; Demidova, G.L. Travel Activity Based Stochastic Modelling of Load and Charging State of Electric Vehicles. *Sustainability* **2021**, *13*, 1550. [CrossRef]
3. Mulenga, E.; Bollen, M.H.J.; Etherden, N. A review of hosting capacity quantification methods for photovoltaics in low-voltage distribution grids. *Int. J. Electr. Power Energy Syst.* **2019**, *115*, 105445. [CrossRef]
4. Bajaj, M.; Singh, A.K. Grid integrated renewable DG systems: A review of power quality challenges and state-of-the-art mitigation techniques. *Int. J. Energy Res.* **2020**, *44*, 26–69. [CrossRef]

5. de Oliveira, T.E.C.; Carvalho, P.M.S.; Ribeiro, P.F.; Bonatto, B.D. PV hosting capacity dependence on harmonic voltage distortion in low-voltage grids: Model validation with experimental data. *Energies* **2018**, *11*, 465. [CrossRef]
6. Liu, D.; Wang, C.; Tang, F.; Zhou, Y. Probabilistic assessment of hybridwind-pv hosting capacity in distribution systems. *Sustainability* **2020**, *12*, 2183. [CrossRef]
7. Vinnal, T.; Puusepp, H.; Shabbir, N.; Iqbal, L.N. Case study of non-linear pv inverter devices attached to the lv distribution network. *Agron. Res.* **2020**, *18*, 2639–2652. [CrossRef]
8. *EN 50160:2010*; Voltage Characteristics of Electricity Supplied by Public Distribution Networks. Cenelec: Newark, DE, USA, 2010.
9. *IEEE Standard II59-1995*; IEEE Recommended Practice for Monitoring Electric Power Quality. IEEE: Piscataway, NJ, USA, 1995.
10. Sezgin, E.; Gol, M.; Salor, O. Determination of harmonic current contributions of plants supplied from PCC based on state estimation. In Proceedings of the 2015 23nd Signal Processing and Communications Applications Conference (SIU), Malatya, Turkey, 16–19 May 2015; pp. 2062–2065. [CrossRef]
11. *Electromagnetic Compatibility (EMC)—Part 4–7: Testing and Measurement Techniques—General Guide on Harmonics and Interharmonics Measurements and Instrumentation, for Power Supply Systems and Equipment Connected Thereto*; IEC: Geneva, Switzerland, 2002.
12. Blanco, A.M.; Yanchenko, S.; Meyer, J.; Schegner, P. Impact of supply voltage distortion on the current harmonic emission of non-linear loads. *Dyna* **2015**, *82*, 150–159. [CrossRef]
13. Peterson, B.; Rens, J.; Desmet, J. Harmonic emission assessment on a distribution network: The opportunity for the prevailing angle in harmonic phasors. *CIRED—Open Access Proc. J.* **2017**, *1*, 668–671. [CrossRef]
14. Hansen, S.; Nielsen, P.; Blaabjerg, F. Harmonic cancellation by mixing nonlinear single-phase and three-phase loads. *IEEE Trans. Ind. Appl.* **2000**, *36*, 152–159. [CrossRef]
15. Ye, G.; Cuk, V.; Cobben, J.F.G. A study on harmonic current summation using field measurement data. In Proceedings of the 2016 IEEE International Conference on Power System Technology (POWERCON), Wollongong, NSW, Australia, 28 September–1 October 2016; pp. 1–6. [CrossRef]
16. *Electromagnetic Compatibility (EMC)—Part 3-6: Assessment of Emission Limits for the Connection of Distorting Installations to MV, HV and EHV Power Systems*; IEC: Geneva, Switzerland, 2008.
17. Iqbal, M.N.; Lauri, K. Impact of Cable Impedance on the Harmonic Emission of LED Lamps. In Proceedings of the 21st International Scientific Conference on Electric Power Engineering (EPE), Prague, Czech Republic, 19–21 October 2020; pp. 1–6.
18. Santos, A.; Duggan, G.P.; Young, P.; Frank, S.; Hughes, A.; Zimmerle, D. Harmonic cancellation within AC low voltage distribution for a realistic office environment. *Int. J. Electr. Power Energy Syst.* **2022**, *134*, 107325. [CrossRef]
19. Iqbal, M.N.; Jarkovoi, M.; Kutt, L.; Shabbir, N. Impact of LED thermal stability to household lighting harmonic load current modeling. In Proceedings of the 2019 Electric Power Quality and Supply Reliability Conference (PQ) and 2019 Symposium on Electrical Engineering and Mechatronics (SEEM), Kärdla, Estonia, 12–15 June 2019. [CrossRef]
20. Jarkovoi, M.; Iqbal, M.N.; Kutt, L. Analysis of harmonic current stability and summation of LED lamps. In Proceedings of the 2019 Electric Power Quality and Supply Reliability Conference (PQ) and 2019 Symposium on Electrical Engineering and Mechatronics (SEEM), Kärdla, Estonia, 12–15 June 2019; pp. 1–8. [CrossRef]
21. Iqbal, M.N.; Kütt, L.; Asad, B.; Shabbir, N.; Rasheed, I. Time-dependent variations in current harmonic emission by LED lamps in the low-voltage network. *Electr. Eng.* **2021**, *103*, 1525–1539. [CrossRef]
22. *Electromagnetic Compatibility (EMC)—Part 4–30: Testing and Measurement Techniques—Power Quality Measurement Methods*; IEC: Geneva, Switzerland, 2003.
23. Iqbal, M.N.; Kutt, L.; Shabbir, N.; Asad, B. Comparison of Current Harmonic Emission by Different Lighting Technologies. In Proceedings of the 2020 IEEE 61th International Scientific Conference on Power and Electrical Engineering of Riga Technical University (RTUCON), Riga, Latvia, 5–7 November 2020; pp. 1–6. [CrossRef]
24. Markiewicz, H.; Klajn, A. *Standard EN 50160—Voltage Characteristics in Public Distribution Systems: Voltage Disturbances*; European Copper Institute: Brussels, Belgium, 2004.
25. Meyer, J.; Blanco, A.-M.; Domagk, M.; Schegner, P. Assessment of Prevailing Harmonic Current Emission in Public Low-Voltage Networks. *IEEE Trans. Power Deliv.* **2017**, *32*, 962–970. [CrossRef]
26. Kutt, L.; Saarijarvi, E.; Lehtonen, M.; Molder, H.; Niitsoo, J. Estimating the harmonic distortions in a distribution network supplying EV charging load using practical source data—Case example. In Proceedings of the IEEE Power and Energy Society General Meeting, National Harbor, MD, USA, 27–31 July 2014. [CrossRef]
27. Paget, M. Summary of Results: Round 13 of Product Testing. 2009; pp. 1–33. Available online: http://apps1.eere.energy.gov/buildings/publications/pdfs/ssl/caliper_round13_summary.pdf%5Cnpapers2://publication/uuid/86DAF28E-BE4C-480C-8775-898D90AD5627 (accessed on 16 November 2021).
28. Iqbal, M.N.; Kütt, L.; Daniel, K.; Asad, B.; Ghahfarokhi, P.S. Estimation of harmonic emission of electric vehicles and their impact on low voltage residential network. *Sustainability* **2021**, *13*, 8551. [CrossRef]
29. Kutt, L.; Saarijärvi, E.; Lehtonen, M.; Mõlder, H.; Niitsoo, J. Electric Vehicle Charger Load Current Harmonics Variations due to Supply Voltage Level Differences-Case Examples. In Proceedings of the 2014 International Symposium on Power Electronics, Electrical Drives, Automation and Motion, Ischia, Italy, 18–20 June 2014. [CrossRef]
30. Iqbal, M.N.; Kütt, L.; Daniel, K.; Jarkovoi, M.; Asad, B.; Shabbir, N. Bivariate stochastic model of current harmonic analysis in the low voltage distribution grid. *Proc. Est. Acad. Sci.* **2021**, *70*, 190. [CrossRef]

Publication III

K. Daniel, L. Kütt, M. N. Iqbal, N. Shabbir, M. Parker and M. Jarkovoi, “Waveform Variation Defined Model for Harmonic Current Emissions Including Cross-Order Supply Voltage Harmonics Influence,” in *IEEE Access*, vol. 11, pp. 42276–42289, 2023, doi: 10.1109/ACCESS.2023.3270805.

IEEE Access
Multidisciplinary | Rapid Review | Open Access Journal

IEEE POWER & ENERGY SOCIETY SECTION

Received 30 March 2023, accepted 21 April 2023, date of publication 26 April 2023, date of current version 3 May 2023.

Digital Object Identifier 10.1109/ACCESS.2023.3270805

RESEARCH ARTICLE

Waveform Variation Defined Model for Harmonic Current Emissions Including Cross-Order Supply Voltage Harmonics Influence

KAMRAN DANIEL[1,2], (Graduate Student Member, IEEE), LAURI KÜTT[1], (Senior Member, IEEE), MUHAMMAD NAVEED IQBAL[1,3], NOMAN SHABBIR[4], (Senior Member, IEEE), MARTIN PARKER[1], AND MAREK JARKOVOI[1]

[1]Department of Electrical Power Engineering & Mechatronics, Tallinn University of Technology, 19086 Tallinn, Estonia
[2]Department of Electrical Engineering, University of Engineering and Technology, Lahore 54000, Pakistan
[3]Department of Electrical Engineering, GC University Lahore, Punjab 54000, Pakistan
[4]FinEST Center for Smart Cities, Tallinn University of Technology, 19086 Tallinn, Estonia

Corresponding author: Kamran Daniel (kdanie@taltech.ee)

This work was supported by the Estonian Research Council Grant PSG142.

ABSTRACT The paper reports an experimental non-linear load evaluation regarding current harmonics sensitivity to supply voltage harmonics. A base for the model is proposed relying on the time-domain waveform variations, rather than impedance or conductance approach. The proposed Waveform Variation Defined Model is able to detail to provide improved correspondence for the actual load physical operation on the emergence of cross-order coupling between the supply voltage and current harmonics variations. Model proposal specifies to implement non-impedance relation and separated phase and magnitude response components, in empirical outcome of the voltage-to-current harmonic variation relation. It will be shown that the model proposed is able to provide an accurate estimation on cumulative influence of different supply voltage harmonics included, for the most probable supply voltage harmonics in the residential grid, for the low order odd harmonics. Model results present outstanding match of the harmonic voltage influence estimations on the load current harmonics levels measured, phase and magnitude values included.

INDEX TERMS Power quality, current harmonic addition, harmonic estimation, harmonic sensitivity.

I. INTRODUCTION

This low voltage distribution network (DN) loads' harmonic current emissions are known to have a response to the harmonics present in the supply voltage [1], [2]. DNs are designed to supply constant RMS magnitude and frequency AC supply voltage with small tolerance around rated values in normal operation [3], [4]. However, as modern energy-efficient electrical devices utilize DC voltage for their operation, power input is commonly delivered by converting the mains AC voltage to DC voltage for power electronic (PE) units using full-bridge rectifiers [5].

In order to model the current waveform response of several power electronic loads in DN system, analysis is often performed in the frequency domain [6], [7], [8], assuming sinusoidal supply voltage. Harmonic current emission assumed as constant $\boldsymbol{I}_{\boldsymbol{h}}^{*} = I_{hM,const} \angle \varphi_{Ih,const}$ is one of the common presentations for harmonic [9], [10] fingerprinting. It faces clear limits for DN supply voltage having some voltage harmonic content, as an evident coupling/sensitivity emerges from measurements [11]. In the following paper, for the benefit of clarity, the current waveform harmonic components are nominated as vectors $\boldsymbol{I}_{\boldsymbol{x}}^{*}$, with "$x$" stating the current harmonic order observed; whereas supply voltage harmonic components are nominated as vectors $\boldsymbol{U}_{\boldsymbol{y}}^{*}$ with "y" stating the voltage harmonic order observed, if different form "x".

A Norton model employs two current harmonic components, a constant current source with current $\boldsymbol{I}_{\boldsymbol{x,Base}}^{*}$ and a linear impedance reaction $\boldsymbol{I}_{\boldsymbol{x,Z}}^{*}$ [12], [13]. $\boldsymbol{I}_{\boldsymbol{x,Base}}^{*}$ emerges as a constant value, upon non-distorted sinusoidal voltage supply. On a vector plot, Norton model proposes that the current

The associate editor coordinating the review of this manuscript and approving it for publication was Elisabetta Tedeschi.

emission of the device resides around an acceptable reference quantity, that is, an ideal sinusoidal voltage condition current emission (modeled as a constant current source) and is linear for minor deviations. If a voltage harmonic influence is represented by a vector $\boldsymbol{U}_x^* = U_{xM} \angle \varphi_{Ux}$, a response on the load's harmonic current would emerge as

$$I_{x,Z}^* = \frac{U_x \angle \varphi_{Ux}}{Z_x \angle \varphi_{zx}} \tag{1}$$

However, Norton model lacks the explanation on several aspects evident in the measurement results. It is unable to accurately present how a supply voltage harmonic of a specific order imposes variation on the current harmonic of another order (cross-order coupling) and is limited to describe the variations for different supply voltage levels.

As more sophisticated models for providing a multi-influence response forming the total $\boldsymbol{I}_{x,FCM}^*$, frequency coupling matrix (FCM) is one of the most discussed models at the time [14]. Utilizing impedance or conductance values for accounting for influence arising from different voltage harmonic orders, the FCM addresses the Norton model circuit base approach and assumes the total $\boldsymbol{I}_{x,FCM}^*$ arises from a cumulation of multiple sub-reactions. Using FCM, the x-th harmonic current vector could be written as

$$\boldsymbol{I}_x^* = \boldsymbol{I}_{x,Base} + [\boldsymbol{U}^*][\boldsymbol{Y}_{xy}^*] \tag{2}$$

Here $[\boldsymbol{U}^*]$ is a supply voltage vector matrix, enclosing voltage harmonic component vectors of different harmonic orders, $[\boldsymbol{Y}_{xy}^*]$ is the frequency coupling admittance matrix between the x-th harmonic current component and each y-th voltage harmonic component in $[\boldsymbol{U}^*]$ [15].

Challenges of FCM arise again as the modeling of practical devices in practical networks results in deviations. While the impedance-based products of harmonic voltage $\boldsymbol{U}_y^*$ phase influences are used, these are best to describe $\boldsymbol{I}_x^*$ circular vector plot result patterns [16]. However, $\boldsymbol{U}_y^*$ phase influence patterns are often elliptical in form (see also Chapter IV in this paper). It has been provided that to describe the elliptical result pattern, another set of variables should be included via negative-sequence FCM [6], [17], [18] or additional frequency component factor [19]. These make the FCM more heavy for calculation and parameter estimation. While the FCM would be capable of providing a current harmonic magnitude response, it does not include a direct physical phenomenon description for the harmonic cross-order coupling [14], [20], [21]. Remaining complexity and the deviation in $\boldsymbol{I}_x^*$ phase result will provide limitations of range for the FCM, as the cumulative assessment of total $\boldsymbol{I}_y^*$ different sub-reactions via (10) also means cumulation of deviations.

In this paper, a novel model is proposed for establishing a total $\boldsymbol{I}_x^*$ estimation model, able to include harmonic cross-coupling physical phenomenon and load current elliptical response reasons to $\boldsymbol{U}_y^*$ phase variation. It will be presented that due to physical phenomenon of the operation of the rectifier circuits; there is more optimal way of describing the time-difference reactions via separate time-difference/phase-difference coefficients and magnitude difference via separate magnitude difference coefficients. For the voltage waveform having the same harmonic RMS-value but a different harmonic phase angle value, the rectifier conduction initiation moment of the current waveform is unique, defining phase shift variation. Furthermore, the duration as well as the peak of the load current pulse are also dependent on the incident harmonic phase angle value. These coefficients would invalidate the total harmonic presentation through complex impedance variables.

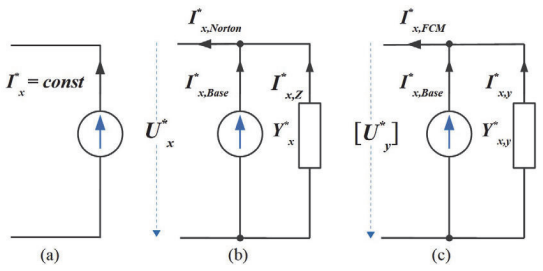

FIGURE 1. Harmonic load reaction models, (a) constant source (b) Norton equivalent (c) FCM [22], [23].

II. EXPERIMENTAL SETUP

The more detailed analysis of the loads $\boldsymbol{U}_y^*$ sensitivity relied on a systematic scan, similar to [24] and [25], performed on different loads exhibiting similar load current characteristics (load types, see further [26]). For the test system, dynamic high-resolution control of the waveform of supply voltage for measured load is a primary feature. Supply voltage is output through a high-precision amplifier, provided with reference from 16-bit waveform synthesizer, updated in every 10 seconds for different harmonic voltage content. The supply voltage output momentary value is established using equation (3).

$$u_{test}(t) = \sum_{y=1}^{N} \sqrt{2} U_y \sin\left(2\pi f_y t + \alpha_y\right) \tag{3}$$

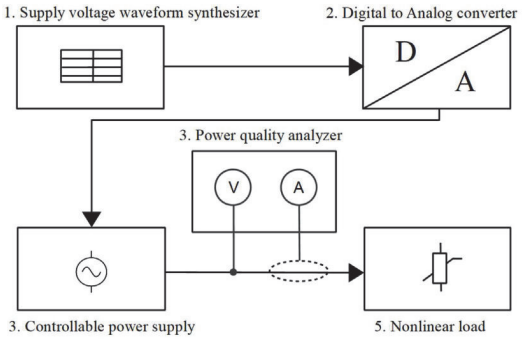

FIGURE 2. Measurement setup [27].

U_y is the rms value of any particular harmonic. The harmonic frequency is shown by f_y and sampling interval by t_s. The number of samples needed for the specific duration (T_m) of the voltage output from the controllable power supply can be calculated by (3).

Supply waveform is generated with the sampling frequency of 100 kS/s; meaning 2000 points for every 50 Hz cycle. Measurements are done via measurement unit having 41 kS/s sampling frequency, with waveform recordings and 1-second averaging of the harmonics used. Extracted values for current harmonics were recorded with a magnitude and phase response values, correlated to the waveform-sampled values.

Commencing the more detailed analysis several criteria was considered for more accurate measurements. First, time dependency of harmonic emission profiles of switch-mode power supplies (SWMPs) [28] was considered. Measurements are done only after the thermal stability of the load, warmup period 60 minutes was applied. Continuous power is provided to loads during testing pauses to maintain a working temperature [29].

During the characteristic scan of the loads, miniature though stable and repeatable variations of the harmonic current component phase and magnitude values were recorded. This was verified with discrete Fourier transform (DFT) of the current waveform. The measurement analyzer used in this study was commercially certified to carry out accurate and repeatable measurements of such order of level magnitude and phase angle variations [30].

Main load characteristics scan is done through scenarios such as presented in Table 1 for the 5th harmonic. As the first test supply voltage combination, the harmonic currents of the load are recorded for input voltage containing only the fundamental component U_1. After that, each input voltage combinations are present for 10 seconds. 24 combinations implement injection of voltage harmonic to the supply voltage, having identical 5th harmonic voltage U_5 level but phase angle at 15-degree steps. This was repeated with different level of influencer U_5 magnitude applied.

TABLE 1. An example of supply voltage combination when adding single harmonic to supply voltage.

Combinations	U^*_1	U^*_3		U^*_5		U^*_7	
	U_1, V	U_3, V	φ_{U3} °	U_5, V	φ_{U5} °	U_7, V	φ_{U7} °
1	230	0	0	0	0	0	0
24	230	0	0	3	0-15 …345	0	0

III. LOAD SCAN RESULTS

The LED lamps commercially available in the market are can be categorized based on the waveform of the drawn current by LED [26] shown in Fig. 3; the shape of the current waveform depend on the presence or absence of the waveform control or filter in the circuit of lamps [31], [32], [33], [34]. In this study, randomly chosen LED lamps of Type A [26] are observed, and evaluated for the odd harmonic contents and reaction for the harmonic orders 3, 5 and 7.

Starting with a time-domain observation, Figure 4 describes the current waveform as a LED lamp is subjected to pure sinewave supply voltage, compared to the supply voltage waveform having a specific harmonic voltage component magnitude level, injected with a specific phase angle towards the main harmonic phase. Figure 4 describes a selection of the current waveforms outcome of a scan result when 5th voltage harmonic was applied with a defined level, and the harmonic injection phase angle varied in 15-degree steps while the harmonic voltage level preserved (see Table 1). Measured

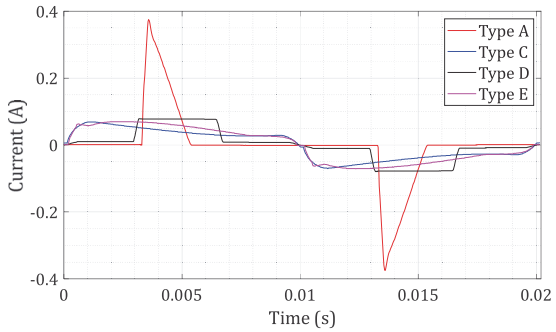

FIGURE 3. Load types of LED lamps tested.

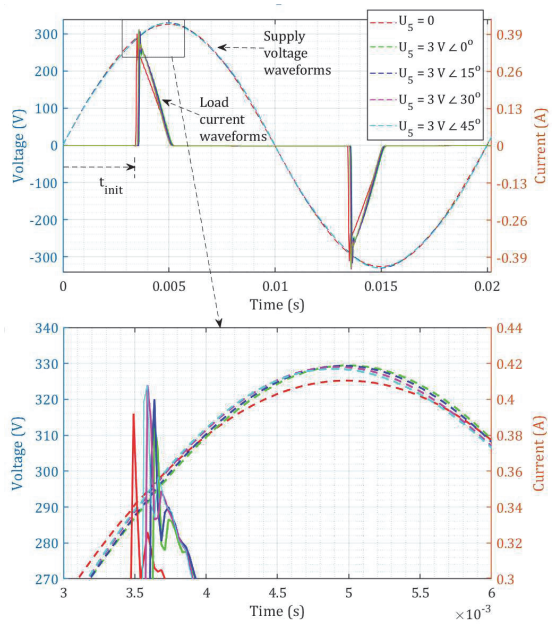

FIGURE 4. Current waveform initiation moment affected by the phase angle of 5th order supply voltage harmonic, measurement results. Dashed lines – supply voltage waveforms; continuous lines – load current waveforms.

current waveforms have been synchronized to the voltage waveform main harmonic zero phase instant.

A distinctive quantity of the current waveform is the point of rectifier conduction initiation time instant t_{init}. Here current provides highest gradient and peaks some moment later. The rectifier current instantaneous peaks provide a characteristic quantity for the magnitude, and another distinctive time-domain characteristic would be the total conduction time of the rectifier.

The current waveform of all the LEDs tested shows similar characteristics of response to voltage harmonics added to the input voltage. Fig. 4 shows the former effect, in terms of amplitude and phase angle of the harmonic current, and it is clear that change in phase angle of the fifth voltage harmonic affects the harmonic currents across the spectrum. The initiation moment given as main harmonic phase angle value (φ_{init}), could be seen to determine to deviation of the LED harmonic current pattern. Time-domain differences have been regarded towards phase angle variation in the literature [35], [36], however not used for base assumption.

The time domain outcome thus establishes a hypothesis if the initiation phase angle would be responsible for the LED current harmonic phase angle variations throughout. The hypothesis proposed refers that the current harmonic phase angles will be directly related to the rectifier physical operation in the time-domain.

IV. PHASOR PLOT PRESENTATION

Measurements thus directly have revealed that due to added voltage harmonics, there are influences to both current conduction initiation time instant (i.e., phase angle) and current magnitude values. For the detailed characterization of frequency approach, total $\boldsymbol{I}_x^*$ was recorded for supply voltage with the specific harmonic component constant magnitude, while rotating in smaller steps through the 360 degrees phase angle. Results present a well-reported [14], [18], [25], [37], [38], though less-approached outcome.

In the following, the harmonic current vector (example of $\boldsymbol{I}_7^*$ in plot Figure 5) difference to base point $\boldsymbol{I}_{7,Base}^*$ is observed as

$$\begin{cases} dI_{x,Uy} = I_{x,Uy} - I_{x,Base} \\ d\varphi_{Ix,Uy} = \varphi_{Ix,Uy} - \varphi_{Ix,\mathrm{Base}} \end{cases} \tag{4}$$

where $\mathrm{d}I_{x,Uy}$ is the measured harmonic current $\boldsymbol{I}_x^*$ magnitude difference due to included $\boldsymbol{U}_y^*$, compared to $\boldsymbol{I}_x^*$ magnitude $I_{x,Base}$ emerging in pure sinewave voltage supply conditions;

$\varphi_{Ix,Uy}$ is the measured harmonic current $\boldsymbol{I}_x^*$ phase angle due to included $\boldsymbol{U}_y^*$, compared to $\boldsymbol{I}_x^*$ phase angle $\varphi_{Ix,Base}$ emerging in pure sinewave voltage supply conditions.

Plot in Figure 5 presents the common measurement outcome for the influence of $\boldsymbol{U}_5^*$ added to the sinusoidal supply voltage, with φ_{U5} rotation applied for full circle (through 360°) and magnitude U_5 held constant. The response of $\boldsymbol{I}_7^*$ endpoints makes up an ellipse, but also $\varphi_{dI7,U5}$ is going through a rotation of exactly 360°. This is evident also for other all other current harmonics, regardless of their frequency value.

While linear impedance can explain the current difference component phase rotation, this is only valid for the harmonic of same order, i.e., identical frequency. As this emerges for all harmonics, for example added $\boldsymbol{U}_3^*$ rotated through $\varphi_{U3} = \{0 \ldots 360°\}$ again provides $\varphi_{dI7,U3}$ rotation through 360°, then this cannot be considered an impedance-based relation. This will follow the coefficient proposals for model for calculating the harmonic current values.

It emerges that reaction plot is rather well symmetrical towards the pure-sinusoidal voltage supply product of $\boldsymbol{I}_x^*$, termed here as the base harmonic current response $\boldsymbol{I}_{x,Base}^*$. Response towards both phase and magnitude response is proportional to the voltage harmonic influencer magnitude value I_{hM}. It raises the model description to the response as

$$\begin{cases} I_x = I_{x,\mathrm{base}} + \Delta I_{x,y} \\ \varphi_{Ix} = \varphi_{Ix,\mathrm{base}} + \Delta\varphi_{Ix,y} \end{cases} \tag{5}$$

where $\Delta I_{x,y}$ is the harmonic current $\boldsymbol{I}_x^*$ magnitude variation estimation due to included $\boldsymbol{U}_y^*$, compared to $\boldsymbol{I}_x^*$ magnitude $I_{x,Base}$ emerging in pure sinewave voltage supply conditions;

$\Delta\varphi_{Ix,y}$ is the is the harmonic current $\boldsymbol{I}_x^*$ phase angle magnitude estimation due to included $\boldsymbol{U}_y^*$, compared to $\boldsymbol{I}_x^*$ phase angle $\varphi_{Ix,Base}$ emerging in pure sinewave voltage supply conditions.

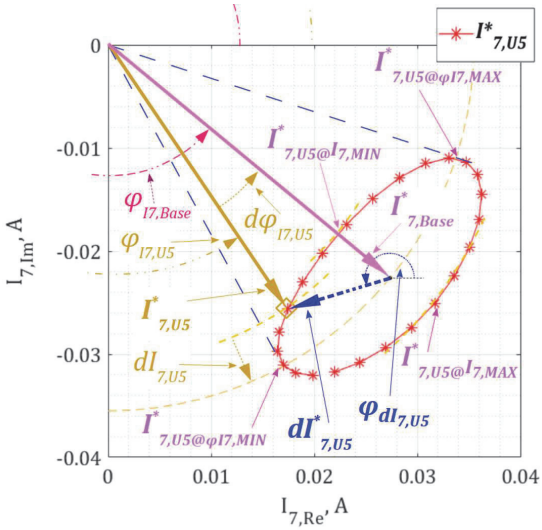

FIGURE 5. Vector component plot for the harmonic load current component analysis. $\boldsymbol{I}_7^*$ vector endpoints' ellipse points plot, for $\boldsymbol{U}_5 = 3$ V, $\varphi_{U5} = 0, 15, 30 \ldots 345°$.

This presentation is following the basic Norton or FCM concepts. However, for the reasons laid out in the following chapter, and relying on the physical rectifier operation phenomenon, it is justified to keep the magnitude and phase

variation quantities independent rather than confined through complex impedance relation.

A. CURRENT HARMONIC PHASE ANGLE VARIATIONS

The initiation angle of the current conduction (φ_{init}) is a time instance where the rectifier starts to conduct for charging the tank capacitor after the rectifier. This initiation angle is determined as

$$\varphi_{init} = f \cdot 360^{o} \cdot \mathrm{d}t_{init} \tag{6}$$

where $\mathrm{d}t_{init}$ – time-difference of the supply voltage main harmonic zero phase instant and current conduction initiation moment. Shown in Table 2, initiation phase is referred to varying $\boldsymbol{U}_{\mathbf{5}}^{*}$ added to the voltage supply. Measurement results in Table 2 present the summary of the results, where

$$\begin{cases} d\varphi_{init,Uy} = \varphi_{init,Uy} - \varphi_{init,\mathrm{base}} \\ d\varphi_{Ix,Uy} = \varphi_{Ix,Uy} - \varphi_{Ix,\mathrm{base}} \end{cases} \tag{7}$$

where $\varphi_{init,Uy}$ is the initiation moment phase with $\boldsymbol{U}*_{\mathbf{y}}$ injected to the supply voltage; $\varphi_{Ix,Uy}$ is the phase angle of the response current vector with $\boldsymbol{U}*_{\mathbf{y}}$ injected to the supply voltage, and "$_{Base}$" notates the values upon sinusoidal supply voltage conditions (i.e., only fundamental voltage component present).

TABLE 2. Initiation moment and phase angles of harmonics in load current, for different magnitude levels of harmonic voltage*.

U_5, V	φ_{U5}, °	$\varphi_{init,0}$, ° (50 Hz phase value)	φ_{I1}, °	φ_{I3}, °	φ_{I5}, °	φ_{I7}, °
0	–	62.1	18.0	231.6	87.2	304.2
		$\Delta\varphi_{init}$, °	$\Delta\varphi_{I1}$, °	$\Delta\varphi_{I3}$, °	$\Delta\varphi_{I5}$, °	$\Delta\varphi_{I7}$, °
1	180	–0.9	0.6	2.0	3.6	5.5
	345	1.1	–0.8	–2.5	–4.2	–6.2
3	180	–2.9	2.0	6.5	11.5	17.7
	345	2.9	–2.4	–6.9	–11.8	–17.4
5	180	–4.7	3.6	11.3	20.4	32.0
	345	4.6	–3.6	–10.7	–18.3	–26.8

* Phase angle accuracy/resolution has been provided for more detailed comparison

TABLE 3. Difference in Phase Angles of Harmonics in Load Current, For Different Magnitude Levels of Harmonic Voltage, determined by (9).

U_5, V	φ_{U5}, °	φ_{init}, °	$\Delta\varphi_{init}$, °	$\Delta\varphi'_{I1,U5}$, °	$\Delta\varphi'_{I3,U5}$, °	$\Delta\varphi'_{I5,U5}$, °	$\Delta\varphi'_{I7,U5}$, °
0	-	62.1					
1	180	61.2	0.9	-0.7	-0.7	-0.7	-0.8
	345	63.2	-1.1	0.8	0.8	0.8	0.9
3	180	59.2	2.9	-2.1	-2.2	-2.3	-2.5
	345	65.0	-2.9	2.3	2.3	2.4	2.5
5	180	57.4	4.7	-3.6	-3.8	-4.1	-4.6
	345	66.7	-4.6	3.5	3.6	3.7	3.8

* Phase angle accuracy/resolution has been provided for more detailed comparison

TABLE 4. Maximum and minimum of peak load current ($I_{l\,Peak}$) according to φ_{u5}.

U_5, V	φ_{U5}, °	$I_{L\,Peak}$, A	$\Delta I_{L\,Peak}$, A	$\Delta I_{1,U5}$, mA	$\Delta I_{3,U5}$, mA	$\Delta I_{5,U5}$, mA	$\Delta I_{7,U5}$, mA
0	-	0.40					
1	270	0.38	0.02	0.05	0.30	0.67	1.13
	90	0.42	-0.02	-0.06	-0.28	-0.73	-1.19
3	270	0.34	0.06	0.21	0.83	1.74	3.0
	90	0.45	-0.06	-0.06	-0.76	-2.05	-3.5
5	255	0.30	0.10	0.29	1.50	3.8	6.3
	105	0.49	-0.10	-0.25	-1.21	-3.1	-5.1

Normalizing the phase angles towards the initiation influencing component $\boldsymbol{U}_{\mathbf{5}}^{*}$, and observing the relation towards the current harmonic $\boldsymbol{I}_{\boldsymbol{x}}$ of order x, it is revealed to have a ratio of closely common to

$$\Delta\varphi'_{I_{x,Uy}} = \Delta\varphi_{init,Uy} \cdot x \cdot k_{WF} \tag{8}$$

where k_{WF}– waveform coefficient, with almost same value for the discussed current harmonic orders ($x = 3, 5, 7$). The initiation phase angle φ_{init} is in direct and proportional ratio to the φ_{I1}, resulting from a frequency domain transfer of t_{init} (φ_{init}). The statement above reveals that the variation of harmonic current phase angles, observed due to $\boldsymbol{U}_{\mathbf{5}}^{*}$, is directly relational and proportional to the initiation angle φ_{init}.

It is important to point out that the harmonic phase angle values are all varying, if the voltage harmonic phase angle is varying. This is a key aspect to explain the harmonic cross-coupling phenomenon, considering that the phase angle variation of the $\boldsymbol{U}_{\boldsymbol{y}}^{*}$ of a specific order will bring along a dedicated response to current harmonic phase angle of another order.

Table 3 presents the maximum and minimum value of initiation moment of the current waveforms, corresponding to φ_{U5} value extreme points, calculated as

$$\Delta\varphi'_{I_{x,y}} = \frac{\Delta\varphi_{Ix,y}}{x} \tag{9}$$

where x is the current harmonic order, further confirming the equation (8). Furthermore, the fundamental current harmonic component phase variation defines phase variations for all other load harmonics, given through fundamental component phase shift multiplied by the observed harmonic current order number. It has to be noted that the magnitude of the incident voltage harmonic (U_5) provides a proportional impact on the initiation moment and the $\boldsymbol{I}_{\boldsymbol{x}}^{*}$ phase angle φ_{Ix} variation range. The phase angles are seen to pose a high and low value responsive to φ_{U5} rotation of almost 180°.

B. CURRENT HARMONIC MAGNITUDE VARIATIONS

Similarly, the highest value of the load currents ($I_{x,y,max}$) is also linked with the phase angle of influencing supply voltage harmonic (φ_{Uy}) on almost 180° rotation. Table 3 illustrates the behavior of time-domain waveform $I_{L,peak}$, corresponding

to φ_{U5}, providing maximum and minimum $\boldsymbol{I_x^*}$ magnitude I_x values with value range shown. It has to be noted, that the highest and lowest current magnitude occurrence are also found at nearly orthogonal (90°) values towards the φ_{U5} value for peak and minimum φ_{Ix} variation values.

Table 4 presents expectedly, that the harmonic magnitudes are directly proportional to the level of the added voltage harmonic (in this case it is $\boldsymbol{U_5^*}$). The proportion origins are evident from time-domain waveform peak current levels, deployed to the current harmonics observed, presenting a physical background for the cross-order harmonic coupling appearance for the magnitude portion.

V. MODEL OF HARMONIC RESPONSE CURRENTS CHARACTERIZATION OF PRACTICAL LOADS

Provided the phase angle and magnitude variation consideration in the previous chapter, it has to be pointed out that the physical characterization to the time-domain origins of the $\boldsymbol{I_x^*}$ components provides justification to model the phase angle φ_{Ix} and magnitude portions I_x independent of each other. This is due to non-impedance origins of the $\boldsymbol{I_x^*}$ variations in time-domain current presentation, discussed in previous chapter.

In the following, a load current model will be described, providing the correspondence of the current harmonic variations, detailed in the previous chapter. The load current harmonic vector $\boldsymbol{I_x^*}$ for a particular harmonic order x is formed of following parts (see also Figure 6):

1. A constant current source part of the harmonic current, $\boldsymbol{I_{x,Base}^*}$ respective for current magnitude component $I_{x,Base}$, and the current phase angle component $\varphi_{Ix,Base}$. This is the value obtained from device test with pure sinusoidal supply voltage.
2. A linear current component part $\Delta\boldsymbol{I_{x,LIN}^*}$, respective for current magnitude component $\Delta I_{x,LIN}$, and the current phase angle component $\Delta\varphi_{Ix,LIN}$. These are calculated as a cumulation of all linear components due to each $\boldsymbol{U_y^*}$ in the supply voltage, for every $\boldsymbol{I_x^*}$.
3. A nonlinear current component part $\Delta\boldsymbol{I_{x,NL}^*}$, respective for current magnitude component $\Delta I_{x,\mathrm{NL}}$, and the current phase angle component $\Delta\varphi_{Ix,\mathrm{NL}}$. The nonlinear part emerges from the fact that the current harmonic response on the ellipse is non-symmetrical. These parts are calculated as a cumulation of all linear components due to each $\boldsymbol{U_y^*}$ in the supply voltage, for every $\boldsymbol{I_x^*}$.

The load harmonic current will be presented as

$$\begin{cases} I_{x,WVDM} = I_{x,\mathrm{Base}} + \Delta I_{x,LIN} + \Delta I_{x,NL} \\ \varphi_{Ix,WVDM} = \varphi_{Ix,\mathrm{Base}} + \Delta\varphi_{Ix,LIN} + \Delta\varphi_{Ix,NL} \end{cases} \tag{10}$$

The main proportion of the current harmonic variation will be provided by the linear part, calculated as

$$\Delta I_{x,LIN} = \boldsymbol{U_y} \cdot \boldsymbol{G_x} \cdot \cos(\boldsymbol{\alpha_x} - \varphi_{\boldsymbol{Uy}}), \tag{11}$$

where $\boldsymbol{U_y}$ is the $\boldsymbol{U_y^*}$ magnitude matrix in form

$$\boldsymbol{U_y} = [U_3\ U_5\ \ldots\ U_N]$$

$\boldsymbol{G_x}$ is the current harmonic I_x magnitude sensitivity coefficient matrix in form

$$\boldsymbol{G_x} = \begin{bmatrix} G_{x3} \\ G_{x5} \\ \ldots \\ G_{xN} \end{bmatrix}$$

where G_{x3} presents I_x sensitivity to the 3rd supply voltage harmonic magnitude U_3 respectively, (units A/V = S), and

$$\cos(\boldsymbol{\alpha_x} - \varphi_{\boldsymbol{Uy}}) = \begin{bmatrix} \cos(\alpha_{x3} - \varphi_{U3}) \\ \cos(\alpha_{x5} - \varphi_{U5}) \\ \ldots \\ \cos(\alpha_{xN} - \varphi_{UN}) \end{bmatrix},$$

where α_{x3} is the specific phase coefficient for calculating I_x related to φ_{U3}, latter presenting the supply voltage harmonic $\boldsymbol{U_3^*}$ actual phase angle value.

Similarly, the main current harmonic phase angle variation will be provided by the linear part, calculated as

$$\Delta\varphi_{Ix,LIN} = \boldsymbol{U_y} \cdot \boldsymbol{k_x} \cdot \sin(\boldsymbol{\alpha_x} - \varphi_{\boldsymbol{Uy}}), \tag{12}$$

$\boldsymbol{k_x}$ is the current harmonic $\boldsymbol{I_{x,LIN}^*}$ phase angle $\Delta\varphi_{Ix}$ sensitivity coefficient matrix in form

$$\boldsymbol{k_x} = \begin{bmatrix} k_{x3} \\ k_{x5} \\ \ldots \\ k_{xN} \end{bmatrix}$$

where k_{x3} presents $\Delta\varphi_{Ix}$ sensitivity to the 3rd supply voltage harmonic magnitude U_3 respectively, (units °/V), and

$$\sin(\boldsymbol{\alpha_x} - \varphi_{\boldsymbol{Uy}}) = \begin{bmatrix} \sin(\alpha_{x3} - \varphi_{U3}) \\ \sin(\alpha_{x5} - \varphi_{U5}) \\ \ldots \\ \sin(\alpha_{xN} - \varphi_{UN}) \end{bmatrix}.$$

Here the coefficients G_{xy}, k_{xy} and α_{xy} are determined through load measurements, presented in the next chapter.

The nonlinear part of current will be calculated for supply voltage harmonic components as

$$\Delta I_{x,NL} = \boldsymbol{U_y} \cdot \left[\boldsymbol{A_{1m}} \sin\left(\boldsymbol{\varphi_{Uy}} + \boldsymbol{C_{1m}}\right) + \boldsymbol{A_{2m}} \sin\left(\boldsymbol{2\varphi_{Uy}} + \boldsymbol{C_{2m}}\right)\right] \tag{13}$$

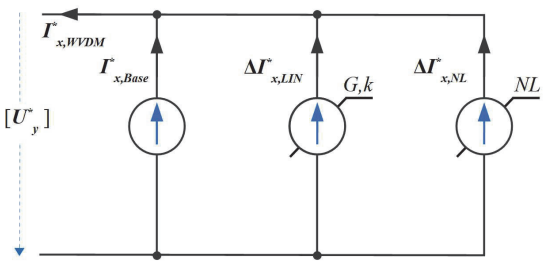

FIGURE 6. Schematic description for harmonic current component $\boldsymbol{I_x^*}$ of order x modeling.

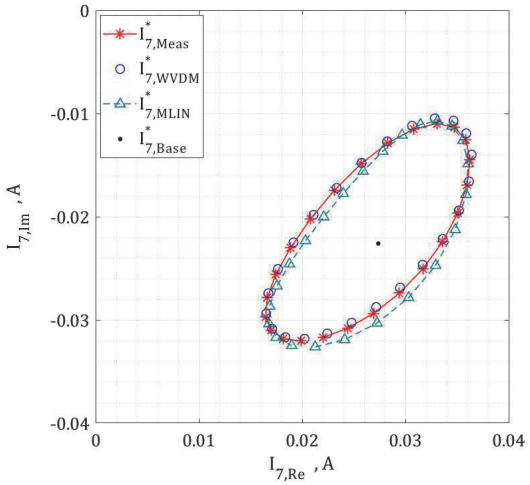

FIGURE 7. Presentation of roles of different harmonic current model components.

where A_{1m}, A_{2m}, C_{1m}, C_{2m} are first and second order polynomial expressions related to harmonic current order and harmonic voltage orders. Similarly nonlinear part for phase angle part will be calculated as

$$\Delta\varphi_{Ix,NL} = U_y \cdot \left[A_{1p} \sin\left(\varphi_{Uy} + C_{1p}\right) + A_{1p} \sin\left(1\varphi_{Uy} + C_{1p}\right)\right] \tag{14}$$

where $A_{1p}, A_{2p}, C_{1p}, C_{2p}$ are second order polynomial expressions related to harmonic current order and harmonic voltage orders.

The particular derivation of the polynomials as calculation of the nonlinear parts will be presented in further upcoming papers by the authors, as this will need extended consideration.

The role of the different components shown here are laid out in Figure 7 below. The main base of the harmonic current vector, $I^*_{7,Base}$ is presented with a dot as the vector endpoint, while its start-point is zero coordinate, corresponding to load current upon pure sinusoidal supply voltage. Red asterisks are forming a presentation of measured harmonic current results, subjected to supply including a single harmonic voltage U^*_5, included with various phase angles $\Delta\varphi_{U5}$ but identical magnitude. Adding the linear parts ΔI_7 and $\Delta\varphi_{I7}$ make up a pattern represented by triangles, forming a specific ellipse shape. Still, there would be a noticeable deviation between the linear-part-included harmonic current results and measurement results. Therefore, the nonlinear part is added to provide improved correspondence to the actual measurement outcome. The final harmonic current response pattern, including the linear and nonlinear parts, is presented as circles' pattern.

VI. DETERMINATION OF COEFFICIENTS

In the following, the main outline will be discussed for the coefficient estimation, used in the harmonic current calculation model. An example of I^*_7 current component will be used, influenced by the effect of the U^*_5 supply voltage harmonic. Here $x = 7$ is the current harmonic order, $y = 5$ is influencing voltage harmonic order. The quantities observed are referred to on the basis of Figure 5.

Ideally, for ΔI_x to reach from $\Delta I_{x,MAX}$ to almost equal to zero, i.e., current vector magnitude is similar to the sinusoidal supply voltage component response vector $\Delta I_{x,Base}$, base harmonic vector; the difference in φ_{Uy} is nearly 90 degrees. At the voltage harmonic phase angle providing harmonic current I_x of base magnitude, the φ_{Ix} phase deviation is highest. Finding the influencing supply voltage phase angles φ_{Uy} corresponding to the minimum and maximum deviation of the magnitude I_x, allows to specify the base phase shift component

$$\alpha_{xy} = \frac{\varphi_{Uy@\varphi Ix,MAX} + \varphi_{Uy@\varphi Ix,MIN}}{2} \tag{15}$$

referring to measurement quantities as in Figure 5. Given the data provided in Table 5, the α_{75} is found to be close to value of 230°. As the measurement steps are 15°, better accuracy is not available. Given the orthogonal shift of $\varphi_{Uy} = 90°$ to find the maximum and minimum magnitude points, the α_{75} should be calculated as

$$\alpha_{xy} = \frac{\varphi_{Uy@Ix,MAX} + \varphi_{Uy@Ix,MIN}}{2} + 90° \tag{16}$$

Data in Table 5 provides that the α_{75}, calculated based on minimum and maximum magnitude, will be around 240°. The proposed value of coefficient of current magnitude sensitivity G_{xy} can be found using maximum and minimum I^*_x magnitude difference value i.e., dI_x maximum and minimum values (referring to Figure 5)

$$G_{xy} = \frac{\left(\left|dI_{x,Uy@Ix,MAX}\right| - \left|dI_{x,Uy@Ix,MIN}\right|\right)}{2} \Big/ U_y \tag{17}$$

TABLE 5. Proposing Alpha Value Form Measurements.

		φ_{U5}	$\varphi_{U5\_MAX} - \varphi_{U5\_MIN}$	φ_{U5_CENTRE}	α_{75} for $dI_7 \approx 0$	α_{75}
dI_{7_MAX}	6.6 mA	225°	-150°	150°	240°	233°
dI_{7_MIN}	-4.9 mA	75°				
$d\varphi_{I7\_MAX}$	21.7°	315°	-165°	233°	233°	
$d\varphi_{I7\_MIN}$	-21.5°	150°				

TABLE 6. Comparison Of Voltage Harmonic Amplitude Change To Current Harmonic Phase Deviation.

Load	U_5	K_{35}, °/V	G_{35}, mA/V	K_{55}, °/V	G_{55}, mA/V	K_{75}, °/V	G_{75}, mA/V
1	1 V	3.17	0.22	5.3	0.63	7.5	1.08
	3 V	3.16	0.23	5.3	0.65	7.6	1.11
	5 V	3.16	0.27	5.3	0.70	7.5	1.14

TABLE 7. Model Parameters of Test Loads.

	I_x order	3			5			7		
U_y order	Load	α_{3y}, °	G_{3y}, mA/V	k_{3y}, °/V	α_{5y}, °	G_{5y}, mA/V	k_{5y}, °/V	α_{7y}, °	G_{7y}, mA/V	k_{7y}, °/V
3		25	0.07	2.16	26	0.18	3.6	28	0.39	5.1
5	1	218	0.24	3.2	220	0.67	5.3	223	1.13	7.5
7		48	0.51	3.6	52	1.22	6.2	57	1.96	8.9
3		29	0.12	2.12	31	0.42	3.6	35	0.75	5.1
5	2	223	0.51	2.95	226	1.27	5.0	233	1.91	7.3
7		53	0.92	3.1	59	2.06	5.4	71	3.03	8.1
3		28	0.10	2.13	29	0.31	3.6	32	0.60	5.1
5	3	221	0.39	2.99	224	1.01	5.1	229	1.58	7.3
7		512	0.74	3.3	57	1.69	5.6	66	2.57	8.3

TABLE 8. Comparison of measured and model calculated Harmonic current values $U_1 = 230$ V; $U_5 = 3$ V.

I/P	*Measured values*				*Model with linear part result*				*Deviation for model with linear part*		*Full model result*		*Full model deviation from measurement*	
φ_{U5}, °	$I_{7,MEAS}$, mA	$\varphi_{I7,MEAS}$, °	$dI_{7,MEAS}$, mA	$d\varphi_{I7,MEAS}$, °	$\Delta I_{7,MLIN}$, mA	$\Delta\varphi_{I7}$, °	$I_{7,MLIN}$, mA	$\varphi_{I7,MLIN}$, °	$\delta I_{x,MLIN}$, mA	$\delta\varphi_{Ix,MLIN}$, °	$I_{7,WVDM}$, mA	$\varphi_{I7,WVDM}$, °	$\delta I_{x,WVDM}$, mA	$\delta\varphi_{Ix,WVDM}$, °
Max	40.4	-18	6.5	21.7	5.7	21.6	41.2	-18	1.8	1.7	40.3	-17	0.4	-0.2
Min	29.0	-61	-4.9	-21.5	-5.7	-21.6	29.8	-61	-1.0	-3.1	29.0	-61	0.0	-1.0
75	40.4	-34	-4.9	-5.8	-5.3	-8.1	40.8	-31	-0.4	-2.3	40.3	-33	0.1	-0.3
150	36.6	-18	-1.1	-21.5	0.7	-21.6	34.8	-18	1.8	-0.1	36.3	-17	0.3	-0.9
225	29.0	-37	6.5	-2.6	5.7	-3.0	29.8	-37	-0.9	-0.5	29.0	-36	0.0	-0.6
315	35.4	-61	0.1	21.7	0.8	21.5	34.7	-61	0.7	-0.2	35.3	-61	0.1	-0.3
RMS error for 24 U_5 phase angles injected									**0.9**	**2.1**			**0.2**	**0.5**

From the result plots (Figure 5, Figure 7) it is evident that base harmonic current vector $\boldsymbol{I}^*_{\boldsymbol{x,Base}}$ does not lie in the centre of ellipse, and with the non-symmetric part included, the average of $|dI_{x,y@Ix,MAX}|$ and $|dI_{x,y@Ix,MIN}|$ is used to determine the G_{xy} using equation (17). The phase variation margins are well symmetrical to the ellipse centre, and to determine the initial proposed value of coefficient of phase angle change (k_{xy}), the measurement-derived $d\varphi_{Ix,Uy@\varphi Ix,MAX}$ is used as in (18)

$$k_{xy} = \frac{d\varphi_{Ix,Uy@\varphi Ix,MAX}}{U_y} \tag{18}$$

The magnitude of the harmonic current difference vectors is linearly dependent on the U_y. This way, for influencer U_5 increase by 3 (from 1 V to 3 V) times, results emerge for the $d\varphi_{Ix,Uy@\varphi Ix,MAX}$ and similarly $dI_{x,Uy@Ix,MAX}$ and $dI_{x,Uy@Ix,MIN}$ that provide the close values of linear scalar coefficients G_{xy} and k_{xy}. Excellent linearity of the coefficients is evident from Table 6. Using presented procedures in (15),(16) and (18) the linear coefficients for different loads discussed further in this paper are presented in Table 7.

VII. SINGLE SUPPLY VOLTAGE HARMONIC COMPONENT MODELING

For more detailed evaluation, the linear component model results are presented for 3 similar type loads. Main emphasis is on the comparison of the measured vs model calculated results. Coefficients from Table 7 have been implemented for the model calculation with linear part included (see (10)), as

$$\boldsymbol{I_{x,MLIN}} = \boldsymbol{I_{x,Base}} + \boldsymbol{\Delta I_{x,LIN}} \tag{19}$$

$$\boldsymbol{\varphi_{Ix,MLIN}} = \boldsymbol{\varphi_{Ix,Base}} + \boldsymbol{\Delta\varphi_{Ix,LIN}} \tag{20}$$

Deviation of calculation to measured magnitude value is presented as

$$\boldsymbol{\delta I_{x,LIN}} = \left|\boldsymbol{I_{x,Meas}}\right| - \left|\boldsymbol{I_{x,Base}} + \boldsymbol{\Delta I_{x,LIN}}\right|, \tag{21}$$

and similarly

$$\boldsymbol{\delta\varphi_{Ix,LIN}} = \left|\boldsymbol{\varphi_{Ix,Meas}}\right| - \left|\boldsymbol{\varphi_{Ix,Base}} + \boldsymbol{\Delta\varphi_{Ix,LIN}}\right|, \tag{22}$$

where $\delta I_{x,LIN}$ presents the magnitude difference of model (see (10)) result without nonlinear part included, compared to measurement outcome;

$\delta\varphi_{Ix,LIN}$ presents the phase difference of model (see (10)) result without nonlinear part included, compared to measurement outcome.

The full model calculation outcome, including the nonlinear part is calculated according to (10). The deviation between the full model calculation and measurement outcome is calculated as

$$\boldsymbol{\delta I_{x,WVDM}} = \left|\boldsymbol{I_{x,Meas}}\right| - \left|\boldsymbol{I_{x,WVDM}}\right|, \tag{23}$$

TABLE 9. Difference Of Measurement And Estimation For Test Loads; Single supply harmonic $U_5 = 3$ V.

Load		I^*_3						I^*_5						I^*_7					
		$I_{3,MEAS}$, mA	$I_{3,MLIN}$, mA	$I_{3,WVDM}$, mA	$\varphi_{I3,MEAS}$, °	$\varphi_{I3,MLIN}$, °	$\varphi_{I3,WVDM}$, °	$I_{5,MEAS}$, mA	$I_{5,MLIN}$, mA	$I_{5,WVDM}$, mA	φ_{I5_MEAS}, °	$\varphi_{I5,MLIN}$, °	$\varphi_{I5,WVDM}$, °	$I_{7,MEAS}$, mA	$I_{7,MLIN}$, mA	$I_{7,WVDM}$, mA	$\varphi_{I7,MEAS}$, °	$\varphi_{I7,MLIN}$, °	$\varphi_{I7,WVDM}$, °
1	Max	40.4	40.5	40.4	-118	-119	-118	36.3	36.8	36.4	103	103	104	31.0	31.7	31.0	-32	-32	-32
	Min	38.9	39.0	39.0	-137	-137	-137	32.3	32.8	32.4	72	72	72	24.2	24.9	24.4	-78	-78	-77
	RMSE		**0.3**	**0.1**		**0.9**	**0.1**		**0.5**	**0.1**		**1.3**	**0.2**		**0.6**	**0.1**		**2.0**	**0.4**
2	Max	59.4	59.7	59.6	-114	-114	-114	51.0	51.7	51.1	112	112	113	40.4	41.2	40.3	-18	-18	-17
	Min	56.4	56.7	56.5	-131	-131	-131	43.4	44.2	43.6	82	82	83	29.0	29.8	29.0	-61	-61	-61
	RMSE		**0.6**	**0.1**		**1.0**	**0.2**		**0.8**	**0.1**		**1.6**	**0.2**		**0.9**	**0.2**		**2.1**	**0.5**
3	Max	50.8	51.0	51.0	-117	-117	-117	44.3	44.9	44.4	106	106	107	35.9	36.7	35.8	-27	-27	-26
	Min	48.5	48.7	48.6	-135	-135	-135	38.3	38.9	38.4	76	76	76	26.5	27.2	26.5	-70	-70	-70
	RMSE		**0.5**	**0.1**		**1.0**	**0.1**		**0.7**	**0.1**		**1.5**	**0.2**		**0.8**	**0.2**		**2.1**	**0.4**

and similarly

$$\delta\varphi_{Ix,WVDM} = \left|\varphi_{Ix,Meas}\right| - \left|\varphi_{Ix,WVDM}\right|. \tag{24}$$

For the whole $\boldsymbol{U}^*_y$ cycle (360°) rotation the outcome deviation is evaluated using the root-mean-square error (RMSE), listed in tables 8 and 9 is calculated using the following equations,

$$RMSE_{Ix} = \sqrt{\frac{\sum_{i=0}^{N} \delta \boldsymbol{I}_x{}^2}{N}} \tag{25}$$

$$RMSE_{\varphi Ix} = \sqrt{\frac{\sum_{i=0}^{N} \delta \varphi_{Ix}{}^2}{N}} \tag{26}$$

where N_{MEAS} is total number of actual (measurement) points and predicted values (magnitude and phase).

Individual results obtained with model linear part results are rather accurate (Table 8), however, if considering the variation full amplitude of 5.7 mA, the maximum model linear part deviation reaches 1.8°, which is roughly 30% of the full variation amplitude. While good for single harmonic voltage component influence estimation, it will be shown in the following chapters that for the cumulative multiple voltage harmonics influence model to have reasonable outcome, the single harmonic voltage influence would need to have as good correspondence as possible. Thus, the nonlinear part included full model (see (10)) calculation can provide very low RMSE value (Table 8). This is valid for multiple loads tested (see Table 9) where the correspondence between the measured and model calculated values shows very high match.

VIII. CUMULATIVE RESPONSE TO VOLTAGE HARMONICS

The harmonic current calculation model (10) is referred through parts (11, 12) that are making up a scalar product of multiple influences from supply voltage harmonics of different order. This means that the model is able to account for cumulative sum of influences on the harmonic current $\boldsymbol{I}^*_x$ from multiple supply voltage harmonic components. In order to present this, a measurement based cumulative influence analysis is presented. In trivial, the cumulative response is approached in a manner to keep one or multiple supply voltage harmonics as constant vectors while the single other order harmonic voltage component $\boldsymbol{U}^*_y$ is rotated through 360°, keeping the magnitude U_y constant.

TABLE 10. Input-Combination-2 When Adding Multiple Harmonic Voltages to Fundamental Voltage.

No. of supply voltage combinations applied	U^*_1	U^*_3		U^*_5		U^*_7	
	U_1, V	U_3, V	φ_{U3} °	U_5, V	φ_{U5} °	U_7, V	φ_{U7} °
1	230	0	0	0	0	0	0
24	230	3	0-15-345	0	0	0	0
24	230	3	120	3	0-15-345	0	0
24	230	3	315	3	0-15-345	0	0

Staring with initial base harmonic current $\boldsymbol{I}^*_{7,base}$ point (“1” in Figure 8, sinusoidal supply voltage conditions), $\boldsymbol{U}^*_3$ is first applied. The rotation of the $\boldsymbol{U}^*_3$ provides an ellipse common from the previous chapters (see Figure 8, black line and asterisks). Two extreme points of attention have been selected next, having $\boldsymbol{I}^*_7$ with minimum (“2” in Figure 8) and maximum phase value (“3” in Figure 8). Next, using $\boldsymbol{U}^*_3$ respective to the point of interest on graph, $\boldsymbol{U}^*_5$ is added and rotated through 360°. Results have been reported as further ellipses, having their center-points in the points of interest previously identified. Therefore, the geometrical cumulation of influence vectors due to different harmonic orders of supply voltages included, can be directly observed. Here even cumulation of $\boldsymbol{U}^*_3$ and $\boldsymbol{U}^*_5$ can be seen to provide up to 80° $\boldsymbol{I}^*_7$ rotation. The points of $\boldsymbol{I}^*_7$ presented for new origins of ellipses for $\boldsymbol{U}^*_5$ influence (“2” and “3” on Figure 8) would provide good accuracy for including more supply voltage harmonic influence components.

The presentation in Figure 8 allows to propose that the harmonic current $\boldsymbol{I}^*_x$ components, determined respectively

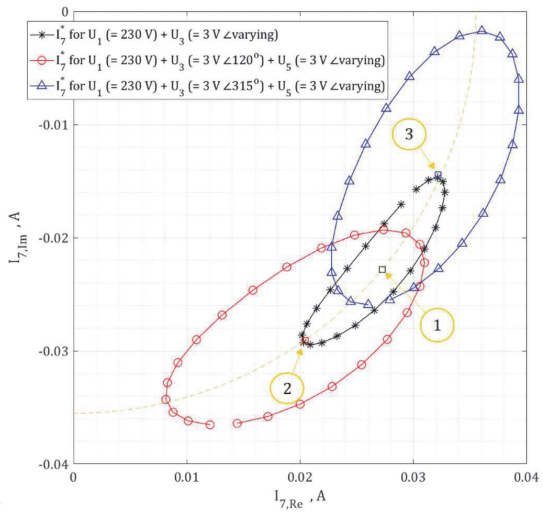

FIGURE 8. Explanation on harmonic current $I*_7$ cumulative products results with $U_1 = 230$ V; U_3 and $U_5 = 3$ V. Red line: $\varphi_{U3} = 105°$, blue line: $\varphi_{U3} = 300°$, φ_{U5} phase values 0,15,30…345, plot of measured response.

TABLE 11. Harmonic Voltage Levels and Phase Ange Present in Residential grid, Flat and Pointed Top Waveforms.

	U^*_1	U^*_3		U^*_5		U^*_7		U^*_9	
	U_1 , V	U_3 , V	φ_{U3} °	U_5 , V	φ_{U5} °	U_7 , V	φ_{U7} °	U_9 , V	φ_{U9} °
Grid-1	230	0.35	51	1.0	224	0.97	15	0	0
Grid-2	230	0.15	80	1.6	296	0.79	37	0	0
Flat top	230	5.5	0	3.8	180	2.0	0	0.57	180
Pointed top	230	6.6	0	4.7	180	1.4	180	0	0

with (10) for each supply voltage harmonic component $\boldsymbol{U}^*_y$ influence individually would be presenting the cumulation in a linear summation as

$$\Delta I_x = \sum_{n=1;y=2n+1}^{N} \Delta I_{x,y} \tag{27}$$

$$\Delta \varphi_{Ix} = \sum_{n=1;y=2n+1}^{N} \Delta \varphi_{Ix,y} \tag{28}$$

where N is the number of odd harmonic components considered. The (27) and (28) are basically subsets of the matrix evaluation provided in (11 – 14). However, the authors express that this cumulation approach should be used with care, as this is providing good accuracy generally for supply voltage harmonics low magnitude levels. For example, the linear relation could be used with voltage harmonics levels of up to 1.5 V, while greater supply voltage harmonic levels would provide a remarkable additional deviation. This can be traced to additional G_{xy} and K_{xy} dependence on the $\boldsymbol{I}^*_x$ ellipse cumulative base point positioning. The authors intend to present work on the stated cumulative $\boldsymbol{I}^*_x$ calculation model in the future.

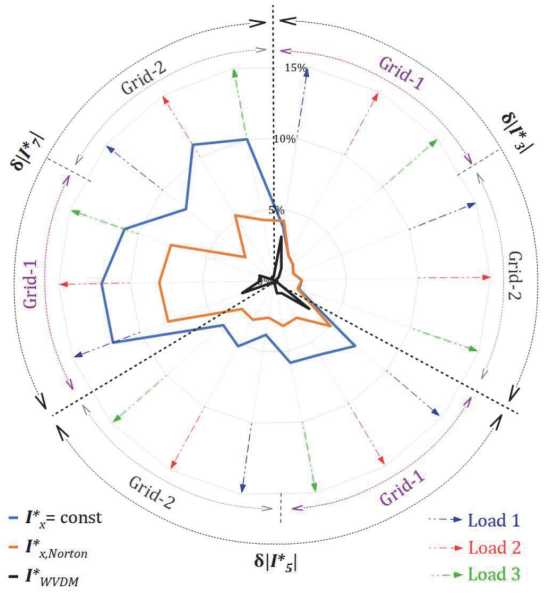

FIGURE 9. Deviation in magnitude between measurements and modelled (constant-current, Norton, proposed model) values, for two residential-area grid waveforms.

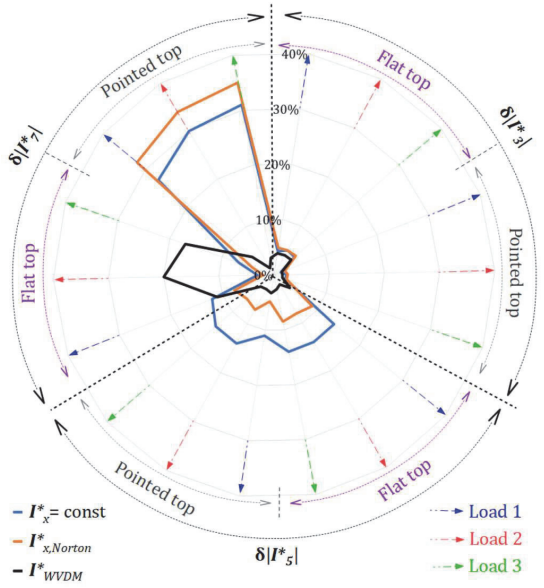

FIGURE 10. Deviation in magnitude between measurements and modelled (constant-current, Norton, proposed model) values, for Flat and pointed-top supply waveforms.

IX. VALIDATION OF PROPOSED MODEL

Even though stating the expected limitations to the cumulative harmonic current evaluation in the previous chapter, the linear cumulative $\boldsymbol{I}^*_x$ model can be seen to provide

TABLE 12. Difference of Estimations and Measurement for tested residential and industrial voltage supply waveform.

Load	Waveform type	Estimation technique	Difference					
			% $\delta\|I^*_3\|$	$\delta\varphi_{I3}$	% $\delta\|I^*_5\|$	$\delta\varphi_{I5}$	% $\delta\|I^*_7\|$	$\delta\varphi_{I7}$
1	Grid-1	I^*_x = const	3.8	<1	7.2	1	12	3
		$I^*_{x,Norton}$	4.2	<1	5.0	2	7.9	4
		I^*_{WVDM}	3.1	1	3.1	2	2.4	3
	Grid-2	I^*_x = const	1.4	5	3.8	8	7.9	11
		$I^*_{x,Norton}$	1.4	5	2.6	<1	2.6	14
		I^*_{WVDM}	0.1	<1	0.1	1	0.1	2
	Flat top	I^*_x = const	4.3	20	14	40	12	65
		$I^*_{x,Norton}$	4.9	14	9.0	25	7.7	48
		I^*_{WVDM}	3.9	<1	3.7	3	12	9
	Pointed top	I^*_x = const	1.3	15	12	27	28	44
		$I^*_{x,Norton}$	2.1	8	4.8	8	33	53
		I^*_{WVDM}	1.5	1	3.3	2	5.1	5
2	Grid-1	I^*_x = const	2.0	1	6.0	3	12	7
		$I^*_{x,Norton}$	2.0	2	3.0	3	8.0	<1
		I^*_{WVDM}	1.0	<1	1	<1	1.0	<1
	Grid-2	I^*_x = const	1.9	5	5.2	7	11	9
		$I^*_{x,Norton}$	1.9	4	3.1	<1	5.3	12
		I^*_{WVDM}	0.2	<1	0.2	1	0.3	2
	Flat top	I^*_x = const	5.0	18	14	38	3.0	63
		$I^*_{x,Norton}$	5.0	12	8.0	22	2.0	47
		I^*_{WVDM}	4.0	2	2.0	1	20	3
	Pointed top	I^*_x = const	2.3	16	15	30	30	51
		$I^*_{x,Norton}$	2.5	8	7.1	10.	34	61
		I^*_{WVDM}	1.5	<1	2.9	2	1.4	6
3	Grid-1	I^*_x = const	1.7	1	5.8	3	12	7
		$I^*_{x,Norton}$	1.7	2	3.2	3	7.6	<1
		I^*_{WVDM}	0.4	<1	0.9	<1	1.1	<1
	Grid-2	I^*_x = const	1.8	5	4.7	8	10	9
		$I^*_{x,Norton}$	1.7	4	3.0	<1	4.3	13
		I^*_{WVDM}	0.1	<1	0.2	1	0.3	2
	Flat top	I^*_x = const	4.9	19	14	38	6.8	64
		$I^*_{x,Norton}$	5.2	12	8.5	23	4.2	47
		I^*_{WVDM}	4.1	2	2.6	2	17	6
	Pointed top	I^*_x = const	2.1	16	14	29	31	48
		$I^*_{x,Norton}$	2.4	8	6.5	9	35	58
		I^*_{WVDM}	1.6	<1	3.2	2	3.1	6

considerably improved performance and accuracy compared to the previously available models. In order to present this, specific waveforms listed in Table 11 will be used.

As the residential grid supply tend to have small harmonic magnitudes, the resultant load current harmonics have nonlinear part insignificant as compared to linear part. More extreme cases are available in the industrial grids, where ''pointed and flat-top'' supply voltage waveform could emerge more often. The latter exceed the proposed model accuracy range; however, could be used for reference of different model presentations.

For load current harmonic fingerprint estimation using the proposed model, 2 recorded residential grid voltage waveforms have been used (Grid-1 and Grid-2, in Table 11). Similarly, but for more extensive industrial case presentation through ''flat top'' and ''pointed top'' waveforms are presented only as reference (Table 11).

For the loads discussed in the previous chapters, the measurements were carried out as the loads were supplied the waveforms in question, using similar grounds as (chapter II).

Table 12 depicts the measurement and proposed model estimation accuracy comparison of different techniques by modeling response of the loads for the targeted waveforms using (11 – 14). The deviation in harmonic currents magnitude $\delta|\boldsymbol{I}^*_h|$ is presented for different harmonic models (see also Figure 9 and 10). The constant harmonic current injection ($\boldsymbol{I}^*_x$ = const) and Norton model ($\boldsymbol{I}^*_{x,Norton}$) waveforms have been compared; the proposed model ($\boldsymbol{I}^*_{x,WVDM}$) presents considerable accuracy improvement. Table 12 readings have been compared to on Figures 9 – 10 for the magnitude result analysis. It has to be noted, that the phase angle values for all considered $\boldsymbol{I}^*_x$ observed, are presenting less than 10° difference compared to the measured values. Figure 11 presents the comparison of load current harmonic measurements and modeled response of different harmonic modeling

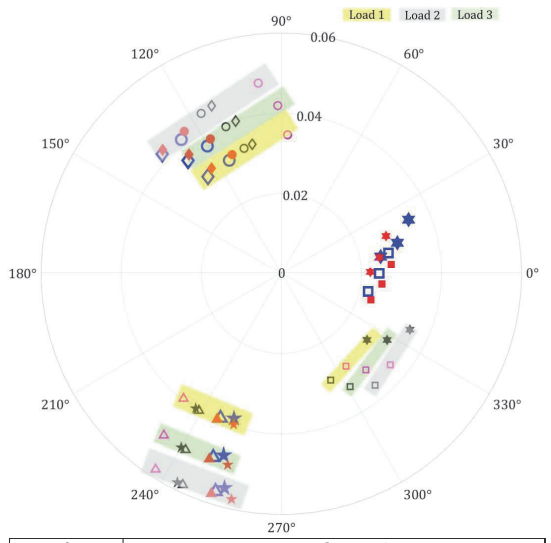

Waveform	Current harmonics		
Pure sine	△ $I^*_{3,Base}$	○ $I^*_{5,Base}$	□ $I^*_{7,Base}$
Flat top	△ $I^*_{3,Meas\_FT}$	○ $I^*_{5,Meas\_FT}$	□ $I^*_{7,Meas\_FT}$
	△ $I^*_{3,Norton\_FT}$	○ $I^*_{5,Norton\_FT}$	□ $I^*_{7,Norton\_FT}$
	▲ $I^*_{3,WVDM\_FT}$	● $I^*_{5,WVDM\_FT}$	■ $I^*_{7,WVDM\_FT}$
Pointed top	★ $I^*_{3,Meas\_PT}$	◇ $I^*_{5,Meas\_PT}$	✱ $I^*_{7,Meas\_PT}$
	★ $I^*_{3,Norton\_PT}$	◇ $I^*_{5,Norton\_PT}$	✱ $I^*_{7,Norton\_PT}$
	★ $I^*_{3,WVDM\_PT}$	◆ $I^*_{5,WVDM\_PT}$	✱ $I^*_{7,WVDM\_PT}$

FIGURE 11. Comparison of load current harmonic measurements and modeled response of different harmonic modeling techniques, for flat-top (FT) and pointed-top (PT) voltage waveforms (see Table 12).

techniques, for flat-top (FT) and pointed-top (PT) voltage waveforms.

The proposed model harmonic current estimation is rather usable even for the industrial cases presented, however this is not valid for all industrial waveform presentations. The phase margin tends to present more accurate estimation outcome, result of improved phase results due to cross-order harmonic coupling evaluation.

X. CONCLUSION

In the presentation above, a novel approach to model the supply voltage harmonics effect to load current of a non-linear load presented very good outcome and correspondence of measured harmonic current levels and phase angles. The type A LED presents a solid example for this model, given the excellent correlation between the time-domain initiation moment shift derived harmonic phase angle variations. In previous network modeling techniques such as Norton equivalent model, the consideration of cross-order harmonic influence for current and voltage is not available, however, this makes up a significant proportion to, for example, 7th harmonic current estimation. Frequency coupling matrix modeling contains many admittance matrix parameters to account cross-order coupling, however the results provide considerable deviations and no physical ground to the emergence of cross-order coupling. The proposed timed-domain waveform variation defined model provides a detailed understanding of the interaction between the supply voltage and current harmonics variations and their cross-order coupling.

Nevertheless, authors point out that the linearity assumption in the harmonic current components cumulative assessment has narrow application span. The discussed lower order harmonics' model is acceptable until ∼1.5 V of supply voltage harmonic levels used. In order to improve this model accuracy, a non-linear approach would be needed for the total harmonic current calculation. The present model, however, has been verified to provide good outcome for residential grid supply voltage harmonic cases. The use of this linear model would be especially feasible for residential harmonic current level estimation, where the harmonic vectors are considered. Authors aim to address the cumulative multiple influencer modelling with accurate nonlinear part estimation details in future publications.

REFERENCES

[1] I. Santiago, M. A. López-Rodríguez, A. Gil-de-Castro, A. Moreno-Munoz, and J. J. Luna-Rodríguez, "Energy consumption of audiovisual devices in the residential sector: Economic impact of harmonic losses," *Energy*, vol. 60, pp. 292–301, Oct. 2013, doi: 10.1016/j.energy.2013.08.018.

[2] T. Vinnal, M. Jarkovoi, and L. Kutt, "Harmonic currents and voltages in LV networks of Estonia: Measurement results, case studies," in *Proc. IEEE 59th Int. Sci. Conf. Power Electr. Eng. Riga Tech. Univ. (RTUCON)*, Nov. 2018, pp. 1–7, doi: 10.1109/RTUCON.2018.8659875.

[3] *Electromagnetic Compatibility (EMC)—Part 3-2: Limits—Limits for Harmonic Current Emissions (Equipment Input Current 16 A Per Phase)*, Standard IEC 61000-3-2:2018, 2018.

[4] N. Shabbir, L. Kütt, M. Jarkovoi, M. N. Iqbal, A. Rassõlkin, and K. Daniel, "An overview of measurement standards for power quality," *Agron. Res.*, vol. 19, no. 1, pp. 944–960, 2021, doi: 10.15159/AR.21.074.

[5] X. Xu, A. J. Collin, S. Z. Djokic, S. Yanchenko, F. Möller, J. Meyer, R. Langella, and A. Testa, "Analysis and modelling of power-dependent harmonic characteristics of modern PE devices in LV networks," *IEEE Trans. Power Del.*, vol. 32, no. 2, pp. 1014–1023, Apr. 2017, doi: 10.1109/TPWRD.2016.2574566.

[6] P. W. Lehn and K. L. Lian, "Frequency coupling matrix of a voltage-source converter derived from piecewise linear differential equations," *IEEE Trans. Power Del.*, vol. 22, no. 3, pp. 1603–1612, Jul. 2007, doi: 10.1109/TPWRD.2006.886779.

[7] M. N. Iqbal, L. Kutt, B. Asad, and N. Shabbir, "Impact of cable impedance on the harmonic emission of LED lamps," in *Proc. 21st Int. Sci. Conf. Electric Power Eng. (EPE)*, Oct. 2020, pp. 1–6, doi: 10.1109/EPE51172.2020.9269271.

[8] A. Gil-De-Castro, R. Medina-Gracia, S. K. Ronnberg, A. M. Blanco, and J. Meyer, "Differences in the performance between CFL and LED lamps under different voltage distortions," in *Proc. 18th Int. Conf. Harmon. Quality Power (ICHQP)*, May 2018, pp. 1–6, doi: 10.1109/ICHQP.2018.8378918.

[9] L. Kutt, E. Saarijarvi, M. Lehtonen, H. Molder, and J. Niitsoo, "Estimating the harmonic distortions in a distribution network supplying EV charging load using practical source data—Case example," in *Proc. IEEE Power Energy Soc. Gen. Meeting*, Oct. 2014, pp. 4–8, doi: 10.1109/PESGM.2014.6939267.

[10] A. J. Collin, X. Xu, S. Z. Djokic, F. Moller, J. Meyer, L. Kutt, and M. Lehtonen, "Survey of harmonic emission of electrical vehicle chargers in the European market," in *Proc. Int. Symp. Power Electron., Electr. Drives, Autom. Motion (SPEEDAM)*, Jun. 2016, pp. 1208–1213, doi: 10.1109/SPEEDAM.2016.7526005.

[11] A. Kalair, N. Abas, A. R. Kalair, Z. Saleem, and N. Khan, "Review of harmonic analysis, modeling and mitigation techniques," *Renew. Sustain. Energy Rev.*, vol. 78, pp. 1152–1187, Oct. 2017, doi: 10.1016/j.rser.2017.04.121.

[12] A. Taghvaie, F. Zare, R. Sharma, and D. Kumar, "Impacts of grid impedance on power quality of converters in distribution networks," in *Proc. 48th Annu. Conf. IEEE Ind. Electron. Soc. (IECON)*, Oct. 2022, pp. 1–6, doi: 10.1109/IECON49645.2022.9968362.
[13] H. Rathnayake, K. G. Khajeh, F. Zare, and R. Sharma, "Harmonic analysis of grid-tied active front end inverters for the frequency range of 0-9 kHz in distribution networks: Addressing future regulations," in *Proc. IEEE Int. Conf. Ind. Technol. (ICIT)*, Feb. 2019, pp. 446–451, doi: 10.1109/ICIT.2019.8755015.
[14] J. Yadav, K. Vasudevan, J. Meyer, and D. Kumar, "Frequency coupling matrix model of a three-phase variable frequency drive," *IEEE Trans. Ind. Appl.*, vol. 58, no. 3, pp. 3652–3663, May 2022, doi: 10.1109/TIA.2022.3156104.
[15] J. Yadav, K. Vasudevan, J. Meyer, and D. Kumar, "Modelling three phase variable frequency drive using a frequency coupling matrix," in *Proc. IEEE 1st Int. Conf. Smart Technol. Power, Energy Control (STPEC)*, Sep. 2020, pp. 1–6, doi: 10.1109/STPEC49749.2020.9297761.
[16] Y. Xiao and X. Yang, "Harmonic summation and assessment based on probability distribution," *IEEE Trans. Power Del.*, vol. 27, no. 2, pp. 1030–1032, Apr. 2012, doi: 10.1109/TPWRD.2012.2187124.
[17] R. Savoor and K. Meier-Hellstern, "Estimating the frequency coupling matrix from network measurements," *IEEE Trans. Control Netw. Syst.*, vol. 7, no. 2, pp. 353–388, Sep. 2020, doi: 10.1201/9781315208787-16.
[18] R. Langella, A. Testa, J. E. Caicedo, A. A. Romero, H. C. Zini, J. Meyer, and N. R. Watson, "On the use of Fourier descriptors for the assessment of frequency coupling matrices of power electronic devices," in *Proc. 18th Int. Conf. Harmon. Quality Power (ICHQP)*, May 2018, pp. 1–6, doi: 10.1109/ICHQP.2018.8378908.
[19] K. J. Son, G. S. An, K. D. Nam, and T. G. Chang, "An advanced frequency estimation algorithm based on analytic compensation of effects of dominant harmonic in power systems," *IEEE Access*, vol. 9, pp. 146568–146577, 2021, doi: 10.1109/ACCESS.2021.3122469.
[20] Y. Sun, G. Zhang, W. Xu, and J. G. Mayordomo, "A harmonically coupled admittance matrix model for AC/DC converters," *IEEE Trans. Power Syst.*, vol. 22, no. 4, pp. 1574–1582, Nov. 2007, doi: 10.1109/TPWRS.2007.907514.
[21] L. F. Beites, J. G. Mayordomo, and X. Yang, "The harmonically coupled admittance matrix of the single-phase diode rectifier," *IEEE Access*, vol. 9, pp. 128023–128031, 2021, doi: 10.1109/ACCESS.2021.3110597.
[22] K. Daniel, L. Kutt, M. N. Iqbal, N. Shabbir, and M. Jarkovoi, "Description of practical load harmonic current emission due to voltage harmonic variation," in *Proc. IEEE 62nd Int. Sci. Conf. Power Electr. Eng. Riga Tech. Univ. (RTUCON)*, Nov. 2021, pp. 1–6, doi: 10.1109/RTUCON53541.2021.9711594.
[23] M. Ramzan, A. Othman, and N. R. Watson, "Accurate harmonic analysis of distribution systems," in *Proc. 7th IEEE Workshop Electron. Grid (eGRID)*, Nov. 2022, pp. 1–5, doi: 10.1109/eGRID57376.2022.9990007.
[24] M. N. Iqbal, L. Kütt, B. Asad, N. Shabbir, and I. Rasheed, "Time-dependent variations in current harmonic emission by LED lamps in the low-voltage network," *Electr. Eng.*, vol. 103, no. 3, pp. 1525–1539, Jun. 2021, doi: 10.1007/s00202-020-01175-4.
[25] D. Gallo, R. Langella, M. Luiso, A. Testa, and N. R. Watson, "A new test procedure to measure power electronic devices' frequency coupling admittance," *IEEE Trans. Instrum. Meas.*, vol. 67, no. 10, pp. 2401–2409, Oct. 2018, doi: 10.1109/TIM.2018.2819318.
[26] M. N. Iqbal, L. Kutt, N. Shabbir, and B. Asad, "Comparison of current harmonic emission by different lighting technologies," in *Proc. IEEE 61th Int. Sci. Conf. Power Electr. Eng. Riga Tech. Univ. (RTUCON)*, Nov. 2020, pp. 1–5, doi: 10.1109/RTUCON51174.2020.9316615.
[27] M. N. Iqbal, L. Kütt, K. Daniel, M. Jarkovoi, B. Asad, and N. Shabbir, "Bivariate stochastic model of current harmonic analysis in the low voltage distribution grid," *Proc. Est. Acad. Sci.*, vol. 70, no. 2, pp. 190–206, 2021, doi: 10.3176/proc.2021.2.08.
[28] M. N. Iqbal, L. Kütt, B. Asad, T. Vaimann, A. Rassõlkin, and G. L. Demidova, "Time dependency of current harmonics for switch-mode power supplies," *Appl. Sci.*, vol. 10, no. 21, pp. 1–12, 2020, doi: 10.3390/app10217806.
[29] M. N. Iqbal, M. Jarkovoi, L. Kutt, and N. Shabbir, "Impact of LED thermal stability to household lighting harmonic load current modeling," in *Proc. Electr. Power Quality Supply Rel. Conf. (PQ) Symp. Electr. Eng. Mechatronics (SEEM)*, Jun. 2019, pp. 1–6, doi: 10.1109/PQ.2019.8818226.
[30] M. N. Iqbal, "Measurement based approach for residential customer stochastic current harmonic modelling," Ph.D. dissertation, Tallinn Univ. Technol., Tallinn, Estonia, Tech. Rep. 43/2021, doi: 10.23658/taltech.43/2021.
[31] J. Cunill-Solà and M. Salichs, "Study and characterization of waveforms from low-watt (≪25 W) compact fluorescent lamps with electronic ballasts," *IEEE Trans. Power Del.*, vol. 22, no. 4, pp. 2305–2311, Oct. 2007.
[32] D. Chakravorty, J. Meyer, P. Schegner, S. Yanchenko, and M. Schocke, "Impact of modern electronic equipment on the assessment of network harmonic impedance," *IEEE Trans. Smart Grid*, vol. 8, no. 1, pp. 382–390, Jan. 2017, doi: 10.1109/TSG.2016.2587120.
[33] A. J. Collin, S. Z. Djokic, J. Drapela, Z. Guo, R. Langella, A. Testa, and Neville . R. Watson, "Analysis of approaches for modeling the low frequency emission of LED lamps," *Energies*, vol. 13, no. 7, pp. 1–33, 2020, doi: 10.3390/en13071571.
[34] J. Molina and L. Sainz, "Compact fluorescent lamp modeling for large-scale harmonic penetration studies," *IEEE Trans. Power Del.*, vol. 30, no. 3, pp. 1523–1531, Jun. 2015, doi: 10.1109/TPWRD.2014.2363143.
[35] A. Alduraibi, J. Yaghoobi, and F. Zare, "Impacts of grid voltage harmonics amplitude and phase angle values on power converters in distribution networks," *IEEE Access*, vol. 9, pp. 92017–92029, 2021, doi: 10.1109/ACCESS.2021.3093026.
[36] J. Drapela, R. Langella, A. Testa, and V. Vendemia, "A new analytical model of single-phase diode bridge rectifiers in the presence of interharmonics in supply voltage," *IEEE Open Access J. Power Energy*, early access, Feb. 13, 2023, doi: 10.1109/OAJPE.2023.3244330.
[37] J. Kwon, X. Wang, F. Blaabjerg, C. L. Bak, A. R. Wood, and N. R. Watson, "Harmonic instability analysis of a single-phase grid-connected converter using a harmonic state-space modeling method," *IEEE Trans. Ind. Appl.*, vol. 52, no. 5, pp. 4188–4200, Sep./Oct. 2016, doi: 10.1109/TIA.2016.2581154.
[38] D. Kumar and F. Zare, "Harmonic analysis of grid connected power electronic systems in low voltage distribution networks," *IEEE Trans. Emerg. Sel. Topics Power Electron.*, vol. 4, no. 1, pp. 70–79, Mar. 2016, doi: 10.1109/JESTPE.2015.2454537.

KAMRAN DANIEL (Graduate Student Member, IEEE) received the B.Sc. degree in electronics engineering from The Islamia University of Bahawalpur, in 2008, and the M.S. degree from the University of South Asia, Lahore, Pakistan. He is currently pursuing the Ph.D. degree with the Tallinn University of Technology, Estonia. He is a Lecturer with the University of Engineering and Technology at Lahore. His research interests include network harmonic modeling, power line diagnostics, power quality, and electromagnetic compatibility.

LAURI KÜTT (Senior Member, IEEE) received the B.Sc. degree in computer and automation technology and the M.Sc. degree in electrical power engineering from the Tallinn University of Technology, Tallinn, Estonia, in 2002 and 2004, respectively, and the Ph.D. degree from the Department of Energy and Geotechnology, Tallinn University of Technology, in 2012. He is currently a Professor with the Department of Electrical Power Engineering and Mechatronics, Tallinn University of Technology. His current research interests include fast transients on electric power lines, power line diagnostics, power quality, and electromagnetic compatibility.

MUHAMMAD NAVEED IQBAL received the B.Sc. degree in electronics engineering from The Islamia University of Bahawalpur, Pakistan, in 2008, the M.S. degree from the University of New South Wales, Australia, in 2010, and the Ph.D. degree from the Department of Electrical Power Engineering and Mechatronics, Tallinn University of Technology, Estonia, in 2021. He is currently an Assistant Professor with the Department of Electrical Engineering, Government College University Lahore, Pakistan. His current research interests include power line diagnostics, power quality, and electromagnetic compatibility.

NOMAN SHABBIR (Senior Member, IEEE) received the B.S. degree in computer engineering from COMSATS, Lahore, Pakistan, and the M.S. degree in electrical engineering from BTH, Sweden. He is currently a Research Fellow with the FinEST Center for Smart Cities, Tallinn University of Technology, Estonia. He is also an Assistant Professor with GC University Lahore, Pakistan. His research interests include renewable energy systems, smart grids, machine learning, and ICT.

MARTIN PARKER received the B.Sc. and M.Sc. degrees in mechatronics from the Tallinn University of Technology, in 2011 and 2013, respectively. He is currently a Junior Researcher with the Department of Electrical Power Engineering and Mechatronics, Tallinn University of Technology. His current research interests include metrology, measurement instrumentation, and lighting technologies.

MAREK JARKOVOI received the M.Sc. (Hons.) and Ph.D. degrees from the Tallinn University of Technology, in 2013 and 2019, respectively. He is currently an Engineer, a Researcher, and an Electronics Development Engineer with the Tallinn University of Technology. He is an expert in areas on measurement models and methods. His current research interests include applied electromagnetics and electromagnetic compatibility and electric power quality, focused on harmonic distortions.

Publication IV

K. Daniel, L. Kütt, M. N. Iqbal, N. Shabbir, M. Jarkovoi and M. Parker, “Voltage Main Harmonic Level Influence on Harmonic Current Emission Modeling,” *2023 International Conference on Future Energy Solutions (FES)*, Vaasa, Finland, 2023, pp. 1–6, doi: 10.1109/FES57669.2023.10183302.

Voltage Main Harmonic Level Influence on Harmonic Current Emission Modeling

Kamran Daniel
Dept. of Electrical Power Engineering & Mechatronics
Tallinn University of Technology
Tallinn, Estonia
kdanie@taltech.ee

Lauri Kütt
Dept. of Electrical Power Engineering & Mechatronics
Tallinn University of Technology
Tallinn, Estonia
lauri.kutt@taltech.ee

Muhammad Naveed Iqbal
Dept. of Electrical Power Engineering & Mechatronics
Tallinn University of Technology
Tallinn, Estonia
miqbal@taltech.ee

Noman Shabbir
FinEST center for Smart Cities
Tallinn University of Technology
Tallinn, Estonia
noman.shabbir@taltech.ee

Marek Jarkovoi
Dept. of Electrical Power Engineering & Mechatronics
Tallinn University of Technology
Tallinn, Estonia
marek.jarkovoi@taltech.ee

Martin Parker
Dept. of Electrical Power Engineering & Mechatronics
Tallinn University of Technology
Tallinn, Estonia
martin.parker@taltech.ee

2023 International Conference on Future Energy Solutions (FES) | 979-8-3503-3230-8/23/$31.00 ©2023 IEEE | DOI: 10.1109/FES57669.2023.10183302

***Abstract*—This paper presents an experimental evaluation on the load current harmonic sensitivity to supply voltage main component level. While most often, the current harmonic model components are presented as constants regardless of U_1 level, the measurements indicate that the role of the U_1 is significant and needs attention. Large experimental result set is used in this paper to describe the possible modeling approach for the U_1 inclusion. Empirical trends of the measurement outcome indicate that a linear relation towards the relative U_1 level is justified to represent the load current harmonics dependence. A waveform variation-dependent model (WVDM) for load current harmonics is further elaborated to provide a U_1 dependent part.**

Keywords—Harmonic analysis, cross-order harmonic coupling, harmonic sensitivity, harmonic estimation

I. INTRODUCTION

The harmonic currents emitted by low voltage distribution network (DN) loads are known to be influenced by the harmonics in the supply voltage [1]. DNs are designed to provide a constant RMS magnitude and frequency AC supply voltage with slight variations around the rated values under normal operating conditions [2][3]. However, as modern energy-efficient electrical devices use DC voltage, the AC voltage from the mains is usually converted to DC voltage for power electronic (PE) units using full-bridge rectifiers [4]. Due to the excess of harmonic distortion added by the non-linear loads to the supply grid, the utility grid struggles to maintain a stable voltage supply level for the end user. The voltage variation can be up to ±10 % of nominal i.e., 230 V.

Of the most common models to describe the load harmonic currents, one can find current source models, whether having a permanent current model (voltage harmonics independent) [5][6], Norton model with a constant current source and added impedance for voltage harmonic response, or frequency coupled admittance matrix (FCM) [7] [8]. The latter is able to include cumulative effects the multiple orders of voltage harmonics, yet still relying on the constant current source base component. Recently the authors of this paper introduced a time domain waveform based model (*WVDM*) for modeling the current harmonics behavior[9]. Still, a base constant current harmonic component is present in this model also.

The constant current source is key feature of the load current response model. In testing, it has been revealed that the load current response vector is seemingly following a cyclic pattern around centrepoint, this is the base harmonic vector. This has given ground to impedance-based modeling approaches, where the supply voltage harmonic component inflicted load current component is added to the base vector. For example, the FCM-based model uses form of

$$\boldsymbol{I_y^* = I_{y,base} + U_x^* Y_{xk}^*} \quad (1)$$

While impedance-based models propose that load response to voltage harmonic is following circular pattern, instead for simpler power electronic loads, the load current response is presenting an elliptic response pattern [10]. The WVDM model separates the magnitude and phase variations to different categories, on physical operation built grounds. An ellipse response pattern of a load current harmonic component, measured as a response of the supply voltage harmonic component injection, has been presented in Fig 1.

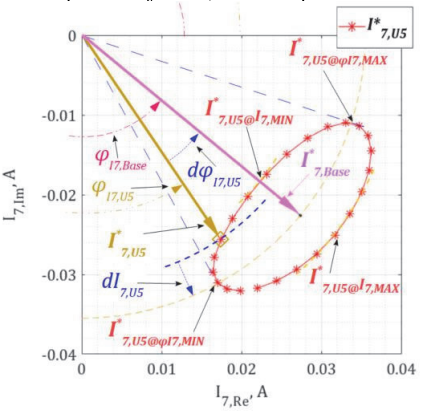

Fig. 1. Vector component plot for the harmonic load current component analysis. I^*_7 vector endpoints' ellipse points plot, for $U_5 = 3$ V, $\boldsymbol{\varphi}_{U5} = 0, 15, 30 \ldots 345^o$.

The WVDM targets the evaluation of phase and magnitude variations of the response. The WVDM proposed form in [9] uses 3 components to describe the model. The initial model is presented based on the rated voltage (230 V) level measurements. In further measurements, however, it has been revealed that any other supply level voltage value, particularly main harmonic U_1 level, will provide an impact to basically all model components. This includes the base harmonic current as well as model coefficients.

This paper will look into details on the load harmonic current modeling, focusing on the base point relations to the supply voltage level. In addition, the variations of the current harmonics' magnitude and phase response will be addressed. The paper raises the relations to describe the load current response components related to U_1 level. The latter has been poorly if at all described in the literature.

II. CHARACTERIZATION OF THE LOAD CURRENT RESPONSE

Lighting loads are a considerable portion of devices connected to the grid. LED lamps as a replacement for older technologies, which can substantially reduce power consumption. However, it is important to note that these LED lamps contain circuits that may interfere with power quality by introducing current harmonics. As a result, the widespread use of LED lamps could potentially impact the distribution grid's power quality. Figure 2 presents the load current waveform of a commercially available LED lamp.

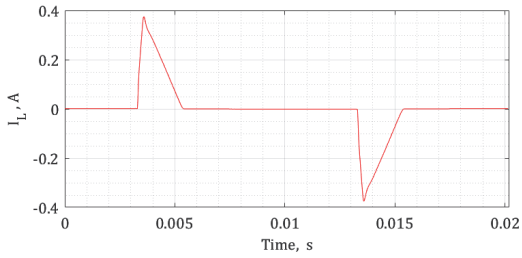

Fig. 2. Load current waveshape of LED lamps tested

Load base current harmonic vector is basically a centrepoint of the harmonic current response vector. Commonly this is evaluated as the response to the sinusoidal supply voltage conditions.

In response to supply voltage harmonics, load current harmonics always provide a variation. The current harmonics response is related to the time-domain waveform variation, see [9]. For example, observing 3º phase shift of 3rd order harmonic current is due to the rectifier conduction initiation moment variation. This propagates as 5º phase shift of 5th order, 7º phase shift of 7th order current harmonic etc. Every voltage harmonic, injected to the power supply with the magnitude of U_y will provide a maximum current harmonic phase influence instance at specific phase value $\angle\varphi_{Uy}$, similarly minimum ($I_{x,min@Uy}$) and maximum ($I_{x,max@Uy}$) magnitude response phase values. The magnitude and phase variations are proportional to the U_y magnitude. These minimum and maximum points establish, for example WVDM coefficient values.

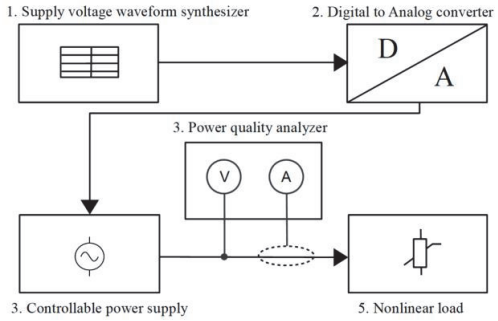

Fig. 3. Measurement setup [11]

The sensitivity analysis of the loads on the U_1 levels was conducted using a systematic scan, similar to the method described in [9] [12][13]. The supply voltage was output from a high-precision amplifier and value is established using equation (3).

$$u_{test}(t) = \sum_{y=1}^{N} \sqrt{2}\ U_y \sin\left(2\pi f_y t + \alpha_y\right) \qquad (2)$$

The extracted values of the current harmonics were recorded with magnitude and phase response values, correlated to the waveform-sampled values.

During the load characteristic scan, minor but stable and repeatable variations in the harmonic current component magnitude and phase values were recorded and verified using the current waveform's discrete Fourier transform (DFT). The main load characteristic scan was carried out using various scenarios, presented in Table I.

TABLE I. SUPPLY VOLTAGE COMBINATIONS, ADDING SINGLE HARMONIC TO SUPPLY VOLTAGE

Combi-nations	U_1	U_3		U_5		U_7	
	U_1, V	U_3, V	φ_{U3} º	U_5, V	φ_{U5} º	U_7, V	φ_{U7} º
5	207, 218, 230, 241, 253	0	0	0	0	0	0
120	207, 218, 230, 241, 253	3	0-15 …345	0	0	0	0
120	207, 218, 230, 241, 253	0	0	3	0-15 …345	0	0
120	207, 218, 230, 241, 253	0	0	0	0	3	0-15 …345

This study evaluated five LED lamps for their odd harmonic content, specifically for harmonics 3, 5, and 7.

III. BASE POINT VARIATIONS

The fundamental response current harmonic (base point) $\boldsymbol{I^*_{5,Base}}$ values for different fundamental voltage U_1 magnitude levels (i.e., 230±10% V) are presented in Fig. 4. With the increase in U_1 magnitude values, the base point value for any response harmonic face a gradual shift; further more, if another influencer voltage harmonic ($\boldsymbol{U^*_x}$) is included in supply the resultant current response vectors also face the similar shift. '○'and '△' patterns are $\boldsymbol{I^*_5}$ response vectors present in load current when U^*_5 is included in supply for two different U_1 levels (207 V, 253 V). Base point $\boldsymbol{I^*_{x,Base}}$ values of dominant low order current harmonics U_1 magnitude levels is presented in table II.

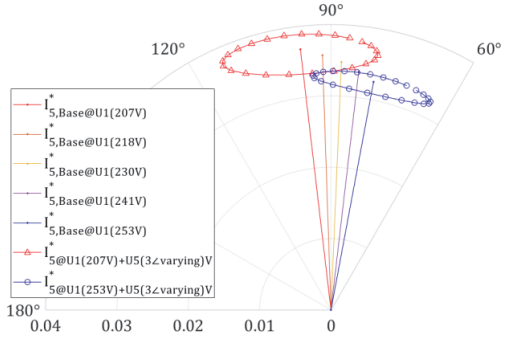

Fig. 4. Ellipses: 5th harmonic currents , 5 levels of U_1

TABLE II. BASE POINT COORDINATES (3RD, 5TH, 7TH)

U_1 , V	$I_{3,Base}$, mA	$\varphi_{I3,Base}$, º	$I_{5,Base}$, mA	$\varphi_{I5,Base}$, º	$I_{7,Base}$, mA	$\varphi_{I7,Base}$, º
207	43.4	-123	36.8	97	28.5	-41
218	41.5	-125	35.7	92	28.4	-48
230	39.8	-128	34.8	88	28.3	-55
241	37.9	-130	33.6	83	27.9	-61
253	36.3	-133	32.5	79	27.5	-67

IV. PHASE AND MAGNITUDE RANGE VARIATIONS

Figures 5 & 6 show the sensitivity of current harmonics for including influencers (voltage harmonics) to the supply voltage waveform and the magnitude of the fundamental voltage component (U_1) in the supply. Harmonic component I^*_7 is selected for presentation here, as the base point magnitude I_7 is rather persistent; and basepoint phase angles are changing. Fig 5 shows I^*_7 response for $\boldsymbol{U^*_3}$ inclusion ($\angle U_3 \rightarrow 360^o$ rotation) in supply voltage for U_1 253 V (230 V+10%), 230 V, and 207 V (230 V–10%); the base point for each elliptical pattern undergoes a similar shift in the phase angle. The spread and compression of $\boldsymbol{I^*_7}$ response vectors related to the U_1 levels is elaborated in Figures 6 and 7, supporting the cumulation hypothesis claimed by *WVDM*.

The dispersion of the phase and magnitude response of the load current harmonic components can be presented as the range of deviation from the base vector point. For the current variation, the highest deviations will be used for the deviation range as

$$dI_{x,y,MAX} = \frac{\left(\left|dI_{x,Uy@Ix,MAX}\right| - \left|dI_{x,Uy@Ix,MIN}\right|\right)}{2} \quad (3)$$

and for the phase angle variation

$$d\varphi_{Ix,y,MAX} = \frac{d\varphi_{Ix,Uy@\varphi Ix,MAX} - d\varphi_{Ix,Uy@\varphi Ix,MIN}}{2} \quad (4)$$

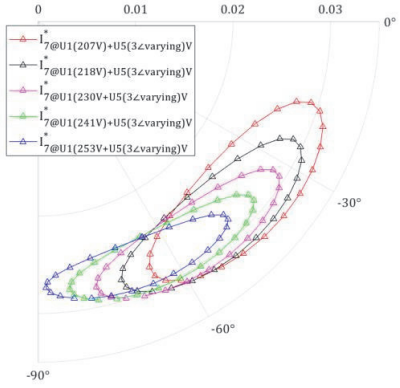

Fig. 5. 7th harmonic response for supply containing U_1 (varying) + U_5 (3V)

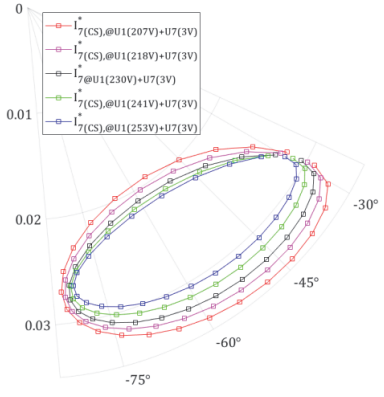

Fig. 6. 7th harmonic response (shifted to identical basepoint phase angle position) for supply voltage U_1 (varying) + added U_3 (3V)

TABLE III. MAXIMUM MAGNITUDE DIFFERENCE & MAXIMUM PHASE DIFFERENCE QUANITIES, BETWEEN BASE POINT & CURRENT HARMONIC VECTORS (3RD, 5TH, 7TH), (U_y = 3V)

U_1, V	Influencing U_h order, y	$dI_{3,max}$, mA	$d\varphi_{3;max;@dI3=0}$, °	$dI_{5,max}$, mA	$d\varphi_{5;max;@dI5=0}$, °	$dI_{7,max}$, mA	$d\varphi_{7;max;@dI7=0}$, °
207	3	0.3	07	1.0	12	1.9	17
207	5	1.3	10	3.5	17	5.4	25
207	7	2.6	11	6.1	19	9.1	28
218	3	0.2	07	0.8	12	1.6	16
218	5	1.1	10	3.0	17	4.7	24
218	7	2.2	11	5.3	19	8.2	28
230	3	0.2	07	0.6	11	1.3	15
230	5	0.8	09	2.5	16	4.1	23
230	7	1.9	11	4.6	19	7.3	27
241	3	0.2	06	0.5	10	1.1	15
241	5	0.7	09	2.1	16	3.5	22
241	7	1.6	11	4.1	18	6.5	26
253	3	0.2	06	0.4	10	0.9	14
253	5	0.6	09	1.7	15	2.9	21
253	7	1.4	11	3.5	18	5.8	26

V. VARIATON PRESENTATION USING WVDM

WVDM [9] describes the total $\boldsymbol{I^*_x}$ is through separate time-difference/phase-difference and magnitude difference coefficients, which captures the physical operation of rectifier circuits.

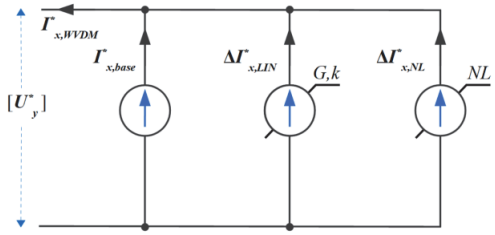

Fig. 7. Schematic description for harmonic current component I^*_x of order x modeling[9].

The load current harmonic component values in WVDM are modeled through 3 component values. These are basepoint value $I_{x,Base}$, linear component, and non-linear component. Respectively, similar component values are for the phase values modeling. (see fig. 2)

$$\begin{cases} I_{x,WVDM} = I_{x,Base} + \Delta I_{x,LIN} + \Delta I_{x,NL} \\ \varphi_{Ix,WVDM} = \varphi_{Ix,Base} + \Delta\varphi_{Ix,LIN} + \Delta\varphi_{Ix,NL} \end{cases} \quad (5)$$

The linear part provides the main proportion of the current harmonic variation, calculated as (4). Similarly, the main current harmonic phase angle variation will be provided by the linear part, calculated as (5)

$$\Delta I_{x,LIN} = \boldsymbol{U_y} \cdot \boldsymbol{G_x} \cdot \cos(\boldsymbol{\alpha_x} - \boldsymbol{\varphi_{Uy}}) \quad (6)$$

$$\Delta\varphi_{Ix,LIN} = \boldsymbol{U_y} \cdot \boldsymbol{k_x} \cdot \sin(\boldsymbol{\alpha_x} - \boldsymbol{\varphi_{Uy}}) \quad (7)$$

where $\boldsymbol{U_y}$ is the $\boldsymbol{U^*_y}$ magnitude matrix in form, $\boldsymbol{G_x}$ is the current harmonic I_x magnitude sensitivity coefficient matrix in form (units A/V = S) when U_1 level is 230 V, and a specific phase coefficient α_{x3} is used for calculating I_x in relation to the actual phase angle value of the supply voltage harmonic $\boldsymbol{U^*_3}$, represented by φ_{U3}. $\boldsymbol{k_x}$ is the current harmonic $\boldsymbol{I^*_{x,LIN}}$ phase angle $\Delta\varphi_{Ix}$ sensitivity coefficient matrix in form (units °/V), when U_1 level is 230 V. The linear part will determine the variation of the main current harmonic phase angle.

$$\boldsymbol{U_y} = [U_3 \;\; U_5 \;\; \ldots \;\; U_N]$$

$$\boldsymbol{G_x} = \begin{bmatrix} G_{x3} \\ G_{x5} \\ \ldots \\ G_{xN} \end{bmatrix} \quad , \quad \cos\left(\boldsymbol{\alpha_x} - \boldsymbol{\varphi_{Uy}}\right) = \begin{bmatrix} \cos(\alpha_{x3} - \varphi_{U3}) \\ \cos(\alpha_{x5} - \varphi_{U5}) \\ \ldots \\ \cos(\alpha_{xN} - \varphi_{UN}) \end{bmatrix}$$

$$\boldsymbol{k_x} = \begin{bmatrix} k_{x3} \\ k_{x5} \\ \ldots \\ k_{xN} \end{bmatrix} \quad , \quad \sin(\boldsymbol{\alpha_x} - \boldsymbol{\varphi_{Uy}}) = \begin{bmatrix} \sin(\alpha_{x3} - \varphi_{U3}) \\ \sin(\alpha_{x5} - \varphi_{U5}) \\ \ldots \\ \sin(\alpha_{xN} - \varphi_{UN}) \end{bmatrix}$$

The coefficients G_{xy}, k_{xy} and α_{xy} are determined through load measurements [9]. Following chapter will present the discussion on the determination on the G and k values.

VI. Phasor Plot Presentation and Determination of Coefficients for Harmonic Component Modeling

Based on the WVDM model, the linear part coefficients are to present the proportion between the magnitude variation range and load current harmonic current parameter. The $dI_{x,y,MAX}$ and supply voltage influencing voltage harmonic U_y proportional coefficient G_{xy} (see (4)) can be calculated as

$$G_{xy} = \frac{dI_{x,MAX}}{U_y} \tag{8}$$

Similarly, the $d\varphi_{Ix,y,MAX}$ and supply voltage influencing voltage harmonic U_y proportional coefficient k_{xy} (see (4)) can be calculated as

$$k_{xy} = \frac{d\varphi_{x,y,MAX}}{U_y} \tag{9}$$

Using the values for harmonic current parameters' variation in Table III, the coefficients discussed have been presented in Table IV.

TABLE IV. *G,K* COEFFICIENT VALUES FOR DIFFERENT HARMONICS COMBINATIONS, MEASUREMENT OUTCOME.
(U_y= 3V), *y*=influencer harmonic order, and *x*=response harmonic order

U_1, V			G_{xy}, mA/V	k_{xy}, °/V	G_{xy}, mA/V	k_{xy}, °/V	G_{xy}, mA/V	k_{xy}, °/V
	y	*x*	3	3	5	5	7	7
207	3		0.09	2.4	0.29	4.0	0.56	5.6
218	3		0.08	2.3	0.23	3.8	0.47	5.3
230	3		0.07	2.2	0.18	3.6	0.39	5.1
241	3		0.07	2.1	0.14	3.4	0.32	4.8
253	3		0.07	2.0	0.10	3.3	0.26	4.6
207	5		0.37	3.4	0.96	5.7	1.52	8.2
218	5		0.30	3.3	0.80	5.5	1.31	7.9
230	5		0.24	3.2	0.66	5.3	1.13	7.6
241	5		0.19	3.1	0.55	5.2	0.96	7.3
253	5		0.15	3.0	0.45	5.0	0.81	7.0
207	7		0.71	3.7	1.63	6.4	2.50	9.4
218	7		0.59	3.7	1.40	6.3	2.22	9.2
230	7		0.50	3.6	1.20	6.1	1.96	8.9
241	7		0.42	3.6	1.03	6.1	1.70	8.7
253	7		0.35	3.6	0.88	6.0	1.49	8.6

VII. Basepoint Sensitivity Model

The main harmonic level U_1 influence to the actual harmonic outcome presents a major influence. In itself, the base point excursion can be modeled with impedance relation, although with negative value. Noted in the table above (Table IV), the coefficients *G* and *k* values are also U_1 level dependent. This presents an additional layer for the model to calculate the estimated harmonic current levels upon expected distribution network mains voltage value ranges.

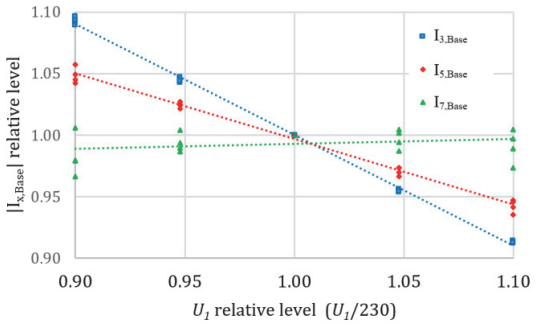

Fig. 8. Relative relation between $|\boldsymbol{I^*_{x,Base}}|$ and fundamental harmonic voltage level.

On the model calculation roots, the sensitivity on U_1 is well correlated to the main harmonic relation to the reference value (see Figures 4, 5 and 6). Deviation in $I_{x,Base}$ are well described by the trends shown in Fig. 8. The linear relation approach is a good tool to deliver the dependency. The relative effect of the U_1 levels on $\boldsymbol{I^*_{x,Base}}$, G_{xy}, and k_{xy} is determined using the following general empirical trend equation (10) inferred from measurements. For example, the base point of the harmonics, the suitable relations can be found as

$$m_{q,U1} = K_{RVL,q} \cdot \left(\frac{U_1}{230}\right) + (1 - K_{RVL,q}) \tag{10}$$

where $k_{RVL,q}$ is the empirical linear '*relative voltage level – RVL*' coefficient and $(1 - k_{RVL,q})$ forms the offset part to the trend. 'q' marks a coefficient identity, where multiplier is used (see Table V). The respective scalar multiplier $m_{q,U1}$ should obtain value 1.0 upon U_1 relative value 1.0. Based on actual U_1 level, for base point $\boldsymbol{I_{x,Base,U1}}$ this multiplier is used to find the respective harmonic base point magnitude value.

$$\boldsymbol{I_{x,Base,U1}} = [m_{b3}\, m_{b5} \ldots m_{bN}] \cdot \boldsymbol{I_{x,Base}} \tag{11}$$

Base point phase value will be defined for phase offset calculation. Phase value offset component is to be resolved through linear trend, relative to voltage U_1 relative level. The basepoint phase offset is an absolute phase shift quantity, added to the base point U_1 nominal level value

$$\boldsymbol{\varphi_{I,Base,U1}} = \boldsymbol{k_{b\varphi}} \cdot \left(\frac{U_1}{230} - 1\right) + \boldsymbol{\varphi_{I,Base}} \tag{12}$$

Figures 9 and 10 indicate the linear dependency of the model coefficients (G_{xy} & k_{xy}) on U_1 relative value and m_{gU1} and m_{kU1} are scalars values to multiply with a value obtained at nominal U_1. Again, multipliers are included to $\boldsymbol{G_{x,U1}}$, $\boldsymbol{k_{x,U1}}$, for making correction based on U_1 relative level. A general trend equation (10) can be suggested to all these.

Equations (10) and (12) are then used to establish $WVDM_{U1}$ model parameter values as:

$$\boldsymbol{G_{x,U1}} = \begin{bmatrix} m_{gX3}\, m_{gX5} \ldots m_{gXN} \end{bmatrix} \begin{bmatrix} G_{x3} \\ G_{x5} \\ \ldots \\ G_{xN} \end{bmatrix}$$

$$\boldsymbol{k_{x,U1}} = [m_{kX3}\ m_{kX5} \dots m_{kN}] \begin{bmatrix} k_{x3} \\ k_{x5} \\ \dots \\ k_{xN} \end{bmatrix}$$

The model equations are updated from (5) as

$$\begin{cases} I_{x,WVDM,U1} = I_{x,base,U1} + \Delta I_{x,LIN,U1} + \Delta I_{x,NL} \\ \varphi_{Ix,WVDM,U1} = \varphi_{Ix,Base,U1} + \Delta\varphi_{Ix,LIN,U1} + \Delta\varphi_{Ix,NL} \end{cases} \quad (13)$$

The WVDM model linear part, calculated using (13) will also be upgraded to U_1 sensitive variables.

$$\Delta I_{x,LIN,U1} = \boldsymbol{U_y} \cdot \boldsymbol{G_{x.U1}} \cdot \cos(\boldsymbol{\alpha_x} - \boldsymbol{\varphi_{Uy}}) \quad (14)$$

$$\Delta\varphi_{Ix,LIN,U1} = \boldsymbol{U_y} \cdot \boldsymbol{k_{x,U1}} \cdot \sin(\boldsymbol{\alpha_x} - \boldsymbol{\varphi_{Uy}}) \quad (15)$$

VIII. Verification

Type-A LED lamps (chapter II) are used for analysis in this study. Load harmonic currents are recoded for all the input combinations mentioned in Table I. The accuracy of the models proposed will be analyzed using a similar approach as presented in Chapter III. The harmonic voltage component is rotated through 24 different phase angles. The magnitude of the supply (U_1) is gradually increased (form 207 V (90% of 230 V) to 253 V (110% of 230 V)) to observe the influence of U_1 on current harmonics. Influencers (voltage harmonics) are added to the supply while rotating through 360º (24 steps). For example, added U_3 is rotated through φ_{U3} = {0 … 360º}, while keeping U_1 at a particular level. Current harmonics are modelled using several estimation techniques and compared to measured readings; and root mean square error (*rmse*) is calculated using all 24 point deviations. U_1 sensitivity coefficients are determined as presented above using multiple lamps in Table V.

Comparison is presented using models as below:

1. $I_{h,const,230}$, assuming I_h persistence regardless of U_1 or any added U_y;
2. $I_{h,const,U1}$, assuming I_h relation to U_1 but persistence regardless of any added U_y;
3. *WVDM* (see equation (5))
4. $WVDM_{U1}$ (see equation (13))

Table VI presents the comparison in maximum deviation (δ_{MAX}) and *rmse* of harmonic modeling techniques for one load. The effect of influencing voltage harmonic is explained in [9] so far, but considering U_1 influence in the estimation model leads to more accurate values. $WVDM_{U1}$ shows the least *rmse* values after estimation, regardless of voltage harmonic influencer or current harmonic order.

It has to be noted, that for the non-linear WVDM part, authors plan to provide further information on the calculation, specifically the current magnitude component $\Delta I_{x,NL}$ and the current phase angle component $\Delta\varphi_{Ix,NL}$, in upcoming papers. This is because these calculations require additional analysis and consideration.

IX. Conclusion

The study presented in this paper aimed to evaluate the relationship between current harmonic sensitivity coefficients (α_{xy} G_{xy} k_{xy}) towards U_1 level of supply voltage. Harmonic estimation techniques like constant current source, Norton, and FCM, generally are presented without consideration of the effect of U_1 level in the supply, on current harmonics; however, the grid supply waveform often shows different levels in U_1. This variation in fundamental component has a definite effect on harmonic fingerprints. The $WVDM_{U1}$ approach is introduced in this paper, which take into consideration of U_1 level while modeling current harmonics. *WVDM* estimation approach was presented by authors, where the fundamental level is taken as fixed level (230V). The results of $WVDM_{U1}$ model show considerable improvement in terms of *rmse* and max deviation compared to previously used models. Therefore, the U_1 level should have a role also in the harmonic current models.

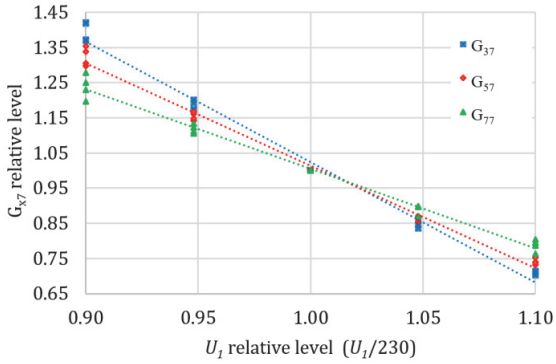

Fig. 9. Relative relation between G_{xy} and fundamental harmonic voltage level.

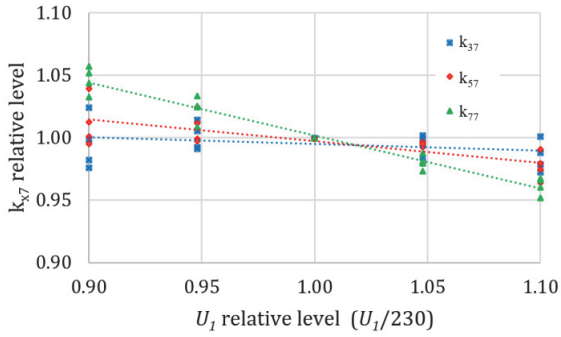

Fig. 10. Relative relation between k_{xy} and fundamental harmonic voltage level.

Acknowledgement

This study was supported by the Estonian Research Council grant PSG-142, "Synthesis of output current waveforms of power electronic converters for increasing the hosting capacity of renewable energy sources in the distribution networks."

TABLE V. DEVIATION COMPARISON OF MODELLED VALEUS FOR DIFFERENT HARMONIC MODELING TECHNIQUES . INFLUENCING U_y LEVEL IS 3 V.

				$\lvert I^*_{x,Base}\rvert$	$\delta\lvert I^*_x\rvert$, mA				$\varphi_{Ix,Base}$	$\delta\varphi_{Ix}$, °			
U_1, V	x	y		, mA	$I_{h,\mathrm{const},230}$	$I_{h,\mathrm{const},U1}$	WVDM	$WVDM_{U1}$	, °	$I_{h,\mathrm{const},230}$	$I_{h,\mathrm{const},U1}$	WVDM	$WVDM_{U1}$
207	3	3	δ_{MAX}	43.4	4.0	0.3	3.8	0.1	-123	12	7	6	<1
218	3	3		41.5	1.9	0.2	1.7	0.2	-125	9	7	3	<1
230	3	3		39.8	0.2	0.2	0.0	0.0	-128	7	7	<1	<1
241	3	3		37.9	2.1	0.2	1.9	0.2	-130	9	6	3	<1
253	3	3		36.3	3.7	0.2	3.6	0.1	-133	11	6	5	<1
207	*3*	*3*	**rmse**		3.7	0.2	3.6	**0.1**		*7*	*5*	*5*	**<1**
218	3	*3*			1.7	0.2	1.7	**0.2**		*5*	*5*	*2*	**<1**
230	3	*3*			0.2	0.2	0.0	**0.0**		*5*	*5*	<1	**<1**
241	3	*3*			1.9	0.1	1.9	**0.2**		*5*	*4*	*2*	**<1**
253	3	*3*			3.5	0.1	3.5	**0.1**		*6*	*4*	*5*	**<1**
207	3	7	δ_{MAX}	43.4	5.3	2.6	4.2	0.3	-123	16	11	5	2
218	3	7		41.5	3.0	2.2	2.0	0.5	-125	13	11	2	2
230	3	7		39.8	1.9	1.9	0.3	0.3	-128	11	11	1	1
241	3	7		37.9	3.5	1.6	2.3	0.4	-130	13	11	4	1
253	3	7		36.3	4.9	1.4	4.1	0.2	-133	15	11	6	<1
207	3	*7*	**rmse**		3.8	1.5	3.5	**0.2**		*9*	*8*	*4*	**2**
218	3	*7*			2.0	1.2	1.6	**0.4**		*8*	*8*	*1*	**2**
230	3	*7*			1.0	1.0	0.2	**0.2**		*8*	*8*	*1*	**1**
241	3	*7*			2.1	0.8	2.0	**0.3**		*8*	*8*	*3*	**<1**
253	3	*7*			3.7	0.7	3.6	**0.1**		*9*	*7*	*6*	**<1**
207	5	5	δ_{MAX}	36.8	4.2	3.5	2.7	0.5	97	26	17	11	1
218	5	5		35.7	2.8	3.0	1.3	0.2	92	21	17	5	1
230	5	5		34.8	2.5	2.5	0.2	0.2	88	16	16	<1	<1
241	5	5		33.6	3.2	2.1	1.6	0.3	83	20	15	5	<1
253	5	5		32.5	4.0	1.7	2.9	0.4	79	23	15	10	1
207	*5*	*5*	**rmse**		2.8	2.0	2.1	**0.3**		*15*	*12*	*9*	**1**
218	*5*	*5*			1.9	1.6	1.0	**0.1**		*12*	*12*	*4*	**1**
230	*5*	*5*			1.4	1.4	0.1	**0.1**		*11*	*11*	<1	**<1**
241	*5*	*5*			1.7	1.1	1.2	**0.2**		*12*	*11*	*5*	**<1**
253	*5*	*5*			2.5	0.9	2.3	**0.3**		*14*	*11*	*9*	**<1**
207	7	5	δ_{MAX}	28.5	5.3	5.4	1.3	1.2	-41	38	25	17	5
218	7	5		28.4	4.6	2.7	0.7	0.7	-48	30	16	8	4
230	7	5		28.3	4.1	4.1	0.2	0.2	-55	23	23	1	1
241	7	5		27.9	3.8	3.5	0.9	0.4	-61	28	22	8	1
253	7	5		27.5	3.7	2.9	1.6	0.8	-67	33	21	15	4
207	*7*	*5*	**rmse**		3.2	3.2	0.9	**0.7**		*22*	*17*	*13*	**5**
218	*7*	*5*			2.7	0.0	0.5	**0.5**		*18*	<1	*6*	**4**
230	*7*	*5*			2.3	2.3	0.1	**0.1**		*16*	*16*	<1	**<1**
241	*7*	*5*			2.0	2.0	0.5	**0.2**		*17*	*15*	*7*	**<1**
253	*7*	*5*			1.9	1.7	1.0	**0.7**		*20*	*15*	*13*	**4**

REFERENCES

[1] I. Santiago, M. A. López-Rodríguez, A. Gil-de-Castro, A. Moreno-Munoz, and J. J. Luna-Rodríguez, "Energy consumption of audiovisual devices in the residential sector: Economic impact of harmonic losses," *Energy*, vol. 60, pp. 292–301, 2013, doi: 10.1016/j.energy.2013.08.018.

[2] L. Kütt, E. Saarijarvi, M. Lehtonen, H. Mõlder, and J. Niitsoo, "Estimating the harmonic distortions in a distribution network supplying EV charging load using practical source data - Case example," *IEEE Power Energy Soc. Gen. Meet.*, vol. 2014-Octob, no. October, pp. 4–8, 2014, doi: 10.1109/PESGM.2014.6939267.

[3] A. J. Collin *et al.*, "Survey of harmonic emission of electrical vehicle chargers in the European market," *2016 Int. Symp. Power Electron. Electr. Drives, Autom. Motion, SPEEDAM 2016*, pp. 1208–1213, 2016, doi: 10.1109/SPEEDAM.2016.7526005.

[4] A. R. Kalair, N. Abas, A. R. Kalair, Z. Saleem, and N. Khan, "Review of harmonic analysis, modeling and mitigation techniques," *Renew. Sustain. Energy Rev.*, vol. 78, no. February, pp. 1152–1187, 2017, doi: 10.1016/j.rser.2017.04.121.

[5] P. W. Lehn and K. L. Lian, "Frequency coupling matrix of a voltage-source converter derived from piecewise linear differential equations," *IEEE Trans. Power Deliv.*, vol. 22, no. 3, pp. 1603–1612, 2007, doi: 10.1109/TPWRD.2006.886779.

[6] M. N. Iqbal, L. Kütt, B. Asad, and N. Shabbir, "Impact of Cable Impedance on the Harmonic Emission of LED Lamps," *21st Int. Sci. Conf. Electr. Power Eng.*, no. December, pp. 1–6, 2020, doi: 10.1109/EPE51172.2020.9269271.

[7] A. J. Collin, J. Drapela, R. Langella, A. Testa, S. Z. Djokic, and N. R. Watson, "Harmonic modelling of LED lamps by means of admittance frequency coupling matrices," *2019 IEEE Milan PowerTech, PowerTech 2019*, pp. 1–6, 2019, doi: 10.1109/PTC.2019.8810803.

[8] S. Z. Djokic and Z. Iqbal, "Non-Fourier Fundamental Components for the Mitigation of Waveform Distortions," *2019 20th Int. Symp. Power Electron. Ee 2019*, pp. 19–24, 2019, doi: 10.1109/PEE.2019.8923243.

[9] K. Daniel, L. Kütt, M. N. Iqbal, N. Shabbir, M. Parker, and M. Jarkovoi, "Waveform Variation Defined Model for Harmonic Current Emissions Including Cross-Order Supply Voltage Harmonics Influence," vol. XX, 2023, doi: 10.1109/ACCESS.2023.3270805.

[10] K. Daniel, L. Kütt, M. N. Iqbal, N. Shabbir, and M. Jarkovoi, "Description of Practical Load Harmonic Current Emission due to Voltage Harmonic Variation," *2021 IEEE 62nd Int. Sci. Conf. Power Electr. Eng. Riga Tech. Univ. RTUCON 2021 - Proc.*, pp. 1–6, 2021, doi: 10.1109/RTUCON53541.2021.9711594.

[11] M. N. Iqbal, L. Kütt, K. Daniel, M. Jarkovoi, B. Asad, and N. Shabbir, "Bivariate stochastic model of current harmonic analysis in the low voltage distribution grid," *Proc. Est. Acad. Sci.*, vol. 70, no. 2, pp. 190–206, 2021, doi: 10.3176/proc.2021.2.08.

[12] M. N. Iqbal, L. Kütt, B. Asad, N. Shabbir, and I. Rasheed, "Time-dependent variations in current harmonic emission by LED lamps in the low-voltage network," *Electr. Eng.*, 2021, doi: 10.1007/s00202-020-01175-4.

[13] D. Gallo, R. Langella, M. Luiso, A. Testa, and N. R. Watson, "A new test procedure to measure power electronic devices' frequency coupling admittance," *IEEE Trans. Instrum. Meas.*, vol. 67, no. 10, pp. 2401–2409, 2018, doi: 10.1109/TIM.2018.2819318.

Publication V

K. Daniel, L. Kütt, M. N. Iqbal, N. Shabbir, M. Jarkovoi and M. Parker, “Load Current Harmonic Model Complexity Reduction through Empirical Pattern Analysis,” *2023 IEEE 17th International Conference on Compatibility, Power Electronics and Power Engineering (CPE-POWERENG)*, Tallinn, Estonia, 2023, pp. 1–6, doi: 10.1109/CPE-POWERENG58103.2023.10227474.

2023 IEEE 17th International Conference on Compatibility, Power Electronics and Power Engineering (CPE-POWERENG) | 979-8-3503-0004-8/23/$31.00 ©2023 IEEE | DOI: 10.1109/CPE-POWERENG58103.2023.10227474

Load Current Harmonic Model Complexity Reduction through Empirical Pattern Analysis

Kamran Daniel
Dept. of Electrical Power Engineering & Mechatronics
Tallinn University of Technology
Tallinn, Estonia
kdanie@taltech.ee

Lauri Kütt
Dept. of Electrical Power Engineering & Mechatronics
Tallinn University of Technology
Tallinn, Estonia
lauri.kutt@taltech.ee

Muhammad Naveed Iqbal
Dept. of Electrical Power Engineering & Mechatronics
Tallinn University of Technology
Tallinn, Estonia
miqbal@taltech.ee

Noman Shabbir
FinEST center for Smart Cities
Tallinn University of Technology
Tallinn, Estonia
noman.shabbir@taltech.ee

Marek Jarkovoi
Dept. of Electrical Power Engineering & Mechatronics
Tallinn University of Technology
Tallinn, Estonia
marek.jarkovoi@taltech.ee

Martin Parker
Dept. of Electrical Power Engineering & Mechatronics
Tallinn University of Technology
Tallinn, Estonia
martin.parker@taltech.ee

***Abstract*— This paper presents an experimental evaluation of coupling coefficients used to describe the harmonic load current dependency on the supply voltage waveform harmonics. This investigation presents an insight to the common behavior of the LED lamps same type circuits. Accounting the cross-order harmonic coupling, assumptions laid out in this paper provide ground to build up less complex models with least measurement to characterize the load. The calculation approach proposed reveals benefits to declare parameters for harmonic coupling modeling of rectifier-based circuits with linear equations. This allows more prominent model parameters' estimations to be done using fewer load-device individual current harmonic sensitivity characterization measurements. This study presented is focusing mainly on specific types of LED lamp structures, expected to have highest share of usage in the field.**

Keywords—Harmonic coupling, harmonic sensitivity, harmonic estimation, power quality.

I. INTRODUCTION

Harmonic load currents of contemporary loads in low voltage distribution networks are affected by supply voltage harmonics. The load current harmonic emissions are inevidable for practically all modern loads due to the conversion units of AC to DC in modern energy-efficient devices [1][2][3]. One of the most frequent AC loads is the modern LED lamp, found in multiples in every household. While low in power, these units can impose significant load current harmonics. Through harmonic voltage drop and impedance characteristics, the high harmonic load current can become a burden for the voltage waveform. Excess load harmonic levels can cause voltage supply instability, with variations of up to ±10% of nominal voltage [4][5][6].

For the calculation of the LED lamp harmonic load currents, available models include current source and Norton models with a constant current source and added impedance. One of the most actively discussed is frequency coupled admittance matrix (FCM) [7][8][9]. The latter can account for cumulative voltage harmonic effects, relying on a constant current source with added harmonic voltage-influenced current component. The authors of this paper recently proposed a time-domain waveform-originated load current response model [10]. While more complex in their expression, these models aim to tackle the multivariate input and influence challenges, revealed by systematic testing.

In this paper, a more common "type A" LED lamp [11][12] circuits' operation and harmonic load response is observed. Internal block diagram of such type, commercially available LED lamps is presented in Fig. 1. An inrush limiting resistor R_{INR}, rectifier circuit, bulk capacitor (C_B), DC-DC converter unit (U_{CONV}) and LEDs [13][14][15][16] make up most common circuits.

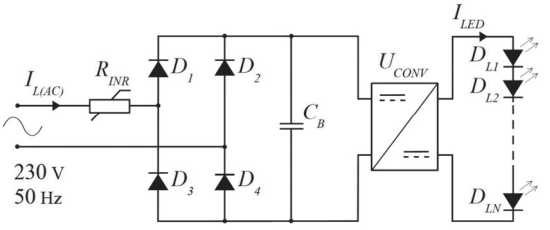

Fig. 1. Internal block diagram of a typical type A LED lamp.

Better-performing LED lamp load current models are able to include the AC load current variations due to voltage harmonics included in the AC supply voltage waveforms. Observing the load harmonic currents as vectors, it is revealed in testing that the actual response to voltage harmonics is laid out by a ellipse-like pattern around the base harmonic vector centre point ($I_{X,Base}$). Research suggests that power electronic loads like energy-efficient LEDs show an elliptic response pattern to voltage harmonics, described by different impedance-based models[17]. The WVDM model categorizes similar magnitude and phase variations based on physical operating principles [10]. WVDM aims to evaluate phase and magnitude variations using a three-part model proposed in [10], initially based on 230 V measurements. Still, the number of variables to be used for full modelling is rather high, therefore requiring high measurement effort. The quantification efficiency is more critical, as it has been revealed that U_1 level will also have a significant effect to the real LED current outcome [18]. Figure 1 illustrates the elliptical response pattern of a load current harmonic component in response to the injection of the supply voltage harmonic component, for different levels of fundamental component level (U_1 level).

In this paper measurement results are analyzed and it will be revealed that there are clear and firm patterns, representing the sensitivity of the load current harmonics to the supply voltage harmonics. All measurements are taken using the

measurement setup and measurement conditions described in [10]. Analysis and input to the variables' modeling will be described. While presented according to the WVDM model quantification approach, similar considerations can be implemented for the FCM models variable definitions.

II. Response Characterization of LED Lamps Towards Supply Voltage Harmonics

A distorted supply voltage can be characterized by a content of harmonic voltage components, having a defined order y (i.e frequency of *y* times main harmonic frequency, e.g 50 Hz), magnitude and phase angle towards the main harmonic zero phase angle.

If a LED lamp with AC frontend description as in Fig. 1 is supplied with the distorted AC voltage, it will draw current with a slightly different load current waveform compared to when it is supplied with undistorted AC voltage. The LED load current waveform non-sinusoidality means that the LED load has a high portion of harmonics included. Waveform variation in turn refers that the harmonic components go through a variation. Latter is evident by variation of a current harmonic components' magnitude and phase value variations.

Figure 2 presents a result plot of load current vectors, where each point displayed is presents a vector endpoint, if subjected to different supply voltage conditions. The elliptic patterns reflect the response to supply voltage harmonic, if this is included with identical magnitude, however different phase angle.

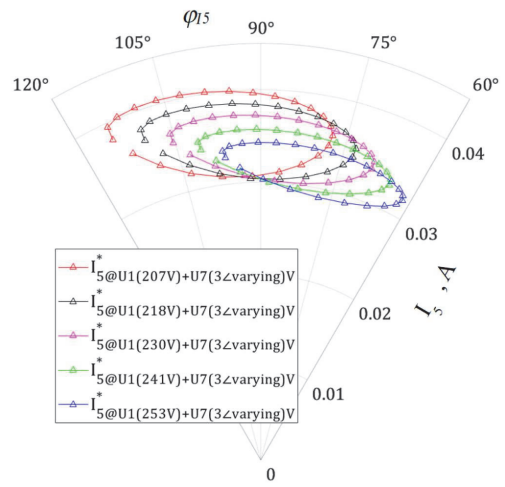

Fig. 2. Example of 5th harmonic response (shifted to identical basepoint phase angle position) for supply voltage U_1 (varying) + added U_7 (3 V).

The characterization of the load current response is thus presented in a geometrical viewpoint. Fig. 3 provides the details on the elements of the analysis of the current harmonic vectorial variation. The base vector $I^*_{7,Base,}$ is the load current harmonic component vector, emerging upon non-distorted supply voltage conditions. Deviation of the actual load vector, upon distorted supply voltage component is described by a deviation vector dI^*_7. Another option is to present the deviation as a polar coordinate variation, as deviation of magnitude and phase quantities. These response deviation quantities are the targets of modeling to calculate the accurate harmonic load response.

III. Magnitude and Phase Variation Coefficients

In the following, the phase and magnitude variation components are approached in polar component analysis. Measurement outcome of the load currents upon supply voltage distortion variation reveals the load current magnitude and phase response extreme point characterization is rather well described through linear proportion

$$dI_{x,MAX} = k_{IM} \cdot U_y \tag{1}$$

$$d\varphi_{x,y,MAX} = k_{\varphi} \cdot U_y, \tag{2}$$

Where k_φ is the coefficient of the phase response (units °/V, or rad/V), and k_{IM} (units A/V) is the response coefficient of the magnitude response. In more general view, these coefficients are elaborated into supply voltage influencing voltage harmonic U_y proportional coefficient G_{xy} calculated as

$$G_{xy} = \frac{dI_{x,MAX}}{U_y}, \tag{3}$$

and supply voltage influencing voltage harmonic U_y proportional coefficient k_{xy} can be calculated as

$$k_{xy} = \frac{d\varphi_{x,y,MAX}}{U_y} \tag{4}$$

Such coefficients are used, for example, by the waveform variation defined model [10] to calculate the load harmonic exact values for distorted supply conditions. It has to be pointed out that each of these coefficients are harmonic order specific and include cross-order harmonic influences. For the complete modeling set, the coefficients $\boldsymbol{G_x}$ and $\boldsymbol{k_x}$ would emerge as matrixes [10] as presented below

$$\boldsymbol{G_x} = \begin{bmatrix} G_{x3} \\ G_{x5} \\ \dots \\ G_{xN} \end{bmatrix}, \qquad \boldsymbol{k_x} = \begin{bmatrix} k_{x3} \\ k_{x5} \\ \dots \\ k_{xN} \end{bmatrix}$$

Table II represents the values of these modelling coefficients for voltage harmonic influencers. Determining all these coefficient values requires a large experimental result set; this invokes the need to develop a method to reduce the measurement effort.

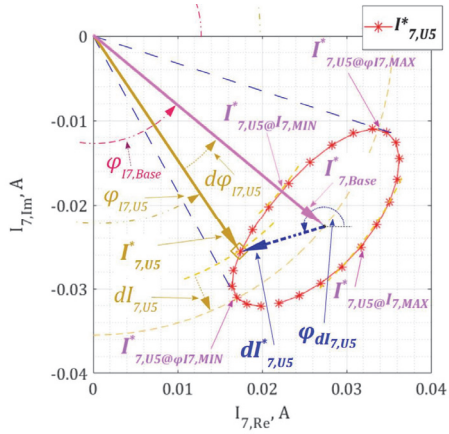

Fig. 3. Vector component plot for the harmonic load current component analysis. $\boldsymbol{I^*_7}$ vector endpoints' ellipse points plot, for $U_5 = 3$ V, $\boldsymbol{\varphi}_{U5} = 0, 15, 30 \dots 345°$.

IV. MAGNITUDE COEFFICIENT TREND MODELS

Next effort will be provided to the coefficients G_{xy} and k_{xy} mathematical descriptions. This is done in order for the coefficients to be calculated from relatively small data without going through larger set of measurements. The model is developed based on the likely input data set of supply voltage and load current. Input to the model will consist of supply voltage harmonic component data, including the harmonic component order y, scalar voltage level U_y and voltage component phase angle φ_{Uy}.

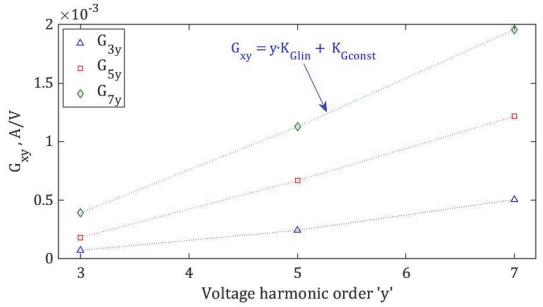

Fig. 4. Magnitude variation coefficient patterns for WVDM against influenecr voltage order *y*.

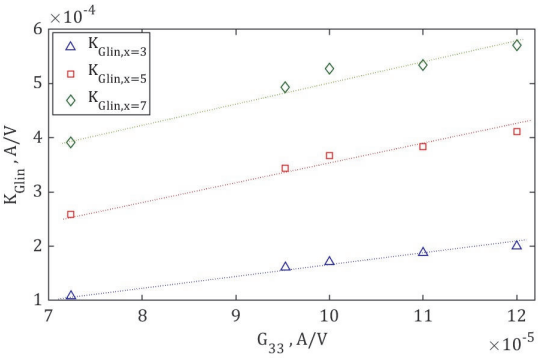

Fig. 5. Linear variable K_{Glin} relation to G_{33} measured values.

TABLE I
MODEL LINEAR COEFFICIENT AND CONSTANT-COEFFICIENT PARAMETERS OF TEST LOADS
current harmonic order '*x*'

	load 1		load 2		load 3		load 4		load 5	
x	K_{Glin}	K_{Gconst}	K_{Glin}	K_{Gconst}	K_{Glin}	K_{Gconst}	K_{Glin}	K_{Gconst}	K_{Glin}	K_{Gconst}
7	39.1	79.7	57.1	95.7	49.3	88.3	52.7	96.4	53.4	89.5
5	25.9	60.5	41.1	80.5	34.4	71.7	36.7	78.5	38.4	75.6
3	10.8	26.8	20	48.4	16.1	39.6	17.1	42.3	18.8	45.7

*all coefficient values are multiplied by 10^5 to enhance readability

The relationship between influencer order '*y*' and G_{xy} value can be seen in Fig 4. As a first-order equation (see Fig. 4) provides a good match with a linear portion (K_{Glin}) and constant portion (K_{Gconst}), written as

$$G_{xy} = K_{Glin} \cdot y + K_{Gconst} \quad (5).$$

Table I shows linear coefficient (K_{Glin}) and constant coefficient (K_{Gconst}) values extracted for the 5 test loads considered in this paper. In relation towards the measurement-based quantities, the K_{Glin} values are revealed to pose a linear relation to G_{33} value, as shown in Fig 5. A good correlation to K_{Glin} can be specified as

$$K_{Glin} = 0.84 \cdot G_{33} \cdot (x - 1) \quad (6)$$

For example, in the case of I_7 , $K_{Glin} = 5.07G_{33}$; for the fifth and third order, slop values to find linear coefficient value are 3.55 and 1.66, respectively (see Fig 5).

The constant coefficient K_{Gconst} can also be traced to the relation between current harmonic order *x* and G_{33}. The following equation can be specified for a constructing K_{Gconst} coefficient of (5)

$$K_{Gconst} = 4 \cdot G_{33} + \left(\frac{-2(x-3)^2+20(x-3)+1}{100000}\right) \quad (7)$$

Thus, by implementing K_{Glin} and K_{Gconst} values obtained in analysis, only G_{33} would be necessary as a load-specific parameter, and can be used to find other magnitude variation coefficients G_{xy} corresponding to any current and voltage harmonic order. This applies to basically all lamps in the test set considered. It has to be pointed out that this is only valid for similar type LED lamps. In essence, such coefficient calculation options provide a significant shortcut compared to measurements to extract the respective G_{xy} coefficients in the matrixes specified.

TABLE II
MODEL PARAMETERS OF TEST LOADS
harmonic voltage order '*y*'

Load		G_{3y}, mA/V		G_{5y}, mA/V		G_{7y}, mA/V		k_{3y}, °/V		k_{5y}, °/V		k_{7y}, °/V	
	y	*Measured*	*Calculated*	*Measured*	*Calculated*	*Measured*	*Calculated*	*Measured*	*Calculated*	*Measured*	*Calculated*	*Measured*	*Calculated*
1	3	0.07	0.07	0.18	0.11	0.39	0.32	2.16	2.12	3.60	3.54	5.08	4.95
	5	0.24	0.31	0.67	0.60	1.13	1.05	3.16	3.00	5.31	5.00	7.54	7.00
	7	0.51	0.55	1.22	1.08	1.96	1.78	3.63	3.67	6.17	6.12	8.91	8.57
2	3	0.12	0.12	0.42	0.40	0.75	0.85	2.12	2.12	3.56	3.54	5.10	4.95
	5	0.51	0.52	1.27	1.21	1.91	2.06	2.95	3.00	5.01	5.00	7.26	7.00
	7	0.92	0.92	2.0	2.0	3.03	3.27	3.11	3.67	5.39	6.12	8.08	8.57
3	3	0.1	0.09	0.31	0.25	0.6	0.57	2.13	2.12	3.57	3.54	5.07	4.95
	5	0.39	0.41	1.01	0.89	1.58	1.53	2.99	3.00	5.08	5.00	7.29	7.00
	7	0.74	0.73	1.69	1.53	2.57	2.49	3.25	3.67	5.59	6.12	8.26	8.57
4	3	0.1	0.09	0.32	0.28	0.62	0.62	2.15	2.12	3.60	3.54	5.11	4.95
	5	0.41	0.43	1.05	0.95	1.66	1.63	3.08	3.00	5.28	5.00	7.48	7.00
	7	0.78	0.77	1.79	1.62	2.73	2.64	3.39	3.67	5.79	6.12	8.51	8.57
5	3	0.11	0.10	0.39	0.34	0.7	0.73	2.12	2.12	3.57	3.54	5.10	4.95
	5	0.48	0.47	1.18	1.08	1.79	1.84	2.95	3.00	5.02	5.00	7.27	7.00
	7	0.86	0.84	1.93	1.82	2.83	2.95	3.12	3.67	5.39	6.12	8.07	8.57

V. PHASE VARIATION COEFFICIENT MODELS

Phase variation coefficient k_{xy} is response for the WVDM modelled values spread on the complex plane. Form the measured values of k_{xy} (present in Table II), a constant ratio emerges between phase variation coefficient, current harmonic order x and voltage harmonic order y, present by the following equation

$$k\_ratio = \frac{k_{xy}}{x\sqrt{y}} \tag{8}$$

Furthermore, while developing the solid relationship for k_{xy}, another coefficient is defined as

$$C_k = \frac{x}{\sqrt{2}} \tag{9}$$

C_k is consistant part of calculated k_{xy} ($k_{xy,calc}$). Table III shows the equations used to determine the phase variation coefficient values, which can be further used to model harmonic current for any influencer order.

TABLE III
RELATION BETWEEN PHASE VARIATION COEFFICIENT, CURRENT AND VOLTAGE HARMONIC ORDER

y	x	$k_{xy,calc}$
3	3 5 7	$\frac{x}{\sqrt{2}}$
5	3 5 7	$\frac{x(x-1)}{2}$
7	3 5 7	$\frac{x\sqrt{3}}{\sqrt{2}}$

VI. VALIDATION

Validation of the proposed G_{xy} and k_{xy} calculation models will be based on the measurement result comparison. In the first step, the accuracy of the G_{xy} and k_{xy} proposed models is evaluated based on the comparison of measurement-originated coefficient values. The measurement specifics have been presented in [10] whereby the coefficient values are extracted from direct results as

$$G_{xy,meas} = \frac{\frac{\left(\left|dI_{x,Uy@Ix,MIN}\right| - \left|dI_{x,Uy@Ix,MAX}\right|\right)}{2}}{U_y} \tag{10}$$

$$k_{xy,meas} = \frac{d\varphi Ix,Uy@\varphi Ix,MAX}{U_y} \tag{11}$$

where $dI_{x,Uy@Ix,MIN}$ is the minimum and $dI_{x,Uy@Ix,MAX}$ maximum measured magnitude deviation from the base vector $I_{x,BASE}$ magnitude value; $d\varphi_{Ix,Uy@\varphi Ix,MAX}$ is the maximum phase deviation from the base vector $I_{x,BASE}$ phase value. Proposed G_{xy} and K_{xy} calculation values are obtained using (5) and relations provided in Table III, respectively. The statistical dispersion is presented as

$$\delta G_{xy,AVG} = average\left\{\left|G_{xy,meas}\right| - \left|G_{xy,calc}\right|\right\} \tag{12}$$

$$\delta k_{xy,AVG} = average\left\{\left|k_{xy,meas}\right| - \left|k_{xy,calc}\right|\right\} \tag{13}$$

where the average is calculated based on difference margin of all 5 loads tested. General show there is no considerable difference between both estimated values in most cases, however, some harmonic order combination coefficients show up to 20% deviation. In order to specify the significance of the difference found, the next validation step is looking into using the calculated G_{xy} and K_{xy} values in total load current deviation calculations.

The load current deviation evaluation, using load models with coefficients calculated according to the scheme proposed is more critical point as this is related to the total harmonic current output estimation. Here for total load current estimation, accounting the voltage harmonic components effects, the WVDM model [10] is used. The total load current deviation is calculated via

$$\begin{cases} dI_{x,WVDM} = \Delta I_{x,LIN} + \Delta I_{x,NL} \\ d\varphi_{Ix,WVDM} = \Delta\varphi_{Ix,LIN} + \Delta\varphi_{Ix,NL} \end{cases} \tag{14}$$

where $d_{Ix,WVDM}$ and $d\varphi_{Ix,WVDM}$ is the deviation from the base load current component $I_{x,Base}$, and phase $\varphi_{Ix,Base}$; with the linear parts $\Delta I_{x,LIN}$ and $\Delta\varphi_{Ix,LIN}$ found as

$$\Delta I_{x,LIN} = \boldsymbol{U_y} \cdot \boldsymbol{G_x} \cdot \cos(\boldsymbol{\alpha_x} - \boldsymbol{\varphi_{Uy}}) \tag{15}$$

$$\Delta\varphi_{Ix,LIN} = \boldsymbol{U_y} \cdot \boldsymbol{k_x} \cdot \sin(\boldsymbol{\alpha_x} - \boldsymbol{\varphi_{Uy}}) \tag{16}$$

where α_x is a load-specific phase offset quantity, φ_{Uy} is the phase angle of the voltage harmonic component U_y of order y. Details for the nonlinear part ($\Delta I_{x,NL}$ and $\Delta\varphi_{Ix,NL}$) is described in [10]; the particular calculation of the nonlinear parts will be presented in further upcoming papers by the authors, as this would need extended consideration.

For the measurement-result based quantities, WVDM model coefficients G_{xy} and k_{xy} are obtained through (10) and (11), while the WVDM results with proposed model to calculate coefficients G_{xy} and k_{xy} are provided for comparsion. In order to present the highest differences, the deviation maximum values $dI_{x,MAX}$ are compared.

Magnitude variation coefficients determined by (5), for all tested loads, are presented in Table II. Table IV shows the deviation from the measured value of G_{xy} (See Table II). Similarly, calculated phase variation coefficients (determined using variables established in Table III) are presented in Table II. Table IV also shows the deviation in measured and modelled values of k_{xy} (See Table II). The results in Table V present deviation between measurement and load current calculation result with WVDM-based values.

- $WVDM_{Gk,mea}$ uses G_{xy} and k_{xy} coefficients that are determined directly from measurements, and
- $WVDM_{Gk,calc}$ uses G_{xy} and k_{xy} variation coefficients calculated using (5) and relations provided in Table III.

TABLE IV
AVERAGE DEVIATION OF MODELLED VARIATION COEFFICIENTS

		$\delta G_{xy,AVG}$			$\delta k_{xy,AVG}$		
y	**x**	3	5	7	3	5	7
3		6%	18%	9%	1%	1%	3%
5		8%	9%	5%	2%	2%	5%
7		3%	7%	6%	12%	9%	4%

VII. CONCLUSION

It has been established, that the supply voltage harmonics have direct and significant influence on the LED lamps' load current harmonic patterns. In order to properly evaluate the performance and behavior of electrical loads, models with cross-harmonic order impact of supply voltage harmonics on load current are crucial. For describing the latter, coupling coefficients are often used in modelling to quantify the

strength of the voltage-current interaction. In literature, FCM is a well-known approach, similarly WVDM uses calculation with multiple coefficients to describe this interaction. However, either of these estimation techniques require high number of coefficients. In FCM, with the increase in influencer voltage harmonics orders accounted, admittance coefficients in the admittance matrix are increased in multiples. Similarly, in WVDM, coupling/sensitivity coefficients determination requires thorough measurement. Previously, these coefficients have not been shown to emerge in a systematic manner.

In this paper, the simplification of the coupling coefficient calculation has been proposed, relying on the empirical patterns extracted through measurements. It was shown that the relations are usable with fair linear properties. If using the coupling coefficient calculation proposals, the total deviation of the model output is expected to remain less than 10%. This is usually acceptable, as there is dispersion associated with any practical load current harmonic estimation models. Combining the WVDM models with the presented coefficient calculation trends, can significantly reduce the load-characterizing modelling and measurement burden. If the deviations are acceptable, only G_{33} is needed to be established for any load in similar class (Type-A LED) via measurements. This eases the complexity of the models by a huge margin.

The LED lamps discussed here are of one of the simplest circuit types on market; however, their share in lamps used is the highest. More complex loads featuring higher component count and load current waveform correction, can have different waveforms and thus the coefficient estimation and calculation is likely different.

ACKNOWLEDGEMENT

This study was financed by the Doctoral School of Energy and Geotechnology - III, supported by the European Union, European Regional Development Fund (Tallinn University of Technology's ASTRA "TTÜ arenguprogramm aastateks 2016-2022") and Estonian Research Council grant PSG-142, "Synthesis of output current waveforms of power electronic converters for increasing the hosting capacity of renewable energy sources in the distribution networks."

TABLE V
COMPARISON OF MODELLED AND MEASURED VALUES

			x	***3***				***5***				***7***			
y, (U_y=3V)	***Load***		dI_{max}, mA	$d\varphi_{max}$, °	$\delta(dI_{max})$, mA	$\delta(d\varphi_{max})$, °	dI_{max}, mA	$d\varphi_{max}$, °	$\delta(dI_{max})$, mA	$\delta(d\varphi_{max})$, °	dI_{max}, mA	$d\varphi_{max}$, °	$\delta(dI_{max})$, mA	$\delta(d\varphi_{max})$, °
3	***1***	*Measurement*	0.22	6.5			0.54	10.8			1.18	15.2		
		$WVDM_{Gk,mea}$	0.21	6.6	0.01	<1	0.53	11.0	0.01	<1	1.16	15.5	0.01	<1
		$\boldsymbol{WVDM_{Gk,calc}}$	0.21	6.7	0.01	<1	0.74	11.2	0.20	<1	1.39	15.9	0.22	<1
	2	*Measurement*	0.36	6.3			1.25	10.7			2.24	15.3		
		WVDM	0.36	6.5	0.00	<1	1.23	10.9	0.01	<1	2.24	15.5	0.00	<1
		$\boldsymbol{WVDM_{Gk,calc}}$	0.36	6.5	0.00	<1	1.27	10.9	0.02	<1	1.92	16.0	0.32	<1
	3	*Measurement*	0.29	6.4			0.94	10.7			1.79	15.2		
		$WVDM_{Gk,mea}$	0.28	6.5	0.00	<1	0.93	10.9	0.01	<1	1.79	15.4	0.00	<1
		$\boldsymbol{WVDM_{Gk,calc}}$	0.28	6.5	0.00	<1	1.11	11.0	0.17	<1	1.85	15.8	0.06	<1
	4	*Measurement*	0.30	6.4			0.95	10.8			1.86	15.3		
		$WVDM_{Gk,mea}$	0.30	6.5	0.00	<1	0.95	10.9	0.01	<1	1.85	15.4	0.00	<1
		$\boldsymbol{WVDM_{Gk,calc}}$	0.30	6.6	0.00	<1	1.05	11.1	0.10	<1	1.85	15.9	0.01	<1
	5	*Measurement*	0.33	6.3			1.16	10.7			2.09	15.3		
		$WVDM_{Gk,mea}$	0.33	6.5	0.00	<1	1.15	10.8	0.01	<1	2.09	15.4	0.01	<1
		$\boldsymbol{WVDM_{Gk,calc}}$	0.33	6.5	0.00	<1	1.29	10.9	0.13	<1	1.97	15.9	0.12	<1
7	***1***	*Measurement*	1.49	10.9			3.61	18.4			5.87	26.7		
		$WVDM_{Gk,mea}$	1.54	11.5	0.05	<1	3.71	19.4	0.10	0.9	5.93	28.5	0.07	1.8
		$\boldsymbol{WVDM_{Gk,calc}}$	1.44	11.4	0.05	<1	4.00	19.4	0.39	1.0	6.37	28.8	0.51	2.0
	2	*Measurement*	2.76	9.4			6.19	16.2			9.13	24.2		
		$WVDM_{Gk,mea}$	2.84	9.7	0.07	<1	6.34	16.3	0.16	<1	9.23	24.3	0.11	<1
		$\boldsymbol{WVDM_{Gk,calc}}$	2.83	8.1	0.06	1.3	6.45	14.2	0.26	2.0	8.61	22.8	0.52	1.4
	3	*Measurement*	2.21	9.8			5.08	16.8			7.70	24.8		
		$WVDM_{Gk,mea}$	2.27	10.2	0.06	<1	5.21	17.2	0.13	0.4	7.76	26.2	0.06	1.4
		$\boldsymbol{WVDM_{Gk,calc}}$	2.29	9.0	0.08	<1	5.62	15.7	0.54	1.1	7.97	26.1	0.27	1.3
	4	*Measurement*	2.34	10.2			5.36	17.4			8.18	25.5		
		$WVDM_{Gk,mea}$	2.41	10.5	0.07	<1	5.52	17.7	0.15	<1	8.26	25.9	0.07	<1
		$\boldsymbol{WVDM_{Gk,calc}}$	2.43	9.7	0.09	<1	5.94	16.7	0.58	0.7	8.49	25.7	0.31	<1
	5	*Measurement*	2.58	9.4			5.79	16.2			8.52	24.1		
		$WVDM_{Gk,mea}$	2.65	9.7	0.07	<1	5.93	16.3	0.15	<1	8.63	24.1	0.11	<1
		$\boldsymbol{WVDM_{Gk,calc}}$	2.69	8.0	0.11	1.3	6.21	14.1	0.42	2.0	8.33	22.6	0.19	1.5

REFERENCES

[1] M. N. Iqbal, L. Kütt, B. Asad, T. Vaimann, A. Rassõlkin, and G. L. Demidova, "Time dependency of current harmonics for switch-mode power supplies," *Appl. Sci.*, vol. 10, no. 21, pp. 1–12, 2020, doi: 10.3390/app10217806.

[2] M. N. Iqbal *et al.*, "Estimation of harmonic emission of electric vehicles and their impact on low voltage residential network," *Sustain.*, vol. 13, no. 15, pp. 1–17, Aug. 2021, doi: 10.3390/su13158551.

[3] L. Kütt, E. Saarijarvi, M. Lehtonen, H. Mõlder, and J. Niitsoo, "Estimating the harmonic distortions in a distribution network supplying EV charging load using practical source data - Case example," *IEEE Power Energy Soc. Gen. Meet.*, vol. 2014-Octob,

no. October, pp. 4–8, 2014, doi: 10.1109/PESGM.2014.6939267.

[4] B. Mitra, A. Singhal, S. Kundu, and J. P. Ogle, “Analyzing Distribution Transformer Degradation with Increased Power Electronic Loads,” *2023 IEEE Power Energy Soc. Innov. Smart Grid Technol. Conf. ISGT 2023*, no. ii, 2023, doi: 10.1109/ISGT51731.2023.10066387.

[5] S. Galla and A. Szewczyk, “The measurement of input power of power supply in network disturbed by low frequency distortions,” *Prz. Elektrotechniczny*, vol. 92, no. 11, pp. 27–30, 2016, doi: 10.15199/48.2016.11.07.

[6] K. O’Connell, M. Barrett, J. Blackledge, and A. Sung, “Cable heating effects due to harmonic distortion in electrical installations,” *Lect. Notes Eng. Comput. Sci.*, vol. 2198, no. July, pp. 928–933, 2012.

[7] J. Yadav, K. Vasudevan, J. Meyer, and D. Kumar, “Frequency Coupling Matrix Model of a Three-Phase Variable Frequency Drive,” *IEEE Trans. Ind. Appl.*, vol. 58, no. 3, pp. 3652–3663, 2022, doi: 10.1109/TIA.2022.3156104.

[8] A. J. Collin, J. Drapela, R. Langella, A. Testa, S. Z. Djokic, and N. R. Watson, “Harmonic modelling of LED lamps by means of admittance frequency coupling matrices,” *2019 IEEE Milan PowerTech, PowerTech 2019*, pp. 1–6, 2019, doi: 10.1109/PTC.2019.8810803.

[9] R. Langella *et al.*, “On the use of fourier descriptors for the assessment of frequency coupling matrices of power electronic devices,” *Proc. Int. Conf. Harmon. Qual. Power, ICHQP*, vol. 2018-May, pp. 1–6, 2018, doi: 10.1109/ICHQP.2018.8378908.

[10] K. Daniel, L. Kütt, M. N. Iqbal, N. Shabbir, M. Parker, and M. Jarkovoi, “Waveform Variation Defined Model for Harmonic Current Emissions Including Cross-Order Supply Voltage Harmonics Influence,” *IEEE Access*, vol. 11, no. March, pp. 42276–42289, 2023, doi: 10.1109/ACCESS.2023.3270805.

[11] X. Xu, A. Collin, S. Z. Djokic, R. Langella, A. Testa, and J. Drapela, “Experimental evaluation and classification of LED lamps for typical residential applications,” *2017 IEEE PES Innov. Smart Grid Technol. Conf. Eur. ISGT-Europe 2017 - Proc.*, vol. 2018-Janua, pp. 1–6, 2017, doi: 10.1109/ISGTEurope.2017.8260292.

[12] M. N. Iqbal, L. Kutt, N. Shabbir, and B. Asad, “Comparison of Current Harmonic Emission by Different Lighting Technologies,” *2020 IEEE 61st Annu. Int. Sci. Conf. Power Electr. Eng. Riga Tech. Univ. RTUCON 2020 - Proc.*, pp. 1–5, 2020, doi: 10.1109/RTUCON51174.2020.9316615.

[13] R. M. Abdalaal, C. Ngai, and M. Ho, “Characterization of Commercial LED Lamps for Power Quality Studies Caractérisation des lampes commerciales à diodes électroluminescentes DEL pour une étude qualitative de l’énergie électrique,” *IEEE Can. J. Electr. Comput. Eng.*, vol. 44, no. 2, p. 2021, 2021, doi: 10.1109/ICJECE.2019.2951031.

[14] Y. Tang *et al.*, “Research on load characteristics of energy-saving lamp and LED lamp,” *2016 IEEE Int. Conf. Power Syst. Technol. POWERCON 2016*, no. 51377046, 2016, doi: 10.1109/POWERCON.2016.7753932.

[15] J. T. Hwang, K. Cho, D. Kim, M. Jung, G. Cho, and S. Yang, “A simple LED lamp driver IC with intelligent power-factor correction,” *Dig. Tech. Pap. - IEEE Int. Solid-State Circuits Conf.*, pp. 236–237, 2011, doi: 10.1109/ISSCC.2011.5746299.

[16] L. Yu and J. Yang, “The topologies of white LED lamps’ power drivers,” *2009 3rd Int. Conf. Power Electron. Syst. Appl. PESA 2009*, 2009.

[17] K. Daniel, L. Kütt, M. N. Iqbal, N. Shabbir, and M. Jarkovoi, “Description of Practical Load Harmonic Current Emission due to Voltage Harmonic Variation,” *2021 IEEE 62nd Int. Sci. Conf. Power Electr. Eng. Riga Tech. Univ. RTUCON 2021 - Proc.*, pp. 1–6, 2021, doi: 10.1109/RTUCON53541.2021.9711594.

[18] K. Daniel, L. Kütt, M. N. Iqbal, N. Shabbir, M. Jarkovoi, and M. Parker, “Voltage Main Harmonic Level Influence on Harmonic Current Emission Modeling,” no. 1, pp. 1–6.

Publication VI

K. Daniel, L. Kütt, M. N. Iqbal, N. Shabbir and M. Jarkovoi, “Estimation of Peak Voltage value and Its Occurrence Timing upon Non-Sinusoidal Supply Voltage,” *2024 IEEE 18th International Conference on Compatibility, Power Electronics and Power Engineering (CPE-POWERENG)*, Gdynia, Poland, 2024, pp. 1–6.

Estimation of peak voltage value and its occurrence timing upon non-sinusoidal supply voltage

Kamran Daniel
Dept. of Electrical Power Engineering & Mechatronics
Tallinn University of Technology
Tallinn, Estonia
kamran.daniel@taltech.ee

Lauri Kütt
Dept. of Electrical Power Engineering & Mechatronics
Tallinn University of Technology
Tallinn, Estonia
lauri.kutt@taltech.ee

Muhammad Naveed Iqbal
Department of Engineering, School of Digital Technology, Innovation & Business
Staffordshire University
Stoke-on-Trent, United Kingdom
naveed.iqbal@staffs.ac.uk

Noman Shabbir
FinEST center for Smart Cities
Tallinn University of Technology
Tallinn, Estonia
noman.shabbir@taltech.ee

Marek Jarkovoi
Dept. of Electrical Power Engineering & Mechatronics
Tallinn University of Technology
Tallinn, Estonia
marek.jarkovoi@taltech.ee

***Abstract*—This paper presents a base for analytical expression development related to physical operation of the components in rectifier circuits. The relations are to be employed for explaining the dependency of harmonic load current on the harmonics of the supply voltage waveform. This study offers insights into the typical behaviour of circuits featuring single phase power electronic AC/DC converters, for example, LED lamps. By considering harmonic phase angle coupling, the assumptions presented can further be used to construct more effective and accurate models for load harmonic currents characterization. Proposed calculation approach defines the peak voltage values present for the bulk capacitor used along with rectifier, also peak timing respective to the main harmonic waveform presentation.**

Keywords—Harmonic analysis, power quality, voltage peak estimation

I. INTRODUCTION

In electrical supply systems, the presence of harmonics can lead to peak voltage values[1]. To gain a comprehensive understanding of this phenomenon, it is essential to first comprehend harmonics and their impact on voltage waveforms [2][3]. Typically, non-linear loads such as computers, variable speed drives, and other electronic devices that consume non-sinusoidal current from the power source, are responsible for generating harmonics [4][5]. These loads are capable of distorting the current waveforms they draw from the power source, which can result in peak voltage distortion [6]. Peak voltage distortion occurs when voltage waveform peaks exceed the ideal sinusoidal waveform due to the harmonic currents generated by non-linear loads [7].

Harmonic currents flow through the impedance of the power distribution system, which can cause voltage distortion, leading to higher peak voltage values. This can adversely affect the power system and equipment, resulting in increased insulation stress, equipment overheating, decreased power quality, and inefficient energy consumption[8]. Understanding and mitigating the effects of harmonics is crucial in maintaining electrical distribution network reliability and efficiency [9]. Supply voltage waveform can be represented as

$$u_{LVAC}(t) = u_1(t) + u_2(t) + u_3(t) + \cdots + u_n(t) \quad (1)$$

Ideally, series (1) contains all harmonics however usually, odd harmonics have a much more dominant role in the waveshape. Majority of the energy efficient devices commercially available contains rectifier circuitry. Figure 1 shows the rectifier circuit commonly present in energy-efficient LED lamps. Rectification operation is dependent on supply voltage waveform shape; When rectified voltage appearing on capacitor terminal reaches its peak value, the current conduction stops[10][11][12]. The end-of-conduction time varies depending upon the peak value instant of the voltage waveform[13][14]. The effect of different supply voltage harmonics, on the operation of rectifier circuits are analysed empirically in [15]–[17]. Most of the typical current waveshape of a common LED lamp is shown in Figure 2, which indicates the conduction starting and ending time.

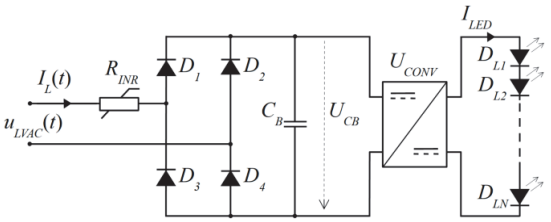

Fig. 1. Rectifier circuit in LED lamp[18]

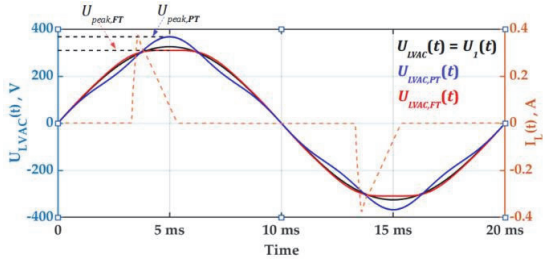

Fig. 2. Supply voltage (pure-sine Flat-top(FT) & pointed-top(PT) waveforms and Current waveform of LED lamp.

The time of peak (t_{peak})value in voltage waveform is dependent on the amplitude and phase angle of the voltage harmonic present[19], [20]; this t_{peak} is end-of-conduction moment of the current of rectifier[21]. This mean harmonic presents in the load current also dependent on the resultant delay in the resultant peak voltage; [22] presents performance comparison of different models for non-sinusoidal supply. In pure sinusoidal signal, peak is supposed to occur at 90 degrees; but with voltage harmonic present in the supply, the resultant peak does not occur at 90 degrees.

The amount and type of the load connected to network changes continuously, so the voltage at point of common connection (PCC); the supply voltage may contain multiple harmonics with various magnitude and phase angles. Figure 3 shows the resultant flat and pointed top waveforms that are usually available as supply voltage in the LV network. In both

cases, the peak voltage available for the rectifier's capacitor charging operation will differ. Also, process itself and end of the rectifier conduction instant will vary.

In this paper analytical approach has been defined that would provide a more detailed and general expression on the formulation of the rectifier circuit operation. Target of the expressions derivation is to provide analytical format to the peak voltage timing (related to rectifier diode conduction cut-off) and peak voltage level (related to the bulk capacitor voltage level at conduction cut-off). Discussion presented aims to provide base for the AC load current harmonic model development for rectifier circuit based load devices taking into account supply voltage harmonics presence.

II. VOLTAGE WAVEFORM NUMERICAL ANALYSIS

In discussing the influence of harmonics on peak voltage, it is essential to consider the role of the phase angle of harmonic voltage in altering the supply waveform. A significant factor in this alteration is the expected shift in peak value moments ($\Delta\varphi_{peak}$) associated with the phase shift of harmonic voltage, as illustrated in Fig 3. The resulting symmetrical shape, as depicted in Fig 4 and 5, reflects the impact of a single voltage harmonic with varying amplitudes on the peak value moment shift. Notably, the severity of the peak shift varies across quadrants.

Mains AC supply voltage, assumed to be composed of multiple harmonic sinusoidal components (1) can be written as

$$u_{LVAC}(t) = U_1 \cdot \sin(\omega_1 t + \varphi_1) + U_2 \cdot \sin(\omega_2 t + \varphi_2) + \cdots + U_N \cdot \sin(\omega_N t + \varphi_N) \quad (2)$$

where N is the total number of harmonic components present. While commonly more dominant in the power grids the odd order harmonic components will be discussed in this paper.

In the following context, let us assume there is just two components present in the supply voltage waveform, the main harmonic with magnitude value U_1 and a harmonic component of order x with magnitude value U_x. In essence, the peak voltage value can be calculated at any time instant, using the common expression of sine components as

$$U_{Peak} = U_1 \cdot \sin(\omega_1 \cdot t_{peak}) + U_x \cdot \sin(x \cdot \omega_1 \cdot t_{peak} + \varphi_x) \quad (3)$$

or expressed phase-wise towards main harmonic 0 phase as

$$U_{Peak} = U_1 \cdot \sin(\varphi_{Peak}) + U_x \cdot \sin(x \cdot \varphi_{Peak} + \varphi_x) \quad (4)$$

It is noteworthy that the main harmonic initiation (zero phase) is assumed to occur at time $t = 0$. Here the φ_x is the harmonic voltage component U_x phase angle from the main harmonic zero phase value and U_x is the harmonic voltage component magnitude value.

Analytically, the peak instant (end of conduction time of capacitor) can be found where the voltage derivative approaches to zero; as expressed in the following equation.

$$\mathrm{Max}\{u_{LVAC}(t)\} \Rightarrow \frac{du_{LVAC}(t)}{dt} = 0 \quad (5)$$

the voltage on capacitor (U_{CB}) in rectifier circuit reaches to its peak when $u_{LVAC}(t)$ reaches its maximum.

$$U_{CB_{MAX}} = max\{u_{LVAC}(t)\}|_{T_{50Hz}} \quad (6)$$

Numerically the peak voltage value is straightforward to find. For any input U_x and φ_x the waveform could be assumed through finite time-step calculation and using (3) for any time step. An example of the outcome of numerical calculations is presented in Fig. 7.

In order to find the analytical expressions of the characteristic parameters of the peak voltage absolute value and it's timing a more universal approach will be needed. Assuming the harmonic voltage component could have any phase angle and any magnitude the numerical descriptions may lack effectiveness for universal analysis. The complexity of the voltage peak moment timing is presented through expressions for peak phase value range in Fig. 4. And Fig. 5 for the peak value range. The eccentricity expression found in the numerical results refers to examples of Kepler equation, known to be unsolvable by geometric relations.

Details on the expressions of the peak voltage have more support from the analysis on dynamics of the supply voltage sinewave components. For the voltage peak time instant t_{peak}, the first order differentials of fundamental and influencer harmonic are equal in magnitude. Referring to (5)

$$\frac{d}{dt}u_1(t_{peak}) = -\frac{d}{dt}u_x(t_{peak}) \quad (7)$$

$$U_1 \cdot \omega_1 \cdot \cos(\omega_1 t_{peak}) = -U_x \cdot \omega_1 \cdot x \cdot \cos(x\omega_1 t_{peak} + \varphi_x) \quad (8)$$

Simplified into

$$U_1 \cdot \cos(\omega_1 t_{peak}) = -U_x \cdot x \cdot \cos(x\omega_1 t_{peak} + \varphi_x) \quad (9)$$

The characteristic peak voltage observation cases will be listed below.

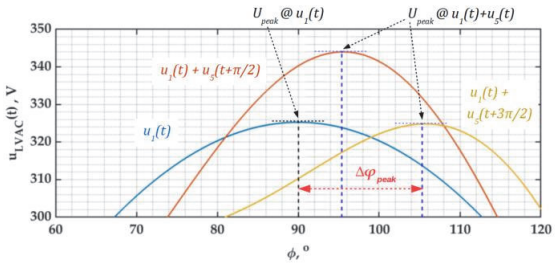

Fig. 3. Variation in peak instant depending on harmonic phase angle.

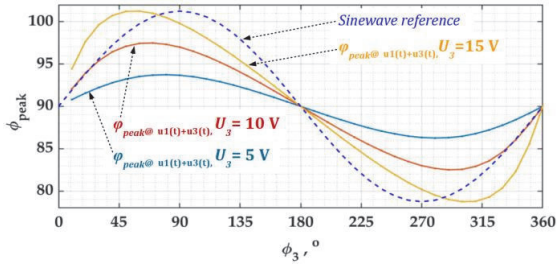

Fig. 4. Variation in peak instant depending on harmonic phase angle. Make blue reference line dashed line

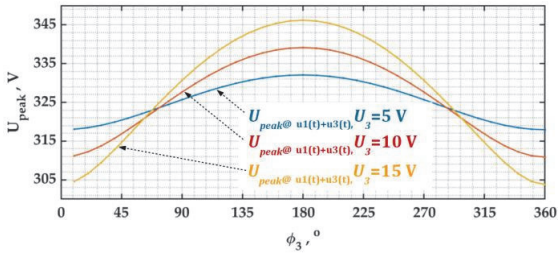

Fig. 5. Variation in peak depending on harmonic phase angle. Dynamic expressions for peak voltage instant

Case 1. Peak voltage highest and lowest magnitude expressions

Search for the peak voltage maximum possible value reveals that upon time instant when $u_1(t_{peak})$ and $u_x(t_{peak})$ components are both at maximum. Here sum of magnitude values will provide U_{peak}. This is when the sin components will both yield value of "1" i.e. the sin argument is π/2

$$U_{peak,max} = U_1 \cdot \sin\left(\frac{\pi}{2}\right) + \mathrm{U}_x \cdot \sin\left(\frac{\pi}{2}\right) \quad (10)$$

given that harmonic phase angle is at x times higher than the main harmonic, the harmonic component angle which provides the π/2 at the time of U_1 magnitude peak will be

$$\varphi_{x,peak,max} = x \cdot \pi/2 \quad (11)$$

In case of odd harmonics, it should be noted that system with only 3rd harmonic added will provide peaking when $\varphi_{U3} = -90^o$ while for 5th harmonic added will respond with peak voltage maximum when $\varphi_{U5} = 90^o$. Similarly, the lowest magnitudes will be provided by harmonic phase angles with 180 ° modification.

Case 2. Maximum shift of the peak time instant from peak instant of only fundamental component (i.e 90° or π/2) $\Delta\varphi_{peak,max}$.

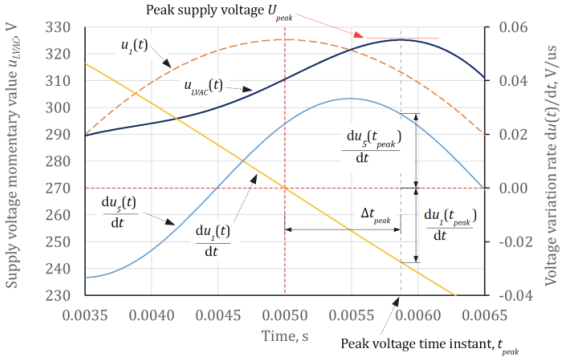

Fig. 6. Variation in peak time instant depending on harmonic phase angle.

The peak time instant maximum shift $t_{peak,\Delta\varphi max}$ occurs when the first order derivative of the harmonic component variation is at its maximum; therefore

$$\left\{\frac{d}{dt}u_x\left(t_{peak,\Delta\varphi_{max}}\right)\right\}_{max} = U_x \cdot x \cdot \omega_1 \quad (12)$$

Assuming (10) this occurs at time instant when $(x{\cdot}\omega{\cdot}t_{peak} + \varphi_{Ux})$ provides total of 0. Therefore, the peak phase excursion occurs at instant for the harmonic when

$$\varphi_{Ux} = x \cdot \omega_1 \cdot t_{peak}$$

from (12)

$$\cos\left(\omega_1 t_{peak,\Delta\varphi_{max}}\right) = \frac{U_x}{U_1}x$$

and replacing

$$A = \frac{U_1}{U_x}$$

the expression will be

$$t_{peak,\Delta\varphi_{MAX}} = \frac{\cos^{-1}\frac{x}{A}}{\omega_1} \quad (13)$$

Case 3. Instant when peak voltage level of the combined waveform with $U_1 + U_x$ is ***equal*** to fundamental harmonic waveform peak; it is the point when there is peak voltage equal to magnitude level of U_1

$$U_1 = U_1 \sin(\omega_1 \cdot t) + U_x \sin(x\omega_1 t + \varphi_x) \quad (14)$$

Here U_1 is the magnitude of fundamental component i.e. for 230 V_{rms} this will have level of 325 V. U_x is the amplitude of supply voltage harmonic component, φ_x is the phase angle of the voltage harmonic component.

Empirical value calculation of the crossing point of harmonic (U_x) near 90° of fundamental harmonic on fundamental harmonic scale

$$t_{cross,x} = \frac{T_1}{x}\left(\frac{1}{4}(x+1) - \frac{\varphi_x}{2\pi}\right) \quad (15)$$

$$\varphi_{cross,x} = 2\pi\frac{t_{cross,x}}{T_1} \quad (16)$$

Where x is a harmonic number. $T_1 = 0.02$ s time-period of fundamental harmonic. Now, transforming the equations (3) and (7) to phase angle domain

$$U_1 = U_1 \sin\left(90^o - \varphi_{peak}\right) + U_x \sin\varphi_{x,c} \quad (17)$$

$$U_1 \cos\left(90^o + \varphi_{peak}\right) = -x \cdot U_x \cdot \cos\varphi_{x,c} \quad (18)$$

Here φ_{peak} is phase distance between peak of fundamental component (i.e. 90° or π/2) and peak of $u_{LVAC}(t)$ expressed in degrees on fundamental harmonic scale and $\varphi_{x,c}$ is distance between peak of $u_{LVAC}(t)$ and the zero crossing instant of the voltage harmonic component.

From (17)

$$\sin\varphi_{x,c} = \frac{U_1}{U_x} - \frac{U_1}{U_x}\sin\left(90^o - \varphi_{peak}\right)$$

$$\sin\varphi_{x,c} = A\left[1 - \cos\varphi_{peak}\right] \quad (19)$$

From (18)

$$\frac{U_1}{U_x \cdot x}\cos\left(90^o + \varphi_{peak}\right) = -\cos\varphi_{x,c}$$

As *cos* is an even function

$$\frac{A}{x}\cos\left(90^o + \varphi_{peak}\right) = \cos\varphi_{x,c}$$

$$\frac{A}{x}\cos\left(90^o + \varphi_{peak}\right) = 1 - [\sin\varphi_{x,c}]^2$$

$$\sin\varphi_{x,c} = \sqrt{1 - \left[\frac{A}{x}\cos\left(90^o + \varphi_{peak}\right)\right]^2} \quad (20)$$

Equating (17) and (18) provides

$$A^2\left[1-\cos\left(\varphi_{peak}\right)\right]^2 = 1-\left[\frac{A}{x}\cos\left(90^o+\varphi_{peak}\right)\right]^2 \quad (21)$$

and this can be developed into

$$\left[A^2-\frac{A^2}{x^2}\right](\cos\varphi_{peak})^2 - 2A^2\cos\varphi_{peak} + \\ +A^2+\frac{A^2}{x^2}-1=0 \quad (22)$$

Substituting $y = \cos(\varphi_{peak})$

$$\left[1-\frac{1}{x^2}\right]\cdot y^2 - 2\cdot y + 1 + \frac{1}{x^2} - \frac{1}{A^2} = 0 \quad (23)$$

Coefficients of quadratic equations are

$a = \left(1-\frac{1}{x^2}\right)$, b = – 2 and $c = 1+\frac{1}{x^2}-\frac{1}{A^2}$.

from value of $cos(\varphi_{peak})$ by quadratic solution, $\boldsymbol{\varphi_{peak}}$ can be determined.

Now in order to determine the value of $\boldsymbol{\varphi_{x,c}}$, similar expressions with (17) and (18) can be used. For development of relation for $\boldsymbol{\varphi_{x,c}}$, (17) will be expressed as

$$\sin\left(90^o-\varphi_{peak}\right) = 1+\frac{U_x}{U_1}\sin\varphi_{x,c}$$

and

$$\cos\varphi_{peak} = 1+\frac{\sin\varphi_{x,c}}{A} \quad (24)$$

Now (18) becomes

$$\cos\left(90^o+\varphi_{peak}\right) = -\frac{U_x}{U_1}\cdot x\cdot\cos\varphi_{x,c}$$

$$-\sin\varphi_{peak} = -\frac{x\cdot\cos\varphi_{x,c}}{A} \quad (25)$$

Squaring and adding (24) and (25)

$$\left(\frac{x\cdot\cos\varphi_{x,c}}{A}\right)^2+\left(1+\frac{\sin\varphi_{x,c}}{A}\right)^2 = 1$$

$$(1-x^2)\left(\sin\varphi_{x,c}\right)^2 - 2A\sin\varphi_{x,c} + x^2 = 0 \quad (26)$$

Coefficients of quadratic equations are

$a = (1-x^2)$, b = –2A and $c = x^2$.

from value of $sin(\varphi_{x,c})$ by quadratic solution, $\varphi_{x,c}$ can be determined.

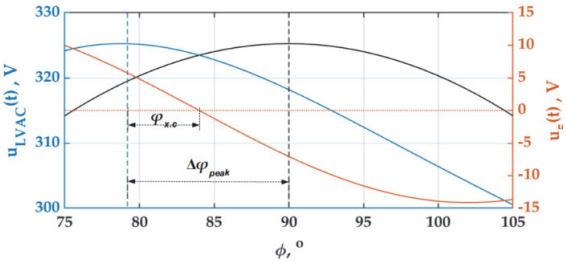

Fig. 7. Distance calculation of zero crossing of influencer harmonic and fundamental-componant's peak toward peak instant of $u_{LVAC}(t)$.

TABLE I

MODELLED/CALCULATED VALUE OF MAXIMUM PEAK STRETCH ON TIME AXIS FOR ANY LEVEL OF INFLUENCER HARMONIC

Harmonic order	U_{xRMS} level	$\varphi_{peak,max}$		$t_{peak,\Delta\varphi max}$
x	V	°	rad	ms
3	5	86.3	1.506	4.79
	10	82.5	1.440	4.58
	15	78.7	1.374	4.37
	20	74.9	1.307	4.16
	25	71.0	1.239	3.94
5	5	83.8	1.462	4.65
	10	77.4	1.352	4.30
	15	71.0	1.239	3.94
	20	64.2	1.121	3.57
	25	57.1	0.996	3.17
7	5	81.2	1.418	4.51
	10	72.3	1.262	4.02
	15	62.8	1.097	3.49
	20	52.5	0.916	2.92
	25	40.5	0.706	2.25

TABLE II

COMPARISON OF MEASURED AND CALCULATED VALUE OF RESULTANT PEAK STRETCH OF $U_{LVAC}(T)$, MAGNITUDE IDENTICAL TO FUNDAMENTAL COMPONENT

x	U_{xRMS}, V	$\varphi_{peak,meas}$, °	$\varphi_{peak,calc}$, °	$\varphi_{x,c,meas}$, °	$\varphi_{x,c,calc}$, °	$\varphi_{cross,x,meas}$, °	$\varphi_{cross,x,calc}$, °
3	5	86.3	**86.3**	6.2	**5.6**	87.9	**88.1**
	10	82.6	**82.6**	11.1	**10.9**	86.3	**86.4**
	15	79.1	**79.2**	15.6	**15.9**	84.8	**84.7**
	20	75.9	**75.8**	20.4	**20.4**	83.2	**83.2**
	25	72.8	**72.7**	24.7	**24.5**	81.8	**81.8**
5	5	84.0	**84.0**	14.2	**14.8**	87.2	**87.0**
	10	78.8	**78.8**	26.2	**26.2**	84.8	**84.8**
	15	74.4	**74.4**	34.2	**34.4**	83.2	**83.1**
	20	70.7	**70.7**	40.5	**40.4**	81.9	**81.9**
	25	67.4	**67.4**	45.0	**45.0**	81.0	**81.0**
7	5	82.1	**82.1**	26.1	**25.7**	86.3	**86.3**
	10	76.6	**76.5**	40.6	**39.7**	84.2	**84.3**
	15	72.3	**72.1**	48.1	**47.7**	83.1	**83.2**

TABLE III

MEASURED VALUES AT CHARACTERISTIC POINTS OF RESULTANT PEAK PHASE STRETCH OF $U_{LVAC}(T)$,

	x	3		5	
	u_{xRMS}, V	$\Delta\varphi_{peak}$, °	φ_x, °	$\Delta\varphi_{peak}$, °	φ_x, °
$\Delta\varphi_{peak}$ = max	5	3.8	80	6.2	120
	10	7.5	68	12.6	155
	15	11.3	55	18.8	185
ΔU_{peak} = 0	5	3.7	85	6.0	105
	10	7.4	79	11.3	120
	15	10.9	73	15.7	135
ΔU_{peak} = (max/min)	5				
	10	0	0;180	0	0;180
	15				

III. RESULTS AND VERIFICATION

Form equation (22) and (26)

$$\varphi_{peak} = \cos^{-1}\left\{\frac{-(-2)\pm\sqrt{(-2)^2-4\left(1-\frac{1}{x^2}\right)\left(1+\frac{1}{x^2}-\frac{1}{A^2}\right)}}{2\left(1-\frac{1}{x^2}\right)}\right\} \quad (27)$$

$$\varphi_{x,c} = \sin^{-1}\left\{\frac{-(-2A)\pm\sqrt{(-2A)^2-4(1-x^2)x^2}}{2(1-x^2)}\right\} \quad (28)$$

Mathematically, there are two possible solutions for every quadratic equation. And depending on the value of coefficients, one or both of the solutions can result a complex value. Equation (24) calculates the distance of zero crossing of the harmonic component and the modified peak of the resultant waveform; out of two quadratic solutions, the positive-real solution is taken as argument of inverse sine function ($\sin^{-1}$), in equation (24). With U_{xRMS} = 10 V and U_{1RMS} = 230 V, 'A' becomes 23; the x = 5 for supply harmonic order 5. The quadratic solutions here are 0.442 and –2.36. As the argument of inverse sine can be {–1…1} one value of a solution remains

$$\varphi_{x,c} = \sin^{-1}(0.4417) = \begin{cases} 26.3^o \\ -26.3^o \end{cases}$$

It has to be noted that $\varphi_{x,c}$ is x-times smaller on the fundamental harmonic scale i.e. 5.25°. Furthermore, $\varphi_{x,c}$ refers to the exact instant where $u_1(t)$ and $u_{LVAC}(t)$ waveforms cross each other (see Fig.7). Similarly, the φ_{peak} can be calculated using the inverse cosine (cos^{-1}) function to the solution of quadratic equation mention in (22). For the above-mentioned values of harmonic amplitudes and included voltage harmonic order, the calculated cos^{-1} argument value is 1.1025 and 0.9808. Similar to the inverse sine function, the argument of cos^{-1} also cannot exceed the range {–1…1}, so φ_{peak} is calculated as

$$\varphi_{peak} = \cos^{-1}(0.9808) = 78.8^o$$

Hereby, the peak shift for the fundamental component timing will be

$$\Delta\varphi_{peak} = |90^o - 78.8^o| = 11.2^o.$$

These calculated values (φ_{peak} , $\Delta\varphi_{peak}$ and $\varphi_{x,c}$) match the measured values, as illustrated in Fig. 7 below and Table I. The value of $\Delta\varphi_{peak}$ can be converted to equivalent time precisely i.e. $t_{peak,\Delta U=0}$. Fig. 8 illustrates the measured phase angle values of above calculated values.

Table I show the calculated values (referring to equation (13)) of maximum shift of peak phase instant,$\Delta\varphi_{peak,max}$, peak time instant maximum shift $t_{peak,\Delta\varphi max}$, referred as ***case 1***. It has to be noted that as the amplitude level of the higher harmonics (for example 7th) increases, the resultant voltage waveform will have multiple peak or have two equal peaks. Therefore the calculation values can point out only one dominant value out of multiple peak values. Table II presents the comparison of measured and calculated values of peak instant phase values and harmonic component zero crossing instants; under the equations (27 & 28) mentioned under ***case 2***. As mentioned earlier in this paragraph, 7th harmonic starts showing equal multiple peaks for amplitude levels higher than 15 V (aspect not discussed in detail within context of this paper). The value presented in table II provides considerable accuracy to measurements. The proof of accuracy of the developed equation can be further acquired by comparing with measurements recorded (for a dedicated amplitude and phase of influencer harmonic) as mentioned in table III. Figure 8 indicates the ΔU_{peak} and $\Delta\varphi_{peak}$ values of the $u_{LVAC}(t)$ containing 3rd harmonic voltage, when 3rd harmonic voltage phase angle φ_{U3} is rotated from 0 to 360°; showing values of all above-mentioned cases.

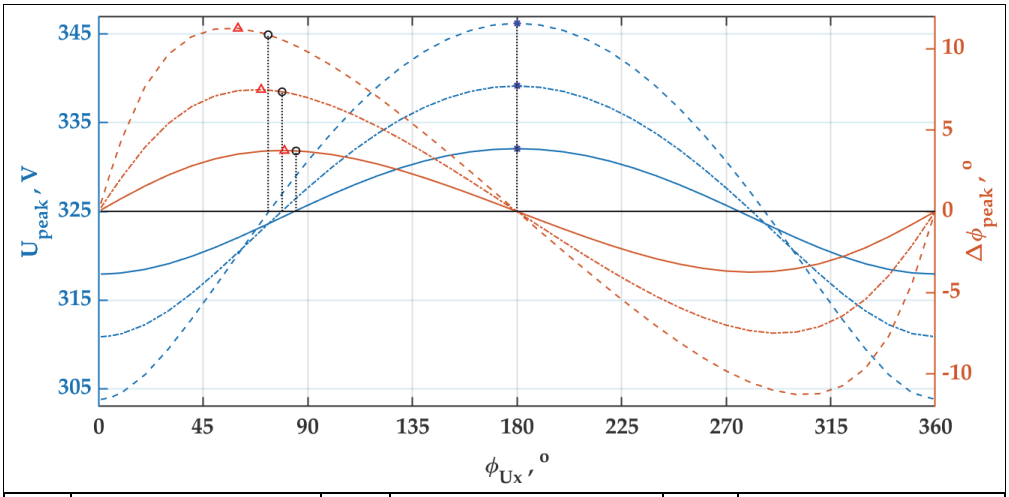

———	ΔU_{peak} @U_3=5 V	-·-·-	ΔU_{peak} @U_3 = 10 V	- - -	ΔU_{peak} @U_3=15 V
—✱—	$\Delta U_{peak,max}$ @U_3=5 V	-·✱·-	$\Delta U_{peak,max}$ @U_3 = 10 V	- ✱ -	$\Delta U_{peak,max}$ @U_3=15 V
———	$\Delta\varphi_{peak}$ @U_3=5 V	-·-·-	$\Delta\varphi_{peak}$ @U_3 = 10 V	- - -	$\Delta\varphi_{peak}$ @U_3=15 V
—○—	$\Delta\varphi_{peak,\Delta U=0}$ @U_3=5 V	-·○·-	$\Delta\varphi_{peak,\Delta U=0}$ @ U_3 = 10 V	- ○ -	$\Delta\varphi_{peak,\Delta U=0}$ @U_3=15 V
—△—	$\Delta\varphi_{peak,max}$ @U_3=5 V	-·△·-	$\Delta\varphi_{peak,max}$ @ U_3 = 10 V	- △ -	$\Delta\varphi_{peak,max}$@ U_3=15 V

Fig. 8. Results of peak mangitude and maximum phase instant of $u_{LVAC}(t)$

IV. Conclusions

Analytic expressions provided for the key waveform points were derived as one of the most characteristic properties of the peak voltage level and timing evaluation. The proposed solutions to the quadratic expressions reveal the nature of the peak voltage and peak timing phase to be sin^{-1} or cos^{-1} functions related. With these functions having a close-to-linear response for the small argument values, the peak instant characteristics and timing relations might seem linear in the empirical assessment. The linear response is easy to disappear with harmonic order increase, where already 7th harmonic voltage component low level can lead to nonlinear outcome.

With the expressions provided more insight to the near-elliptical rectifier circuit harmonic load component relation [9] on the complex plain. Further analysis is required, as the expressions here reveal only part of the analytical description of the rectifier DC side behaviour, related to the expected load current formation upon distorted supply voltage waveforms. The idealistic case here omits all circuit characteristics of the rectifier itself, therefore the actual capacitor peak voltage value and timing could differ to some extent compared to the cases presented here.

Acknowledgement

This study was supported by the Estonian Research Council grant PSG-142, "Synthesis of output current waveforms of power electronic converters for increasing the hosting capacity of renewable energy sources in the distribution networks."

References

[1] M. H. Rashid, "Power Electronics Circuits Devices and Application," 2014.

[2] M. Jarkovoi, M. Naveed Iqbal, and L. Kutt, "Analysis of harmonic current stability and summation of LED lamps," *2019 Electr. Power Qual. Supply Reliab. Conf. 2019 Symp. Electr. Eng. Mechatronics, PQ SEEM 2019*, pp. 1–8, 2019, doi: 10.1109/PQ.2019.8818237.

[3] A. M. Blanco, S. Yanchenko, J. Meyer, and P. Schegner, "Impact of supply voltage distortion on the current harmonic emission of non-linear loads," *DYNA*, vol. 82, no. 192, pp. 150–159, Aug. 2015, doi: 10.15446/dyna.v82n192.48591.

[4] L. Kütt, E. Saarijarvi, M. Lehtonen, H. Mõlder, and J. Niitsoo, "Estimating the harmonic distortions in a distribution network supplying EV charging load using practical source data - Case example," *IEEE Power Energy Soc. Gen. Meet.*, vol. 2014-Octob, no. October, pp. 4–8, 2014, doi: 10.1109/PESGM.2014.6939267.

[5] M. N. Iqbal *et al.*, "Estimation of harmonic emission of electric vehicles and their impact on low voltage residential network," *Sustain.*, vol. 13, no. 15, pp. 1–17, Aug. 2021, doi: 10.3390/su13158551.

[6] M. N. Iqbal, L. Kutt, N. Shabbir, and B. Asad, "Comparison of Current Harmonic Emission by Different Lighting Technologies," *2020 IEEE 61st Annu. Int. Sci. Conf. Power Electr. Eng. Riga Tech. Univ. RTUCON 2020 - Proc.*, pp. 1–5, 2020, doi: 10.1109/RTUCON51174.2020.9316615.

[7] K. Daniel, L. Kütt, M. N. Iqbal, N. Shabbir, M. Jarkovoi, and M. Parker, "Voltage Main Harmonic Level Influence on Harmonic Current Emission Modeling," *2023 Int. Conf. Futur. Energy Solut.*, no. 1, pp. 1–6, doi: 10.1109/FES57669.2023.10183302.

[8] M. N. N. Iqbal, K. Lauri, L. Kütt, B. Asad, and N. Shabbir, "Impact of Cable Impedance on the Harmonic Emission of LED Lamps," *21st Int. Sci. Conf. Electr. Power Eng.*, no. December, pp. 1–6, 2020, doi: 10.1109/EPE51172.2020.9269271.

[9] K. Daniel, L. Kütt, M. N. Iqbal, N. Shabbir, M. Parker, and M. Jarkovoi, "Waveform Variation Defined Model for Harmonic Current Emissions Including Cross-Order Supply Voltage Harmonics Influence," *IEEE Access*, vol. 11, no. March, pp. 42276–42289, 2023, doi: 10.1109/ACCESS.2023.3270805.

[10] J. Liu, J. K. Motwani, D. Zhang, and D. Dong, "Unidirectional Hybrid Multilevel Rectifier Family for MV/HV Applications: Analysis and Comparative Evaluation," *IEEE Trans. Power Electron.*, vol. 39, no. 3, pp. 1–13, 2023, doi: 10.1109/tpel.2023.3337772.

[11] S. Gupta, N. Vamanan, and V. John, "A Diode Bridge Rectifier with Improved Power Quality Using the Capacitive Network," *IEEE Trans. Ind. Appl.*, vol. 54, no. 2, pp. 1563–1572, 2018, doi: 10.1109/TIA.2017.2785354.

[12] X. Yue and S. Du, "A Synchronized Switch Harvesting Rectifier With Reusable Storage Capacitors for Piezoelectric Energy Harvesting," *IEEE J. Solid-State Circuits*, vol. 58, no. 9, pp. 2597–2606, 2023, doi: 10.1109/JSSC.2023.3260145.

[13] J. K. Han, J. W. Kim, and G. W. Moon, "A High-Efficiency Asymmetrical Half-Bridge Converter with Integrated Boost Converter in Secondary Rectifier," *IEEE Trans. Power Electron.*, vol. 32, no. 11, pp. 8237–8242, 2017, doi: 10.1109/TPEL.2017.2675283.

[14] S. Sharifi, M. Monfared, and M. Babaei, "Ferdowsi Rectifiers - Single-Phase Buck-Boost Bridgeless PFC Rectifiers with Low Semiconductor Count," *IEEE Trans. Ind. Electron.*, vol. 67, no. 11, pp. 9206–9214, 2020, doi: 10.1109/TIE.2019.2955430.

[15] M. Melquíades Silva, M. Losada Y Gonzalez, and S. Rocha Silva, "A new analytical model for evaluating loads supplied by sinusoidal and non-sinusoidal voltage sources," *2010 IEEE/PES Transm. Distrib. Conf. Expo. Lat. Am. T D-LA 2010*, pp. 824–831, 2011, doi: 10.1109/TDC-LA.2010.5762980.

[16] S. Elphick, P. Ciufo, and S. Perera, "Laboratory investigation of the input current characteristics of modern domestic appliances for varying supply voltage conditions," *ICHQP 2010 - 14th Int. Conf. Harmon. Qual. Power*, pp. 1–7, 2010, doi: 10.1109/ICHQP.2010.5625397.

[17] M. Rylander, W. M. Grady, and M. Narendorf, "Experimental apparatus, testing results, and interpretation of the impact of voltage distortion on the current distortion of typical single-phase loads," *IEEE Trans. Power Deliv.*, vol. 24, no. 2, pp. 844–851, 2009, doi: 10.1109/TPWRD.2008.2002874.

[18] K. Daniel, L. Kütt, M. N. Iqbal, N. Shabbir, M. Jarkovoi, and M. Parker, "Load Current Harmonic Model Complexity Reduction through Empirical Pattern Analysis," *Int. Conf. Compat. Power Electron. Power Eng. (CPE-POWERENG 2023) JUNE 14 – 16,Tallinn, Est.*, pp. 1–6, 2023, doi: 10.1109/CPE-POWERENG58103.2023.10227474.

[19] R. S. Thallam, M. T. Doyle, S. D. Krein, M. J. Samotyj, A. Mansoor, and W. M. Grady, "Effect of Supply Voltage Harmonics on the Input Current of Single-Phase Diode Bridge Rectifier Loads," *IEEE Trans. Power Deliv.*, vol. 10, no. 3, pp. 1416–1422, 1995, doi: 10.1109/61.400924.

[20] J. J. Mesas, L. Sainz, and J. Molina, "Parameter estimation procedure for models of single-phase uncontrolled rectifiers," *IEEE Trans. Power Deliv.*, vol. 26, no. 3, pp. 1911–1919, 2011, doi: 10.1109/TPWRD.2011.2120629.

[21] Z. Chen, Y. Han, Y. Wu, Z. Lu, and X. Liu, "A Low Voltage Stress PFC Rectifier Based on Nonoverlapping Strategy Using Resonant Switched-Capacitor Converter," *IEEE Trans. Ind. Electron.*, vol. 69, no. 12, pp. 12728–12738, 2022, doi: 10.1109/TIE.2021.3135643.

[22] T. Busatto, S. K. Rönnberg, and M. H. J. Bollen, "Comparison of models of single-phase diode bridge rectifiers for their use in harmonic studies with many devices," *Energies*, vol. 15, no. 1, 2022, doi: 10.3390/en15010066.

Curriculum vitae

Personal data

Name:	Kamran Daniel
Date of birth:	01.10.1986
Place of birth:	Pakistan
Citizenship:	Pakistan

Contact data

E-mail:	kamran.daniel@taltech.ee
Address:	Tallinn University of Technology, School of Engineering, Department of Power Engineering and Mechatronics, NRG-311, Ehitajate tee 5, 19086 Tallinn Estonia
Phone:	+372 59 138 125

Education

2020–2024	Tallinn University of Technology Estonia, PhD
2015–2116	University of South Asia Lahore Pakistan, MSC
2004–2008	Islamia University Bahawalpur Pakistan, BSC
2001–2003	BISE Bahawalpur Pakistan, HSSC

Language competence

English	Fluent
Urdu	Fluent (Native)
Punjabi	Fluent

Professional employment

2020–2024	Tallinn University of Technology Estonia, Early-Stage Researcher
2009–2020	University of Engineering and Technology Lahore Pakistan, Lecturer

Main track of research

Electrical engineering, Power quality, Signal processing, measurement of AC quantities

Research Projects

2018–2021	PSG142 “Synthesis of the output waveform of semiconductor converters to increase the possibility of connecting renewable energy sources to the network” (1.01.2018−31.12.2021); Responsible executor: Lauri Kütt; Tallinn University of Technology, School of Engineering, Department of Electrical Power Engineering and Mechatronics; Financier: Estonian Science Agency Foundation.
2024–2028	PRG2055 “Efficient, reliable and safe partial power electronic systems” (1.01.2024−31.12.2028); Responsible executor: Andrii Chub; Tallinn University of Technology, School of Engineering, Department of Electrical Power Engineering and Mechatronics; Financier: Estonian Science Agency Foundation.

Elulookirjeldus

Isikuandmed

Nimi:	Kamran Daniel
Sünniaeg:	01.10.1986
Sünnikoht:	Pakistan
Kodakondsus:	Pakistani

Kontaktandmed

E-post:	kamran.daniel@taltech.ee
Aadress:	Tallinna Tehnikaülikool, Inseneriteaduskond, energeetika ja mehhatroonika instituut, NRG-311, Ehitajate tee 5, 19086 Tallinn Eesti
Tel:	+372 59 138 125

Hariduskäik

2020–2024	Tallinna Tehnikaülikool, Eesti, PhD
2015-2016	Lõuna-Aasia ülikool Lahore Pakistan, MSc
2004–2008	Bahawalpuri Islamia Ülikool, Pabistan, BSC
2001–2003	BISE Bahawalpur Pakistan, keskharidus

Keelteoskus

Inglise keel	Kõrgtase
Urdu keel	Kõrgtase (emakeel)
Pandžabi keel	Kõrgtase

Teenistuskäik

2020–2024	Tallinna Tehnikaülikool, doktorant-nooremteadur
2009–2020	University of Engineering and Technology Lahore Pakistan, lektor

Peamine uurimistöö

Elektrotehnika, elektrikvaliteet, signaalitöötlus, vahelduvvoolusuuruste mõõtmine

Uurimisprojektid

2018–2021	PSG142 “Pooljuhtmuundurite väljundvoolukuju süntees taastuvenergiaallikate võrguga liitmisvõimaluse suurendamiseks” (1.01.2018−31.12.2021); Vastutav täitja: Lauri Kütt; Tallinna Tehnikaülikool; Finantseerija: Sihtasutus Eesti Teadusagentuur; Pooljuhtmuundurite väljundvoolukuju süntees taastuvenergiaallikate võrguga liitmisvõimaluse suurendamiseks.
2024–2028	PRG2055 “Tõhusad, töökindlad ja turvalised osavõimsusega elektroonilised süsteemid” (1.01.2024−31.12.2028); Vastutav täitja: Andrii Chub; Tallinna Tehnikaülikool; Finantseerija: Sihtasutus Eesti Teadusagentuur

ISSN 2585-6901 (PDF)
ISBN 978-9916-80-165-9 (PDF)